KAUNAS UNIVERSITY OF TECHNOLOGY

SHARATH PEETHAMBARAN SUBADRA

A STUDY ON IMPACT PERFORMANCE OF FIBRE REINFORCED POLYMER COMPOSITES BY ANALYSING THE EFFECTS OF NANO-FILLERS, HYBRIDISATION AND FIBRE WAVINESS

Doctoral dissertation
Technological Sciences, Mechanical Engineering (T 009)

2023, Kaunas

This doctoral dissertation was prepared at Kaunas University of Technology, Faculty of Mechanical Engineering and Design, Department of Mechanical Engineering during the period of 2018–2022.

The doctoral right has been granted to Kaunas University of Technology together with Vytautas Magnus University.

Scientific Supervisor:

Prof. Dr. Paulius GRIŠKEVIČIUS (Kaunas University of Technology, Technological Sciences, Mechanical Engineering, T 009).

Edited by: English language editor Brigita Brasienė (Publishing House *Technologija*), Lithuanian language editor Aurelija Gražina Rukšaitė (Publishing House *Technologija*)

Dissertation Defense Board of Mechanical Engineering Science Field:

Prof. Dr. Giedrius JANUŠAS (Kaunas University of Technology, Technological Sciences, Mechanical Engineering, T 009) – **chairperson**;

Dr. Andrey ANISKEVICH (University of Latvia, Latvia, Technological Sciences, Materials Engineering, T 008);

Dr. Gintautas DUNDULIS (Kaunas University of Technology, Technological Sciences, Mechanical Engineering, T 009);

Prof. Dr. Valdas EIDUKYNAS (Kaunas University of Technology, Technological Sciences, Mechanical Engineering, T 009);

Prof. Dr. Juozas PADGURSKAS (Vytautas Magnus University, Technological Sciences, Mechanical Engineering, T 009).

The public defense of the dissertation will be held at 10 a.m on 28 August, 2023 at the public meeting of Dissertation Defense Board of Mechanical Engineering Science Field in Rectorate Hall at Kaunas University of Technology.

Address: K. Donelaičio 73-402, Kaunas, LT-44249, Lithuania
Phone: (+370) 608 28 527; e-mail doktorantura@ktu.lt

The doctoral dissertation was sent out on 28 July, 2023.
The doctoral dissertation is available on the internet http://ktu.edu and at the libraries of Kaunas University of Technology (Gedimino 50, Kaunas, LT-44239 Lithuania) and Vytautas Magnus University (K. Donelaičio 52, Kaunas, LT-44244, Lithuania).

KAUNO TECHNOLOGIJOS UNIVERSITETAS

SHARATH PEETHAMBARAN SUBADRA

PLUOŠTU ARMUOTŲ POLIMERINIŲ KOMPOZITŲ SMŪGINĖS ELGSENOS TYRIMAI ANALIZUOJANT NANOUŽPILDŲ HIBRIDIZAVIMO IR PLUOŠTŲ BANGUOTUMO ĮTAKAS

Daktaro disertacija
Technologijos mokslai, mechanikos inžinerija (T 009)

2023, Kaunas

CONTENTS

LIST OF TABLES

LIST OF FIGURES

8

LIST OF ABBREVIATIONS

BPO – benzoyl peroxide
CDM – continuum damage mechanics
CNT – carbon nanotubes
CVD – chemical vapor deposition
DFAILC – compressive failure strain
DFAILM – matrix failure strain
DFAILT – tensile failure strain
DI – ductility index
E_1/E_2 – Young's modulus in the principal material direction
E_x/E_y – Young's modulus in the body coordinates
FBRT – strength reduction parameter
FCNT – functionalised carbon nanotubes
FGA – functionalised graphene
FGCE – functionalised glass carbon nanotubes epoxy
FGGE – functionalised graphene glass epoxy
G_{12}/G_{13} – shear modulus in the principal material direction
GA – graphene
GHGE – greenhouse gas emissions
GPa – giga pascal
G_{xy}/G_{yz} – shear modulus in the body coordinates
ISO – international organisation for standardisation
MAT – material model
MMA – methylmethacrylate
MWCNT – multi-walled carbon nanotubes
PFM – progressive failure model
PMMA – poly(methylmethacrylate)
PS – parametric study
SC – shear strength
SEM – scanning electron microscope
TGA-DTG – thermogravimetric/derivative thermogravimetric analysis
XC – fibre compressive strength
XT – fibre tensile strength
YCFAC – strength reduction parameter
YC – matrix compressive strength
YT – matrix tensile strength
ν_{12} – Poisson's ration

INTRODUCTION

Motivation and importance of the problem

The demand for polymeric composites has seen an upswing over the past few decades owing to their light weight, damage tolerance, high specific strength, durability, maturity in processing, lower gas emissions, lower fuel consumption etc., compared to metals [1–3]. However, these materials are prone to sudden failure because of their delicate and brittle nature; thus, for cautious functioning, higher safety factors are applied for portions made from fibre reinforced composites. This could lead to the overdesigned portions in components made of composites, hence altering their potential weight saving benefits. In this context, introducing ductility into brittle composites could engineer gradual failure (during impact events) akin to metal, thus enhancing their usability and expanding their application scope [4, 5].

While being used in day-to-day applications, the composites are subjected to occasionally low velocity impact. The examples include bird strikes on aircraft composite parts, tool drops during in station work etc. Even though the damages are unavoidable, the composite structures are designed to consider the presence of flaws. During the impact event, the incident energy is expended through various damage mechanisms [6, 7], and an impact resistant structure should be able to avoid the damage mechanisms (matrix cracks, delamination, fibre rupture etc.). However, during an impact event, the initial failure is initiated by the formation of matrix cracks within plies, and this is due to the out-of-plane shear stresses generated by an out-of-plane impact force [8]. The matrix cracks latter develop into delaminations initiated by opening forces, mainly driven by interlaminar shear stress (mode II) induced by bending of the laminate [9].

The brittle nature of resins (epoxy) used in composites renders them susceptible to impact induced damage, such as delamination. Thus, an ideal approach to make composites impact resistant would be to strengthen the matrix system by enhancing its energy absorption capabilities. This has been achieved through various filler materials dispersed within the matrix [9, 10]. In addition to these, through the thickness reinforcement methods, the nanofillers intended for reinforcements in the nanoscale are gaining wide scale prominence.

Carbon nanofibers, nanoclays, graphene and carbon nanotubes are a few of the nanofillers used to strengthen the matrix in composite architectures. Carbon nanotubes, in particular, are used extensively owing to its properties associated with large aspect ratio and specific surface area in conjunction with high longitudinal modulus [11]. Impact strength improved significantly with 0.5% weight of Multi-Walled Carbon Nanotubes (MWCNT) [12]; likewise, several studies have proven to positively affect the mechanical properties of composites when reinforced with either nanotubes or graphenes [13–20]. However, the downside to both carbon nanotubes and graphene is that they agglomerate while being dispersed in the matrix, and hence, they should be either functionalized before being introduced into the matrix, or more sophisticated mechanical methods, e.g., three roll mills, should be employed [11, 21–

23]. Hence, more cost-effective methods to develop impact resistant composites should be explored.

Hybridization of composite architecture could be a cost-effective game changer to enhance the impact resistance of polymer composites. The basic rationale being the addition of tough fibres leads to enhanced impact resistance without significant drop in mechanical properties [24]. Hybrid composite architectures are made by combining two or more different fibres in a matrix [25]. The stacking sequence of different fibres to obtain an optimum impact resistance remains unknown, as various combinations have achieved results, which seem promising and at the same time, have some drawbacks. Few design parameters in hybrid composites that affect their impact resistance are stacking sequence, thickness and geometry. Various studies have shown the ability of hybrid architecture in composites to reduce the impact induced damage governed basically by the stacking sequence [26, 27]. Hybrid composites were even found to exhibit a gradual flexural behaviour, which in turn helps to infer their more gradual behaviour during impact [24, 27], and this gradual behaviour can be termed as the ductility effect [27]. While being subjected to impact, stresses that are caused by bending are the major cause of delamination and a matrix dominant phenomenon [5]. As matrix dominant properties play such an important role in determining the long-term stability of composites, an alternative to epoxy should be explored to render these highly engineered materials environmentally friendly. As epoxy-based composites are hard to recycle, an alternative resin material exhibiting similar mechanical properties should be investigated, and one such replacement could be poly(methylmethacrylate)-PMMA. It remains to be explored if the ductility effect can be seen in other resins, such as PMMA, during the impact event.

Hybrid effect and the effect of waviness in such resins need to be ascertained to understand the behaviour of resins better when contributing to the long-term stability of composites, and hence, make them an ideal low weight replacement. Even though the presence of waviness in composites might mimic out-of-plane reinforcements, in reality, it is a problem associated with thick composite structures. The primary cause of such problems is residual stress, originated during curing and local buckling of fibres during filament winding [28–30]. Loading of composite structures with ply waviness causes a three-dimensional stress state that ideally reduces the stiffness and strength [31]. Fabricating composite architectures to achieve gradual failure with flexural loading could pave the way to make them more predictable. As mentioned previously, hybridizing the architecture could help in achieving this, but the effect of waviness can as well lend such behaviour but with reduced modulus of elasticity. The effect of waviness can help to understand the effect of shear on the stability of composites better. Thus, matrix dominant properties play an important role [31, 32] in the presence of waviness, and hence, the effect of waviness in different matrix should be studied.

Aim and objectives of the PhD dissertation

The aim of this doctoral dissertation is to explore and analyse the effect of nanoparticles, hybridizations and waviness on impact characteristics of fibre reinforced polymer composites.

Polymer composites subjected to low velocity impact loading undergone damage, which is matrix dominant. The above-mentioned aim was formulated to understand the effect on matrix and hence the impact damage. Thus, based on the formulated aim, the following objectives can be established:

1. To determine the effect of carbon nanotubes and graphene on the impact performance of composites under low velocity impact loading;

2. To ascertain the effectiveness of hybrid architecture in composites under impact loading with two different matrixes, namely, epoxy and PMMA;

3. To quantify the hybrid effect in terms of energy and arrive at a quantifiable term/index;

4. To deduce the effect of waviness (both in-plane and out-of-plane) on flexural loading prevalent as global bending during the impact loading;

5. To ascertain the effectiveness of in-plane waviness against different fibre orientations during the impact loading;

6. To develop a numerical model on LS-DYNA to correctly ascertain the effect of fibre and matrix-based failure strains respectively during flexure and impact loading.

Thus, the current PhD dissertation is an attempt to realise 6 objectives elaborated above starting with nanofiller reinforcements to using an easier method, such as hybridization, and studying the effect of associated parameters directly dependent on resin to improve the impact resistance of polymer composites.

Research methodology

The basic structure of the research could be broken down into two broad categories where the first part deals with nanoscale reinforcements (chapters 2 and 3) and focuses on the material characterisation. Even though it does not categorically form a part of the current study, it helps in further developing ideas for the second part (which would be chapters 4, 5 and 6). The second part deals with the mechanics of composite from the perspective of impact loading and further delves deeply on the role of energies that play an important role in damage formations. The aspect of sustainability is a common thread that runs through this work from chapter 2 in order to bring the reader's attention to the ability of polymer composites to be recycled effectively.

The effect of matrix on the composite material's stability while under impact loading is very crucial, and hence, the way to improve the impact resistance by enhancing the strength of the matrix is obvious. Thus, the methodology that has been adopted during this research follows the logical order of published results that are presented in sub-chapters of chapter 2 to chapter 5. Initially an attempt to evaluate the mechanical and impact performance of composites with nano reinforcements in the forms of CNTs and graphene were adopted. In order to study the mechanical

properties in terms of strength and modulus, ISO 527-2 was adopted as a standard, while for the impact, the specimen size of 80 x 80 mm with a thickness of 1 mm was fabricated. The impact energy was kept constant at 50 J throughout the experimentations to attain complete perforation. Based on the results and conclusions drawn from these experimentations, the next stage incorporates ductility into composites. The first stage of the research concludes with chapter 3.

In the next stage, a gradual shift to explore the hybridised composite structures was initiated with an emphasis on PMMA to study the effect of alternative resin materials. The energy-based failure characterisation technique was explored, which could quantify the hybrid effect in composites when subjected to impact loading. Hence, the term ductility index-DI for composites, which takes into consideration the failure characterisation in terms of elastic and inelastic energies, was recommended. In order to further understand the hybrid effect, the composite panels were subjected to impact at higher temperatures, and microscopic characterisations were performed to study the damage and correlate them to the energy-based failure. Chapter 4 deals with these aspects and covers the methodology and results that have been obtained.

The same chapter covers a comprehensive review on recycling and thermoplastic resins to emphasize the role of composites as an alternative and sustainable material for future green tech revolution in the wind sector. Chapter 5 covers flexural aspects that have been encountered when subjected to impact and delves on the waviness both in-plane and out-of-plane in determining the role of matrix in improving the performance of composites while being subjected to impact loading. This chapter deals with numerical modelling techniques in understanding the strains related to the matrix and fibre directions in composites in determining performance under flexure. The conclusions briefly elaborate on relations between waviness, strains, flexural response and eventually on the impact performances. Chapter 6 explores in-plane waviness in composites and its performance when subjected to impact. Thus, in-plane waviness is incorporated into unidirectional composites, and its impact performance is compared with various other architectures, such as twill woven, unidirectional etc. The sub-chapters are related to the methodologies and each of them covers an article published during the course of this research.

Scientific novelty

- Brittleness in composites is responsible for catastrophic failure: this is reduced by introducing hybrid architecture.
- The achieved reduction in brittleness is converted to pseudo-ductility, thus making composite failure more predictable during the impact event.
- In-plane waviness introduced in unidirectional composites improves the impact performance by increasing the impact load and energy absorption characteristics.

Statements for the defence

- The hybrid effect is quantified through the energy model while under impact loading.
- The model gives an appropriate amount of energy expended in the form of elastic and inelastic energies.
- In-plane waviness positively affects the flexural response, while out-of-plane waviness affects it negatively.
- In-plane waviness increases the impact load and energy absorption when compared to unidirectional composites.

Practical value of the research

- The introduction of hybrid effect reduces the brittleness in composites, thus making them tougher and predictable when undergoing failure.
- PMMA is an effective alternative to epoxy in composites, thus rendering them recyclable and more sustainable.
- In-plane waviness in unidirectional composites improved their impact performance, and hence, the applications involving these composites cannot be restricted owing to poor impact performance.

Approbation

The scientific results that have been obtained during the course of current research were published in six publications: 4 of them in international journals referred in *ISI Web of Scinece*, one in a local journal referred in *ISI Web of Science* and one accepted as a proceeding in an international conference. In addition to this, the results were presented in two international conferences held in Lisbon (presented as a presentation) and Riga (online presentation).

Structure of the thesis

The thesis begins with an introduction, then follows six main chapters, conclusions, summary, list of references, curriculum vitae, list of publications along with the attended conferences and copies of scientific publications. The volume of the dissertation is 108 pages, but the main part covers 72 pages, which include 28 figures, 26 equations, 8 tables, 89 bibliographic references and copies of 5 publications.

- The first chapter is a review of two important aspects covered in the thesis, namely, the study of waviness and numerical modelling. It is a review to establish the mathematical aspect of waviness and affected composite properties and understand the Chang–Chang failure criterion that was used to predict the flexure in sub-chapter 2.5.
- Chapters 2 to 5 elaborate on the five publications covering the aim that has been set in this thesis. Chapters 2 and 3 deal with nano reinforcements; chapter 4 deals with the aspects of hybridisation and the two resins. It as well deals with the aspects of hybrid effect and the necessities of exploring an alternative resin, such as PMMA, for the purpose of making composites sustainable. Chapter 5 explores the flexural response that has been seen as global bending during impact and again

deals with the aspects of hybridisation and the effect of in-plane and out-of-plane waviness. Chapter 6 elaborates on the 5th objective, i.e., to explore the effect of in-plane waviness on the impact performance.

- Chapter 7 concludes the thesis based on the set objectives.

Author's contribution

A1: "High-performance fibreglass/epoxy reinforced by functionalized CNTs for vehicle applications with less fuel consumption and greenhouse gas emissions" [33]. **Sharath P. Subadra** contributed to the experimental study (data curation, mechanical and impact assessment), software. **Samy Yousef** contributed to the conceptualisation, formal analysis, writing of the original draft. **Paulius Griskevicius** contributed to the writing, reviewing and editing, and lastly, **Vidas Makarevicius** contributed to the visualisation. This article is reviewed in chapter 2.

A2: "Superhydrophilic functionalized graphene/fibreglass/epoxy laminates with high mechanical, impact and thermal performance and treated by plasma" [34]. Second co-author **Sharath P. Subadra** was involved in the formal analysis, investigation (experimental, mechanical and impact assessment), methodology formulation, writing of the original draft. **Samy Yousef** dealt with the formal analysis, funding acquisitions, investigation, methodology, writing of the original draft, review and editing. **Paulius Griskevicius** as well dealt with writing of the original draft. **Sarunas Varnagiris** dealt with the investigation, methodology, writing of the original draft and formal analysis. **Darius Milcius** was involved in writing the original draft and formal analysis, and lastly, **Vidas Makarevicius** dealt with the methodology and visualization. This article is reviewed in chapter 3.

A3: "Low velocity impact and pseudo-ductile behaviour of carbon/glass/epoxy and carbon/glass/PMMA hybrid composite laminates for aircraft application at service temperature" [35]. **Sharath P. Subadra** was involved in the methodology (ductility investigations, energy model formulation), formal analysis, investigation (experimental), visualisation (optical microscopic investigation), writing of the original draft. **Paulius Griskevicius** was involved in the original draft editing and review, formal analysis and investigation. **Samy Yousef** dealt with fund acquisition, formal analysis, methodology and formal analysis. This article is reviewed in chapter 4.

A4: "Sustainability of polymer composites and its critical role in revolutionising wind power for green future" [36]. **Sharath P. Subadra** dealt with the formal analysis, review of articles, writing of the original draft. **Paulius Griskevicius** dealt with reviewing and editing of the article. This article is reviewed in chapter 4.

A5: "Effect of hybridization and ply waviness on the flexural strength of polymer composites: An experimental and numerical study" [37]. **Sharath P. Subadra** dealt with the conceptualisation, methodology, software (LS DYNA), validation, formal analysis and investigation, resources, data curation (experimentation), writing of the original draft, visualisation. **Paulius Griskevicius** dealt with conceptualisation, validation, reviewing, editing, project administration and fund acquisition. This article is reviewed in chapter 5.

16

1. A BRIEF REVIEW OF COMPOSITE APPLICATION AND RELATED MECHANICS IN THE PRESENCE OF FIBRE WAVINESS AND NUMERICAL MODELLING

1.1. Applications of fibre reinforced composites and involved challenges

Fibre reinforced composites are widely used in many applications due to their light weight, high specific strength and stiffness and their ability to impart design flexibility. The composites could be tailored to the specific necessities by tweaking the fibre orientations, using different resins etc. Thus, the composites have found their acceptance in the aerospace, wind energy, automobile sectors, and similarly, many other sectors are gradually adopting them. To put this into perspective, Boeing 787 has 50% of its structure made from composites, and wind turbine blades have their components made of glass fibre reinforced composites [1–3].

Different fibre and resin types make up a composite structure; the choice is being made on the specific requirements and could range from the mechanical properties to the costs involved. Glass, carbon, aramid and natural fibres are the different reinforcement materials that are available. The resins are either thermoset or thermoplastic: the former is the most widely used due to their low costs and good mechanical properties that they exhibit, while the latter is gaining prominence due to being recyclable. Thermoplastics resins (polypropylene, polyether ether ketone) are known to be highly productive, since they could be reused, and this makes them a viable alternative in the automotive sector. In addition to the two basic components mentioned above, nanofillers are used to enhance the internal architecture and hence minimize the classic damages suffered by these materials, such as delamination, debonding etc., when in service [38–40].

During their service life, the composites are subjected to various loading conditions, such as fatigue, impact etc. This leads to a gradual deterioration of the material not by wear and tear as seen in the metals but through delamination, debonding and fibre rupture. These mechanisms are unique to composites; thus, a combination of these damages and ultimate catastrophic failure of the material makes them brittle in nature. A case in study for fatigue loading is the wind turbine blades subjected to high cycle fatigue loads over their operational life [41]. Thus, the failure that is accumulated is non-linear and leads to structural damage and material degradation. In order to predict the failure of composite under fatigue, there are several models available to study the evolution of the damage based on the experimental research [42]. This forms one of the major limitations of composites being used on a large scale, as the catastrophic failure needs to be accounted for while designing by incorporating larger safety factors.

As with fatigue induced damage, the impact event causes damage as well, which has a profound effect on the structural integrity of composite materials. Impact loading suffered by composites can be classified into three groups, namely, low, intermediate, and high velocity impacts. Low velocity impacts as well termed as large mass impact are synonymous with tool drops during composite manufacturing or repair, and velocity is limited to 10 m/s. Secondary blasts debris, hurricane and tornado debris,

debris on roads and runways can be classed under the intermediate velocity impact, and the velocity ranges from 10 to 50 m/s. This impact event is a characteristic of both low and high velocity impact. Impact event resulting from small firearms or blast fragments debris can be classed under high velocity impact (ballistic): a typical velocity in this case is between 50 and 1000 m/s. The mass associated with this event is very small when compared to the low velocity impact event. Each of these velocities is characterised by different damage mechanism. Delamination growth (Fig. 1.1 a, b) is associated with low velocity impacts, while high velocity impacts are characterised by localised damages. The impact induced delamination damage occurs after the threshold energy is reached. Delamination is usually preceded by the matrix cracks and is initiated as mode-I fracture. This is due to the presence of high out-of-plane normal stresses caused by the presence of the matrix cracks and high interlaminar shear stresses along the interface. The matrix crack-initiated delamination is normally due to the development of the interlaminar normal and shear stresses at the interface [31].

a)   b)
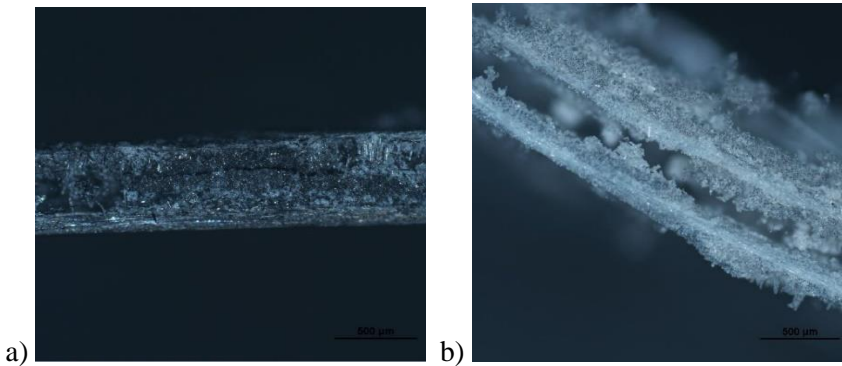
Fig. 1.1. a) Carbon fabric with a crack in the mid layer, b) glass fabric with delamination in the mid layer

1.2. Composites under impact loading in the presence of nano-fillers, hybridization and fibre waviness

Fibre-reinforced composites in structural applications (aerospace, vehicular etc.) are subject to low velocity impact resulting from bird strikes, while the aircraft is parked and taxiing from dropped tools during the assembly and maintenance works (while fabrication or repair of composite parts) or runway debris encountered during the take-off, which can cause damage even at very low impact energies [5]. Laminated composites are more prone to the impact induced damage than its metallic counterparts. These damages are internal in nature, depending on the intensity of the impact event; thus, they are not visible through visual inspection. The damage would have reduced the load bearing capacity of the material to a great extent leading to unforeseen situations in the structural applications [5]. The impact design procedure considering knockdown factors are generally adopted to design impact-resistant structures. The procedure in the beginning includes testing small coupons against impact to determine the energy and load history, damage and flexure. This is followed

by a post-impact compression test, and hence, a limit on allowable strain is determined for design purpose. Allowable laboratory scale strain is applied to the material that is susceptible to the impact failure. Thus, according to the observed behaviour of large scale, the impact requirements will be modified. Since the structure is defined before the actual impact test, the iterative process that has been elaborated above leads to a very conservative design [43]. In this cyclical process, the major reason underlying damage formation is less explored; the role of matrix, especially vis-à-vis matrix cracks and its contribution to delamination, is not given prominence.

The brittleness of the epoxies used in polymeric composites makes them susceptible to damage under various loading conditions. During impact loading of composites, delaminations are a major source of damage, and to make them resistant to such damages, strengthening the matrix would be an ideal solution. This can be achieved by dispersing nanofillers within the resin [9–10], such as graphene, carbon nanotubes (CNTs) etc. Large aspect ratio and specific surface area along with high longitudinal modulus [11] makes CNTs an ideal choice for different applications [16–20]. Along with CNTs, graphene as well enhances the mechanical properties of composites, but both are limited in their applications because of agglomeration when dispersed in matrix. Functionalisation could be an ideal choice to disperse nanofillers uniformly in addition to using three roll mills and such different sophisticated methods [11, 21–23]. A reliable method to fabricate impact resistant composites should be explored, and this method should inculcate ways to make them more predictable (tougher) while undergoing damage.

Service conditions play a role in determining the initiation and propagation of damage in composites. This becomes a critical factor when they are used in marine and aerospace applications. The stressing conditions along with the environmental conditions play a role in determining the impact performance of polymer composites and subsequent failure [24]. The damage suffered by polymer composites at room and higher temperature vary and are complicated [24, 44–47], for instance, the impact induced delamination area decreases as the temperature increases. Thermosets and thermoplastics are the two major classes of resins in use: the formers use exceeds of the latter because it can impregnate the fibres better and allows itself to be moulded into complex shapes. Thermosets are proven to lend itself to the high strengths and stiffness after curing; they have proven chemical resistance, fibre adhesion and good service temperature properties. A blend of thermosets and thermoplastics have been in use to improve the impact performance of composites. Thus, thermosets have been in continuous use, but they are not an environmentally friendly solution, as they are not fully recyclable when used in composites. Thus, a need arises to find better replacements, which are as good as epoxy. Acrylic resins could lend themselves to good wetting of fibres and are known to possess high strength, and hence, they have been used to make ultralight orthopaedic appliances. Poly(methyl methacrylate)-PMMA is an acrylic resin and has been widely used to make prostheses and is non-toxic in nature. It could act as a replacement for epoxy, and its impact properties at room and higher temperatures are studied in this research. An energy-based model

could describe this aspect considering the amount of damage suffered by the material in its entirety better.

Moreover, the inherent limitation of polymer composites is its brittle nature, which makes the failure catastrophic in nature without significant visible damage or warning [48]. Thus, in order to ensure safety, a wider design margin is applied to composites. A pseudo-ductile failure is more desirable, as it makes the material more predictable when vis-à-vis damage is concerned. In order to achieve a pseudo-ductile behaviour, a modification of the composite structure can be carried out. This can be done by hybridising the structure, which is commercially viable when costs and processes are considered. Hybridized composites fail in a gradual manner over a range of strains, and this effect, termed as the hybrid effect, was first demonstrated by Hayashi et al. [49] on a unidirectional glass and carbon hybrid composites. Generally, hybrids show an enhanced strain to failure than those seen in pure single fibre composites. Thus, hybrid effect is defined as an apparent increase in the initial failure strain of low elongation fibres in the hybrid composites, relative to the composite with only low elongation fibres. The hybrid effect is characterised by suppressed delamination and localised fibre ruptures in low strain fibres. The ideal composite architecture for such a scenario is a thin low strain fibre in the middle and high strain fibres stacked on both sides symmetrically with total thickness of high strain fibres exceeding that of the low strain fibres. The ductility to composites, imparted through hybridisation, influences the impact performance of the composites by complicating the damage mechanisms that have been involved during failure. Since there is suppression of delamination when hybridised, the influence of matrix is less explored, and the energy-based model could be relied upon to quantify the hybrid effect during the impact at any given temperature studied.

Impact induced damage, especially delamination, is governed by out-of-plane properties, such as the interlaminar longitudinal shear stress σ_{13} and the interlaminar transverse shear stress σ_{23} [31]. These play a prominent role if the laminates are thicker. The effective interplay of these stress components could be ascertained by creating scenarios, which would mimic through the thickness fibre reinforcements. The ideal way could be the introduction of a waviness, which is normally a manufacturing induced damage. It has been documented extensively that the presence of waviness both in-plane or out-of-plane affect the stiffnesses in the respective planes. The presence of waviness reduces the stiffness in the direction of waves, which is dependent on the wave characteristics, namely, the amplitude and wavelength. This has been proven analytically and experimentally. However, these waves introduce large interlaminar shear, which could make a difference when impact performance is studied. Low velocity impact (sub-perforation impact) causes global bending of the specimens; therefore, the stresses developed during a three-point bending could be comparable to that caused by the low velocity impact. In this context, introducing waviness and studying the out-of-plane shear properties through the standard bending test will give an insight into the interplay of these stress components [5, 50–51].

The interplay of interlaminar stresses can be simulated by numerical methods by employing commercial finite element solvers. A model developed using these

20

solvers could be easily tweaked to match the test results, thus enabling one to produce a generic numerical model that could predict a real time situation accurately. Out of several solvers that are available, LS-DYNA offers several material models for polymer composites based on progressive failure model (PFM) or continuum damage mechanics model (CDM). These models are based on the degradation laws, which degrade the elastic properties of composites, once an initial failure is achieved. LS-DYNA terms these models as material keywords, and hence, MAT22 and MAT54/55 are based on PFM, while MAT58 and MAT162 are based on CDM. In the context of this research to study the interlaminar stresses, a generic model based on PFM would be implemented, and hence, MAT54/55 would be used [52]. The next two sub-chapters deal with the aspect of waviness and numerical modelling. The sub-chapter on waviness elaborates on the materials properties derived in the presence of waviness within composite plies, while the sub-chapter on numerical modelling explains the Chang–Chang failure adopted to study flexure.

1.3. Determining composite material properties in the presence of waviness

The material properties of composites with waviness should be determined in order to form an input for determining their behaviour, while in numerical modelling, the properties were determined using the method adopted by Hsiao et al. [53]. Since the fabricated specimens had uniform waviness in them, it was sufficient to consider the representative volume element of one period of waviness as shown in Fig. 1.2. The volume is divided into small pieces of thickness dx, wherein x is the axis along the aligned fibre loading directions. There, each slice is treated as an off-axis unidirectional lamina, and its compliances are obtained from the compliance transformation operations [54–55]. The elastic properties are obtained from the average strains integrated over one wavelength in the loading directions.
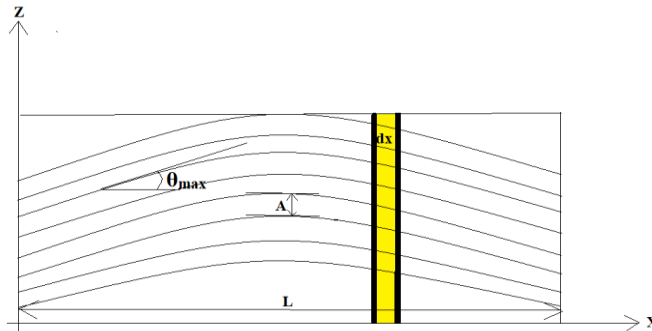
Fig. 1.2. A representative volume element with coordinates for a unidirectional composite with waviness

The fibre waviness is assumed to be a sinusoidal wave in the xz direction with an amplitude defined by:

$$v = A.sin\ (2\pi x/L);\qquad(1)$$

where A and L are the amplitude and wavelength of the wavy fibre.

The transformation equations on stresses in the three coordinate system are elaborated as follows:

$$\sigma_i = C_{ij}\,\varepsilon_j \qquad \text{or} \qquad \varepsilon_j = S_{ij}\,\sigma_i, \tag{2}$$

$$[S_{ij}] = \begin{bmatrix} \dfrac{1}{E_1} & -\dfrac{v_{21}}{E_2} & -\dfrac{v_{31}}{E_3} & 0 & 0 & 0 \\[6pt] -\dfrac{v_{12}}{E_1} & \dfrac{1}{E_2} & -\dfrac{v_{32}}{E_3} & 0 & 0 & 0 \\[6pt] -\dfrac{v_{13}}{E_1} & -\dfrac{v_{23}}{E_2} & \dfrac{1}{E_3} & 0 & 0 & 0 \\[6pt] 0 & 0 & 0 & \dfrac{1}{G_{23}} & n & 0 \\[6pt] 0 & 0 & 0 & 0 & \dfrac{1}{G_{31}} & 0 \\[6pt] 0 & 0 & 0 & 0 & 0 & \dfrac{1}{G_{12}} \end{bmatrix}, \tag{3}$$

$$[\overline{Q}] = [T]_*^{-1}[Q][T]_*^{-T} \text{ wherein } [T]_* = [T]_\alpha {}^*[T]_\beta, \tag{4}$$

where $[T]_\alpha$ and $[T]_\beta$ are expanded below:

$$[T]_\alpha = \begin{bmatrix} m^2 & n^2 & 0 & 0 & 0 & 2mn \\ n^2 & m^2 & 0 & 0 & 0 & -2mn \\ 0 & 0 & 1 & 0 & 0 & 0 \\ 0 & 0 & 0 & m & n & 0 \\ 0 & 0 & 0 & -n & m & 0 \\ -mn & mn & 0 & 0 & 0 & m^2-n^2 \end{bmatrix} \text{ and}$$

$$[T]_\beta = \begin{bmatrix} m^2 & 0 & n^2 & 0 & 2mn & 0 \\ 0 & 1 & 0 & 0 & 0 & 0 \\ n^2 & 0 & m^2 & 0 & -2mn & 0 \\ 0 & 0 & 0 & m & 0 & -n \\ -mn & 0 & mn & 0 & m^2-n^2 & 0 \\ 0 & 0 & 0 & n & 0 & m \end{bmatrix}$$

wherein $m = cos(\alpha)\,and\,n = sin(\alpha)$ for $[T]_\alpha$ and $m = cos(\beta)\,and\,n = sin(\beta)$ for $[T]_\beta$.

$$[\overline{Q}] = \begin{bmatrix} \overline{Q}_{11} & \overline{Q}_{12} & \overline{Q}_{13} & \overline{Q}_{14} & \overline{Q}_{15} & \overline{Q}_{16} \\ \overline{Q}_{12} & \overline{Q}_{22} & \overline{Q}_{23} & \overline{Q}_{24} & \overline{Q}_{25} & \overline{Q}_{26} \\ \overline{Q}_{13} & \overline{Q}_{23} & \overline{Q}_{33} & \overline{Q}_{34} & \overline{Q}_{35} & \overline{Q}_{36} \\ \overline{Q}_{14} & \overline{Q}_{24} & \overline{Q}_{34} & \overline{Q}_{44} & \overline{Q}_{45} & \overline{Q}_{46} \\ \overline{Q}_{15} & \overline{Q}_{25} & \overline{Q}_{35} & \overline{Q}_{45} & \overline{Q}_{55} & \overline{Q}_{56} \\ \overline{Q}_{16} & \overline{Q}_{26} & \overline{Q}_{36} & \overline{Q}_{46} & \overline{Q}_{56} & \overline{Q}_{66} \end{bmatrix} \tag{5}$$

In equation (4), $[T]_\alpha$ and $[T]_\beta$ represent the in-plane and out-of-plane orientations, respectively. The presence of orientations will mean that the transformed

matrix eq. (5) will have terms in all positions instead of zeros, making the material anisotropic. However, the composite is still orthotropic, but with the presence of undulations, there is coupling between shear strain and normal stresses and between shear stresses and normal strains known as shear-extension coupling. Thus, in body coordinates, a normal orthotropic material appears to be anisotropic. In normal parlance, such a material is termed as generally orthotropic material (in case of composites) because a composite lamina does have orthotropic properties in the principal material coordinates. The extensional stiffness matrix can be calculated from the transformation matrix as seen in eq. (10).

$$A_{ij} = \sum_{k=1}^{N} \overline{(Q_{ij})}_k (z_k - z_{k-1}) \tag{6}$$

From the extensional matrix, the material properties can be estimated by the following set of equations:

$$E_1 = \frac{A_{11}A_{22}A_{33} + 2A_{23}A_{12}A_{13} - A_{11}A_{23}^2 - A_{22}A_{13}^2 - A_{33}A_{12}^2}{A_{22}A_{33} - A_{23}^2},$$

$$E_2 = \frac{A_{11}A_{22}A_{33} + 2A_{23}A_{12}A_{13} - A_{11}A_{23}^2 - A_{22}A_{13}^2 - A_{33}A_{12}^2}{A_{11}A_{33} - A_{13}^2},$$

$$E_3 = \frac{A_{11}A_{22}A_{33} + 2A_{23}A_{12}A_{13} - A_{11}A_{23}^2 - A_{22}A_{13}^2 - A_{33}A_{12}^2}{A_{11}A_{22} - A_{12}^2},$$

$$G_{12} = A_{44}, \ \ G_{13} = A_{66}, \ G_{23} = A_{55},$$

$$v_{12} = \frac{A_{12}A_{33} - A_{13}A_{23}}{A_{22}A_{33} - A_{23}^2}, \ v_{13} = \frac{A_{22}A_{13} - A_{12}A_{23}}{A_{22}A_{33} - A_{23}^2}, \ \ v_{32} = \frac{A_{11}A_{23} - A_{12}A_{13}}{A_{11}A_{22} - A_{12}^2}. \tag{7}$$

From equation (11), the matrix in equation (6) can be filled up. Subsequently, the material properties in the plane xz coordinates can be obtained by averaging the properties over one wavelength of fibre waviness; it is important to relate angle θ to the wave parameters A and L:

$$tan\,\theta = \frac{dv}{dx} = 2\pi\frac{A}{L}cos\frac{2\pi x}{L}. \tag{8}$$

Thus, m and n from the previous equations can be rewritten as:

$$m = cos\,\theta = \left[1 + \left(2\pi\frac{A}{L}cos\frac{2\pi x}{L}\right)^2\right]^{-\frac{1}{2}},$$

$$n = sin\,\theta = 2\pi\frac{A}{L}cos\frac{2\pi x}{L}\left[1 + \left(2\pi\frac{A}{L}cos\frac{2\pi x}{L}\right)^2\right]^{-\frac{1}{2}}. \tag{9}$$

The average transformed compliances, $\bar{S}_{ij}$ over one wavelength can be determined by integrating the same over the wavelength L. Thus, from (5), (13) and integration, the following strains are obtained:

$$\bar{\varepsilon}_x = [S_{11}I_1 + (2S_{12} + S_{66})I_3 + S_{22}I_5]\sigma_x,$$

$$\bar{\varepsilon}_y = [S_{12}I_6 + S_{23}I_8]\sigma_x,$$

$$\bar{\varepsilon}_z = \left[(S_{11}+S_{22}-S_{66})I_3+S_{12}(I_1+I_5)\right]\sigma_x,$$

$$\bar{\gamma}_{xz} = 0; \tag{10}$$

where

$$I_1 = \frac{1+\frac{\alpha^2}{2}}{(1+\alpha^2)^{3/2}},\ I_3 = \frac{\frac{\alpha^2}{2}}{(1+\alpha^2)^{3/2}},\ I_5 = 1-\frac{1+\frac{3\alpha^2}{2}}{(1+\alpha^2)^{\frac{3}{2}}},\ I_6 = \frac{1}{(1+\alpha^2)^{\frac{1}{2}}},\ I_8 = 1-\frac{1}{(1+\alpha^2)^{\frac{1}{2}}},$$

$$\alpha = 2\pi\frac{A}{L}. \tag{11}$$

The effective material properties in xz coordinates can be expressed as follows:

$$E_x = \frac{1}{S_{11}I_1+(2S_{12}+S_{66})I_3+S_{22}I_5},\ E_y = \frac{1}{S_{22}},$$

$$E_z = \frac{1}{S_{11}I_5+(2S_{12}+S_{66})I_3+S_{22}I_1},$$

$$G_{xy} = \frac{1}{2(S_{22}-S_{23})I_8+S_{66}I_6},\ G_{yz} = \frac{1}{2(S_{22}-S_{23})I_8+S_{66}I_8},\ G_{xz} = \frac{1}{4(S_{11}+S_{22}-2S_{12})I_8+S_{66}(I_6-2I_3+I_6)},$$

$$v_{xy} = -\frac{S_{12}I_6+S_{23}I_8}{S_{11}I_1+(2S_{12}+S_{66})I_3+S_{22}I_5},\ v_{xz} = -\frac{(S_{11}+S_{22}-S_{66})I_3+S_{12}(I_1+I_5)}{S_{11}I_1+(2S_{12}+S_{66})I_3+S_{22}I_5},$$

$$v_{yz} = \frac{S_{23}I_6+S_{12}I_8}{S_{22}}. \tag{12}$$

Thus, the material properties that had been obtained would be used numerically to simulate the flexure of composites with waviness in chapter 2 (sub-chapter 2.5). The FEM model to simulate the hybrid effect and composite with waviness was implemented by using LS-DYNA software. In the materials chapter, two composite material properties were defined for carbon and glass. The material properties were determined by static tests for specimens without waviness and for waviness equations derived in [53] was used, for which the input parameters were the material properties of glass, carbon, epoxy and PMMA. Thus, based on the tests and equations [53], the material properties are listed in Table 4.

1.4. Numerical modelling approaches

Commercial codes, such as LS DYNA, ABAQUS Explicit etc., offer a wide range of built-in material models to predict failure in composite structures. The composites are modelled as orthotropic liner elastic materials within the failure surface, and beyond it, the elastic properties are degraded according to the degradation laws [83, 84]. The modelling approaches differ on the specific degradation laws that were used and hence can be divided into progressive failure models (PFM) and continuum damage mechanics model (CDM) [56]. This thesis employs LS DYNA commercial solver for the numerical investigation of composite damage under flexure, which is prevalent during the impact loading. This solver offers PFM based materials models, such as MAT22 and MAT54/55, and CDM based models, such as MAT 58 and MAT 162. Progressive damage models take into account three in-plane failure

modes, namely, matrix cracking, fibre-matrix shearing and fibre rupture. In this case, the fibre rupture and fibre-matrix shearing, for which the level of property degradation within the damaged area depends largely on the span of damage predicted by the fibre failure criterion. Most progressive failure models are defined by the strength-based criterion, which means that when strength within a ply is exceeded, their respective properties are degraded. Ply-by-ply failure leads to a progressive failure within a laminate, and when all plies in the laminate are failed, the respective elements are deleted. Continuum damage mechanics requires material properties in tension, compression and shear to define stress-strain behaviour within a laminate. MAT58, which is a continuum damage-based model, requires the user to specify the in-plane elastic modulus and Poisson's ratio in two directions on LS-DYNA. In addition to these, the maximum strengths in tension, compression and shear are specified at corresponding strain values. The response during tension is initially linear elastic with the modulus being specified as EA. The non-linearity is defined by LS-DYNA, internally based on the theories on continuum damage mechanics. In order to elaborate further on this, XT (maximum strength) is reached; the underlying stresses are reduced based on the value defined for SLIMT1, which is a stress limiting factor. Following this, the stress is held constant at the reduced value until reaching a strain specified by the ERODS parameter. Once this point is reached, the elements are deleted and removed from the solution. Thus, by correctly selecting the SLIM and ERODS, a plastic-like behaviour is incorporated in the model to avoid premature elements failure [57].

Based on the above elaborated differences between MAT54 and MAT58, which in turn is based on PFM and CDM, respectively, the previous model, i.e., MAT54, was adopted in this thesis. This decision was made due to its wide use [39–42, 56–60] and its ease of use while defining various parameters associated with this model. Most of these parameters can be defined by conducting simple static experiments, and the rest of the parameters can be defined by trial and error, which could finally deliver a model that could closely resemble failure when under flexure and impact loading, respectively. As mentioned in the previous paragraph, MAT 54 employs a ply discount method to degrade material properties. In the failure surface, the values of elastic properties in the ply material direction are degraded from an undamaged state, which is 1 to fully damaged state at 0.

In the elastic region, the material stress-strain curves in the fibre region, matrix direction and shear direction are given as follows:

$$\varepsilon_1 = \frac{1}{E_1}(\sigma_1 - v_{12}\sigma_2), \tag{13}$$

$$\varepsilon_2 = \frac{1}{E_2}(\sigma_2 - v_{21}\sigma_1), \tag{14}$$

$$2\varepsilon_{12} = \frac{1}{G_{12}}(\tau_{12} - \sigma\tau_{12}^3). \tag{15}$$

Beyond elastic region, the Chang–Chang failure criterion is employed by the material model MAT54 [60] to determine individual ply failure. In the equations elaborated below, *ef, ec, em* and *ed* are termed as history variables and represent

25

tension and compression for 1-direction and tension and compression along 2-direction. The input parameters: XT-fibre tensile strength, XC-fibre compressive strength, YT matrix tensile strength, YC matrix compressive strength and SC (S_{12})-shear strength are determined experimentally from unidirectional tape lamina.

In the case of tensile fibre mode ($\sigma_{11} \geq 0$):

$$e_f^2 = \left(\frac{\sigma_{11}}{X_T}\right)^2 + \beta \left(\frac{\sigma_{12}}{S_{12}}\right)^2 \left\{ \begin{array}{l} \geq 1 \ failed \\ < 1 \ elastic \end{array} \right. ; \qquad (16)$$

where upon failure: $E_1 = E_2 = G_{12} = v_{12} = v_{21} = 0$. In the above provided equation, β is the shear stress weighing factor, which defines the influence of shear in tensile fibre failure, this term is determined by trial and error.

In the compressive fibre mode ($\sigma_{11} \leq 0$):

$$e_c^2 = \left(\frac{\sigma_{11}}{X_C}\right)^2 \left\{ \begin{array}{l} \geq 1 \ failed \\ < 1 \ elastic \end{array} \right. ; \qquad (17)$$

where upon failure: $E_1 = v_{12} = v_{21} = 0$.
In the tensile matrix mode, when $\sigma_{22} \geq 0$:

$$e_m^2 = \left(\frac{\sigma_{22}}{Y_T}\right)^2 + \beta \left(\frac{\sigma_{12}}{S_{12}}\right)^2 \left\{ \begin{array}{l} \geq 1 \ failed \\ < 1 \ elastic \end{array} \right. ; \qquad (18)$$

where upon failure: $E_2 = v_{21} = G_{12} = 0$.
In compressive matrix mode ($\sigma_{22} \leq 0$):

$$e_d^2 = \left(\frac{\sigma_{22}}{2S_{12}}\right)^2 + \left[\left(\frac{Y_C}{2S_{12}}\right) - 1\right] \frac{\sigma_{22}}{Y_C} \left(\frac{\sigma_{12}}{S_{12}}\right)^2 \left\{ \begin{array}{l} \geq 1 \ failed \\ < 1 \ elastic \end{array} \right. ; \qquad (19)$$

where upon failure: $E_2 = v_{21} = 0 = G_{12} = 0$.

Thus, when one of the above conditions are exceeded in ply and within the element, all the specified elastic properties of that ply are set to zero. Matrix failure corresponds to the first ply failure, and FBRT and YCFAC strength reduction parameters degrade the fibre strengths of the remaining plies, once the matrix failure takes place. These strengths degradations are expressed as follows:

$$XT = XT^* * FBRT, \qquad (20)$$

$$XC = YC^* * YCFAC; \qquad (21)$$

where in FBRT is terms of percentage reduction of tensile fibre strength that can vary from 0 to 1. YCFAC used pristine matrix strength YC in determining the damaged compressive fibre strength; thus, the upper value of YCFAC is not 1, but XC/YC = 7.4. These two terms cannot be determined experimentally and can be known through trial and error.

Along with these strength-based criteria, failure occurs if strains exceed the strain to failure for each ply. For a unidirectional ply, DFAILT and DFAILC are tensile and compressive failure strains in the fibre direction, while DFAILM is the failure strain in the matrix direction. DFAILT must be positive, and DFAILC must be

negative, and when these three parameters are set to zero, the model ignores these parameters, and the failure is by the Chang–Chang failure criterion. If these parameters are non-zero, the failure occurs if one of the strains exceeds the strain to failure. Along with these three strain-based parameters, DFAILS for shear is used in the model, but it does not appear as a criterion for failure. This means that if the shear strain exceeds the assigned value of DFAILS, failure does not occur. In the current research, DFAILT and DFAILM has been investigated, and their influence was ascertained during flexural loading of composites in chapter 5. A parametric study was carried out, and the influence of DFAILM to a greater extent was established in determining the failure when being loaded and hence understanding its effect, while under impact loading, during which event there is global bending that causes delamination and failure [61].

2. FIBREGLASS REINFORCED COMPOSITES WITH FUNCTIONALIZED CNTS: A STUDY ON ITS IMPACT RESISTANCE

This chapter forms a review of the article "High-performance fibreglass/epoxy reinforced by functionalized CNTs for vehicle applications with less fuel consumption and greenhouse gas emissions". The article [33] has been published in the journal *Polymer Testing* and is available online since March 16, 2020. The aim of the article was to ascertain the mechanical and impact characterisations by reinforcing the resin at the nanoscale (carbon nanotubes). Each author's contribution has been reported at the end of the article and at the beginning of this thesis. The first author as well as the corresponding author is the writer of this dissertation, and he contributed to the experimentations involving fabrication of composites, mechanical and impact studies. This article falls into the first stage with the emphasis on nano reinforcements and studies the impact resistance. Environmental assessments through greenhouse gas emissions form a part of this article. A numerical model was developed on LS DYNA to effectively evaluate the effect of impact and hence realise a model that could effectively mimic the experimental study and serve as a tool to further study the impact.

2.1. Experimental and numerical materials, composite fabrication, material characterisation and numerical modelling approach

In this study, CNTs with an average diameter of 30 nm and a few microns in length were synthesized using CVD, the method is explained in [33] elaborately. Epoxy resin and its hardener (EPIKOTE Resin MGD® RIMR 135 and EPIKURE Curing Agent MGS® RIMH 1366), glass fabric, a twill woven 2/2 type, having an areal weight 163 g/m^2, was used for the composite panel preparation. The functionalized carbon nanotubes (FCNTs) were dispersed in epoxy using a sonicator (concentrations ranging from 0.05 to 0.4 wt%, Table 2.1), and later, the solution of FCNTs/epoxy was subjected to ultrasonication and hence obtaining a pre-dispersed solution of the same. The same was later dissolved with hardener according to the ratio: 3-part FCNTs/epoxy and 1-part hardener using a mechanical stirrer.

Later, the preparation of composites was initiated by cutting the glass fabric in size of 270 x 320 mm. The solution prepared earlier was later reinforced with four layers of the cut glass by the vacuum assisted resin transfer method. A neat batch without any FCNTs was prepared for the sake of comparison, and the average thickness of the samples were kept constant at 1±0.05 mm. Initial post curing was carried out by using an infrared lamp at 80 ℃ for 8 hours. Later, the panels were cured in an oven at 80–100 ℃ for 6 hours. Subsequently, the specimens were cut down to dimensions of 25 x 270 mm for tensile tests as per ISO 527-2 and for impact assessment with specimens bearing a dimension of 80 x 80 mm.

Table 2.1. Fibreglass/epoxy laminate nanocomposite panel codes

Sample Code	FGCE0	FGCE1	FGCE2	FGCE3	FGCE4	FGCE05	FGCE6	FGCE7	FGCE8
CNTs (wt.%)	0	0.05	0.15	0.20	0.25	0.30	0.35	0.40	0.45
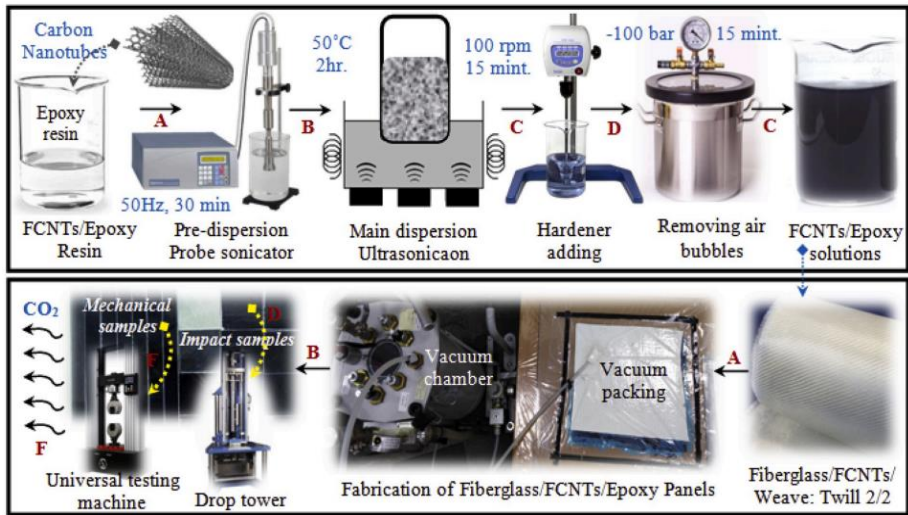
Fig. 2.1. The nano composite panel preparation and characterisation flowchart

In line with the aim of producing composites that are more sustainable, the environmental performance in terms of Greenhouse Gas emission (GHGE) factor of the fabricated panels were evaluated for their potential application in the automotive sector. GHGE factor was calculated based on the approach developed by Turner et al. (2015) and according to ISO-14040 [80, 33]. As per this model, each material has an equivalent CO_2 value that could be decreased by cutting down either their mass or size or density [14, 62]. Thus, the reduction of a vehicular mass by 100 kg saves about 0.7 l fuel for each 100 km leading to decreased CO_2 emissions by 1800 kgCO2-eq/ton [63]. This model was accounted for the current situation where FCNTs were added into the resin material, and hence, this model was reworked to suit the current scenario. More details of this model can be found in the article: after working out the model, a relation on mass reduction (m_R), fuel reduction (F_R) and GHGE factor was calculated.

The characterisation was carried out using Scanning Electron Microscope (SEM) (the equipment was from Carl Zeiss AG), which was used to check the dispersion and morphology of the fabricated panels. Different resolutions were adopted ranging from 100 μm to as low as 3 μm; these resolutions were adopted to

check the fracture, especially those suffered by fibre and check adhesion between fibre and resin. Mechanical tensile properties (5 specimens from each batch) were measured by a Lloyd Universal Testing Machine (model LR10K) connected to a high-resolution camera; the machine had a maximum load capacity of 25 kN. The loading rate was kept constant at 5 mm/min as per ISO standards. The test was carried out until final failure, at which the maximum strength was captured by dividing the maximum load by the cross sectional area of the specimen. The modulus of elasticity or tensile modulus was captured from the slope along the elastic region of the load curve expressed in MPa.

The impact test was conducted on a Coesfeld Magnus 1000 high-speed drop tower with cylindrical steel impactor with 20 mm in diameter and hemispherical end with a mass of 5.129 kg. The entire construct of the equipment was as per ISO 6603-2, and the tests were conducted at a constant impact energy of 50 J at room temperature and at a drop speed of 4 m/s. The test equipment can reach a maximum speed of 50 m/s; thus, its speed range lies within the intermediate range. The specimen was held in position by the pneumatically actuated holder, thus ensuring that the specimen does not slip away due to the speed of impact. The load displacement curve is measured by the system along with the energy, which is the integration of the area underneath the load curve.

The numerical model (Fig. 2.2) to study the evolution of impact event of the specimen with 0.35 wt% of FCNTs is accessed using the commercial solver LS DYNA. The composite plies were modelled by using 4 node shell formulation, while the mesh size was kept constant at 1 mm (dimensions of specimens were kept similar to the one adopted during experimentations, i.e., 80 x 80 mm). Normally, thin composite structures are modelled by using the shell elements against solid elements. Using this approach, composite lay-up is defined by integration points for each of the ply, which has a thickness and ply orientation defined [59]. These definitions can be set in the "Part_Composite" card on LS DYNA keyword manager. The fibre orientations can be set there, which has a direct correlation to the simulation results as the composites structural performance is a direct outcome of the fibre orientations and its interaction with the resin. The specimens were constrained in all degrees of freedom mimicking the experimental reality. The impact was modelled as a rigid body, falling with a speed of 4 m/s and having a mass of 5.129 kg. The interaction between the rigid body impactor and composite laminates are modelled using "Contact_Automatic_Nodes_To_Surface", where the nodes on the impactor are selected as the master segment, and the composite surface is selected as the slave segment. A mass of 5.129 kg is assigned to the impactor in the "Element" section that is available within the library. The composite failure was analysed by using the Chang–Chang failure criterion [64]. The model takes 21 parameters that should be defined, 15 of which are physically based and 6 are numerical parameters. Among the 15 physical parameters, 10 are material constants, and the remaining 5 are tensile and compressive failure strains in the fibre directions, matrix and shear failure strains. The 6 numerical parameters were set at their default values. Among the ten material constants, in-plane Young's modulus (E_x) and in-plane strength (σ_x) were determined

30

from the experiments as elaborated in the previous paragraph. Thus, based on the experimental results, the Ex and σx were input as 8.76 GPa and 249 MPa, respectively. The rest of the material constants were adopted from Table 5.2 in chapter 5.
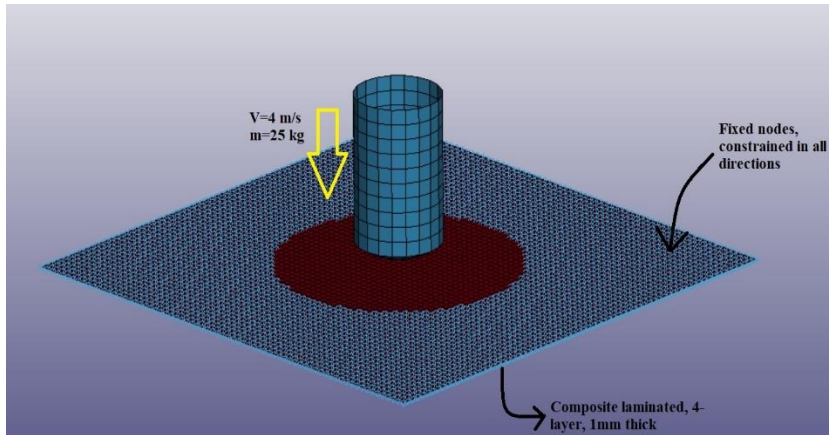
Fig. 2.2. Numerical model as modelled on LS DYNA

2.2. Results and discussions

The dispersion (Fig. 2.3) of the FCNTs was first examined using SEM on the neat sample, sample with 0.35 wt% and 0.4 wt%, respectively. It was observed that at higher resolutions of 3 μm, the features of FCNTs start appearing as forms of very fine particles distributed uniformly inside the panel with strong crosslinking. The cross section of the composite was examined; the fine distribution of resin was observed along the cross section with good adhesion that was observed. The fracture surface was seen to have lot debris, especially those with 0.35 wt% and 0.4 wt% of FCNTs in the samples. This could be attributed to the branching out of cracks and its obstruction by the CNTs and hence strengthening the matrix in the process. It has been observed that higher concentrations lead to agglomeration and hence make the composites more brittle and create more debris during failure as the structure is becoming more brittle.
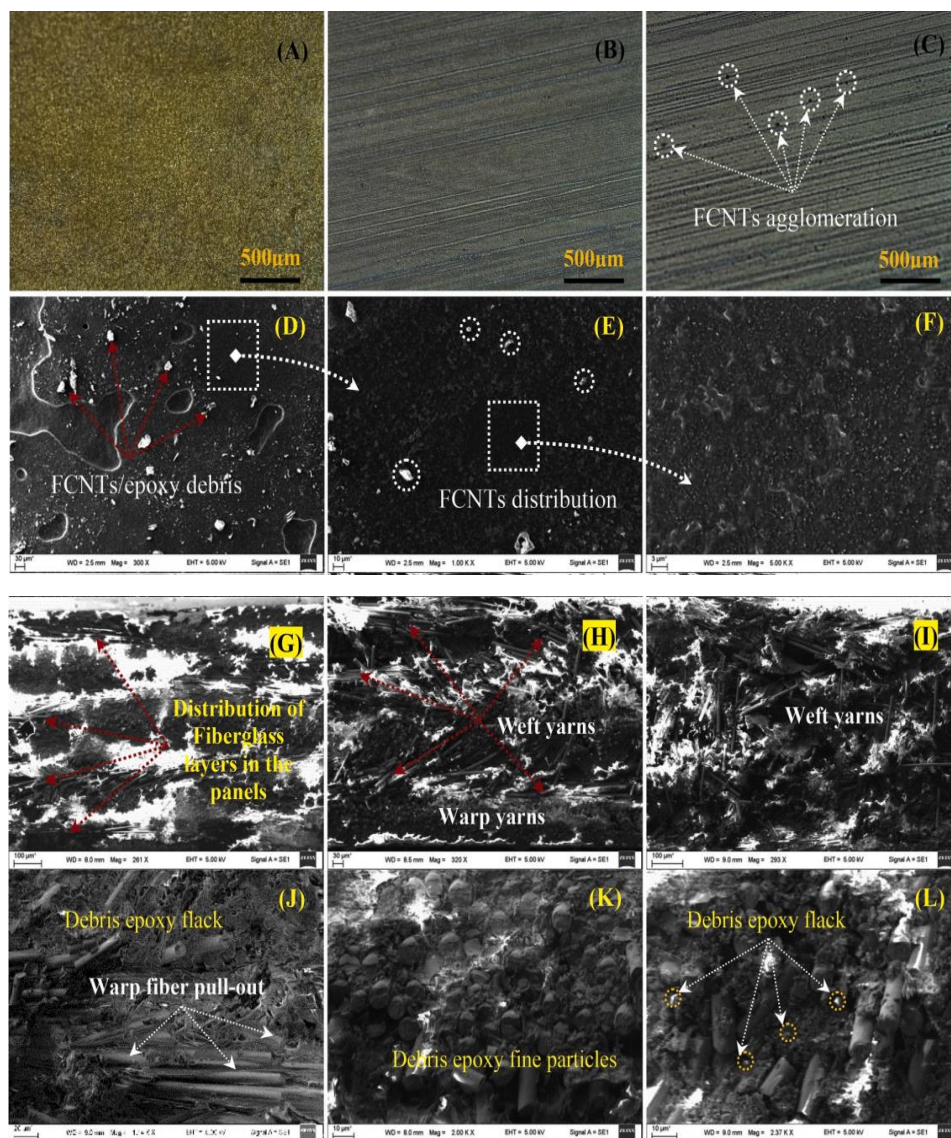
Fig. 2.3. (A–C) Surface morphology of FGCE0, FGCE6 and FGCE7; (D–F) FCNT dispersions in FGCE6 at 30 μm, 10 μm and 3 μm; (G–I) gold coated cross section of FGCE6 to examine fibreglass distribution; (J–L) fracture morphology in FGCE6

The **mechanical characterisation** led to interesting outcomes: there was observed no increase in the strain when loaded under tension, but significant increase in strength and modulus were observed (Fig. 2.4 a). Initially, an increase of ~7% and ~6% (compared to the neat sample) in strength and modulus was observed with the addition of 0.05 wt% of FCNTs, while it increased to 30% and 31%, respectively, with an increase of 0.35 wt%. Any concentrations above 0.35 wt% reduced the

strength and modulus considerably due to the agglomeration. The observed concentration of 0.35 wt% to obtain an increase in strength and modulus was lesser than those reported in literature, which reported an increase only after 0.75 wt% [46–48, 38, 65–66]. It can be concluded that even though the thickness reinforcements with FCNTs are promising, but the process to obtain a uniform distribution on a large scale can be not feasible and hence remains a drawback.

The **impact response** of the panels is seen in Fig. 2.4 b. As it is evident from the impact load characteristics, a steady rise in load was seen in all samples before reaching the maximum load. After reaching the maximum load, the failure is abrupt and then again rises sharply to reach a maximum lesser than the previous, and then the load drops steadily. The first peak corresponds to the maximum impact load that the specimens take, and the second peak represents the fracture impact load. As it is evident from the figure, the addition of FCNTs does improve the impact performance significantly. A 0.35 wt% addition of FCNTs increased the impact load from 2.13 kN to 2.80 kN, which is a ~31% increase. This could be attributed to the thickness reinforcement, which was evident from the SEM observations elaborated above, as these reinforcements create the bridging to crack front and hence strengthen the matrix. However, a wt% more than this creates agglomeration, and the intended effect is not seen. The improvement can be attributed as well to the functionalization of the nanotubes, which creates good bonding between the nanotube surface and epoxy [38, 67].

(a) (b)

(c)
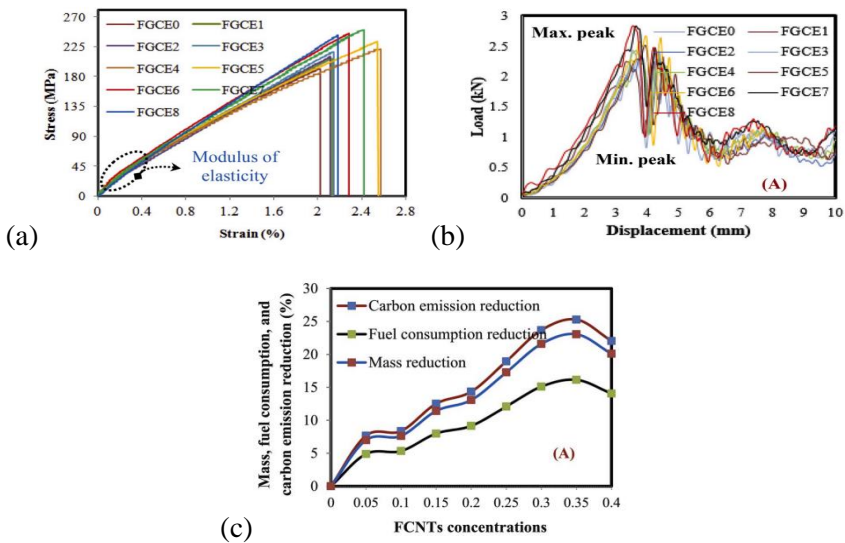
Fig. 2.4. (a) Load displacement curve for all specimen types under tension, (b) load displacement curve for all specimen types under impact loading and (c) FCNTs effect on the mass, fuel and CO2 reduction

The effect of FCNTs on the mass, fuel consumptions and carbon emission reductions obtained from the fabricated panels based on the improved resultant strength and density are shown in Fig. 2.4 c. The three parameters were affected by

the addition of CNTs, for instance, the addition of 0.05 wt% decreased the mass by ~7%, and hence, there was a reduction in fuel consumption and CO_2 by 4.9% and 7.7%, respectively. Similarly, an increase in CNT concentration to 0.35 wt% decreased the mass by ~23%, which caused a significant reduction in the fuel consumption and CO_2 by 16.1% and 25.3%, respectively. However, an increment in the concentration of CNT beyond 0.35 wt% did not show any significant mass reduction, which could be attributed to the agglomeration and hence a comparative reduction in composite strength. Thus, based on these insights, the application of these panels in the structure of vehicles can lead to a decrease in CO_2 emission by -9581 kg CO_2-eq/t and decrease the energy consumption by 16.1%.

Lastly, based on the numerical simulations, a close alignment was seen with respect to the load displacement curve, as seen from the experiments for FCNTs with 0.35 wt%. As seen in the figure below (Fig. 2.5), the model could correctly predict the failure, as seen from the experiments. From the first figure, the model correctly predicts the load in the elastic region of the modelling. The first drop followed by the second eventual drop is not seen in the numerical model. This could be attributed to the non-modelling of the contact between layers, which could model the delamination. This modelling was avoided because delamination was not seen in the experiments as seen below. The distribution of shear stress (seen as red) that is seen in the figure (Fig. 2.5 b) can be seen as partial crack formation in the specimen subjected to the impact (Fig. 2.5 c). Thus, the numerical model that has been developed could easily predict the impact behaviour of composite laminate being subjected to impact. This model can be calibrated according to the experimental conditions to study the impact and determine the effect of various material properties, such as in-plane modulus, shear etc., on the evolution of impact induced damage.
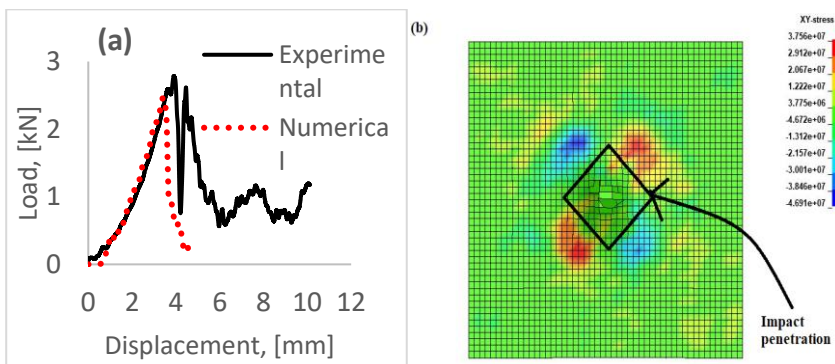
Fig. 2.5. Impact performance assessment from the numerical mode: (a) load displacement curve, (b) shear stress distribution from the model, (c) failure profile during the experimental impact

2.3. Conclusions

This article presents the effect of "through the thickness" reinforcement using functionalised carbon nanotubes (FCNTs), which effectively increased the mechanical, impact strengths along with the sustainability of the fabricated nanocomposite when used in vehicular structures. The FCNTs were dispersed uniformly in the epoxy, which latter was reinforced with glass fibres by vacuum-assisted resin transfer method. The mechanical characterisation showed an increase in mechanical strength by 30%, while the impact strength increased by 31% with an increment of FCNTs by 0.35 wt%. These could be attributed to the nano reinforcements by the FCNTs, which made the panels brittle as well. From the effect on the environment, the greenhouse gas emission (GHGE) was evaluated based on a model that was developed earlier, and according to this model, the panel with 0.35 wt% was seen to reduce fuel consumption and greenhouse gas emission by 16% and 26%, respectively. Thus, based on these assessments, the fabricated fibreglass/epoxy nanocomposites could be grouped as environmentally sustainable material with a good potential to be adopted in the auto industry. Lastly, the numerical model that was developed could predict the load displacement as seen during experimentations; thus, the same model could be recalibrated and used for other sub-chapters of the thesis. A detailed parametric study of the model to predict flexure is carried out in chapter 5.

3. HIGH IMPACT RESISTANCE OF FIBREGLASS REINFORCED COMPOSITES WITH FUNCTIONALIZED GRAPHENE, AN EXPERIMENTAL AND NUMERICAL STUDY

This chapter is a review of the article titled "Superhydrophilic functionalized graphene/fibreglass/epoxy laminates with high mechanical, impact and thermal performance and treated by plasma" [34] that has been published in the journal *Polymer Testing* and is available online since June 24, 2020. The aim was to ascertain the influence of nano reinforcements (graphene) on mechanical and impact characterisations. The second author as well as the corresponding author is the writer of this dissertation, and the contribution was in the form of formal analysis, investigation in the form of panel fabrications and experimentations, formulating the methodology and writing the original draft. This article falls in the first category with the emphasis on nano reinforcements and study of the impact resistance, as explained in the previous chapter.

3.1. Experimental materials, composite fabrication and material characterisation

Epoxy, hardener and fabrics used in this article were the same as the one used in the previous article and hence will not be elaborated. Graphene (GA) that is used in this work was synthesised using multi-roll milling and low-temperature expandable graphite as a raw material [14]. The process of obtaining graphenes that are functionalised are mentioned in [62, 68–69], and the same method was adopted in this research. The dispersion of FGA followed next in the fabrication process, wherein to obtain a uniform dispersion of FGA in epoxy and avoid agglomeration, FGA concentrations of 0.05, 0.1, 0.15, 0.2, 0.25, 0.3, 0.35, 0.4 wt% (relative to epoxy, Table 3.1) was dispersed in acetone under the effect of sound wave for 1 h at 50 kHz [34]. The dispersion and composite panel preparation was similar to the technique that was elaborated in the previous article.

The characterizations were done firstly by using scanning electron microscope (SEM) to observe the GA dispersions, while optical microscope (Hirox digital microscope KH 8700) was used to investigate the impact damage mechanism. The mechanical characterisation was carried out using a Lloyd Testing Machine (model LR10K) connected to a high-resolution camera to study the actual deformation. Coesfeld Magnus 1000 High-speed drop tower with a cylindrical steel impactor with 20 mm in diameter and hemispherical end with a mass of 5.129 kg was used to access the impact performance of the composite laminates. In fact, 5 specimens were tested from each to arrive at a conclusive result.

A numerical model was implemented on LS DYNA, similar to the methodology elaborated in chapter 2 (sub-chapter 2.1). FGCE6 was adopted for this study, as it showed the best impact performance, and hence, a model that could help further ascertain the effect of impact need to be established. Among the ten material constants, in-plane Young's modulus (Ex) and in-plane strength (σx) were determined from the experiments. Thus, based on the experimental results, the Ex and σx were

input as 8.59 GPa and 226 MPa, respectively. The rest of the material constants were adapted from Table 5.2 are elaborated in chapter 5.

Table 3.1. Sample codes of the fabricated FGEC laminates

Sample codes	FGGE0	FGGE1	FGGE2	FGGE3	FGGE4	FGGE5	FGGE6	FGGE7
FGA (wt.%)	0	0.05	0.15	0.20	0.25	0.30	0.35	0.40

3.2. Results and discussions

The dispersion of FGA (Fig. 3.1) was analysed on FGGE0, FGGE1, FGGE6 and FGGE7, using SEM ranging from resolution of 3–30 μm. With regards to FGGE0 and FGGE1, there was no significant change in the micro-structure, as the previous one was a neat sample, and the latter was with the lowest concertation of FGA within the architecture. The fibres in both cases had less adherence of epoxy, which was evident from clean fibre surface, its poor impact performance and unsatisfactory tensile strength. The debris that has been observed was a mix of flakes and small particles, which in the case of FGGE6, coalesced to bulk particles, which implies transformation in the failure mechanism. In conjunction with this observation, the adhesion was intact with the matrix and fabric, thus obtaining reinforcements at the nano scale, which in turn improved the impact resistance of these samples. FGGE6 was seen to have the optimum FGA, and any concentrations above 0.35 wt% were seen to aggravate agglomeration, which drastically affected the mechanical properties.
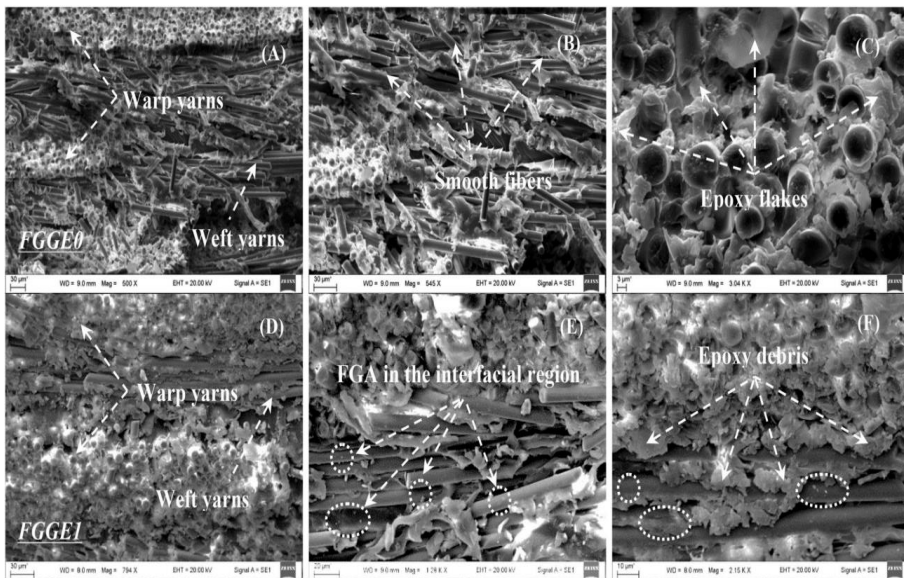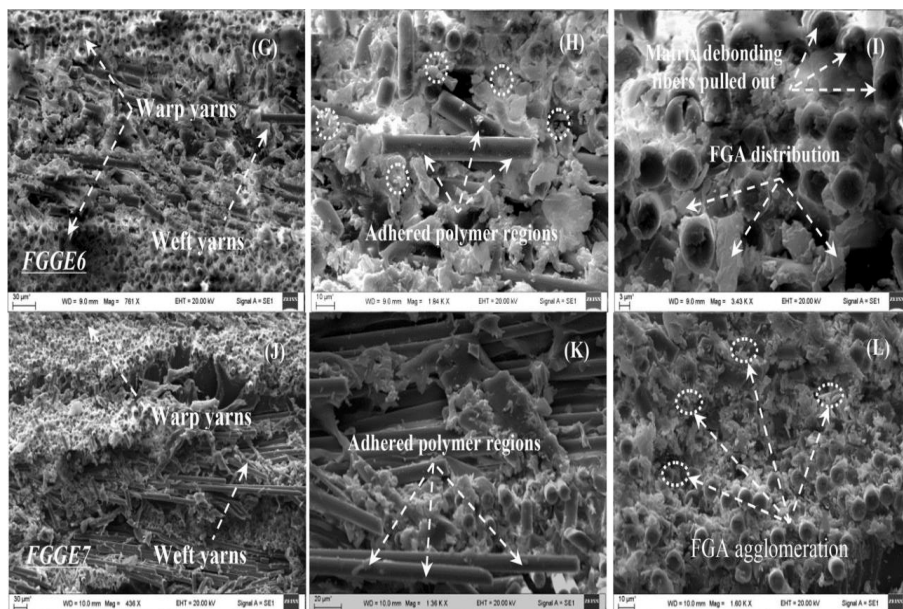
Fig. 3.1. SEM micrographs of FGCE samples

All the samples were subjected to tension (Fig. 3.2 a), and two transformations in terms of strain and strength were observed. FGGE0, FGGE1, FGGE2, FGGE5 and FGGE7 showed no noticeable to insignificant improvement in strengths. In the case of FGGE7, due to the agglomerations, the strength and strain were lower than that of all the samples that studied, even lesser than FGGE0. Three samples stood out in their performance: FGGE3, FGGE4 and FGGE6. The strength increased by 18% when compared to FGGE0 in the case of FGGE6; the strain increased by 16%. This was again true in the case of FGGE3, which exhibited similar increase in strain, but the strength that was observed was modest. FGGE4 showed 14% increment in strength, while at the same time exhibited 23% increment in strain, implying a tougher specimen. This could imply a higher amount of energy being spent on damage mechanisms; thus, the energy that is spent is higher due to the improved adhesion between matrix and fabrics. Therefore, from these observations in conjunction with SEM analysis, it can be conclusively said that "through the thickness" reinforcements by nano-fillers help to improve the toughness and strength of composites.

38

(c)
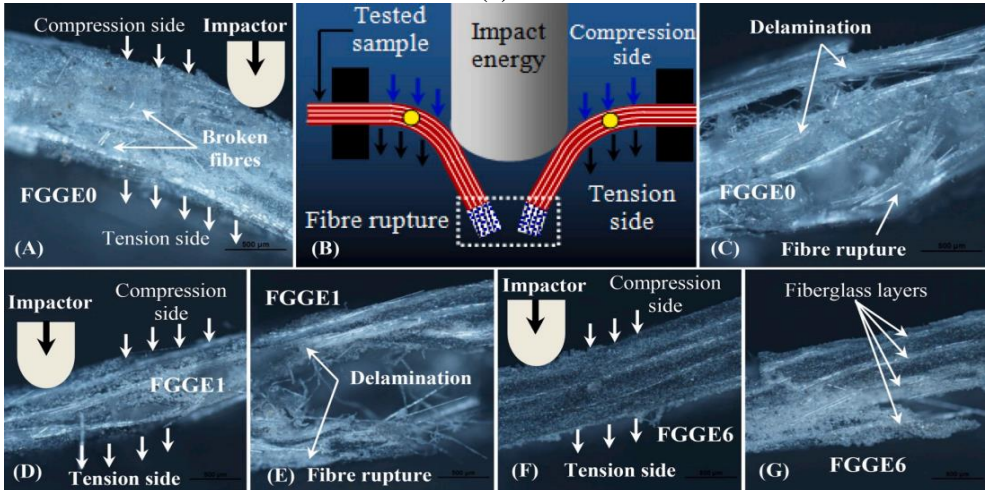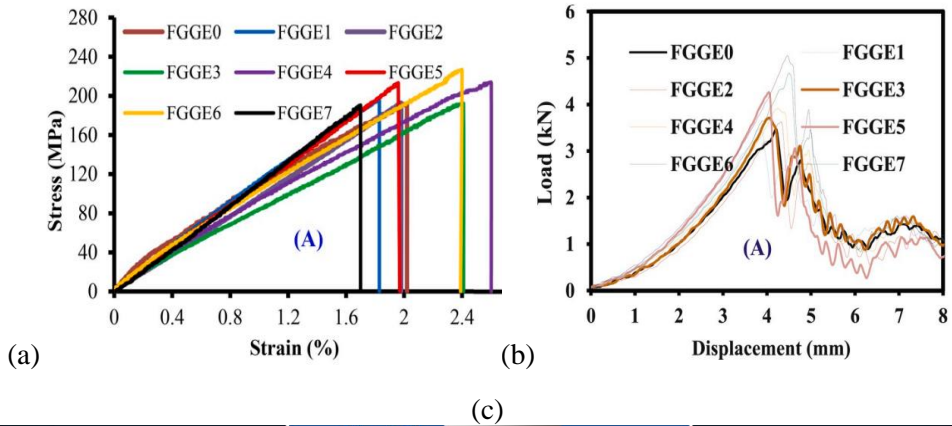
Fig. 3.2. (a) Stress-strain of all the samples subjected to tension, (b) load displacement of all the samples subjected to low velocity impact loading, (c) fractographic analysis of specimens

The impact characterisation showed the best effect in terms of FGA dispersion and "through the thickness" reinforcements. While FGGE0 showed the least impact load of 2.81 kN, FGGE6 with 0.35 wt% exhibited the highest load bearing capacity at 4.78 kN, which is 70% increase. This could be attributed to the toughening effect that is seen through SEM observations in the form of improved adhesion and hence larger debris particles post impact. In order to validate this theory further, the investigations were carried out under optical microscope to check the damage mechanism, and the images are presented in Fig. 3.2 c. The delaminations were observed in samples with no to less concentrations of FGA, while the delaminations were negligent in the case of samples with higher concentrations (FGGE6 in Fig. 3.2 c). Corroborating this with SEM observations, a clear trend with adhesion, is the reason attributed to this, which is positively contributing to the toughening of matrix and hence improving the impact resistance of samples.

Based on the methodology elaborated in chapter 2, a model to predict the impact performance as seen experimentally was established. The brittle nature of failure of FGGE6 was evident from the numerical modelling, as it could be seen in Figure 3.3 a. The numerical model could predict the response quite accurately, and this could be attributed to the failure strains involved while modelling. During numerical studies, it was seen that DFAILT, DFAILM and DFAILC, which are failure strains in the fibre direction and transverse directions, respectively, were seen to influence the outcome to a large extent. A detailed parametric study was carried out and is elaborated in chapter 5 where flexure was studied, which is seen in the form of global [61] bending while under impact loading. Comparing Fig. 3.3 b, c, the diamond/rhombus shaped failure was seen in numerical model and real time experiments, while in the numerical model, the shear stress concentration was seen along the diagonal of the diamond (rhombus).
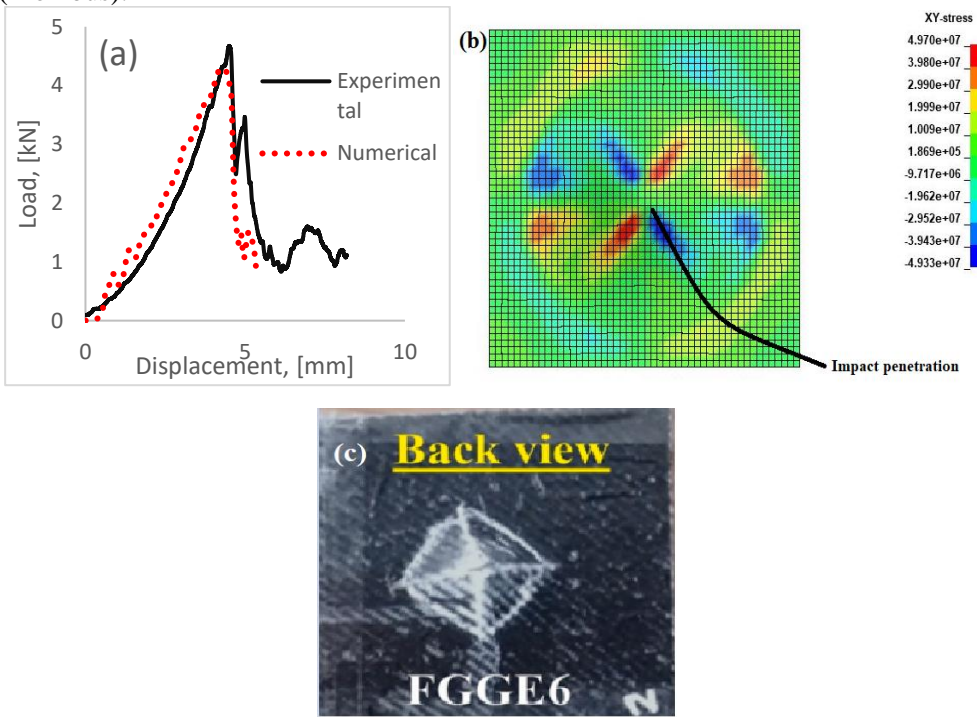
Fig. 3.3. Impact performance assessment from the numerical mode: (a) load displacement curve, (b) shear stress distribution from the model, (c) failure profile during experimental impact

3.3. Conclusions

This article covered another aspect of nano reinforcements using functionalised graphene (FGA). The dispersion of GA within the matrix was checked to see if it is in uniformity, in distribution, and it was observed that higher concentrations

transformed the interaction between matrix and fabric, wherein good adhesion was observed between the two. This adhesion improved the mechanical strength and toughness to significantly higher levels, which in turn lent itself to higher impact performances. The numerical model could predict the impact performance as close as it could be seen in the experiments. The shear stress distribution matches with the diamond shaped failure that is seen in the experiments, even though the loading curve could capture the elastic region closely, the reached maximum load was 2–5% lesser.

Thus, these two articles attempted to highlight the importance of nano-fillers, reinforcing the matrix at nanoscale, and hence, improving the impact resistance in addition to improving other mechanical aspects, such as strength, modulus and strain. Even though it was observed that the impact performance improved significantly with the addition of nanofillers, the process of incorporating them is an additional process, which increases involved manufacturing costs. In addition to this, the precise level of na no-fillers that was required could hinder the reliability of structures, made from such composites, as there is a wide variety of concentrations available in the literature that have improved the mechanical characteristics. Even though in this study it was confirmed that 0.35 wt% of FNCTs/FGAs were sufficient to improve the mechanical performance, this concentration never remains fixed, as there is a wide variety of the same nanofillers that are available, but have different functionalisations. Thus, in order to make the manufacturing easier and cost-effective and make more sustainable composites, the second part of this thesis deals with a new resin, hybridizations, ductility in brittle composites and the issue of recyclability of these materials. It as well deals with the mechanics and numerical modelling to limit the extensive experimentations involved in understanding these engineering materials.

4. AN EXPERIMENTAL STUDY TO CONTROL BRITTLENESS IN COMPOSITES

This chapter is a review of two articles that are both exploring an alternative resin-polymethyl methacrylate (PMMA). The first article is a review of the efficacy of using PMMA and its ability to lend itself to be recycled efficiently; thus, it was adopted as an alternative resin for the second article. The second article deals with epoxy and PMMA in the context of hybrid architecture, built specifically to control brittleness associated with composites. It explores the novel idea of introducing ductility into composites through a hybrid architecture, and hence, making the failure predictable. The first article titled "Sustainability of polymer composites and its critical role in revolutionising wind power for green future" [36] has been published in the journal *Sustainable Technologies for Green Future* and is available online since May 6, 2021. There are two authors, and the first author of the article is the author of this dissertation, and the contribution is equally shared between the two authors. Sub-chapters from 4.1 to 4.3 are attributed to this article. The second article [35] has been published in the journal *Polymer Testing* and is available online since June 30, 2020. There are three authors, and the first author is the defendant of this dissertation, who contributed to the formal analysis, investigation, methodology, writing of the original draft. Sub-chapters from 4.4 to 4.6 are attributed to this article titled "Low velocity impact and pseudo-ductile behaviour of carbon/glass/epoxy and carbon/glass/PMMA hybrid composite laminates for aircraft application at service temperature".

4.1. An alternative resin for fabricating a recyclable and sustainable composite architecture

As it could be seen in the previous two chapters, the composites are fabricated by reinforcing thermoset resins, such as epoxy with fabrics, such as glass, carbon, etc. There are several drawbacks associated with thermosets, some of them are associated with its inability to be remoulded and hence rendering them non-recyclable. Thus, there arises a necessity to investigate the reliability of the other resin type, namely, thermoplastic vis-à-vis thermosets. Hence, in this context, a review of PMMA was carried out, the aim being to highlight its structural reliability when being reinforced with fabrics and its ability to lend itself to be remoulded and recycled. In the next sub-chapter, a brief overview of different methods to recycle epoxy-based composites are elaborated, and in the subsequent sub-chapters, two case studies, pertaining to structural reliability and recycling of PMMA based composites, are elaborated. The two case studies where within the context of wind turbine industry, since decommissioning of old wind turbine blades with composites poses a challenge in terms of their disposability.

4.2. Current techniques to recycle polymer composites

There are three methods available to recycle composites, and they could be broadly classified as mechanical, thermal and chemical recycling [70, 71]. Mechanical recycling involves the use of crushed composites as raw materials for secondary raw

materials. This process is further classed into two sub-processes: the first process is to break up the waste into fine powder, and in the second process, to shred/crush the waste, and hence, the recycled material would go as fillers/reinforcements into cements/concrete. This method is simple and economical, but the final product that has been obtained is of low value, because of the fibre being damaged during the process and its inability to deliver longer fibres [72].

Thermal recycling falls under three broad categories, namely, pyrolysis, fluidised bed recycling process and microwave pyrolysis. The first method involves fibre recovery through the decomposition of resin into organic small molecules using inert gas [73]. The second method uses air as a fluidising gas in a fluidised bed reactor to decompose the matrix through high temperature air heat flow; thus, the generated heat recycles the fibre material [74]. The last method decomposes the resin in the composite material by microwave radiation in a microwave cavity [75].

Chemical recycling is the use of chemicals to chemically modify or decompose to make waste materials into recyclable materials. Supercritical fluid method and solvolysis are the two major methods that fall within the chemical recycling method. The first method refers to a state, in which the temperature and pressure of the fluid exceed its critical temperature and pressure, and at this stage, the fluid can decompose polymer waste wherein water or alcohol are used as the decomposition of medium [76]. The second method, i.e., solvolysis involves depolymerisation of the polymer using the chemical properties of the solvent under heating conditions [77].

4.3. Case studies examining the feasibility of recycling PMMA based composites

Recycling thermosets are limited by its commercial exploitability/viability on a large scale, since the margins on which they operate are small. Thermoplastic, such as PMMA, can limit the extent of downcycling that thermosets might require [78]. In the wind turbine industry, 40% of the costs are associated with labour, and this is related to the cycle time [79]. The cycle time is associated with the polymerisation process, which in the case of thermosets, are longer when compared to thermoplastics. The latter can polymerise at room temperature, thus avoiding tooling for heating, such as ovens for post cure [80]. In addition to room temperature polymerisation, thermoplastics can be reformed by the application of heat enabling maintenance by not degrading the material properties [30]. Based on these advantages associated with thermoplastics, two case studies were performed to understand the structural reliability and recyclability of Elium (based composites) an acrylic resin, which is composed of 2-Propeonic acid, methyl methacrylate monomer (MMA) and acrylic copolymers, in which the MMA undergoes a free radical polymerisation to its respective polymer, i.e., PMMA [35].

Case study 1: R.E. Murray et al. (2021) from the National Wind Technology Centre (NWTC) fabricated a wind turbine blade using Elium, wherein the structural health of this blade was compared with an epoxy-based blade fabricated by TPI composites. As it has been mentioned earlier, there is no requirement for heating equipment, since the resin can polymerise at room temperature, and hence, the manufacturing costs are reduced significantly. The thermoplastic blade had 3–11% more displacement under static load, which was attributed to the fibreglass weight and

adhesives that were used, even though the thermoplastic blade was more flexible than its epoxy counterpart. Meanwhile, fatigue test on both blades revealed less than 0.5% variation in stiffness over a million cycles of loading with no large-scale noticeable degradation in structural or material properties. The study further revealed that the natural frequencies were within 2.5% in both flatwise and edgewise directions, and the structural damping was 5 to 7 times higher in the case of thermoplastic blade. With these observations, which is on par with blade fabricated from epoxy-based composites, Elium being a PMMA based thermoplastic could serve as an ideal replacement within the wind turbine sector [44].

Case study 2: the investigation was carried out by D.S. Cousins et al. (2019) [81], which highlights the feasibility of using Elium, because it can facilitate the recycling of wind turbine parts on a larger scale. Four recycling techniques were implemented thermal decomposition of a polymer matrix, mechanical grinding, thermoforming and dissolution. Thermal decomposition falls within the thermal recycling method, while mechanical grinding and dissolution falls within the mechanical and chemical recycling methods, respectively. Thermoforming involves heating the composite panels above the glass transition temperature and altering the shape in a mould. Based on these four methods, the pros and cons of each of them are weighed.

Thermal decomposition that is termed as pyrolysis required less energy to decompose the polymer matrix compared to other recovery methods. Since there is a loss of high embedded energy polymer, it could be counted as a disadvantage when considering this method. Thermoplastic resins had higher recovery rate compared to the thermoset resins when subjected to dissolution technique, and the glass fabric that was recovered from this method retained its tensile strength with a reduction of only 12%. There was a significant reduction in the mechanical property when fabrics were recovered by pyrolysis. Thermoforming enabled the straightening of a spar cap, hence, demonstrating that the thermoplastics could be downcycled into other products. A feasibility study revealed that recycling thermoplastic composites into its constituent materials can replace the virgin materials within the supply chain [35]. Based on these studies, it can be stated that these methods could be upscaled when used to recycle thermoplastic based composites. Adopting these methods and materials could gradually replace thermosets and pave the way for a fully integrated industrial cycle beginning with the structure, installing the structure, recycling it and using it further.

Thus, based on a comprehensive review conducted in this article, fabricating sustainable composites with recyclable materials were adopted in the subsequent chapters. Elium with PMMA as its main constituent was seen to sustain both loads, i.e., static and dynamic, similar to that of epoxy-based composites and hence could serve as an ideal replacement in the wind turbine sector. Thus, drawing from the results of the two case studies, the composites with epoxy and PMMA need to be investigated for their impact performances, especially at higher temperatures. In order to make composites more impact resistant, there exists a need to make it tougher in terms of energy absorption while undergoing failure. A method adopted in this

research is to make composite architecture hybrid and introduce pseudo-ductility into it while undergoing failure. In order to further develop more impact resistant composites, there exists a necessity to make composites tougher by introducing hybrid architectures. More of these aspects are explored in the subsequent sub-chapters along with establishing a metallic property in an otherwise brittle composite. These aspects are explored in the next sub-chapters of this chapter.

4.4. Experimental materials, composite fabrication and material characterisation

Unidirectional carbon fabrics (areal density-120 g/m^2) and glass fabric Panda^{TM} (2/2 twill weave and weight 163 g/m^2) were sourced from R&G Faserverbunkwerkstoffe GmbH, Waldenbuch in Germany. Epoxy based on Bisphenol A and its hardener (modified cycloaoliphatic polyamine free of alkyl phenol and benzyl alcohol) were as well sourced from the same company mentioned previously, while Methyl methacrylate (MMA: 617H119-Orthocryl Resin) resin and its polymerizer (Benzoyl peroxide-BPO: Orthocryl resin 617P37, Otto Bock) were purchased from Otto Bock.

Thus, 6 set of composite panels were fabricated, each bearing the code T-1, T-2, T-3, T-4, T-5 and T-6. T-1 has four layers of carbon fabric with the fabric orientation being $[0_c/90_c/90_c/0_c]$; T-2 has four layers of glass fabric with orientation being $[0_g/0_g/0_g/0_g]$; T-3 has a hybrid architecture with four layers of glass and one layer of carbon in the middle $[0_g/0_g/0_c/0_g/0_g]$. All three architectures have epoxy as resin. T-4, T-5 and T-6 have the same architecture as T-1, T-2 and T-3, respectively, while the matrix being PMMA. The composite fabrication process was the same as the one adopted in the previous chapters, the difference in this case was attributed to the polymerisation of PMMA. The PMMA resin was prepared by mixing MMA monomer with BPO as an initiator system in the free radical polymerisation with a weight ratio of 100:2 (MMA:BPO). Post curing, the samples were cut with dimensions 80 x 80 mm, and each of the code had 5 samples assigned to them.

The impact test parameters were the same as the one adopted in the previous chapters, but the samples were subjected to the impact loading at three different temperatures: 25 ℃, 60 ℃ and 80 ℃, respectively. These temperature regimes were adopted to study the effect of hybridization at higher temperatures and characterise the damage mechanisms. The damage characterisation, hybrid effect and its quantification were achieved by implementing the energy model put forward by Naaman and Jeong (1995) and Grace et al. (1998) [82, 83]. The model is based on the energy criterion, which subsequently gave way to the index termed as ductility index (DI). The energy model developed by both Naaman and Grace takes into account the total energy (E_{total}), elastic energy ($E_{elastic}$) and failure energy ($E_{in-elastic}$) as elaborated in equations (22) and (23). E_{total} represents the area under the load displacement curve up to failure, which is the total sum of elastic and failure energies. Elastic energy is defined as the area of triangle that is formed at the failure load by the line, having the weighted average slope of two initial straight lines of the load deflection curve, as seen in Fig. 4.1. Since both methods gave accurate results, it served as a strong motivation for their calculation of ductility of several brittle materials, such as

concrete [84]. Hence, both of these methods were implemented to estimate the DI of samples that were studied in this research.

$$DI \text{ (Naaman)} = \frac{1}{2}\left(\frac{E_{total}}{E_{elastic}} + 1\right) \tag{22}$$

$$DI \text{ (Grace's)} = \frac{E_{in\text{-}elastic}}{E_{total}} \tag{23}$$
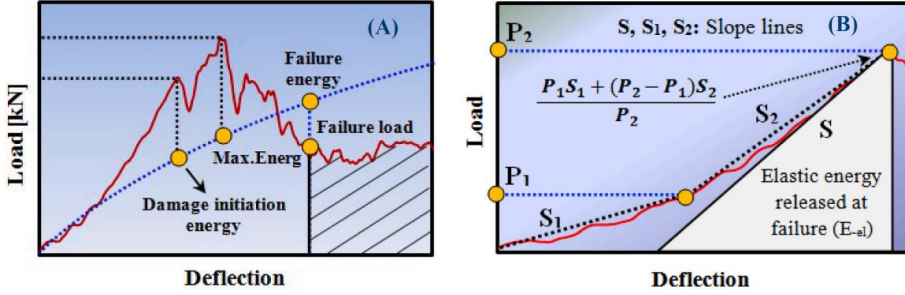
Fig. 4.1. (a) Impact characteristics and (b) evaluation of elastic energy

The numerical model is implemented to capture load displacement characteristic, as it has been done in the previous chapters. The material properties for modelling effort were taken from Table 4 that was elaborated in chapter 5. Thus, 6 separate models were implemented to capture the impact performance of T-1, T-2, T-3, T-4, T-5 and T-6 at room temperature.

4.5. Results and discussions

The load displacement characteristics of T-1, T-2, T-3 and T-4, T-5, T-6 are shown in Fig. 4.2 a, b. As it was expected, carbon composites had the least impact resistance compared to its glass counterparts. This was true with T-1 and T-4 with epoxy and PMMA as resins, respectively, while T-2 and T-5 had an impact resistance that was 6 times higher than that of carbon composites. In between these two extremes, there were the hybrids T-3 and T-6, while T-3 has similar impact strength to that of its glass counterpart T-2; T-6 has reduced the impact strength than T-5. However, both of these hybrids stood unique with respect to the load displacement curves, as it can be noticed in Figure 12. While T-2 and T-5 had a gradual increase in load without any significant drop until it reached the maximum before dropping due to the multiple failure mechanisms culmination with a rupture, T-3 and T-6 had clearly defined elastic limits followed by a limited drop and again reaching a maximum load, which eventually drops again culminating in a rupture of the composites. The addition of a carbon in the midst of glass has reduced the brittleness of glass and make it behave in a pseudo ductile nature as well as making them to fail in a predictable manner, as opposed to a catastrophic failure seen in pure glass composites. Impact resistance should not be just limited to obtaining maximum impact load, it should as well involve composites being tougher while undergoing damage. While glass does have good impact resistance, due to their brittle nature, they fail in an unpredictable manner. The
46

unpredictability is reduced to a large extent by the addition of carbon fabric in the midst of glass fabrics, ideally in the middle.
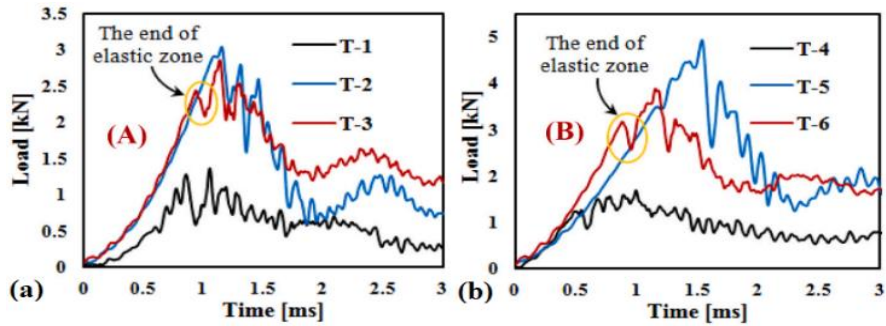
Fig. 4.2. Load time characteristic of (a) carbon, glass and hybrid with epoxy, (b) carbon, glass and hybrid with PMMA

The effect of temperature was assessed on T-1, T-2, T-3, T-4, T-5 and T-6 at room temperature, i.e., 60 ℃ and 80 ℃, respectively. As it could be seen in Fig. 4.3. a, T-1 and T-2 did stay stable while the temperature increased, and this could be attributed to the fact that epoxy tends to retain its ambient temperature characteristics up to 160 ℃ with less degradation. An interesting observation was made regarding T-2 and T-5 (both with glass reinforced in epoxy and PMMA), T-2, even though stable with increasing temperature, saw some increment in load, although insignificant. However,, T-5 saw a 50% increase in load from room temperature, as the temperature increased, and this could be attributed to the increased elastoplasticity of PMMA, as the temperature increased. Another observation could be due to the higher thermal stability compared with epoxy resin, which needs more energy to break the molecular bond of PMMA [76]. The energy absorbed by composites is expended in two ways, i.e., elastic deformation and inelastic deformation; the latter involves all the classic damage mechanisms, such as crack, delamination, debonding and fibre rupture. The maximum energy absorbed at different temperatures by all samples is seen in Fig. 4.2 b; at room temperature, the energy was absorbed through the damage mechanisms mentioned earlier, and as the temperature rose, the energy was spent in the form of elastic deformation and fibre rupture. The maximum energy that was absorbed remained constant in individual cases (constant energy absorption with temperature increase), and this was the case with all samples, except T-5, which took in more energy in the form of elastic deformation, which can be attributed to high strain glass fibres and pliability of acrylic resins [8].
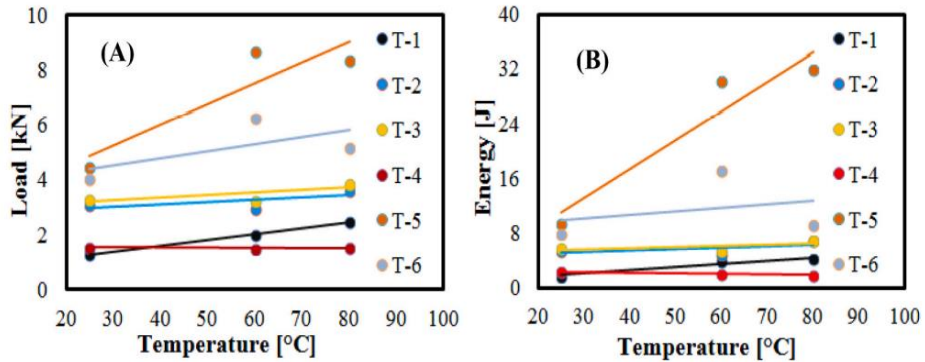
Fig. 4.3. Effect of temperatures on (a) maximum load characteristics and (b) maximum energy characteristics

The two energy components, namely, inelastic and elastic components at different temperatures, are seen in Fig. 4.4 a, b. The inelastic component, which is the major contributor to introducing ductility into composites in the form of damage initiation and propagation, remained constant throughout the temperature profile. The elastic component increased with T-5, showing the maximum; this could be attributed to T-5 being PMMA as resin. Thermoplastics are mouldable at higher temperatures; thus, there should be a natural increase inelastic energy, which contributes to increased mouldability. This observation is significant, because there exists an opportunity for thermoplastic composites lending itself to be recycled. Fig. 4.5 C, D proves that the elastic component of energy absorption was dominant, as there was no perforation. This is in contrast to Fig. 4.5 A, B, where are shown the epoxy-based composites with perforation at higher temperatures.
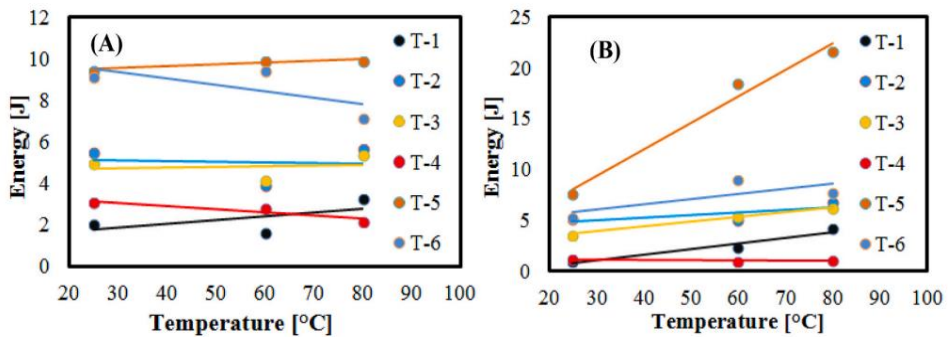
Fig. 4.4. (a) Inelastic energy temperature and (b) elastic energy temperature
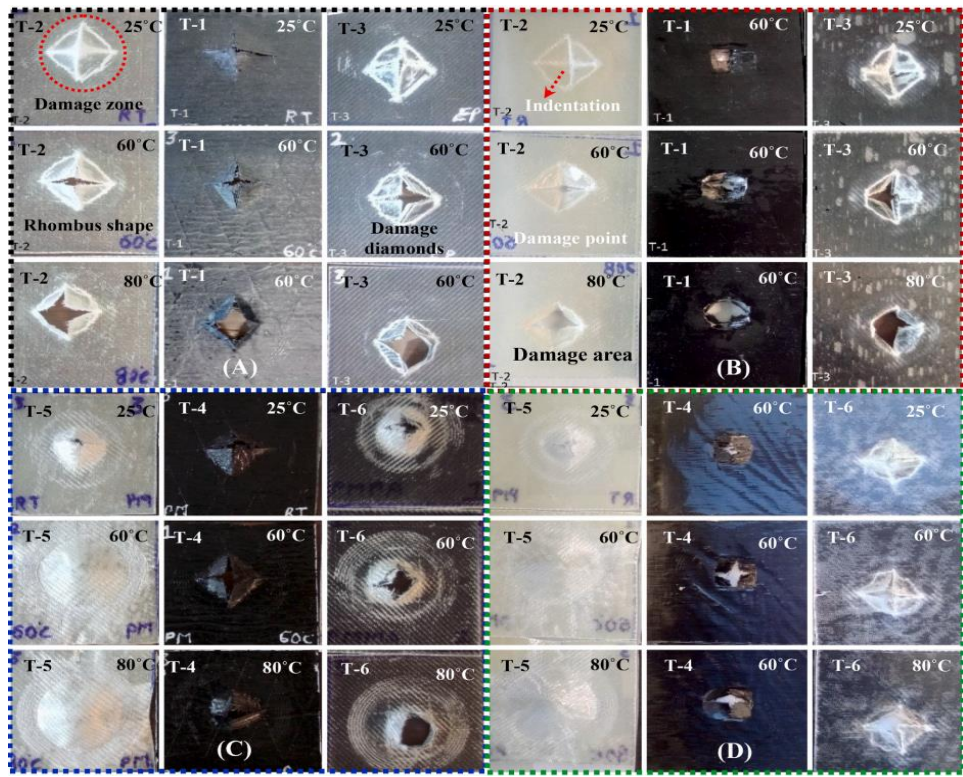
Fig. 4.5. A) Obverse and B) impact side of T-2, T-1 and T-3, C) obverse and D) impact side of T-5, T-4 and T-6

Referring to Fig. 4.5 C, D, there is an observable trend, as the temperature rose from 25 to 80 ℃. At room temperature, there is a perforation as in all of the samples (T-4, T-5 and T-6), but in the case of T-5, the perforation gradually closes to form a circular indentation at 80 ℃. If this is cross checked with the energy profile in Fig. 4.3, T-5 has a constant inelastic component throughout the three temperatures, but the elastic component shot up as temperature rose. This proves that glass with PMMA is ideal for structural applications involving higher temperatures, and the same can be recycled by just remoulding the entire structure.

From the two energy components of the total energy, i.e., the elastic and inelastic energies, the ductility index (DI) can be estimated. Based on the values obtained, the behaviour of the materials can be defined as brittle, if DI is less than 69%, ductile if greater than 75%, and semi-ductile if between 70 and 74% [83]. Thus, based on this inference, Fig. 4.6 a and 4.6 b give an estimate of DI calculated based on the methodology put forward by Naaman et al. (DI-Naaman) and Grace et al. (DI-Grace). According to both these indexes, DI decreased with increasing temperature due to the reduction in the inelastic component. DI quantifies the amount of inelastic energy taken by the composites during damage, and the index developed by Grace is more relevant in this aspect, as it is a ratio of inelastic over the total energy component that is more revealing. T-3 and T-6, which were hybrids, were exhibiting semi-

49

ductility, as both had DI at the range of 66–70%. However, this can be increased to purely ductile if the thickness of the carbon fabric was reduced and introducing them at additional positions, as this would create more bending stiffness mismatch [61] and hence positively contribute to the higher inelastic component and higher DI. T-2 and T-5, both glass-based composites, were brittle at room temperature, having DI ranging from 45 to 55%. Thus, when implementing hybrid architectures, an index based on energy could quantify the hybrid effect, which is nothing more than the quantification of the inelastic component.
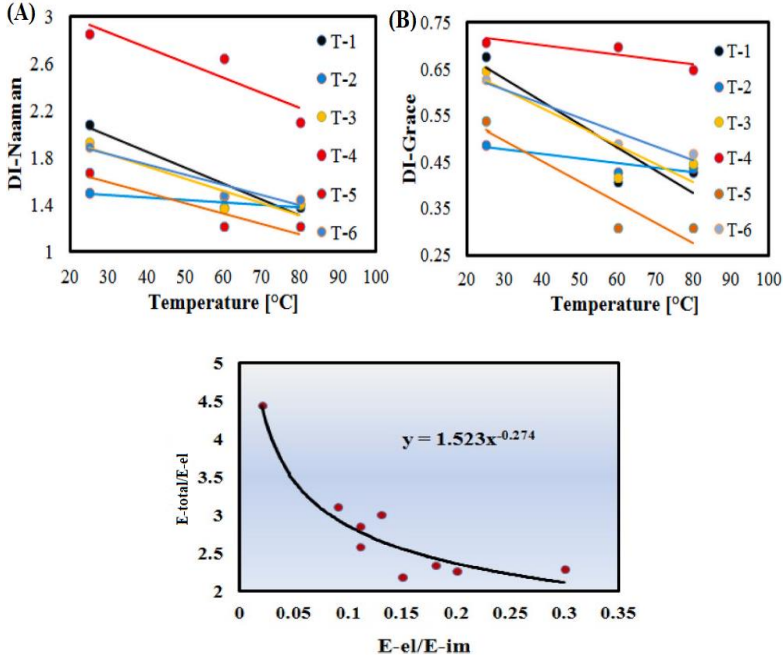
Fig. 4.6. Ductility Index (DI) with respect to temperature, (A) DI-Naaman and (B) DI-Grace, (C) normalized plot for nine specimens at room temperature

An energy-based model to predict the absorbed energies during low velocity impact empirically by Foo et al. [85] for sandwich composites was adopted in this research. The model involves plotting of normalised absorbed energy (E_{total}/E_{el}) against the inverse of the normalised impact energy ratio (E_{el}/E_{imp}) for all the samples (Fig. 4.6 C), where E_{imp} is the incident impact energy of the impact, and in the present case, it is 50 J. The power regression curve was found to be the best fit, and based on this, equation (24) links the absorbed energy to the elastic and incipient impact energy, thus giving an approximate estimate of the total absorbed energy in the form of elastic and inelastic deformations. Thus, according to this empirical relation, the absorbed energies could be estimated by just determining the elastic energies and knowing the impact energy, both of which were estimated during this research.

$$\frac{E_{total}}{E_{el}} = 1.52 * \left(\frac{E_{el}}{E_{imp}}\right)^{-0.27} \tag{24}$$

In order to further ascertain the effect of elastic and inelastic energy components, optical microscopic investigations were carried out to further study the damage mechanisms that were involved under impact. The cross section of the impact region was observed, and Fig. 4.7 shows specimens with epoxy as the resin; namely, T-1, T-2 and T-3; all the observations were carried out for specimens subjected to room temperature and at 80 ℃. Generally, it has been observed that at room temperature, all the classical failure mechanisms were observed, which could be correlated to the high DIs of these composites at room temperature. At high temperature, the DI was reduced due to an increase inelastic deformation, and hence, the appreciation of the elastic component in the DI. Higher elastic deformation is due to the deformations rather than any observable failure, arising from increased pliability with increasing temperature. These observations as well hold true in the case of specimens with PMMA (T-4, T-5 and T-6), and hence, the microscopic observations of this group are not shown.
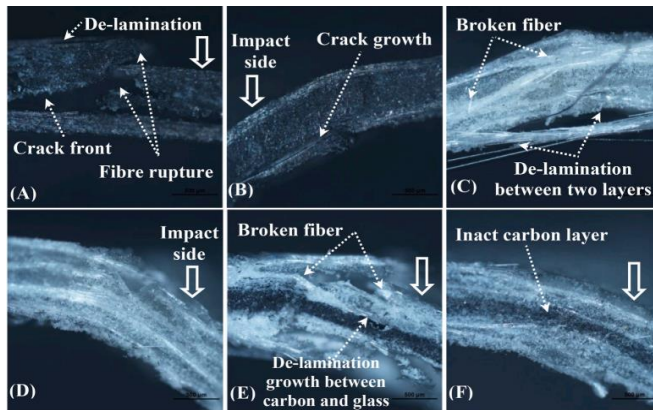
Fig. 4.7. A) and B) are T-1 at 25 ℃ and 80 ℃, respectively; at 25 ℃, unstable propagation of crack is seen especially at the interface between alternatively oriented plies, and at 80 ℃, resin is more plastic and hence more pliable; similar observations hold true

Following the implemented numerical model, Fig. 4.8 elaborates on the obtained results, which has a clear semblance to the experimental observations. The aim was to produce a model that could precisely capture the progression of impact in terms of load displacement and shape of damage that was seen during the experimentations. Thus, according to the set objective, Fig. 4.8 a, b represents the impact characterisation of T-1. While the load curve had slight variations in the elastic region, the maximum load was close to the one seen in the experiments. While the observed damage was in semblance to the one seen in Fig. 4.5 A, i.e., T-1 at 25 ℃. Since T-1 is fabricated using unidirectional carbon fabric, the diamond shaped failure is less obvious, and this has been precisely captured by the model. Fig. 4.8 c, d show the progression of damage in T-2: the diamond shaped damage is not as clearly visible in the model, but the concertation of shear stress is along the edges of the diamond as it is shown in Fig. 4.8 d. The load displacement progression was very precise to the one seen during the experiments. In the case of T-3, the load displacement slightly

51

deviated from the experimental in the elastic region; the max load was correctly captured. The damage seen again was not precisely damage shaped, but as in T-2, the shear stress concentration was along the edges of the diamond, as it could be seen in Fig. 4.8 f, showing a precursor to where the damage could occur.
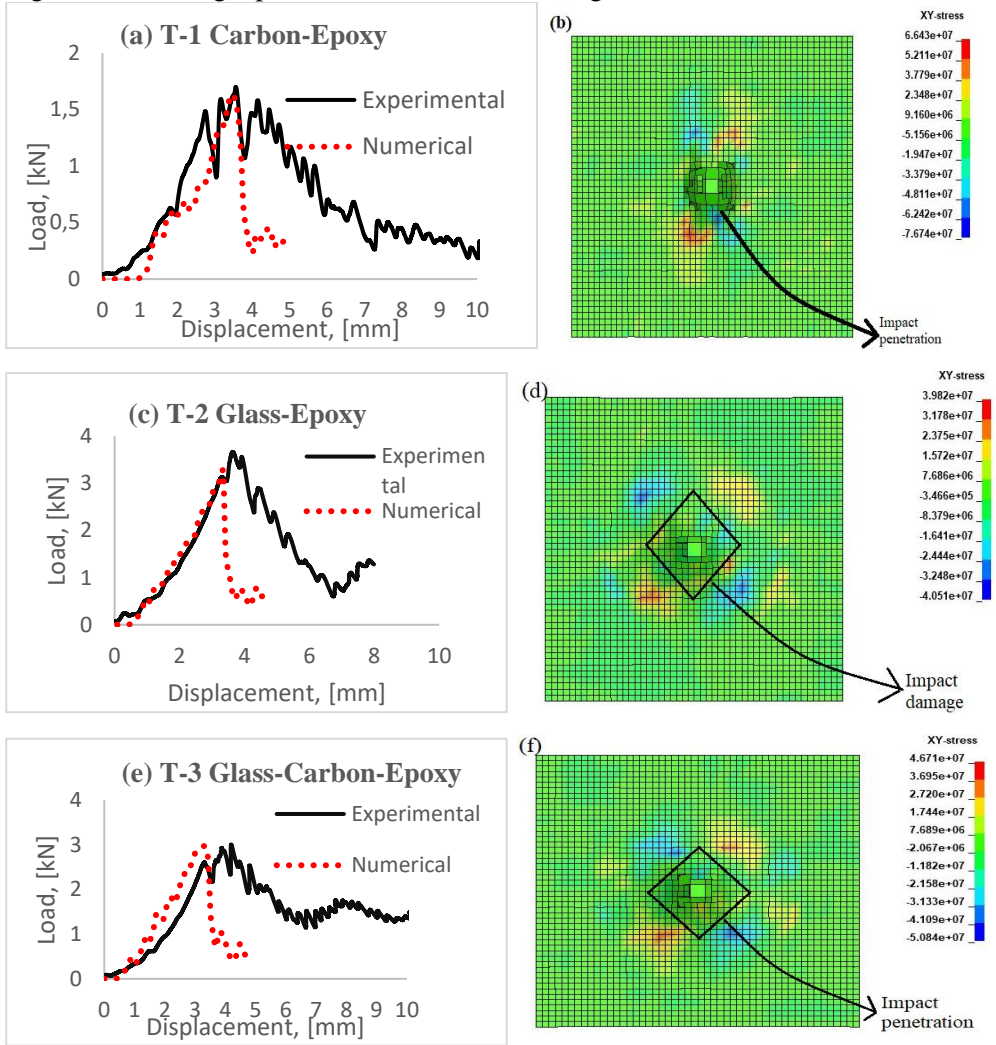
Fig. 4.8. (a) and (b) – T-1 numerical results of carbon and epoxy composite, (c) and (d) T-2 – numerical results of glass and epoxy composite and (e) and (f) – T-3 numerical results of glass carbon epoxy hybrid composite

With regards to T-4, T-5 and T-6, the numerical model studying the evolution of impact damage is seen in Fig. 4.9. Fig. 4.9 a, b shows the evolution of load and damage with respect to carbon with PMMA. The catastrophic failure seen in the numerical model is the same as it was observed during the experiments in the case of T-4 at room temperature, where the failure is seen along the fibre direction without

52

the diamond shape found in the glass based composites. The load curve that was obtained during the numerical model follows the trajectory seen during the experiments. T-5, which is glass and PMMA based composite, shows the diamond shaped fracture in the form of shear stress concentration along the contours, which would ultimately fail along those countoures. The elastic loading range and maximum load is captured closely by the model as seen in Fig. 4.9 c, d. The role of shear, which is predominantly determined by the type of used resin, is explicit in this model, a parametric study of which is carried out in the next chapter. Lastly, in the case of T-6, which is a hybrid combination of glass carbon and PMMA, the diamond shaped failure is evident again in the form of shear stress distribution as contours, along which the damage occurs in the experiments. The load curve captures the maximum load as close as the one seen in the experiments, which is evident in Fig. 4.9 e, f.
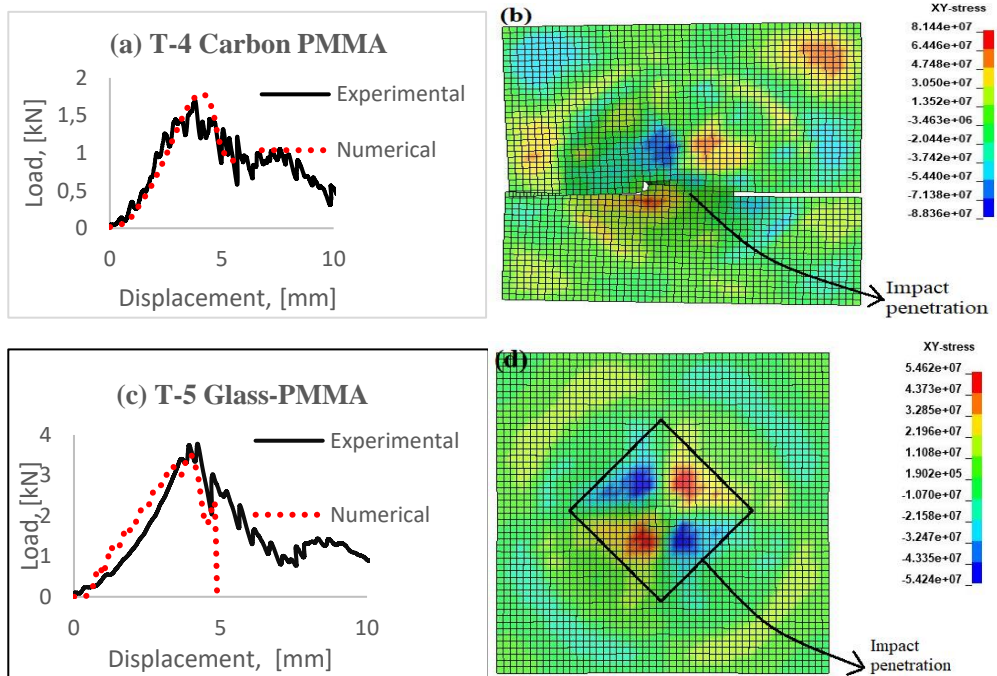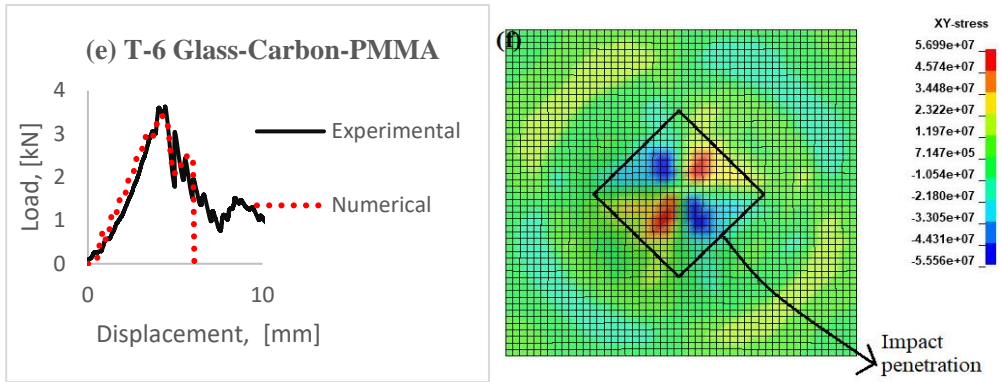
Fig. 4.9. (a) and (b) – T-4 numerical results of carbon and PMMA composite, (c) and (d) – T-5 numerical results of glass and PMMA composite and I and (f) – T-6 numerical results of glass carbon PMMA hybrid composite

4.6. Conclusions

The current chapter firstly delved into the feasibility of adopting PMMA as an alternative to epoxy. It was seen that PMMA could lend itself to be recycled and up scaled to the industrial scale. Later, the study explored the aspect of improving impact performance by introducing hybrid architectures as against introducing nanofiller seen in the previous two chapters, making the process more cost effective in terms of manufacturing. Two broad groups of composites were fabricated, i.e., the first group with epoxy and the second group with PMMA. Impact performances were assessed at room temperature and at higher temperatures, the damage mechanisms due to the hybrid architecture were quantified using an index termed as Ductility Index (DI). The introduction of hybrid architecture improved the toughness of composites without reducing its inherent strengths drastically, and hence, the composites exhibited a pseudo-ductile behaviour, and the toughness can be attributed to this pseudo ductility. However, the pseudo-ductility was lost at higher temperatures, which is not desirable. An energy-based model could predict the total energy absorption if the elastic energy and incident impact energy is known. The stability exhibited by PMMA was instrumental in using it in the next chapter. The global bending seen in composites during impact loading determines the behaviour in terms of damage initiation and its growth. In addition to this, fibre waviness is introduced into the composite architecture to introduce stable failure [86]. Thus, based on these two inferences, next study (chapter 5) in this research would focus on this aspect through an experimental and numerical method.

5. AN EXPERIMENTAL AND NUMERICAL INVESTIGATION OF GLOBAL BENDING THROUGH A FLEXURAL STUDY OF HYBRID ARCHITECTURE

This article titled "Effect of hybridization and ply waviness on the flexural strength of polymer composites: An experimental and numerical study" [37] has been published in the journal *Polymers* and is available online since March 27, 2022. This study explores the flexural behaviour of composites with the same architecture that was adopted in the previous chapter. Carbon was neglected because it was seen to perform poorly during the impact loading.

Flexure is important while under impact loading because there is global bending, and the role of bending stiffness miss match [61] play an important role in making composites semi-ductile in nature. In order to further explore the matrix behaviour, the waviness could be an ideal route, as it induces failure due to the shear dominant properties [86]. An important motivation to conduct these studies through this chapter is to further explore if there is a way to improve impact performance by studying the global bending that has been seen during impact. Global bending introduces stresses within a composite architecture, which leads to its ultimate failure. Introducing waviness into the architecture interferes with these stresses and hence is introduced to understand if it can positively affect flexural behaviour and hence the impact performance itself. There are two authors, and the first author is the defendant of this dissertation who contributed to the conceptualization, methodology, software, validation, formal analysis, investigation, resources, data curation, writing of the original draft, preparation and visualization.

5.1. Experimental materials, composite fabrication and material characterisation

Five sets (Fig. 5.1) of specimens were fabricated by the method elaborated in the previous studies (except for the vacuum bagging method adopted in this study), and they were cut and subjected to flexural tests as per EN ISO 14125:1998/AC, each specimen type, and their architecture is as shown in Table 5.1. This part of the study can be classed into four stages: stage 1 – fabrication of composite panels, stage 2 – investigation of flexural performance, stage 3 – estimation of the ductility of hybrid architectures and stage 4 – validation of the numerical model. With reference to Table 3, T-3, T-4, T-7, T-8 are specimens with out-of-plane waviness; T-3 and T-7 had waviness defined as concave up and T-4 and T-8 as concave down. According to the table, T-9 and T-10 are with in-plane waviness.
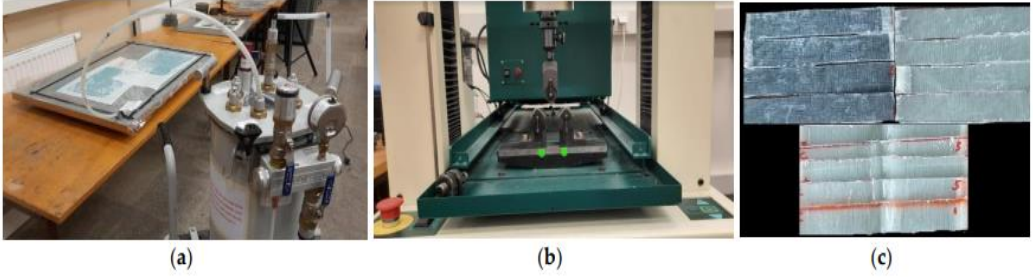
Fig. 5.1. (a) Composite panel preparation using the vacuum bagging method, (b) flexural tests on a specimen with waviness and (c) specimens for flexural tests

Table 5.1. Composite architecture

Specimen code	Symbol	Architecture	Fabric	Fibre orientation	Resin
T-1			Glass	Unidirectional	Epoxy
T-2			Glass and Carbon	Unidirectional	Epoxy
T-3/T-9			Glass	Unidirectional	Epoxy
T-4/T-10			Glass	Unidirectional	Epoxy
T-5	Glass ●		Glass	Unidirectional	PMMA
T-6	Carbon ●		Glass and Carbon	Unidirectional	PMMA
T-7			Glass	Unidirectional	PMMA
T-8			Glass	Unidirectional	PMMA

Table 5.2. Composite specimen properties for numerical modelling: X_T – strength in tension (longitudinal), X_C – strength in compression (longitudinal), Y_T – strength in tension (transverse), Y_C – strength in compression (transverse), S_L – shear strength

Resin Type	E_1 [GPa]	E_2 [GPa]	G_{12}/G_{13} [GPa]	ν_{12}	X_T [MPa]	X_C [MPa]	Y_T [MPa]	S_L [MPa]	Y_C [MPa]
Epoxy/Glass	32.4	8.1	2.6	0.22	680	600	35	37	35
Epoxy/Carbon	63	40	9	0.16	709	473	34	146	199
PMMA/Glass	23.16	2.1	2.62	0.38	325	246	16	42	128
PMMA/Carbon	47	3	1.8	0.13	1,300	882	15	40	120

Further delving into the numerical modelling (Fig. 5.2), the composites were modelled by using 4 node shell structure, while the size of the mesh was kept constant at 1 mm throughout the modelling procedure. The size of the specimens was as per the ISO standard, and the architecture was according to those mentioned in Table 5.1. The boundary conditions were fixed as a pin and roller to represent the flexural experiments [87]. Loading was defined on nodes by using the Boundary_SPC_SET option; later, the loading curve was defined based on the experimental loading conditions. The composite failure was defined using the Chang–Chang failure criterion [64]; this model is elaborated in chapter 1. This failure model in LS DYNA takes 21 parameters that should be defined, i.e., 15 of which are physically based, and 6 are numerical parameters. Among the 15 physical parameters, 10 are material constants (Table 5.2), and the remaining 5 are tensile and compressive failure strains in the fibre directions, the matrix and shear failure strains. The 6 numerical parameters were set at their default values. By conducting a parametric study, it was inferred that only the failure strains in the fibre direction and matrix direction influenced the model to a larger extent, i.e., DFAILT and DFAILM, respectively.
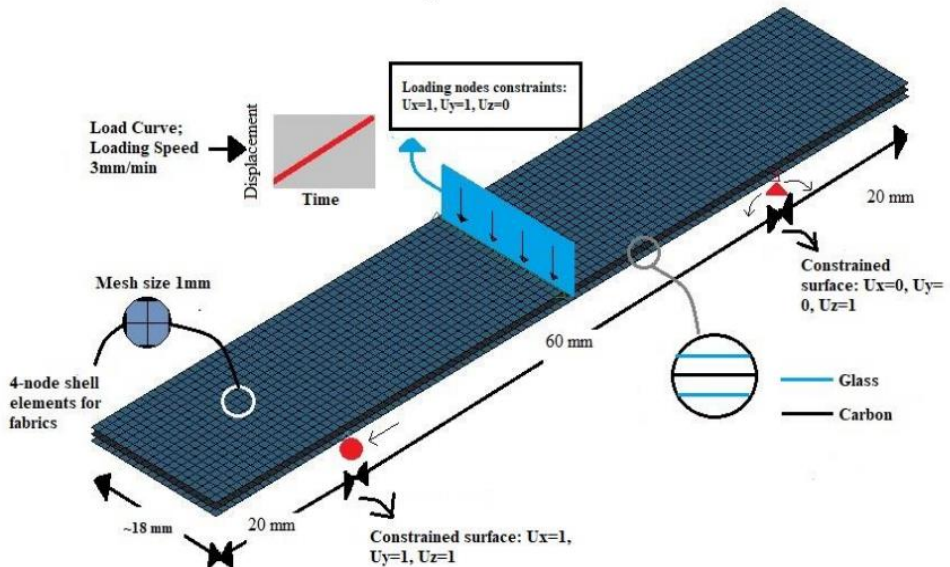
Fig. 5.2. FEM schematic of specimen, including meshing, constraints, loading conditions

5.2. Results and discussion

The load displacement plots for all the tested samples are shown in Fig. 5.3 a, b and c. As it can be seen, the samples with both epoxy and PMMA exhibited similar flexural response in all the samples that were studied. This could be an inference into its eventual replacement of epoxy-based composites and lending itself to better recyclability. Even though hybrids (T-2 and T-6) had reduced loading bearing capacities as against T-1 and T-5, the failure was not abrupt, as it was in the case later. After carrying the maximum load, it failed by intermittent drops in load, which implies higher inelasticity in them. While the specimens with out-of-plane waviness (T-3, T-

4, T-7 and T-8) failed with reduced load, T-7 and T-8 (PMMA samples) tend to carry similar loads with specimens having no waviness in them. T-8 had waviness in the concave down direction, and hence, the geometry of the sample could have been the reason for its higher displacement and better load bearing capacity. T-9 and T-10 samples are with in-plane waviness with root wave angle at ~15º and ~35º, respectively. These samples outperformed T-1, and the increase in load was anticipated, since mathematically, when using classical laminate theory to infer the effect of in-plane waviness on various properties (E_x, E_y, E_z, G_{xy}, G_{yz}, G_{xz}), an increase in G_{xy} is observed. However, in reality, this rise cannot be discerned, owing to interlaminar failure [88], as it was evident in the case of out-of-plane waviness. Further delving into this inference, in Fig. 5.3 e, T-10 failed due to shear before any clearly observable damage. T-10 lost its load bearing capacity due to which intensified the delamination, and hence, the final failure. The delamination in T-10 can be seen along the edges of the central region. A direct outcome of this inference is that the introduction of in-plane waviness increases the in-plane shear modulus, and this could lead to a better load bearing capacity, wherein the load is evenly shared by the fibre and resin within a composite structure. This is yet to be proven, for which further research must be done through dynamic tests, such as fatigue and impact.
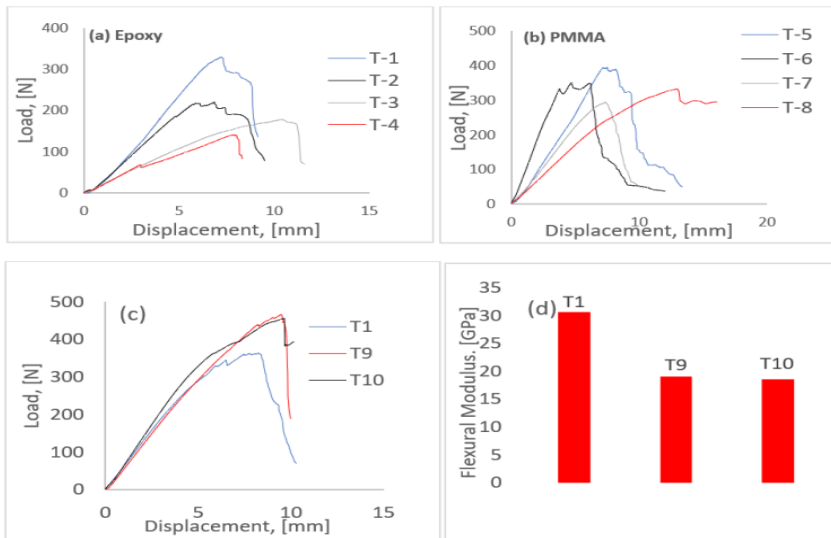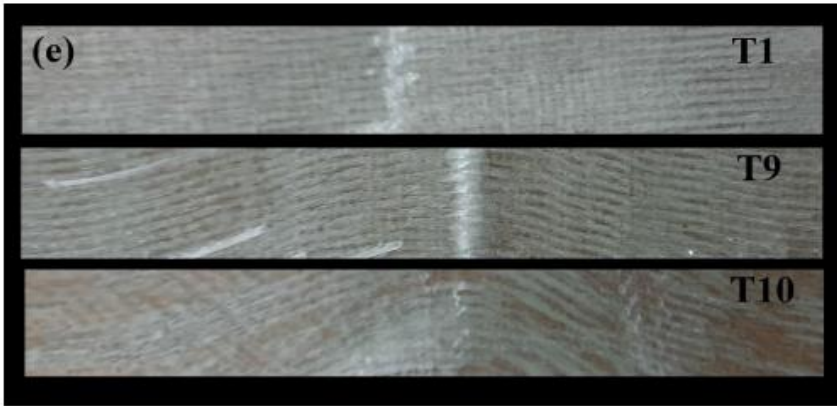
Fig. 5.3. Load displacement curve flexural tests: (a) specimens with epoxy resin, (b) specimens with PMMA resin, (c) specimens with in-plane waviness, (d) flexural modulus of specimens with in-plane waviness and (e) specimens post failure (in-plane waviness)

Figure 5.4 a, b illustrates the maximum strength and flexural stiffness (EN ISO 14125:1998/AC), which can be obtained by the following equations:

$$\sigma_F = \frac{3PL}{2bd^2},$$ (25)

$$E_F = \frac{L^3}{4bd^3}\left(\frac{\Delta F}{\Delta S}\right);$$ (26)

where P, L, b, d, and m are the maximum load, span, width, height and initial slope from the load displacement curve (expressed as change in force divided by the change in displacement, i.e., $\Delta F/\Delta S$ in eq. (26)), respectively. The figure below is the average plot of five samples from each code. As it can be inferred from the figure below, a considerable drop in flexural strength was witnessed with the presence of waviness in the architecture. Even though the drop in the case of the hybrid specimens (T-2) is negligible, the waviness in T-3 and T-4 saw a considerable reduction in strength. Similar results are seen in PMMA samples, thus favouring them to replace the epoxy for better recyclability.
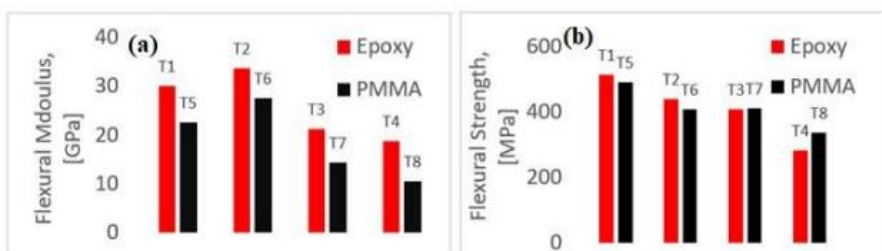
Fig. 5.4. Flexural modulus and strength of pure glass, hybrids and samples with waviness: (a) flexural modulus comparisons from T-1 to T-8 and (b) flexural strength comparisons from T-1 to T-8

The energy model to measure ductility was elaborated in chapter 4; hence, in this sub-chapter, the results will be presented. Fig. 5.5 a, b compares the hybrid T-2 and T-6 with T-1 and T-5, respectively. As it was expected, T-2 and T-6, due to their architecture, fail in a controlled manner, and an increase in ductility is observed. This is due to an increase in the inelastic component of the total energy, which was estimated to be 520 J in the case of T-2 and 861 J in the case of T-6. The hybrid effect can be attributed to the effect of interplay of low strain carbon and high strain glass fibres; the interlaminar stresses as well have an effect and cannot be neglected, as it is evident from the current research. Another important observation is that the elastic component from the total energy, in the case of non-hybrids, was the dominant energy absorption segment. This component makes the material brittle and less predictable while the introduction of hybrids increased the inelastic component, reducing the elastic component to 40% of the total energy. In conclusion, the hybridising of composites can reduce the unpredictability of composites considerably and make them an ideal choice for the structural applications.
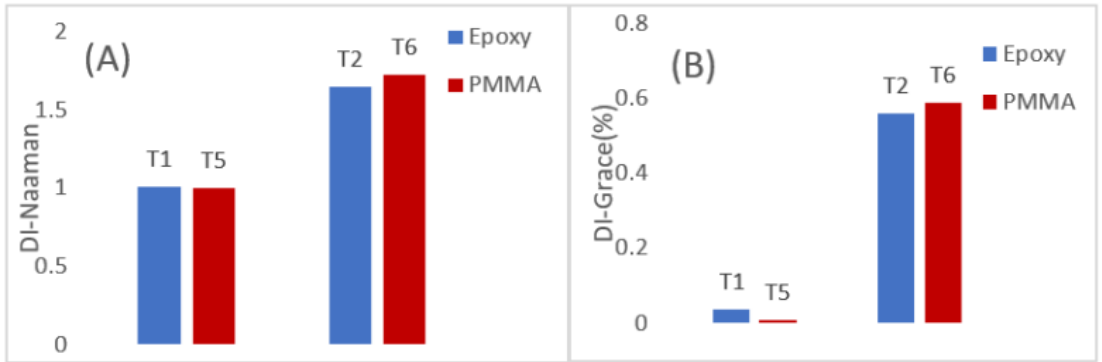
Fig. 5.5. Ductility Index (DI) based on the energy model developed by Naaman et al. and Grace et al., (a) DI-Naaman, (b) DI-Grace

The numerical modelling approach elaborated in sub-chapter 5.1 could generate results that captured the experimental behaviour with acceptable compatibility. This compatibility is elaborated in Table 5.3 and Fig. 5.6, where figures marked as (1, 2, 3) are numerical response to T-1, similarly, (4, 5, 6) are for T-2, (7, 8, 9) for T-3, (10, 11, 12) for T-4, (13, 14, 15) for T-5, (16, 17, 18) for T-6, (19, 20, 21) for T-7 and (22, 23, 24) for T-8, respectively. It is evident that the model was able to capture the load displacement in the elastic region precisely as it could be seen in the experiments. As it was elaborated in chapter 1 sub-chapter 1.4, MAT 54 uses a strain-based criteria to arrive at failure; therefore, in the case of flexure, DFAILT and DFAILM play an important role.

Table 5.3. Comparison of experimental and numerical loads obtained in flexure

Specimen code	T1	T2	T3	T4	T5	T6	T7	T8
Experimental load [N]	329.60	226.25	172.40	139.95	428.21	440.50	230.00	295.20
Numerical load [N]	341.34	229.78	165.92	138.38	439.94	492.21	205.47	296.44

Failure strains DFAILT and DFAILM are calculated by dividing the material modulus by their strengths, i.e., DFAILT = XT/E_1 and DFAILM = YT/E_2. There, a parametric study was performed to ascertain the effect of these two strain parameters, and a range between 0.01 to 0.05 was seen to give good compatibility with the experiments; it must be noted that higher values overestimated the failure load to a large extent. Other MAT 54, such as FBRT, TFAIL, DFAILS, SOFT and YCFAC, were set at its default terms to avoid overlapping outcomes. With these parameters, MAT 54 could be an ideal material model to study the flexural behaviour of composites within any kind of architecture.

Epoxy

62
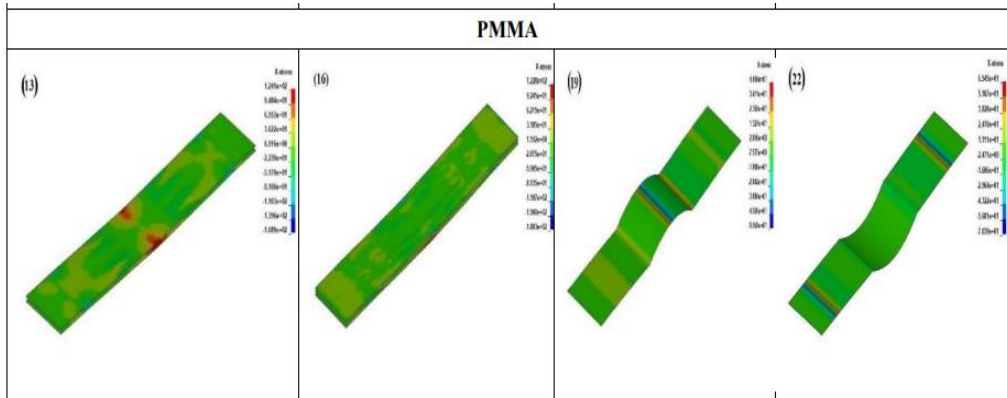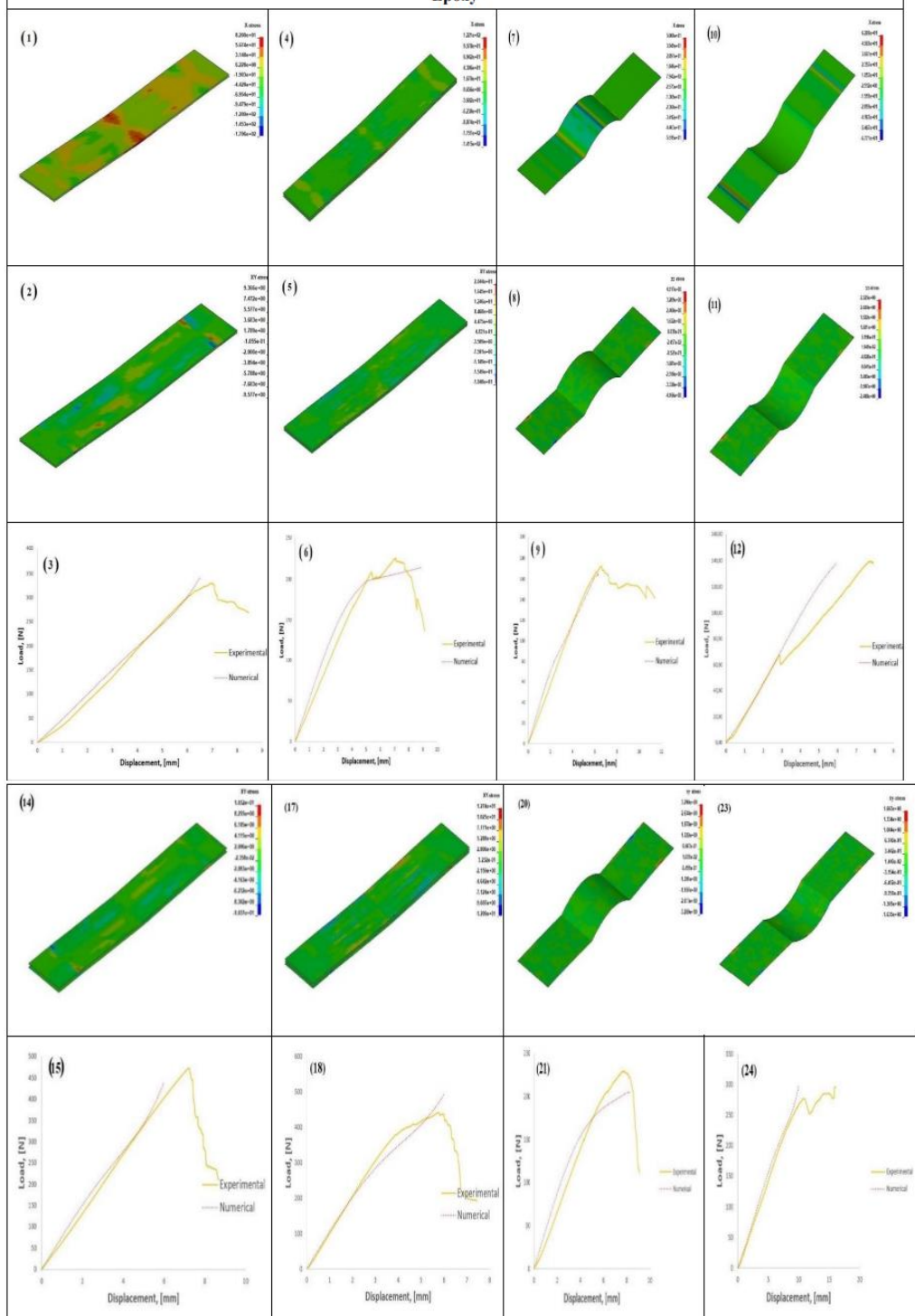
Fig. 5.6 Numerical results (stress fields along the x and xy directions, load displacement plots) captured on LS DYNA for all the studied specimen types: (1) stress in x direction for T-1, (2) stress in xy direction for T-1, (3) load curve for T-1, (4–6) stresses and load curve for T-2, (7–9) stresses and load curve for T-3, (10–12) stresses and load curve for T-4, (13–15) stresses and load curve for T-5, (16–18) stresses and load curve for T-6, (19–21) stresses and load curve for T-7, (22–24) stresses and load curve for T-8

Fig. 5.7 elaborates the theoretical and numerical strain values that were used in the parametric study. The theoretical values were determined through a rule of mixture model that is available in literature [54]. Theoretical strains can be ascertained by having the material properties of the fabric and resin individually. Therefore, the glass fabric stiffness was taken from literature [89] and is elaborated in Table 5.4 along with that of the resin (epoxy). ISO 527(2) tests were conducted to ascertain the resin properties. Since it is difficult and tiresome to estimate the correct calibration parameters experimentally, a parametric study could help to ascertain the influence of various parameters, such as strain (both in fibre and matrix direction) on flexure. The numerical model with these theoretical values can be calibrated quickly and easily, and hence, from the Figure 5.7, DFAILT of 0.048 and DFAILM of 0.1 were used in the parametric study (PS-2 and PS-4, respectively).

Table 5.4. Fibre and matrix mechanical properties

Material	Young's modulus, [GPa]	Tensile strength, [MPa]
Epoxy	3.2	70
Glass fabric	81.0	2,200
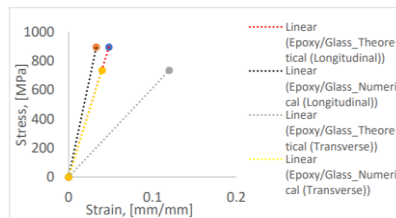
Fig. 5.7. Theoretical and numerical strains for the parametric study

Figure 5.8 highlights the influence of DFAILT and DFAILM on the behaviour of T1 under flexure. Thus, shear stress distribution was studied, because it was inferred that DFAILM (strain in the matrix direction) influenced the failure to a larger extent. As it has been mentioned previously, a parametric study would help to benchmark a modelling approach to validate its use in future studies. Table 5.5 lists the range of different parameters that were studied, and hence, six parametric studies (PS) were conducted on T-1. It has been observed that the material properties in the fibre and matrix direction influenced the flexure to a large extent. Among the six listed PS, PS-1 and PS-6 gave results that were resembling the experiments, whereas PS-2 and PS-4 overestimated the results. DFAILM at 0.1 was the same as obtained theoretically, calibrated the model as closely as seen in the experiments. PS-3 and PS-

4 were seen to underestimate the response and hence were omitted in further study. According these parametric studies, it can be inferred that the max strain in the fibre direction (DFAILT) and the max strain in the matrix direction in tension and compression (DFAILM) influenced the flexural response and govern the outcome during global bending, prevalent during the impact event. Another aspect that should be highlighted is that DFAILM, which is a matrix dominant strain, influences the growth of delamination, and the presence of in-plane waviness has affected DFAILM, which in turn gave higher loads that could be seen in Fig. 5.3 c. This could translate to a better impact performance due to the presence of global bending, which requires more research.

Table 5.5. Parameters adopted for the parametric study

Parametric study (PS)	DFAILT	DFAILM
1	0.033	0.04
2	0.048	0.04
3	0.009	0.04
4	0.1	0.04
5	0.033	0.009
6	0.033	0.1

Fig. 5.8 b highlights the effects of an overestimated DFAILT and DFAILM at 0.1. As it can be seen, at 0.1, the failure strain is very high, which in turn makes the composite stiff in the elastic region. Fig. 5.8 a, d shows the shear stress distribution where the element deletion signifying failure is not seen. At lower strains (0.015), the obtained results were detrimental and hence not considered. The instabilities were seen when strain went below 0.01, signifying non-uniform element failure. DFAILT at 0.09 saw the specimens fail earlier and was less stiff than seen in the experiments (Fig. 5.8 f). Therefore, the ideal strains, which reflect the experimental reality, were 0.033 and 0.04 (Fig. 5.8 e) and hence should be considered. These strains are the baseline values, since with these strains, the model predicts the failure when under flexure.
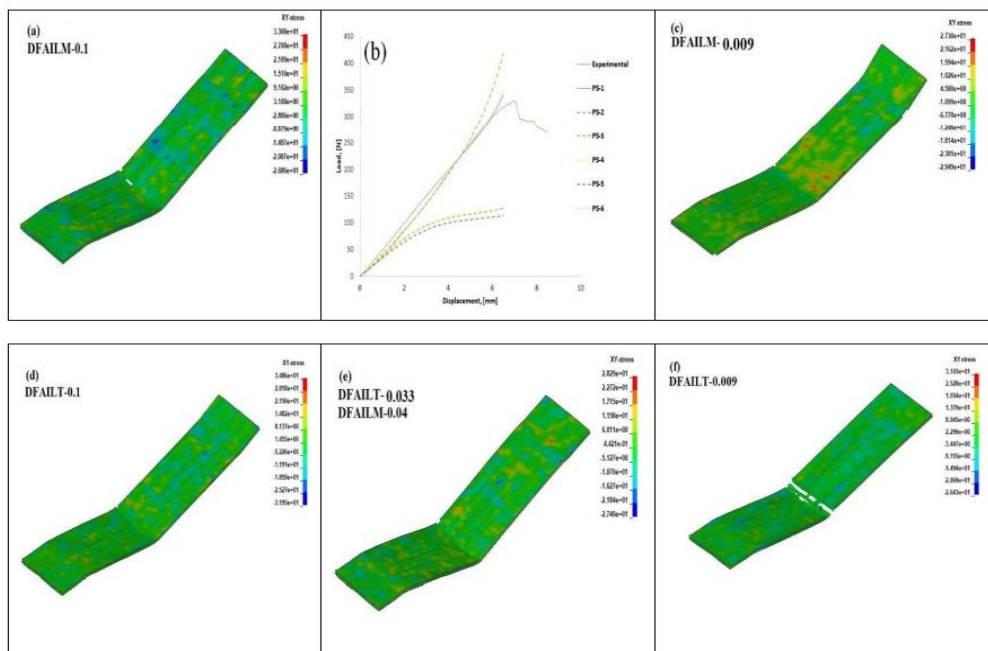
Fig. 5.8. Parametric study on the influence of DFAILT and DFAILM on flexural behaviour of T-1: (a) XY-stress when DFAILM = 0.1, (b) load displacement plot for the six parametric studies listed in Table 7, (c) XY-stress when DFAILM = 0.009, (d) XY-stress when DFAILT = 0.1, (e) XY-stress when DFAILT = 0.033 and DFAILM = 0.04, (f) XY-stress when DFAILT = 0.009

5.3. Conclusions

This chapter attempts to explore the aspect of global bending that is prevalent during impact loading. Thus, moving from a dynamic aspect of loading scenario to the static scenario, flexural tests were conducted on specimen architecture, as seen in chapter 4. The pure carbon specimens were not subjected to flexure, as it was realised that carbon-based composites do not exhibit good impact resistance. The ductility effect was observed in this research, and it can be safely concluded that hybrid architectures provide good impact resistance without the sophistication involved in introducing nano-fillers. In order to further study the role of matrix in impact performance, in-plane and out-of-plane waviness were introduced. Even though out-of-plane waviness affects the flexural performance to a great extent, in-plane waviness was seen to increase the load bearing capacity. Thus, the numerical studies were conducted, and it was seen that matrix-related strain parameter DFAILM had a positive influence in improving or underestimating the flexural response. Therefore, it can be hypothesised that the introduction of in-plane waviness affects the shear properties of the specimen, which is a matrix-related property, and hence, there exists a direct correlation of this property with that of flexural response, and it could improve the impact performance subsequently.

6. EXPERIMENTAL AND NUMERICAL INVESTIGATION OF GLOBAL BENDING THROUGH A FLEXURAL STUDY OF HYBRID ARCHITECTURE

This chapter introduces non-published research in addition to the published research enumerated in the previous chapter, where the effect of ply waviness of composites is studied when subjected to impact loading. This chapter is a conclusion, which studies the final aspect of waviness affecting the impact performance. A set of 5 composite panels with glass as the reinforcing material was used with epoxy as the resin. The first panel has woven glass, the second has $[0/90]_2$ symmetric glass, the third is a unidirectional glass with a certain amount of waviness in the impact region, and the fourth is a purely unidirectional glass composite. All of them had a nominal thickness of 1 mm (4 layers of glass).

6.1. Experimental materials, composite fabrication and material characterisation

Four sets of samples were fabricated by the methods elaborated in the previous chapters. Each of these sets bears the code as elaborated Table 6.1, where the composite architectures are described. The samples had four layers, reaching a thickness of 1 mm. G-1 has woven fabric (2/2 twill weave) in them, bearing an areal weight of 163 g/m^2, G-2, G-3 and G-4 have unidirectional fabric with areal weight of 200 g/m^2. The fabrics were sourced from R&G Faserverbunkwerkstoffe GmbH, Waldenbuch in Germany; the Epoxy based on Bisphenol A and its hardener (modified cycloaoliphatic polyamine, free of alkyl phenol and benzyl alcohol) was sourced from the same company. The impact energy was kept constant at 50 J to achieve complete perforation in all specimens that were studied. The characterisation was in the form load displacement curve, energy and studying the damage in composites.

Table 6.1. Fibre architecture details

Specimen code	Fabric	Fibre orientation	Stacking order	Resin	Comments
G-1	Glass	Woven	[0/0/0/0]	Epoxy	No waviness
G-2	Glass	Unidirectional	[0/90/90/0]	Epoxy	No waviness
G-3	Glass	Unidirectional	[0/0/0/0]	Epoxy	With ply waviness
G-4	Glass	Unidirectional	[0/0/0/0]	Epoxy	No waviness

6.2. Results and discussions

The evolution of damage during impact on different types of glass architecture, as elaborated in Table 6.1, is displayed in Fig. 6.1. The highest impact load was seen in G-1 (Fig. 6.1 a) at 2.8 kN with the shape of the fracture (Fig. 6.1 b), which is a diamond and is typical in woven glass architectures. The major source of energy dissipation during the course of impact is the elastic deformation, which reaches the

maximum of 3.63 mm, following which, there is a split in the shape of diamond along the weave directions. This phenomenon is dominated by fibre dominant characteristics of composites, and hence, the shear dominant properties, which is typically governed by the matrix, do not play any role. This is evident from lesser delamination, which if present would have produced intermittent load drops in the elastic region of load curve. These observations hold true for symmetric G-2 (Fig. 6.1 c, d), which has unidirectional lamina in 0/90/90/0 ply orientations. The damage, even though not diamond shaped seen in G-2, was circular, highlighting complete penetration; the load bore by this architecture was similar to G-1 but with less energy absorption until the max load. However, there was higher energy absorption in the case of G-1, which means that all this energy is in the form of elastic deformation, and the penetration is catastrophic [82–83]. Hence, hybridising this architecture could convert energy for elastic deformation to the energy absorption for introducing the hybrid effect or ductility.

The ductility effect can be realised to an extent by introducing in-plane waviness in a unidirectional composite. Even though the ductility index in term of obtained Grace [83] was 0.53, this is much higher, i.e., to 0.43 in woven glass composites, which is 18% increase. The loads that are seen in G-1, G-2 and G-3 (Fig. 6.1 i) are similar; the increase seen with respect to G-4 is important, which corroborates the finding in the previous chapter where in-plane waviness was seen to improve the flexural response. As explained earlier, by introducing in-plane waviness, the shear component of the composite is activated. An increase in waviness increases the in-plane shear modulus [88] considerably, and this imparts better performance in the case of unidirectional composites under impact loading. Flexure in static is prevalent, as global bending during impact, and if in-plane waviness can improve flexure, the same should be obvious during impact. When comparing the load increase between G-3 and G-4 (Fig. 6.1 i), the increase seen in G-3 is approximately 21% with considerably higher energy in the elastic region. The intermittent load drops seen in G-3 is due to the several damage mechanisms seen in G-3 during the loading phase, and hence, making them comparatively less brittle and tougher.

The damage seen in G-3 is different from the one seen in G-1 and G-2. The diamond shaped damage associated with woven composites and circular damage seen in symmetric G-2 are incomparable to the peanut shaped damage seen in G-3. There is debonding in the central region of impact and fibre breakage along two edges. This is evident from the load being shared equally by the individual components of a composite material, i.e., fabric and resin. In the case of G-4, the lower load could be attributed to the horizontal split seen in the impact region, which means that more load was borne by resin as opposed to the fabric. Thus, if seen from G-1 to G-4, the damage transitions from a diamond to a circular to a peanut shape, and finally, to a line. Among these, the peanut shaped damage, as mentioned before, is the shear effect coming into fruition. If this was a thicker laminate, the performance vis-à-vis a unidirectional composite would be better, and where such composites are subject to impact, a switch over can be made by implementing this simple change in architecture.

As explained in the previous chapter, the effect of DFAILT (failure strain in matrix direction) had a profound effect on the load curve when loaded under flexure. Flexure in the form of global bending is prominent in composites and contributes to the propagation of damage during impact. The failure strain (DFAILT) increases with the introduction of in-plane waviness and significantly increases the load as it is seen. This was seen in the flexure in the previous chapter and during impact loading in this chapter. Thus, the introduction of in-plane waviness, even though detrimental when under compression, tension and fatigue, could help to increase the impact performance of unidirectional composites, where their application is unavoidable and there is a higher possibility of being hit by nearby substances/debris.
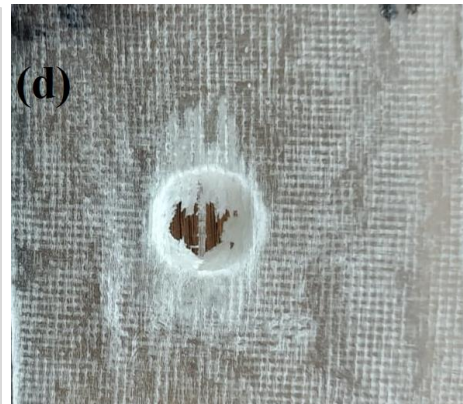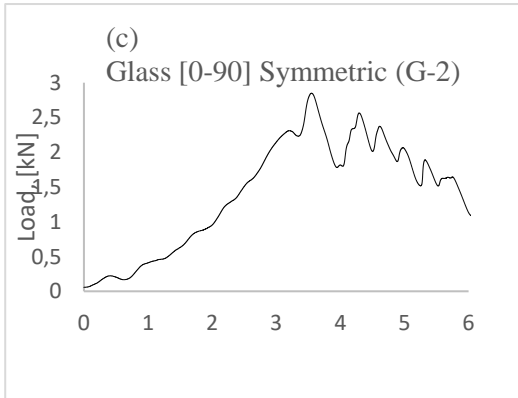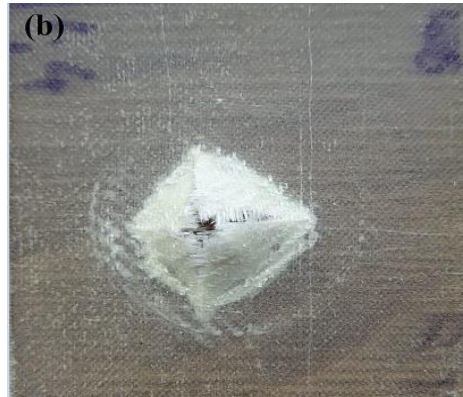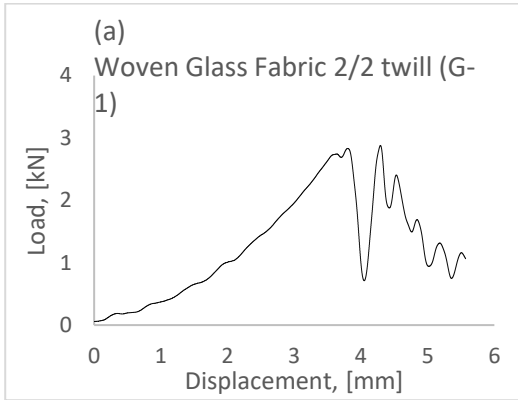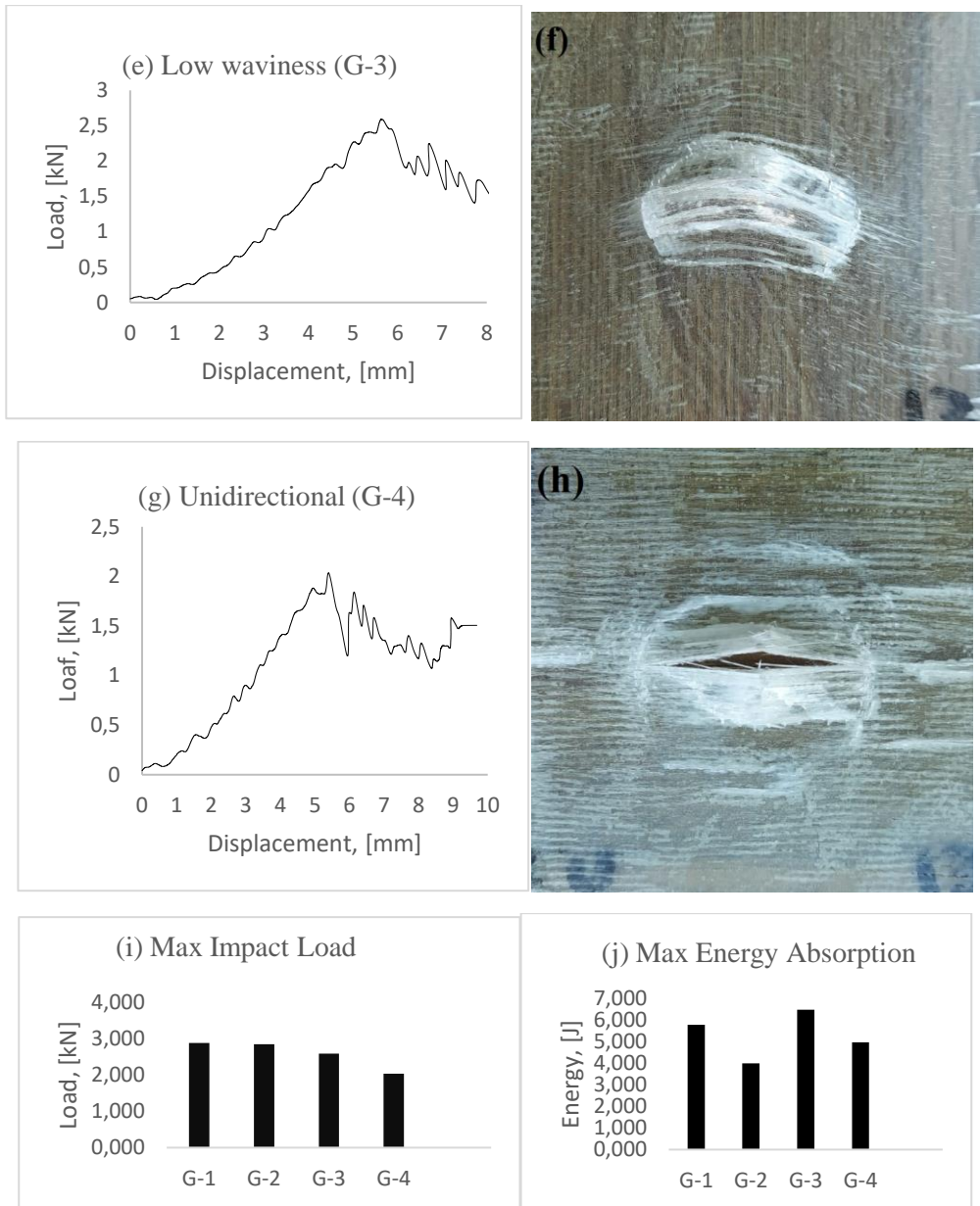
Fig. 6.1. (a, b) G-1 load characteristics with the typical diamond shape fracture seen in the woven fabric, (c, d) G-2 load characteristics with circular penetration seen in the symmetric composites, (e, f) G-3 load characteristics for ply with waviness with a peculiar peanut shaped fracture, (g, h) G-4 load characteristics with split along the middle that is usually seen in unidirectional composites, (i, j) load comparison of all the composite architectures along with energy absorbed during the impact

6.3. Conclusions

The effect of waviness on impact performance was compared with different fibre architecture, namely, woven (G-1), symmetric (G-2) and unidirectional (G-4). The fabrication technique was similar to the one adopted throughout the thesis, the achieved thickness was 1 mm, and the impact energy was 50 J. All the four types of specimens went through penetration, and their load characteristics, energy and damage were analysed. Following these, the load characteristics of G-3 increased with respect to unidirectional G-4. The observed increase was 21%, which was in sync with the flexural strength increase that was seen previously. The observed energy was higher in the case of G-3 when compared to G-1, G-2 and G-4. This can be attributed to the combination of damage mechanisms seen in G-3, which had higher ductility index when compared to the other types that were studied in this sub-chapter. The transition of damage that was seen from G-1 to G-4 can be attributed to the fibre architecture. G-1 and G-2 experienced brittle failure, which was fibre dominant, whereas G-3 and G-4 was seen to have a failure dominated by the interaction of both fibre and resin.

CONCLUSIONS AND PROPOSALS FOR FUTURE STUDIES

Based on the 6 objectives that were set at the beginning of this research, the following conclusions can be drawn from the summary of five research papers related to this PhD dissertation.

1   The introduction of FCNTs (functionalised carbon nanotubes) increased the mechanical and impact strengths of glass reinforced composites, and it was deduced that 0.35 wt% with respect to epoxy was sufficient to increase the mechanical strength by 30%, and the impact strength by 31%. The introduction of FGA-functionalised graphene (the best wt% was found between 0.2 to 0.35 wt%) was seen to increase the strength by 18%, while a noticeable increase in strain was observed. The maximum observed increase in strength was seen at 23%. The impact strength was seen to increase by 70%. Thus, nano reinforcements were seen to increase the strength in terms of loading conditions, namely, tension and impact.

2   Epoxy and PMMA could bear similar impacts loads: their performance at higher temperature was compatible. However, the performance of composites with PMMA was better at higher temperatures, owing to its elastic deformation and minimal observable damage, as there was no perforation seen. The hybrid effect was achieved in both cases at room temperature but was lost at higher temperatures.

3   The hybrid effect was quantified in terms of index, termed as ductility index. Two indices were put forward, namely, Naaman and Grace, both of which showed similar trends. Thus, as per Grace, the ductility index of the composites with hybrid architecture was estimated between the range of 66–70% at room temperature. Whereas in composites with no hybrid architecture, the ductility index was estimated as low as 45%.

4   The effect of in-plane and out-of-plane waviness were explored during flexure, and it was observed that out-of-plane waviness drastically reduced flexural load, while in-plane waviness, improved it.

5   In-plane waviness incorporated into a unidirectional glass composite was seen to perform better when compared to unidirectional specimens without any waviness in them during impact loading. The performance of specimens with waviness was seen on par with composites with woven/symmetric architectures in them.

6   Numerical models were validated to establish a benchmark modelling approach to further explore the effect of matrix on failure initiation and propagation along with those of fibre. It has been noticed that the influence of matrix dominant parameters was underestimating or overestimating flexure, and its relation to waviness was explored. It has been observed that matrix-related strain parameter DFAILM had a positive influence on improving or underestimating the flexural response. It was deduced from this observation that the introduction of in-plane waviness affects the shear properties of the specimen, which in turn affects the flexural response positively and hence imparts better impact resistance.

Proposals for future research

The methods adopted in this research gave an overall view of the impact performance of composites in the presence of nanofillers and hybridization while the presence of waviness on the flexural response was ascertained as well. It as well has some insights on the influence of fibre and matrix direction strain parameters on flexure, evaluated using a numerical model. However, this has to be eventually proven in the context of impact induced global bending. Based on this proposition, a few guidelines for future research can be drawn.

1   Introduction of in-plane waviness improved the flexure and impact response significantly. The experimentations in the realm of impact have been limited, and hence, more experimentations must be performed in addition to the work performed in this thesis on different waviness root angle to deduce where the optimum range lies.

2   The experimentations can be three: pronged, static flexure, fatigue and impact loading. If more results prove it to be right; then, the impact resistant composites can be realised by simple manufacturing techniques, thus cutting down the costs in manufacturing.

SANTRAUKA

Motyvacija ir problemos svarba

Per pastaruosius kelis dešimtmečius polimerinių kompozitų paklausa, palyginti su metalais, smarkiai išaugo dėl jų lengvo svorio, atsparumo pažeidimams, didelio specifinio stiprumo, ilgaamžiškumo, mažesnės dujų emisijos, mažesnių degalų sąnaudų ir kt. [1–3]. Skirtingai nuo šių privalumų, šios medžiagos yra linkusios staigiai suirti dėl savo trapios prigimties, todėl detalėms, pagamintoms iš pluoštu sustiprintų kompozitų, yra taikomi aukštesni saugos koeficientai, užtikrinantys patikimumą. Dėl ko su didesne atsarga suprojektuoti komponentai sumažina svorio taupymo efektą. Trapiems kompozitams suteikus plastiškumo, dinaminės savybės priartėtų prie metalams būdingų aukštų energijos sugėrimo charakteristikų ir tai dar labiau išplėstų kompozitų panaudojimą [4, 5].

Eksploatacijos metu įprasta, kad kompozitinės medžiagos patiria mažo greičio smūgines apkrovas. Pavyzdžiui, paukščių susidūrimai su orlaivių sudedamosiomis dalimis, įrankių kritimai vykdant remonto darbus ir pan. Nors pažeidimai neišvengiami, kompozitinės konstrukcijos gali būti projektuojamos siekiant sumažinti minėtų pažeidimų dydį arba poveikį tolimesniam konstrukcijos mechaniniam atsparumui. Smūgio metu kinetinė energija išeikvojama įvairiems pažeidimo mechanizmams [6,7], o smūgiams atspari konstrukcija turėtų būti tokia, kad būtų galima išvengti pažeidimų mechanizmų (matricos įtrūkimų, delaminacijos, pluošto lūžimo ir kt.). Tačiau smūginių apkrovų metu pradinį pažeidimą inicijuoja matricos įtrūkimų susidarymas sluoksniuose dėl šlyties įtempių, veikiančių statmenai kompozito paviršiui [8]. Matricos įtrūkimai vėliau išsivysto į atsisluoksniavimo defektą, nulemtą tarpsluoksninių šlyties įtempių (II moda), atsirandančių dėl laminato lenkimo [9].

Dėl naudojamų dervų (pvz., epoksidinių) trapumo, kompozitai yra jautrūs smūginių apkrovų poveikiui. Taigi vienas iš būdų padaryti kompozitus atsparius smūgiams būtų koreguoti matricos savybes, didinant jos plastiškumą ir kartu energijos sugerties galimybes. Tai galima įgyvendinti panaudojant įvairius užpildus matricoje [9, 10]. Vis labiau populiarėja - nanoužpildai.

Anglies nanopluoštai, nanoplokštelės, grafenas ir anglies nanovamzdeliai yra keletas nanoužpildų pavyzdžių, naudojamų kompozitinių medžiagų matricai sustiprinti. Ypač plačiai naudojami anglies nanovamzdeliai dėl savo savybių, susijusių su dideliu matmenų santykiu ir specifiniu paviršiaus plotu pasižymintys ypač dideliu išilginiu tamprumo moduliu [11]. Eksperimentiniais tyrimais patvirtinta, kad mechanines kompozitų savybes teigiamai paveikia nanovamzdelių arba grafeno užpildai [13-20], net 0,5 % masės daugiasienių anglies nanovamzdelių (MWCNT) užpildas gali smarkiai padidinti kompozito atsparumą smūginėms apkrovoms [12]. Tačiau anglies nanovamzdelių ir grafeno trūkumas yra tas, kad jie aglomeruojasi matricoje, todėl prieš panaudojant juos matricoje, jie turėtų būti funkcionalizuoti arba

turėtų būti naudojami sudėtingesni mechaniniai metodai, pvz., panaudotos specifinės valcavimo staklės [11, 21-23]. Todėl išlieka aktualumas ieškoti ekonomiškesnių smūgiams atsparių kompozitų kūrimo metodų.

Kompozitinės architektūros hibridizavimas galėtų būti ekonomiškas žaidimo taisyklių pakeitimas, siekiant padidinti polimerinių kompozitų atsparumą smūgiams. Pagrindinė priežastis yra ta, kad, papildžius standžiais pluoštais, padidėja atsparumas smūgiams be reikšmingo mechaninių savybių sumažėjimo [24]. Hibridinės kompozitinės architektūros kuriamos matricoje sujungiant du ar daugiau skirtingų pluoštų [25]. Skirtingų pluoštų sudėjimo tvarka, kad būtų pasiektas optimalus atsparumas smūgiams, lieka nežinoma, nes įvairūs deriniai davė rezultatus, kurie, viena vertus, atrodo daug žadantys, o kita vertus – netenkinami. Kai kurie hibridinių kompozitų projektavimo parametrai, turintys įtakos jų atsparumui smūgiams, yra sluoksniavimo seka, storis ir geometrija. Įvairūs tyrimai parodė, kad kompozitų hibridinės architektūros gebėjimą sumažinti smūgio žalą daugiausia nulemia sluoksniavimo seka [26, 27]. Nustatyta, kad hibridiniai kompozitai gali pasižymėti laipsniško lenkimo elgsena, ir tikėtina, kad panaši elgsena pasireikštų ir smūgio metu [24], kas galėtų būti vadinama plastiškumo efektu [27]. Veikiant smūgiams, lenkimo sukelti įtempiai yra pagrindinė išsisluoksniavimo priežastis, kuri, kaip minėta anksčiau, yra vyraujantis reiškinys matricoje [5]. Kadangi dominuojančios matricos savybės atlieka tokį svarbų vaidmenį, tai, numatant ilgalaikes kompozitų savybes, reikėtų ieškoti alternatyvos epoksidinei dervai, kad šios medžiagos taptų ekologiško. Dėl sunkaus epoksidinės dervos kompozitų perdirbimo aktualu ištirti alternatyvią rišančią polimerinę medžiagą su panašiomis mechaninėmis savybėmis, ir vienas iš tokių pakaitalų galėtų būti poli(metilmetakrilato)-PMMA derva. Todėl kaip alternatyvas epoksidinei dervai svarbu ištirti hibridinio kompozito reakciją į statinio lenkimo bandymus nustatant matricos efektą, pluošto banguotumo sluoksnyje ir statmena kryptimi įtaką. Banguotumas statmena sluoksniui kryptimi galėtų imituoti tarpsluoksnio sustiprinimo efektą. Be eksperimentinio tyrimo, reikėtų atlikti hibridizavimo efekto ir banguotumo skaitmeninį tyrimą, siekiant sukurti etaloninį skaitmeninį modelį, kurį būtų galima naudoti paskutiniuose tyrimo etapuose nepasikliaujant eksperimentiniais tyrimais, nes tai varginantis ir brangus procesas.

Reikia įvertinti tokių dervų hibridizacijos ir banguotumo poveikį, kad būtų galima geriau suprasti dervų elgseną, susijusią su ilgalaikiu kompozitų panaudojimu, taigi, kad jos būtų idealus pakaitalas projektuojant lengvas konstrukcijas. Nors kartais kompozitų banguotumas gali sustiprinti medžiagą, storoms kompozitinėms konstrukcijoms tai yra problema, susijusi su liekamaisiais įtempiais, atsirandančiais kietėjimo metu, ar vietiniu pluoštų deformavimusi vyniojimo metu [28–30]. Apkrovos kompozitinėse konstrukcijose su sluoksnio banguotumu sukelia triašį įtempių būvį, dėl ko sumažėja standumas ir stiprumas [31]. Sudėtinio sluoksniavimo taikymas (hibridizavimas) leidžia pasiekti laipsnišką sluoksnių irimą, gali būti įgyvendintas ir pritaikius banguotumo efektą. Banguotumo poveikis taip pat gali padėti geriau kontroliuoti šlyties poveikį kompozitų stiprumui. Tačiau esant banguotumui svarbų

vaidmenį vaidina dominuojančios matricos savybės [31, 32], kurias svarbu ištirti, siekiant projektuoti pigius ir efektyvius kompozitus.

Daktaro disertacijos tikslas ir uždaviniai

Tikslas yra ištirti nanodalelių, hibridizacijos ir banguotumo poveikį pluoštu armuotų polimerų kompozitų smūginėms savybėms.

Polimeriniuose kompozituose, kuriuos veikia mažo greičio smūgio apkrovos, dominuoja matricoje inicijuoti pažeidimai. Tikslui įgyvendinti suformuluoti uždaviniai:

1. Nustatyti anglies nanovamzdelių ir grafeno poveikį kompozitų smūginiam atsparumui esant mažo greičio smūgio apkrovai.

2. Nustatyti skirtingų matricos medžiagų, t. y. epoksidinės dervos ir PMMA, panaudojimo hibridinės struktūros kompozituose, veikiamuose smūginės apkrovos, efektyvumą.

3. Pritaikius energomechaninius metodus, kiekybiškai, įvertinti hibridizacijos poveikį kompozito smūginiam atsparumui.

4. Nustatyti banguotumo (tiek plokštumoje, tiek per laminato storį) poveikį mechaninei kompozito elgsenai lenkiant, vyraujančiai smūginės apkrovos metu.

5. Nustatyti banguotumo plokštumoje efektyvumą lyginant su skirtingų pluošto orientacijų laminatais smūginės apkrovos metu.

6. Sukurti skaitmeninį LS-DYNA modelį, leidžiantį patikimai prognozuoti pluošto ir matricos irimo deformacijų poveikį laminato elgsenai dėl lenkimo ir smūginių apkrovų.

Tyrimų metodologija

Daktaro disertacijoje parengtoje penkių mokslinių straipsnių pagrindu, nagrinėjama nanoužpildų, hibridizacijos parametrų, tiesiogiai priklausomų nuo dervos, pluošto bei jo banguotumo poveikis polimerinių kompozitų smūginiam atsparumui. Tyrimai suskirstyti į dvi dalis. Pirmoje įvertinamos nano užpildų CNT ir grafenu nanoarmuotų kompozitų mechaninės ir smūginės savybės. Mechaninių savybių, t. y. sluoksnio tamprumo ir stiprumo, parametrų nustatymas atliktas pagal ISO 527-2 standarto reikalavimus, o atsparumui smūginei apkrovai tirti buvo pagaminti 80x80 mm dydžio ir 1 mm storio bandiniai. Viso eksperimento metu buvo naudojama vienoda 50 J smūgio energija, pakankama bandiniui pramušti. Remiantis šių eksperimentų rezultatais ir išvadomis, buvo pradėta kita tyrimų dalis, susijusi su lenkimo charakteristikų analize hibridinėse struktūrose, siekiant padidinti laminato smūginį atsparumą. Tiriant hibridines kompozicines struktūras, daugiausia dėmesio

skirta PMMA dervai. Pritaikius energomechaninius metodus, kiekybiškai įvertintas laminato smūginis atsparumas ir dinaminės apkrovos atsakas į smūgines apkrovas, ir tuo remiantis rekomenduotas kompozitų plastiškumo indekso DI parametras, kuriame atsižvelgiama į irimo charakteristikas pagal tamprumo ir plastiškumo energijas. Siekiant geriau suprasti hibridizavimo efektą, kompozitiniai laminatai buvo tiriami skirtingose temperatūrose, o mikroskopiniai tyrimai buvo atlikti siekiant ištirti pažeidimų pobūdį ir susieti juos su siūlomu energomechaniniu parametru.

Darbe pateikiama išsami perdirbimo ir termoplastinių dervų apžvalga, siekiant pabrėžti kompozitų, kaip alternatyvios ir tvarios medžiagos, vaidmenį būsimai žaliųjų technologijų revoliucijai vėjo energetikoje. Aptariami lenkimo aspektai, atsirandantys veikiant smūginėms apkrovoms, ir gilinamasi į banguotumą tiek plokštumoje, tiek per laminato storį, nustatant matricos vaidmenį gerinant kompozitų veikimą veikiant smūginei apkrovai. Nagrinėjami skaitmeninio modeliavimo metodai, padedantys suprasti su matrica susijusias deformacijas ir pluošto krypčių įtaką kompozitų mechaniniam atsakui į smūgines apkrovas. Išvadose apibendrinamas ryšys tarp banguotumo, ribinių deformacijų ir atsparumo smūgiams.

Darbo mokslinis naujumas

- Kompozitų trapumas nulemia staigų irimą, kuris gali būti sumažintas įdiegus hibridinę architektūrą.
- Pasiektas trapumo sumažėjimas paverčiamas pseudoplastiškumu, todėl kompozito irimas smūgio metu tampa labiau prognozuojamas.
- Vienakrypčio kompozito laminatams banguotumas plokštumoje pagerina smūginį atsparumą padidindamas smūginės apkrovos amplitudę ir sugertos energijos kiekį.

Ginamieji teiginiai

- Hibridizavimo poveikis smūginiam atsakui kiekybiškai įvertinamas naudojant energomechaninį modelį.
- Banguotumas plokštumoje teigiamai veikia smūginį atsparumą, o banguotumas per storį turi neigiamą įtaką.
- Banguotumas plokštumoje pagerina kompozito armuoto vienakrypčiu audiniu smūginį atsparumą, nulemia didesnę smūginės jėgos amplitudę ir sugertos energijos kiekį.

Praktinė tyrimo vertė

- Hibridinio efekto įdiegimas sumažina kompozitų trapumą, taip jie tampa pseudo-plastiškesni, o pagerėjęs smūginis atsparumas padidina ir saugumą.
- PMMA yra veiksminga epoksidinės dervos alternatyva kompozituose, o pakartotinio perdirbimo galimybė suteikia kompozitinei konstrukcijai tvarumo.

1. Didelio veiksmingumo stiklo pluoštas / epoksidinė derva, sustiprinta funkcionalizuotais CNT, skirta naudoti transporto priemonėse, kurių degalų sąnaudos ir šiltnamio efektą sukeliančių dujų kiekis yra mažesnis

Funkcionalizuoti anglies nanovamzdeliai (FCNT) buvo disperguoti epoksidinėje dervoje ultragarsu (koncentracijos svyravo nuo 0,05 iki 0,4 masės %, 9 lentelė), po to FCNT / epoksidinės dervos tirpalas buvo apdorotas ultragarsu ir taip buvo gautas preliminariai disperguotas to paties tirpalas (1.1 pav.). Tada jis vėliau buvo ištirpintas kietikliu santykiu: 3 dalys FCNT/epoksidinės dervos ir 1 dalis kietiklio, naudojant mechaninį maišytuvą. Vėliau buvo pradėtas kompozitų ruošimas pjaustant stiklo audinį 270 mm x 320 mm dydžio. Anksčiau paruoštas tirpalas vėliau buvo sustiprintas keturiais iš anksto supjaustyto stiklo sluoksniais, naudojant dervos vakuumo perdavimo metodą. Palyginimo tikslubuvo paruošta švari partija be jokių FCNT, o vidutinis mėginių storis buvo pastovus $1 \pm 0,05$ mm. Pirminis kietinimas buvo atliktas infraraudonųjų spindulių lempa 80°C temperatūroje 8 valandas. Tada plokštės 6 valandas džiovinamos orkaitėje 80100ºC temperatūroje. Po to bandiniai buvo supjaustyti iki 25 mm x 270 mm matmenų tempimo bandymams pagal ISO 527-2 ir smūgiui vertinti su 80 mm x 80 mm bandiniais.

1.1 lentelė. Stiklo pluošto / epoksidinė dervos sluoksniuotos medžiagos nanokompozitinių plokščių kodai.

Bandinio kodas	FGCE 0	FGCE 1	FGCE 2	FGCE 3	FGCE 4	FGCE 05	FGCE 6	FGCE 7	FGCE 8
CNT masė, %)	0	0.05	0.15	0.20	0.25	0.30	0.35	0.40	0.45
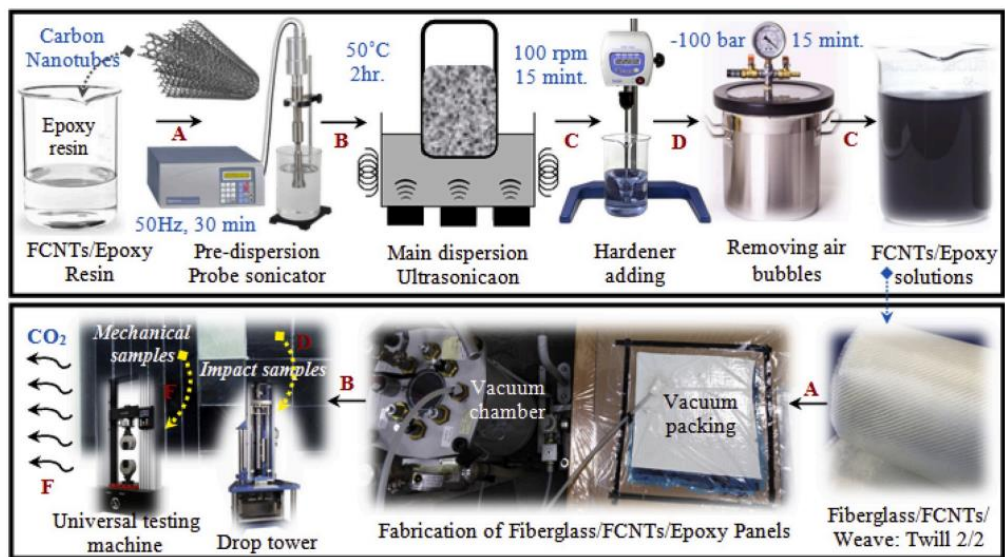
1.1 pav. Kompozitinio laminato su nano užpildais paruošimo schema

Smūgio bandymas buvo atliktas Coesfeld Magnus 1000 didelio greičio smūginių bandymų sistema naudojant 5,129 kg plieninį muštuvą su 20 mm skersmens sferiniu antgaliu. Visa įrangos konstrukcija atitiko ISO 6603-2. Bandymai buvo atliekami esant pastoviai 50 J smūgio energijai, kambario temperatūrai ir 4 m/s kritimo greičiui. Bandinys buvo tvirtinamas pneumatiniu laikikliu, taip sumažinant praslydimo galimybę bandymo metu. Bandymo rezultatas – smūgio jėgos signalas ir prieš pat kontaktą išmatuotas momentinis smūgio greitis. Poslinkio kitimas laike gaunamas kelis integruojant jėgos signalo rezultatus, padalintus iš muštuvo masės. Suintegruota jėgos ir poslinkio priklausomybė laikoma smūgio energija.

Siekiant ištirti FCNT įtaką pažeidimų formavimosi raidai ir kompozitinio laminato mechaninei elgsenai, sudarytas ir validuotas skaitmeninis baigtinių elementų modelis (1.2 pav.) panaudojant komercinį LS-DYNA paketą. Kompozitinis laminatas buvo modeliuojamas naudojant 4 mazgų, 1 mm dydžio kevalinius elementus. Laminato matmenys, įtvirtinimas ir apkrovimo sąlygos atitinka eksperimentuose buvusias sąlygas. Kompozito laminato sluoksniai apibrėžiami integravimo taškais, sluoksnio storiu ir pluošto orientacija naudojant „Part_Composite" komandas [59]. Smūgis buvo imituojamas 4 m/s greičiu krintančiu standžiu sferos formos paviršiaus kūnu, sveriančiu 5,129 kg. Sąveika tarp standaus muštuvo ir bandinio paviršiaus modeliuota naudojant „Contact_Automatic_Nodes_To_Surface". Kompozito pažeidimas buvo modeliuojamas naudojant Chang-Chang irimo kriterijų [64]. Medžiagos modelis apibrėžiamas 21 parametru, nusakančiu medžiagos tamprumo, stiprumo ir irimo charakteristikas (1.2 lentelė).
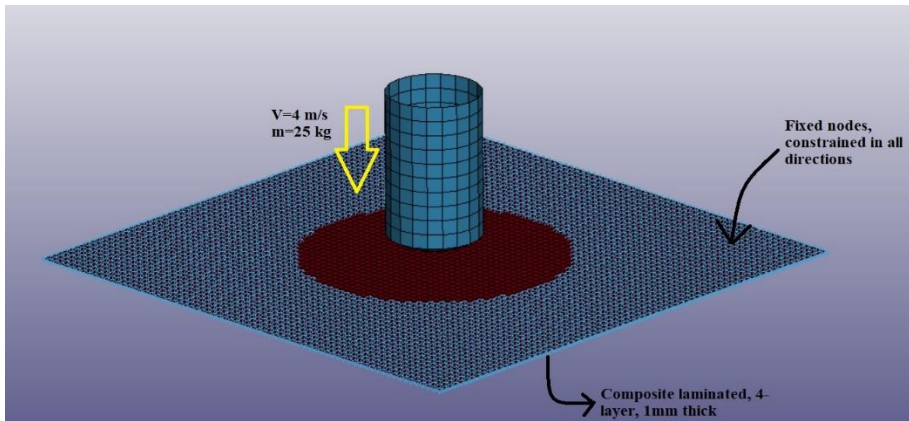
1.2 pav. Baigtinių elementų modelis kompozitų smūginių bandymų analizei su programa LS-DYNA

Rezultatai ir aptarimai

Nanoužpildai nepadidino trūkio deformacijos, tačiau buvo pastebėtas reikšmingas tamprumo modulio ir stiprumo padidėjimas (1.3 pav., a). Iš pradžių, pridėjus 0,05 masės % FCNT, stiprumas ir modulis padidėjo atitinkamai ~7% ir ~6% (palyginti su grynu mėginiu), o padidėjus 0,35 masės %, atitinkamai padidėjo iki 30% ir 31%. Koncentracijos, viršijančios 0,35 % masės, smarkiai sumažina stiprumą ir modulį dėl aglomeracijos. Galima daryti išvadą, kad nors FCNT priedai turi teigiamą efektą, tačiau dideliu mastu vienodo pasiskirstymo procesas gali būti sunkiai įgyvendinamas, ir tai laikoma trūkumu.

Iš smūginės apkrovos charakteristikų pateiktų 1.3 pav.,b, matyti, kad visuose bandiniuose jėga pastoviai didėja, iki pasiekia didžiausią smūgio jėgos vertę. Pasiekus maksimalią apkrovą, staiga atsiranda pažaida, po to vėl didėja smūgio jėga, kol pasiekiamas mažesnis už ankstesnį maksimumas, po kurio jėga tolygiai mažėja. Pirmoji smailė atitinka didžiausią bandinių patiriamą smūginę apkrovą, o antroji smailė – lūžio momentą. Kaip matyti iš paveikslo, pridėjus FCNT, labai pagerėja smūginis atsparumas. Pridėjus FCNT 0,35 % masės, smūgio jėga padidėjo nuo 2,13 kN iki 2,80 kN, t. y. ~31%. Tam galimai turėjo įtakos nanoužpildų teigiamas poveikis tarpsluoksnio stiprumui, kas buvo matoma atlikus SEM nuotraukų analizę. Tačiau didesnis masės % sukuria aglomeraciją, ir laukiamo efekto nematyti. Patobulinimas taip pat gali būti siejamas su nanovamzdelių funkcionalizavimu, kuris sukuria gerą ryšį tarp nanovamzdelio paviršiaus ir epoksidinės dervos [38,67].
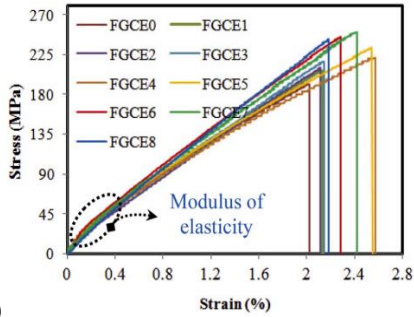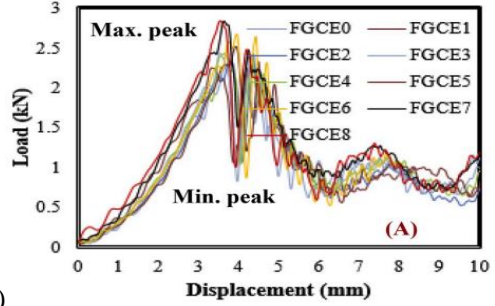
(a)　　　　　　　　　　　　　　　　(b)

1.3 pav. a) įtempių ir deformacijų priklausomybė statinio tempimo bandymu; b) jėgos ir
įlinkio priklausomybė veikiant smūginei apkrovai

Skaitinio modeliavimo ir eksperimentinių rezultatų palyginimas (1.4 pav.)
parodo, kad nustatyti medžiagos tamprumo ir stiprumo parametrai leidžia
prognozuoti pažaidos susidarymo momentą, tačiau irimo kriterijaus ir pažeidimo
augimo parametrai turėtų būti kalibruojami papildomai. Šlyties įtempių
pasiskirstymas (pažymėtas raudonai) paveiksle (1.4 pav., b) gali būti vertinamas kaip
dalinis įtrūkimų susidarymas bandinyje dėl smūginės apkrovos. Taigi, sukurtas
paprastas skaitmeninis modelis gali nesunkiai numatyti kompozitinio laminato elgesį
esant smūgiui. Šis modelis gali būti kalibruojamas pagal eksperimentines sąlygas,
siekiant ištirti poveikį ir nustatyti įvairių medžiagų savybių poveikį smūgio sukelto
pažeidimo raidai.
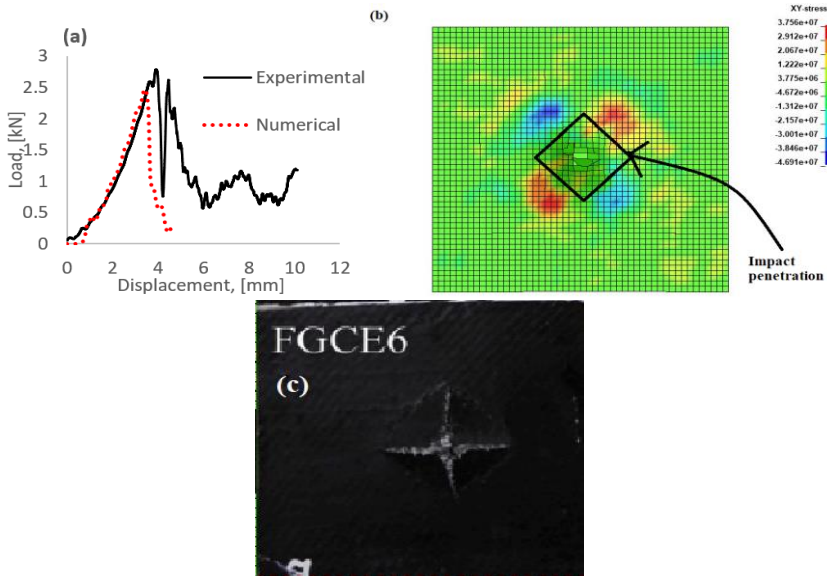
1.4 pav. Smūginio bandymo rezultatai: a) apkrovos -poslinkio kreivė, b) modelio šlyties
įtempių pasiskirstymas (BEA rezultatas), c) pažeidimo vaizdas (eksperimentinis rezultatas).

2. Didelio smūginio atsparumo stiklo pluoštu armuotų kompozitų su funkcionalizuotu grafenu eksperimentiniai ir skaitiniai tyrimai

Darbe naudojamas grafenas (GA) buvo susintetintas naudojant žemoje temperatūroje besiplečiantį grafitą kaip žaliavą [14]. Funkcionalizuoto grafeno gavimo procesas paminėtas [62, 68-69], toks pat metodas buvo pritaikytas ir šiame tyrime, norint gauti vienodą FGA dispersiją epoksidinėje dervoje ir išvengti aglomeracijos. FGA koncentracijos 0.05, 0.1, 0.15, 0.2, 0.25, 0.3, 0.35, 0.4 % epoksidinės dervos masės buvo išsklaidytos acetone veikiant garso bangai 1 val. 50 kHz dažniu [34].

Smūginių bandymų sąlygos ir skaitmeninis modeliavimas buvo identiškas 1 skyriuje aprašytai metodikai.

2.1 lentelė. FGEC kompozitinių laminatų bandinių kodai

Bandinio kodas	FGGE0	FGGE1	FGGE2	FGGE3	FGGE4	FGGE5	FGGE6	FGGE7
FGA (masė %)	0	0.05	0.15	0.20	0.25	0.30	0.35	0.40

Rezultatai ir aptarimai

Statinio tempimo ir smūginio bandymo rezultatai pateikti 2.1 pav. FGGE0, FGGE1, FGGE2, FGGE5 ir FGGE7 bandiniai nepasižymėjo reikšmingu stiprumo pagerėjimu. FGGE7 atveju dėl aglomeracijų stiprumas ir deformacija buvo mažesni nei kituose tirtuose bandiniuose, net mažesni nei FGGE0. Pagal charakteristikas buvo išskirti trys bandiniai – FGGE3, FGGE4 ir FGGE6, kurių stiprumas padidėjo 18%, palyginti su FGGE0, FGGE6 atveju deformacija padidėjo 16%. Tai vėlgi pasakytina apie FGGE3, kuris pasižymėjo panašiu deformacijos padidėjimu, tačiau stiprumas išliko nepakitęs. FGGE4 stiprumas padidėjo 14%, o deformacija 23%. Tai parodo, kad dėl pagerėjusio sukibimo tarp matricos ir audinių daugiau energijos išeikvojama pažeidimo mechanizmams. Įvertinus ir SEM analizės rezutatus galima teigti, kad sutvirtinimas „per storį" nanoužpildais prisideda prie kompozitų atsparumo smūgiams ir stiprumo padidėjimo. FGGE0 atveju maksimali smūgio jėga 2,81 kN, o FGGE6 su 0,35 % masės 4,78 kN, t. y. padidėjimas net 70 proc.

(a)

(b)
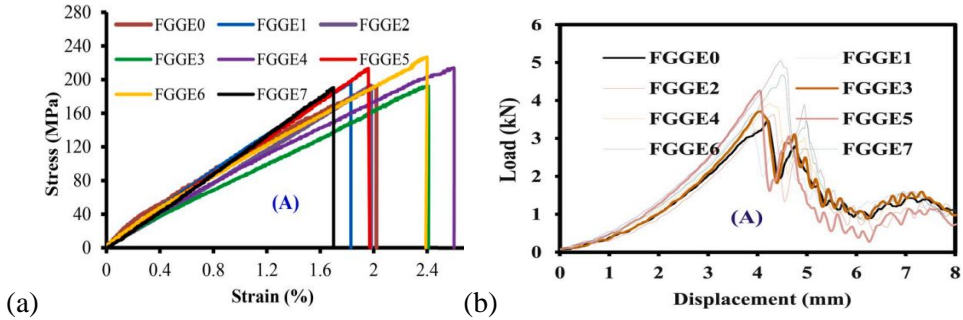
2.1 pav. a) Įtempių ir deformacijų priklausomybė statinio tempimo bandymu; b) jėgos ir įlinkio priklausomybė veikiant smūginei apkrovai

Skaitmeninių tyrimų metu buvo pastebėta, kad medžiagos modelio ribinės deformacijos DFAILT, DFAILM ir DFAILC (atitinkamai irimo deformacijos tempiant pluošto išilgine ir skersine kryptimis bei gniuždymo deformacijos) didžiąja dalimi daro įtaką rezultatui. Smūginiu eksperimentu ir skaitiniu modeliavimu gauti laminato pažeidimo panašūs vaizdai 2.2 pav., b, c, ir jėgos poslinkio kreivės leidžia teigti, kad sudaryti modeliai gana tiksliai atspindi eksperimentinius rezultatus ir gali būti naudojami detalesnei analizei bei smūginiam atsparumui prognozuoti.
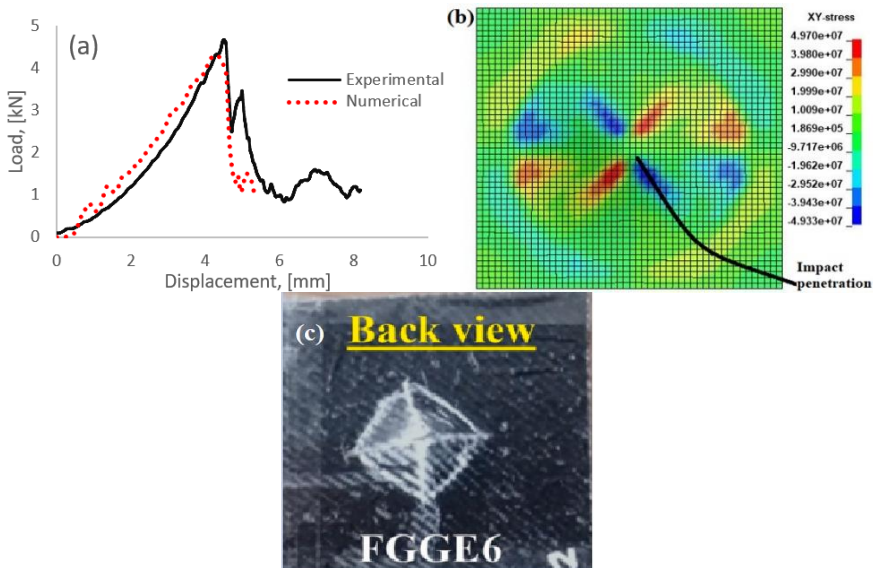
2.2 pav. Smūginio bandymo rezultatai: a) apkrovos-poslinkio kreivė, b) modelio šlyties įtempių pasiskirstymas (BEA rezultatas), c) pažeidimo vaizdas (eksperimentinis rezultatas)

3. Eksperimentiniai trapumo kontrolės kompozituose tyrimai

Panaudojant hibridizaciją t. y. keičiant kompozitinio laminato sluoksnių medžiagas bei kryptis, siekiama padidinti laminato smūginį atsparumą. Identiški bandymai atlikti su epoksidinės dervos ir termoplastikinės (PMMA) dervos kompozitiniais laminatais. Bandinių gamybai naudotos medžiagos įsigytos „R&G Faserverbunkwerkstoffe GmbH", Waldenbuch, Vokietija. Vienakrypčiai anglies audiniai (tankis 120 g/m^2), stiklo pluoštas „Panda™" (ruoželinis pynimas 2/2 ir svoris: 163 g/m2), epoksidinė derva, kurios pagrindą sudaro bisfenolis A ir jo kietiklis (modifikuotas cikloalifatinis poliaminas be alkilfenolio ir benzilo alkoholio). Metilmetakrilato derva (MMA: 617H119-Orthocryl) ir jos katalizatorius benzoilperoksidas (BPO: 617P37-Orthocryl), „Otto Bock", Vokietija.

Buvo pagaminti 6 kompozitinių laminatų rinkiniai, kurių kiekvienas pažymėtas kodais T-1, T-2, T-3, T-4, T-5 ir T-6. T-1 turi keturis anglies audinio sluoksnius, kurių audinio orientacija yra [0_c/90_c/90_c/0_c], T-2 turi keturis stiklo pluošto sluoksnius, orientacija [0_g/0_g/0_g/0_g], T-3 turi hibridinę sandarą su keturiais stiklo sluoksniais ir vienu anglies sluoksniu viduryje [0_g/0_g/0_c/0_g/0_g], visų trijų sandaroje yra epoksidinė derva. T-4, T-5 ir T-6 sandara yra tokia pati, kaip atitinkamai T-1, T-2 ir T-3, tačiau matrica yra PMMA. Epoksidinės dervos kompozito gamybos procesas išliko nepakitęs. PMMA derva buvo paruošta sumaišant MMA monomerą su BPO kaip iniciatoriumi laisvųjų radikalų polimerizacijoje, masės santykis 100:2 (MMA:BPO). Bandiniai po sukietėjimo buvo supjaustyti 80 mm x 80 mm matmenimis, kiekvienam kodui buvo priskirti 5 bandiniai.

Smūginio bandymo parametrai išliko tokie patys (50 J smūgio energija, esant 4 m/s smūgio greičiui), tačiau, siekiant ištirti hibridizacijos poveikį aukštesnėje temperatūroje, bandymai atlikti trijose skirtingose temperatūrose 25ºC, 60ºC ir 80ºC. Pažeidimo charakteristika, hibridinis efektas ir kiekybinis įvertinimas pasiekti pritaikius Naaman ir Jeong (1995) ir Grace ir kt. (1998) pasiūlytus energinius modelius [82-83], taikančius kriterijus, vadinamus plastiškumo indeksu (DI). Naamano ir Grace'o sukurtuose energiniuose modeliuose atsižvelgiama į suminę (E$_{total}$), tamprią (E$_{elastic}$) ir plastinę (E$_{in-elastic}$) energijas, kaip pateikta (1) ir (2) formulėse. Suminė energija E$_{total}$ susideda iš energijos, reikalingos bandinį deformuoti tampriai, ir iš plastinės energijos, kuri apima visus klasikinius pažeidimo mechanizmus, tokius kaip įtrūkimai, atsisluoksniavimas, atplėšimas ir pluošto ir dervos trūkimas (3.1 pav.). Medžiagų elgsena gali būti apibūdinama kaip trapi, kai DI pagal Grace yra mažesnis nei 69%, plastiška, kai DI didesnis nei 75%, ir pusiau plastiška, kai DI yra 70–74% [83].

$$DI\ (Naaman) = \frac{1}{2}\left(\frac{E_{total}}{E_{elastic}} + 1\right) \qquad (1)$$

$$DI\ (Grace's) = \frac{E_{in-elastic}}{E_{total}} \qquad (2)$$
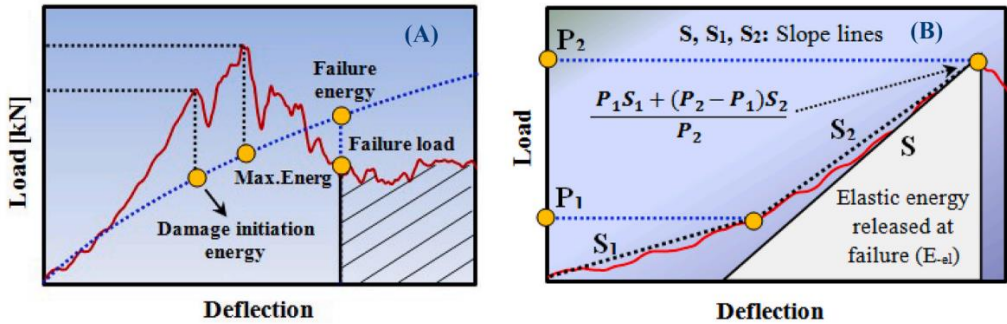
3.1 pav. a) smūginio bandymo jėgos ir poslinkio kreivė, b) tamprumo energijos įvertinimas Pagal anksčiau aprašytą metodiką atliktas ir skaitinis smūginio bandymo modeliavimas. Įvertinus medžiagų savybes, nustatytas laboratorijoje statinio deformavimo bandymais.

Rezultatai ir aptarimai

Smūginių bandymu metu gautos jėgos-poslinkio priklausomybės pateiktos 3.1 pav., a ir b. Kaip ir tikėtasi, anglies kompozitai (T-1, T-4) turi mažiausią atsparumą smūgiams, jų bandymo maksimali jėga, palyginti su stiklo pluoštu armuotais kompozitais (T-2, T-5), buvo net 6 kartus mažesnė. Hibridinių epoksidinės dervos kompozitų (T-3) smūginis stiprumas atitiko stiklo audiniu armuoto kompozito (T-2) stiprumą. Tačiau abu šie hibridiniai kompozitai buvo unikalūs savo apkrovos poslinkio kreivėmis, kaip matyti 3.2 paveiksle. Nors T-1 ir T-5 apkrova laipsniškai didėjo be jokio reikšmingo kritimo, kol pasiekė aukščiausią tašką prieš nukritimą, dėl daugelio pažeidimų mechanizmų, kurių kulminacija buvo plyšimas, T-3 ir T-6 turėjo aiškias tam tikras elastingumo ribas, po to buvo ribotas kritimas, ir vėl pasiekė maksimalią apkrovą, kuri ilgainiui vėl nukrenta ir baigiasi kompozitų plyšimu. Anglies pluošto įterpimas tarp stiklo audinio sluoksnių kompozitiniam laminatui suteikė pseudoplastiškumo. Atsparumą smūgiams apibūdina ne tik maksimalios smūginės apkrovos reikšmė, bet ir laminato smūginis tąsumas, padidinantis ir sugeriamos smūgio energijos reikšmę.
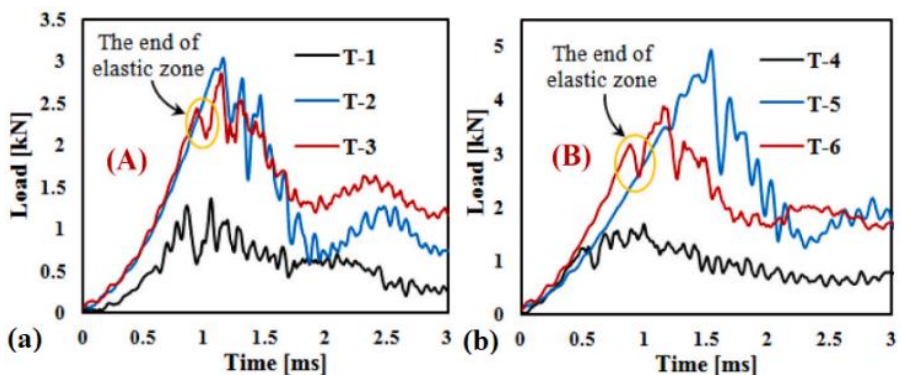
3.2 pav. Jėgos ir įlinkio priklausomybės veikiant smūginei apkrovai kambario temperatūroje: a) epoksidinės dervos kompozitiniai bandiniai, b) PMMA dervos kompozitiniai bandiniai

Temperatūros poveikio rezultatai maksimaliai smūginės jėgos reikšmei ir sugertai energijai pateikti 3.3 pav.
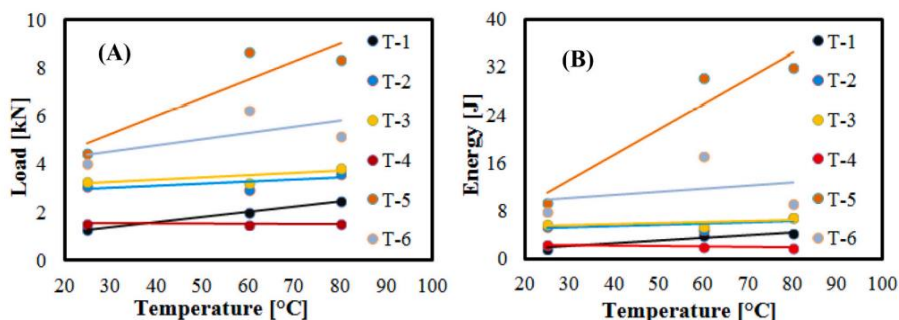
3.3 pav. Temperatūros įtaka smūginėms charakteristikoms: a) maksimalios jėgos reikšmės, b) suminė sugerta smūgio energija

Suminės sugertos energijos kiekius išskaidžius į tamprios ir plastinės deformacijos energijų komponentus (3.4 pav.) išryškėja, būtent tampriosios energijos komponentės augimas didėjant temperatūrai. Vadinasi, kambario temperatūroje energija buvo absorbuojama dėl anksčiau minėtų pažeidimo mechanizmų, o, kylant temperatūrai, didesnė energijos dalis buvo eikvojama tampriosioms laminato deformacijoms, o energijos komponentė priklausanti nuo pažeidimo formavimosi ir plitimo, išliko pastovi visame temperatūros ruože.

85
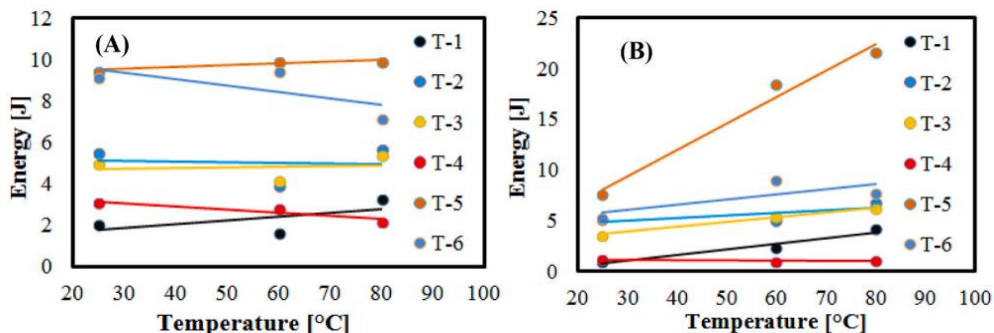
3.4 pav. Temperatūros įtaka plastinėms (a) ir tamprioms (a) deformavimo energijų komponentėms

Pagal energijos komponentus nustatyti Naaman (DI-Naaman) ir Grace'o (DI-Grace) plastiškumo indeksai didėjant temperatūrai sumažėjo. DI leidžia kiekybiškai įvertinti kompozitų sukaupiamą tampriosios energijos kiekį, ir šiuo aspektu Grace pasiūlytas indeksas yra jautresnis. Hibridiniai kompozitiniai laminatai (T-3 ir T-6) kambario temperatūroje pasižymėjo daliniu plastiškumu, nes abiejų DI buvo 6670 %. Stiklo pluošto kompozitai (T-2 ir T-5) kambario temperatūroje buvo trapūs, jų DI svyravo nuo 45–55%, o didėjanti temperatūra smarkiai padidina tamprios deformacijos energijos komponentės dalį. Šis aspektas turėtų būti detaliau nagrinėjamas.
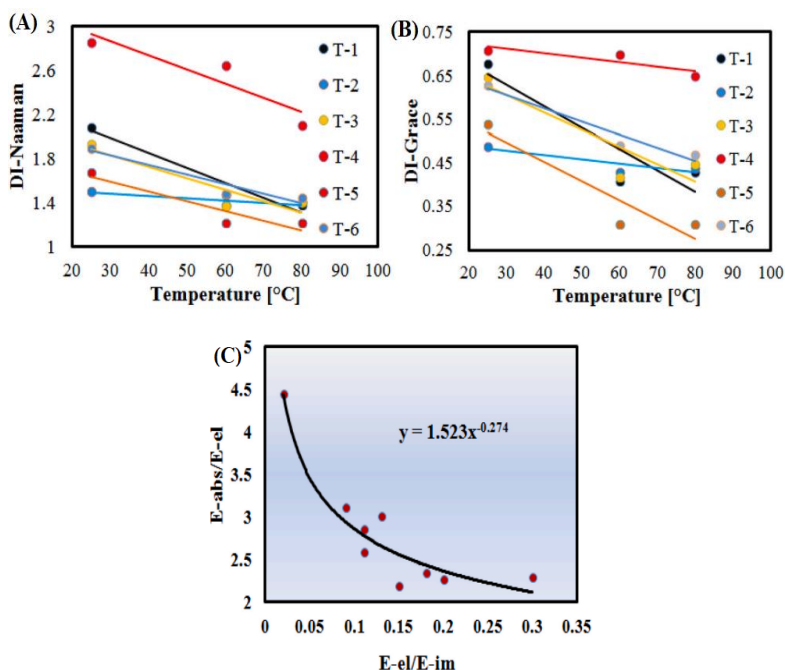
3.5 pav. Plastiškumo indeksų (DI) priklausomybės nuo temperatūros: a) DI-Naamano, b) DI-Grace'o, c) normalizuotas bandinių kambario temperatūroje grafikas

Šiame tyrime pritaikytas Foo ir kt. [85] empirinis energinis modelis (24), skirtas prognozuoti sugertos energijos kiekį sluoksniuotiems kompozitams mažo greičio smūgio metu. Modelis sieja bandinio normalizuotą sugertą energiją (E_{total}/E_{el}) ir normalizuotą smūginę energiją (E_{el}/E_{imp}) (3.5 pav., c), kur E_{imp} yra kritimo smūginė energija, šiuo atveju 50 J. Pagal šį empirinį ryšį, sugertos energijos kiekį būtų galima prognozuoti apskaičiavus tamprumo energijos dalį ir žinant smūginės energijos reikmę.

$$\frac{E_{total}}{E_{el}} = 1.52 * \left(\frac{E_{el}}{E_{imp}}\right)^{-0.27} \qquad (3)$$

Skaitmeninio modeliavimo, sudaryto pagal anksčiau aprašytas sąlygas, rezultatus (36 pav.) palyginus su eksperimentiniais tyrimais, gautas priimtinas sutapimas, leidžiantis skaitinius modelius naudoti smūgio metu atsirandančių pažeidimų kitimo analizei. Tangentinių įtempių, darančių įtaką atsisluoksniavimui, koncentracija leidžia nustatyti pažeidimo pradžios vietas ir stebėti kompozito laminato irimo seką.
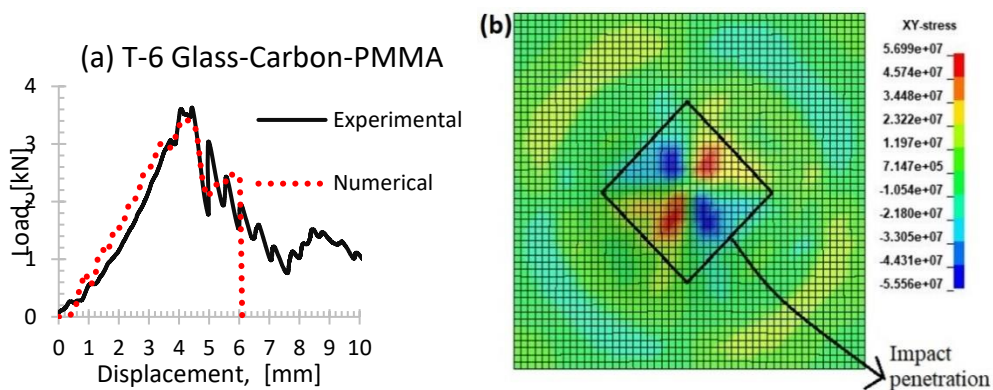
3.6 pav. Smūginio bandymo (T-6) (stiklo/anglies + PMMA laminatas) rezultatai: a) apkrovos-poslinkio kreivės, b) modelio šlyties įtempių pasiskirstymas (BEA rezultatas)

4. Polimerinių kompozitų tvarumas ir jų esminis vaidmuo keičiant vėjo energiją siekiant ekologiškos ateities

Yra trys kompozitų perdirbimo būdai, kuriuos galima suskirstyti į mechaninius, terminius ir cheminius [70-71]. **Mechaninis perdirbimas** apima susmulkintų kompozitų žaliavos naudojimą kaip antrines žaliavas. Šis procesas dar skirstomas į du subprocesus: pirmasis yra atliekų susmulkinimas į smulkius miltelius, o antrasis atliekų susmulkinimas / sutrupinimas, todėl perdirbta medžiaga bus naudojama kaip cemento užpildai / armavimo medžiagos cemente / betone. Šis metodas yra paprastas ir ekonomiškas, tačiau gautas galutinis produktas yra mažos vertės, nes pluoštas proceso metu pažeidžiamas ir negali suteikti ilgesnių pluoštų [72].

Terminis perdirbimas patenka į tris plačias kategorijas, t. y. pirolizę, sūkurinės pakuros perdirbimo procesą ir mikrobangų pirolizę. Pirmasis metodas apima pluošto atkūrimą naudojant inertines dujas, dervą skaidant į mažas organines molekules [73]. Antrasis metodas naudoja orą kaip suskystinimo dujas sūkurinės pakuros reaktoriuje, kad suskaidytų matricą naudojant aukštos temperatūros oro šilumos srautą, o taip susidariusi šiluma perdirba pluoštinę medžiagą [74]. Paskutiniu būdu kompozitinėje medžiagoje esanti derva skaidoma mikrobangų spinduliuote mikrobangų rezonatoriuje [75].

Cheminis perdirbimas – tai cheminių medžiagų naudojimas chemiškai modifikuoti arba skaidyti, kad atliekos būtų paverstos perdirbamomis medžiagomis. Superkritinio skysčio metodas ir solvolizė yra du pagrindiniai metodai, susiję su cheminio apdorojimo metodu. Pirmasis metodas reiškia būseną, kai skysčio temperatūra ir slėgis viršija kritinę temperatūrą ir slėgį, ir šiame etape skystis gali skaidyti polimero atliekas, kur vanduo arba alkoholis yra naudojami kaip terpė skaidyti [76]. Antrasis metodas, t. y. solvolizė, apima polimero depolimerizaciją, naudojant chemines tirpiklio savybes kaitinimo sąlygomis [77].

Alternatyvūs perdirbimo būdai: Kadangi ankstesni metodai buvo susiję su termoreaktyviųjų dervų perdirbimu, kurį riboja jų komercinis panaudojimas dideliu mastu, termoplastikai gali apriboti termoreaktingų dervų perdirbimo mastą [78]. Vėjo turbinų sektoriuje 40% vėjo turbinų menčių sąnaudų sudaro darbo sąnaudos, o šios sąnaudos yra susijusios su ciklo trukme, todėl, termoreaktingas dervas pakeitus termoplastikais, atsirastų galimybė sutrumpinti ciklo laiką [79]. Termoplastiką galima pertvarkyti naudojant šilumą, taip užtikrinant techninę priežiūrą nepabloginant medžiagos savybių [30]. Tuo remiantis šiame tyrime PMMA buvo priimtas kaip epoksidinės dervos pakaitalas, o jo savybės buvo lyginamos su epoksidine derva.

5. Hibridizacijos ir sluoksnių banguotumo poveikis polimerinių kompozitų stiprumui: eksperimentinis ir skaitmeninis tyrimas

Tikslas – eksperimentiškai nustatyti pluošto banguotumo įtaką kompozitinio laminato mechaninėms savybėms, sudaryti validuotus skaitinius modelius, leidžiančius analizuoti pažeidimų formavimąsi ir mechaninę elgseną smūginių apkrovų atveju.

Panaudojant rankinį-vakuuminį formavimo metodą buvo pagaminti penki rinkiniai (5.1 pav.), bandinių su pluošto banguotumu (5.1 lentelė). Mechaninės savybės nustatytos statinio lenkimo bandymu pagal EN ISO 14125:1998. Bandinių grupės pažymėtos: T-1, T-2 neturinčios banguotumo, T-3, T-4, T-7, T-8 turinčios neplokštuminį (statmenai laminato paviršiui) banguotumą, T-9 ir T-10 turinčios banguotumą plokštumoje.
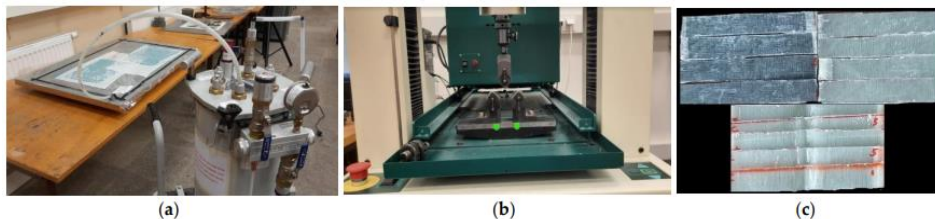
5.1 pav. a) Kompozitinių plokščių paruošimas rankinio-vakuuminio formavimo būdu. b) lenkimo bandymo vaizdas, c) bandinių lenkimui nuotrauka

5.1 lentelė. Kompozitų laminatų tritaškiam lenkimui sandara

Bandinio kodas	Simbolis	Sandara	medžiaga	Pluošto orientacija	Derva
T-1		⬤⬤⬤⬤⬤⬤⬤⬤	Stiklas	Vienakryptis	Epoksidas
T-2		⬤⬤⬤⬤●⬤⬤⬤	Stiklas ir anglis	Vienakryptis	Epoksidas
T-3/T-9		⬤⬤⬤⬤⬤⬤⬤	Stiklas	Vienakryptis	Epoksidas
T-4/T-10		⬤⬤⬤⬤⬤⬤⬤⬤	Stiklas	Vienakryptis	Epoksidas

T-5	Stiklas Anglis	●●●●●●●●	Stiklas	Vienakryptis	PMMA
T-6		●●●●○●●●	Stiklas ir anglis	Vienakryptis	PMMA
T-7		●●●●●●●●	Stiklas	Vienakryptis	PMMA
T-8		●●●●●●●●	Stiklas	Vienakryptis	PMMA

5.2 lentelė. Kompozito bandinių savybės skaitmeniniam modeliavimui. XT: stiprumas tempiant (išilgai pluošto); XC: stiprumas gniuždant (išilginis); YT: stiprumas tempiant (skersinis); YC: stiprumas gniuždant (skersinis); SL: stiprumas šlyčiai

Dervos tipas	E_1 [GPa]	E_2 [GPa]	G_{12} [GPa]	ν_{12}	X_T [MPa]	X_C [MPa]	Y_T [MPa]	S_L [MPa]	Y_C [MPa]
Epoksidas / stiklas	32,4	8,1	2,6	0.22	680	600	35	37	35
Epoksidas / anglis	63	40	9	0.16	709	473	34	146	199
PMMA/stiklas	23,16	2,1	2,62	0.38	325	246	16	42	128
PMMA/anglis	47	3	1,8	0.13	1300	882	15	40	120

Skaitiniu modeliavimu (5.2 pav.) banguotumas įvertintas pakitusiomis mechaninėmis savybėmis, kurios buvo nustatytos statiniais bandymais ir kalibruotos naudojant tritaškio lenkimo eksperimentinius rezultatus. Baigtinių elementų modelio matmenys, apkrovos, įtvirtinimai atitiko eksperimentines sąlygas. Apkrova mazguose buvo nustatyta naudojant komandą „Boundary_SPC_SET". Pažeidimas modeliuotas naudojant Chang-Chang irimo kriterijų [64]. Atlikus parametrinę jautrumo analizę, nustatyta, kad rezultatams didesnį poveikį turėjo tik pluošto ir matricos irimo deformacijos, t. y. atitinkamai DFAILT ir DFAILM.
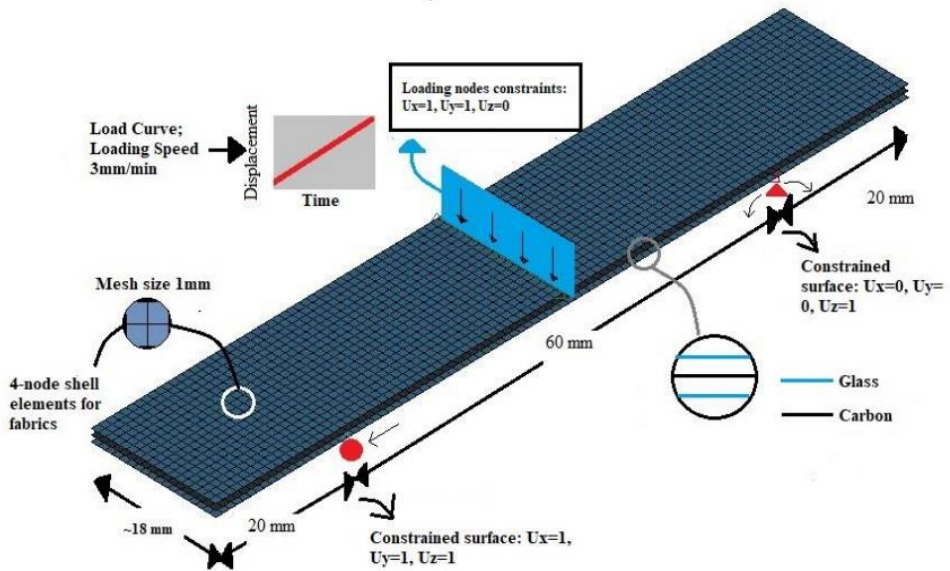
5.2 pav. Baigtinių elementų modelis tritaškio lenkimo bandymo simuliacijai

Rezultatai ir aptarimai

Tritaškio lenkimo bandymų jėgos-poslinkio diagramos pateiktos 5.3 pav. Kaip matyti, visuose tirtuose mėginiuose tiek epoksidiniai, tiek PMMA bandiniai turėjo panašius lenkimo atsakus. Bandinių T-9 ir T-10 turinčių banguotumą plokštumoje, šaknies bangos kampas yra atitinkamai ~15° ir ~35°. Jų stiprumas lenkiant buvo didžiausias iš tirtų.
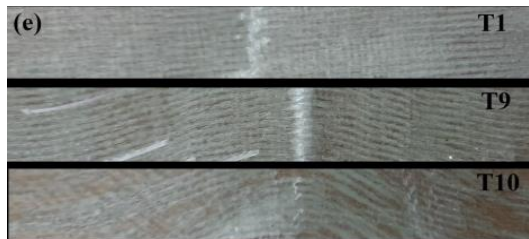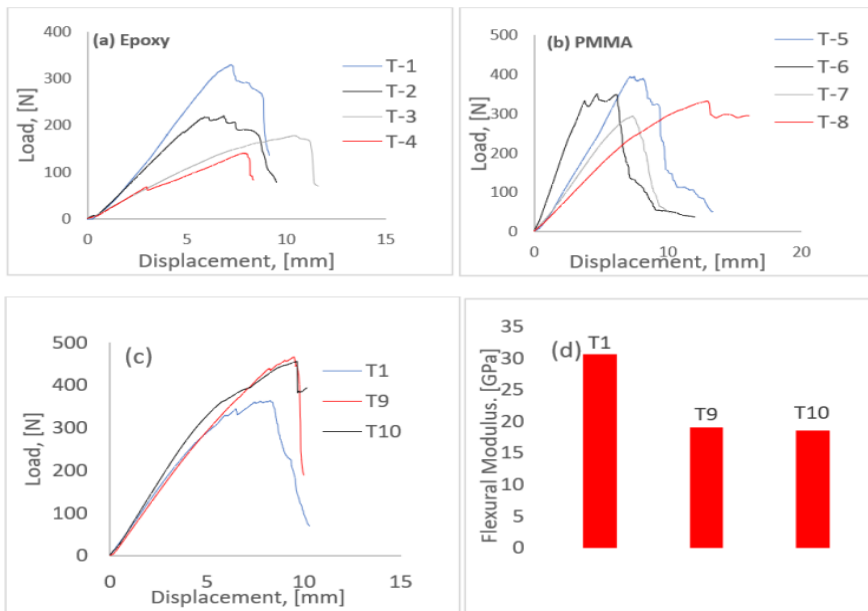
5.3 pav. Tritaškio lenkimo bandymų jėgos-poslinkio diagramos a) bandiniai su epoksidine derva, b) bandiniai su PMMA derva, c) bandiniai su banguotumu plokštumoje ir epoksidine derva, d) bandinių su banguotumu plokštumoje lenkimo modulio reikšmės, e) bandiniai po bandymo (banguotumas plokštumoje)

Stiprumas ir tamprumo modulis lenkiant buvo nustatyti pagal standarto EN ISO 14125:1998 reikalavimus:

$$\sigma_F = \frac{3FL}{2bd^2} \qquad (4)$$

$$E_F = \frac{L^3}{4bd^3}\left(\frac{\Delta F}{\Delta s}\right) \qquad (5)$$

čia F, L, b, d, ir Δs atitinkamai yra lenkimo jėga, atstumas tarp atramų, plotis, aukštis ir įlinkis nuo apkrovos ΔF. Vidutiniai penkių bandinių rezultatai pateikti 5.4 pav. Esant banguotumui statmenai paviršiui, gaunamas stiprumo lenkiant sumažėjimas.
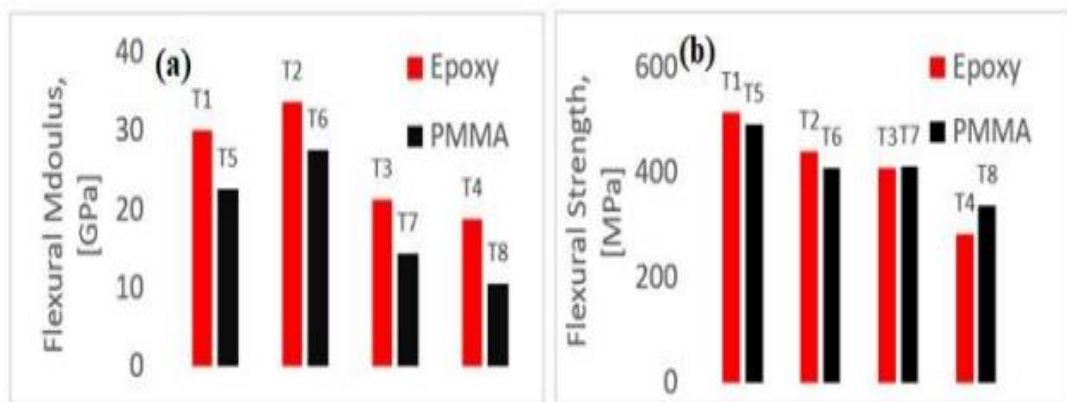
5.4 pav. Tritaškio lenkimo bandymo suvidurkinti rezultatai a) lenkimo modulio kitimas, b) stiprumo lenkiant kitimas

6. Eksperimentinis sluoksniuotų kompozitų su banguotumu plokštumoje atsparumo smūgiams tyrimas

Naudojant tas pačias gamybos sąlygas paruošti keturi bandinių rinkiniai (6.1 lentelė). Bandiniai keturių sluoksnių, 1 mm storio. G-1 pagamintas iš stiklo pluošto audinio (2/2 ruoželinio pynimo), kurio savitasis svoris 163 g/m². G-2, G-3 ir G-4 vienkryptis stiklo pluoštas 200 g/m². Smūgio energija - 50 J, jos pakako, kad kiekvienas bandinys būtų pramuštas.

6.1 lentelė. Pluošto struktūros elementai

Bandinio kodas	Medžiaga	Pluoštas	Sluoksniai	Derva	Pastabos
G-1	Stiklas	Pintas	[0/0/0/0]	Epoksidas	Be banguotumo
G-2	Stiklas	Vienakryptis	[0/90/90/0]	Epoksidas	Be banguotumo
G-3	Stiklas	Vienakryptis	[0/0/0/0]	Epoksidas	Banguotumas plokštumoje
G-4	Stiklas	Vienakryptis	[0/0/0/0]	Epoksidas	Be banguotumo

Rezultatai ir aptarimai

Tipinės jėgos poslinkio kreivės ir bandinių po smūginio eksperimento nuotraukos pateiktos 6.1 pav.

(a) Woven GF 2/2 twill (G-1)

(b)

(b) UD GF [0/90]$_S$ (G-2)

(d)

(e) UD GF [0]$_4$ Low waviness (G-3)

(f)
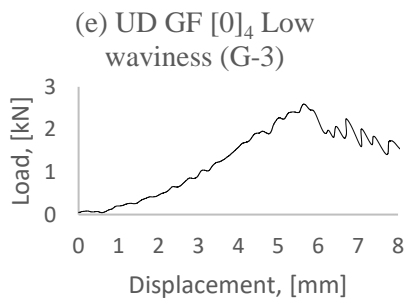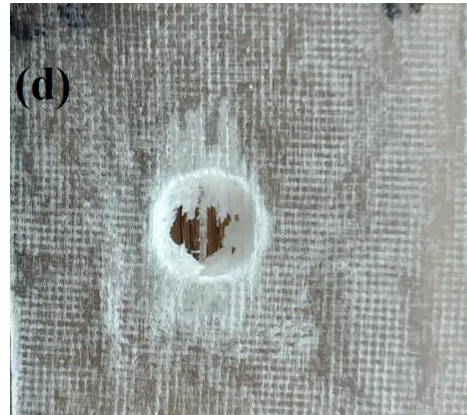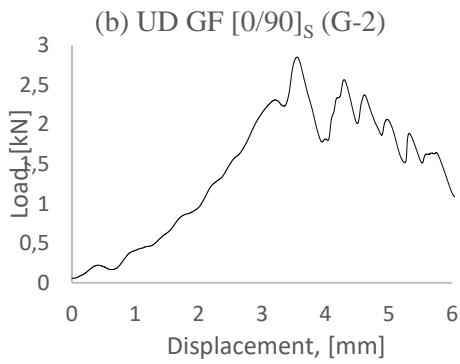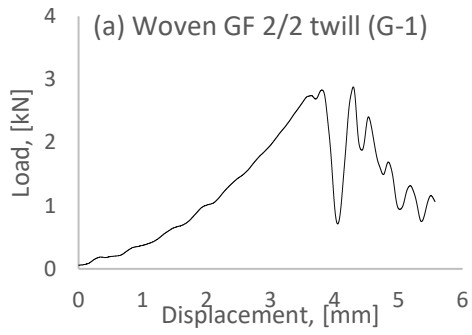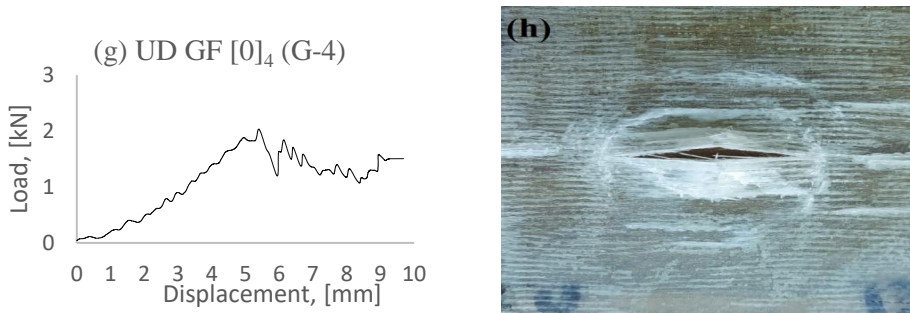
6.1 pav. Smūginių bandymų rezultatai apkrovos-poslinkio kreivės ir suirimo forma: a, b) G-1 stiklo audinys, c, d) G-2 vienakryptis stiklo pluoštas [0/90]$_S$, e, f) G-3 vienakryptis stiklo pluoštas su banguotumu plokštumoje [0]$_4$,g, h) G-4 vienakryptis stiklo pluoštas [0]$_4$

Didžiausia smūgio apkrova ($F_{max} = 2,8$ kN) pasiekiama esant stiklo audiniu armuotam kompozito laminatui, o gautas rombo formos suirimas yra būdingas audinio struktūrai. Šiuo atveju pagrindinis energijos išsklaidymo šaltinis smūgio metu yra elastinė deformacijos energija, kuri bandinį įlenkia iki 3,6 mm, vėliau formuojasi rombo formos pažeidimas. Visų bandinių pažeidimų formos skyrėsi.
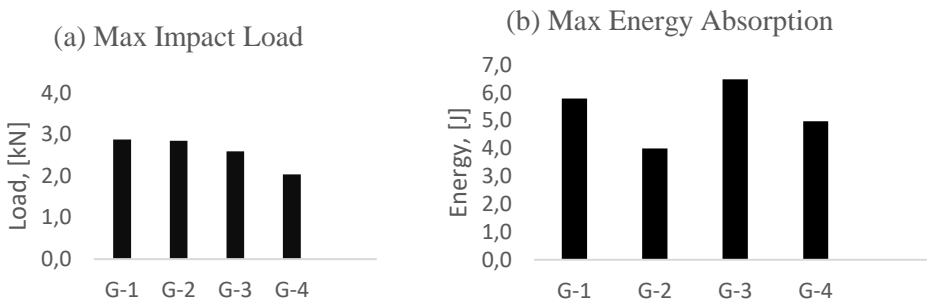
6.2 pav. Smūginių bandymų charakteristikos a) maksimalios smūginės jėgos kitimas, b) maksimalios sugertos energijos kitimas

Pseudo-plastiškumo efektą vienkrypčiam kompozitui galima suteikti panaudojant plokštuminį banguotumą ir taip padidinant šlyties modulį plokštumoje [88] bei pagerinant vienakrypčių kompozitų smūginį atsparumą. Šis efektas buvo pastebėtas tritaškio lenkimo atveju atliekant ankstesnius bandymus ir pasitvirtino esant smūginei apkrovai, kurios metu tirtu atveju dominuoja lenkimo reiškiniai [61]. Lyginant maksimalią smūgio jėgą, bandiniai su banguotumu plokštumoje (G-3) pasižymėjo 20 % didesne jėga nei tokie patys bandiniai su tiesiu pluoštu (G-4), tačiau smūgio jėga buvo mažesnė nei bandinių armuotu audiniu arba turinčių 0 ir 90 laipsnių pluošto kryptis (6.2 pav., a). O bandiniai su banguotumu plokštumoje (G-3) sugėrė daugiausiai smūgio energijos palyginti su likusiomis trimis bandinių grupėmis. Dėl padidėjusių šlyties parametrų galima numatyti, kad, esant storesniam bandiniui, smūginio atsparumo efektas būtų dar didesnis.

7. IŠVADOS IR PASIŪLYMAI ATEITIEMS TYRIMAMS

Remiantis šio tyrimo pradžioje išdėstytais 6-iais uždaviniais, iš penkių mokslinių tyrimų darbų, susijusių su šia daktaro disertacija, santraukos galima padaryti tokias išvadas:

1 Nanoužpildai naudojant funkcionalizuotus anglies nanovamzdelius (FCNT) ir funkcionalizuotą grafeną (FGA) leido sustiprinti sluoksniuotą kompozitą „per storį". FCNT padidino stiklu armuotų kompozitų mechaninį ir smūginį stiprumą. Nustatyta, kad 0,35 % epoksidinės dervos masės atžvilgiu pakako mechaniniam stiprumui padidinti 30 %, o smūginiam stiprumui 31 %. Buvo pastebėta, kad panaudojus FGA (geriausias masės procentas buvo nuo 0,2 iki 0,35 % masės), 18% padidėjo stiprumas, bet ir kartu labai padidėjo irimo deformacija. Didžiausias nustatytas stiprumo padidėjimas buvo 23%, o smūginis atsparumas padidėjo 70%. Taigi buvo pastebėta, kad nanoužpildai padidina tiek statinį stiprumą tempiant, tiek smūginį atsparumą.

2 Sluoksniuotų kompozitų su epoksidine derva ir PMMA smūginis atsparumas panašus. Tačiau pastebėta, kad kompozitai su PMMA aukštesnėje temperatūroje pasižymi geresnėmis savybėmis dėl dominuojančios elastinės-plastinės deformacijos ir pastebimų mažesnių pažeidimų (esant vienodoms sąlygoms PMMA laminatas nebuvo pramuštas). Hibridinis efektas abiem atvejais buvo pasiektas kambario temperatūroje, tačiau buvo prarastas esant aukštesnei temperatūrai.

3 Hibridinis poveikis buvo kiekybiškai įvertintas vadinamuoju plastiškumo indeksu. Buvo taikyti du Naamano ir Grace'o plastiškumo indeksai, abu rodė panašias tendencijas. Pagal Grace'ą, hibridinės architektūros kompozitų plastiškumo indeksas kambario temperatūroje buvo 66–70%, o kompozitų be hibridinės architektūros plastiškumo indeksas siekė 45%.

4 Lenkimo bandymais ištirtas pluošto banguotumo plokštumoje ir per storį poveikis. Pastebėta, kad banguotumas per storį turi neigiamą poveikį atsparumui lenkiant, o banguotumas plokštumoje pagerino stiprumo savybes.

5 Tiriant smūginį atsaką nustatyta, kad vienakrypčio stiklo pluošto kompozito banguotumas plokštumoje suteikia geresnį smūginį atsparumą, palyginti su laminatais, armuotais tiesiu pluoštu. Bandinių, turinčių banguotumą plokštumoje, savybės buvo artimos kompozitams, armuotiems audiniu.

6 Buvo sudaryti ir eksperimentiškai validuoti skaitmeniniai modeliai, leidžiantys prognozuoti sluoksniuoto kompozito pažeidimo inicijavimą ir plitimą statinės ir smūginės apkrovos metu. Nustatyta pluošto banguotumo

įtaka sluoksnio mechaninėms savybėms leido pritaikyti tipinių sluoksniuotų kompozitų modeliavimo metodiką prognozuojant banguotumo įtaką laminato mechaninei elgsenai smūginių apkrovų metu. Pastebėta, kad matricos savybes aprašantis irimo deformacijų parametras DFAILM turi svarią teigiamą įtaką laminato lenkimo savybėms ir smūginiam atsparumui. Tuo pagrindu buvo pagaminti bandiniai su pluošto banguotumu plokštumoje ir eksperimentiškai įsitikinta, kad pluošto banguotumas sukuria pseudo-plastiškumo efektą, pagerinantį sluoksniuoto kompozito smūginį atsparumą.

Pasiūlymai tolimesniems tyrimams

Šiame darbe pritaikyti metodai suteikė bendrą vaizdą apie nanoužpildų, kompozitų hibridazacijos ir pluošto banguotumo įtakas laminato smūginiam atsparumui. Sukurti ir validuoti skaitiniai modeliai leido matyti kompozito pluošto ir matricos savybių įtaką laminato mechaniniam atsakui į lenkimo ir smūgines apkrovas, bet, ieškant optimalių sprendimų, kai kurių parametrų poveikis turi būti ištirtas detaliau:

1. Pluošto banguotumas plokštumoje smarkiai pagerino laminato atsaką į statines lenkimo ir smūgines apkrovas. Tyrimų imtis vertinant banguotumo didumo įtaką yra ribota, todėl, siekiant gauti optimalaus banguotumo parametrus, reikia išplėsti eksperimentų skaičių.

2. Eksperimentai gali būti trijų krypčių – statinio lenkimo, nuovargio ir smūginės apkrovos. Išsamiai ištyrus banguotumo poveikį, būtų galima gaminti smūgiams atsparius kompozitus panaudojant paprastus technologinius sprendimus.

REFERENCES

[1] Djeghader D., Redjel B. Weibull analysis of fatigue test in jute reinforced polyester composite material. Comoposite Communications, Vol 17, 2020, pg. 123-128.

[2] Cheng J., Xu Y., Zhang W., Liu W. A review on the multi-scale simulation of Z-pinned composite laminates. Compos. Struct. Vol 295, 2022, 115834.

[3] Mostafa NH., Ismarrubie ZN., Sapuan SM., Sultan MTH. Effect of fabric biaxial prestress on the fatigue of woven E-glass/polyester composites. Materials and Design, Vol 92, 2016, pg. 579-589.

[4]Swolfs Y., Geboes Y., Gorbatikh L., Pinho ST. The importance of translaminar fracture toughness for the penetration impact behaviour of woven carbon/glass hybrid composites. Compos. Part A. Vol. 103, 2017, p. 1-8.

[5]Randjbaraa E., Zahari R., Jalil NAA., Majid LAA. Hybrid composite laminates reinforced Kevlar/carbon/glass woven fabrics for ballistic impact loading. Hindawi. Vol. 2014, 413753.

[6]Sadighi M., Alderliesten R. Impact fatigue, multiple and repeated low-velocity impacts on FRP composites: A review. Compos. Struct. Vol. 297, 2022, 115962

[7]Soliman EM., Sheyka MP., Taha MR. Low-velocity impact of thin woven carbon fabric composites incorporating multi-walled carbon nanotubes. Int. J. of Impact Eng. Vol. 47, 2012, pg. 39-47

[8]Jiang W., Jin X., Li H., Zhang S., Zhou T., Xie H. Modification of nano-hybrid silicon acrylic resin with anticorrosion and hydrophobic properties. Polym. Test. Vol.82, 2020, 106287.

[9]Pathak AK et.al. Improved mechanical properties of carbon fibre/graphene oxide-epoxy hybrid composites. Compos. Sci. and Tech. Vol. 135, 2016, pg. 28-38.

[10]Mouritz AP. Review of z-pinned laminates and sandwich composites. Composites Part A, Vol. 139, 2020, 106128.

[11]Avramov K., Uspensky B., Sakhno N., Nikonov O. Transient response of functionally graded carbon nanotubes reinforced composites conical shell with ring-stiffener under the action of impact load. European J. of Mechanics-A/Solids. Vol 91, 2022, 104429.

[12]Taraghi I., Fereidoon A., Taheri-Behrooz. Low-velocity impact response of woven Kevlar/epoxy laminated composites reinforced with multi-walled carbon nanotubes at ambient and low temperature. Materials and Design. Vol. 53, 2014, pg. 152-158.

[13]ASTM D 5045. Standard test methods for plane-strain fracture toughness and strain energy release rate of plastic materials. West Conshohocken, PA, USA: ASTM International; 2007.

[14]Yousef S., Mohamed A., Tatariants M. Mass production of graphene nanosheets by multi-roll milling technique. Tribol. Int. Vol. 121, 2018, p. 54-63.

[15]Keyte J., Pancholi J., Njuguna J. Recent developments in graphene oxide/epoxy carbon fibre-reinforced composites, Front. Mater. Vol. 6, 2019, 224.

[16]Hawkins DA., Haque A. Strain energy release rate and mode-I delamination growth in carbon-graphene /epoxy hybrid nanocompsoites. Procedia Eng. Vol. 105, 2015, p. 829-834.

[17]Zeng S., Shen S., Chen L., F. Lu Yang., Xue Y. Mechanical and thermal properties of carbon nanotubes- and graphene-glass fibre fabric-reinforced epoxy composites: a comparative study. Textil. Res. J. Vol. 89, 2019, p. 2353-63.

[18]Asaee Z., Mohamed M., Soumik S., Taheri F. Experimental and numerical characterisation of delamination buckling behaviour of a new class of GNP-reinforced 3D fibre-metal laminates. Thin-Walled Struct. Vol. 112, 2017, p. 208-216.

[19]Seretis GV., Kouzilos G., Manolakos DE., Provatidis CG. On the graphene nanoplatelets reinforcement of hand lay-up glass fabric/epoxy laminated composites. Compos, B Eng. Vol. 118, 2017, p. 26-32.

[20]Jia J., Du X., Chen C., Sun X., Mai YW., Kim JK. 3D network graphene interlayer for excellent interlaminar toughness and strength in fibre reinforced composites. Carbon, Vol. 95, 2015, p. 978-986.

[21]Deep A., Singh KK., Rawat P., Kumar C., Behera RP. Effect of nano and macro carbon fillers on flexural properties of glass/epoxy composite laminates. IOP Conf. Ser. Mater. Sci. Eng. Vol. 455, 2018, 012007.

[22]Dalina WADW., Tan SH., Mariatti M. Properties of fibreglass/MWCNT buckypaper/epoxy laminated compsites. Procedia Chemistry. Vol. 19, 2016, p. 935-942.

[23]Aly K., Li A. Bradford PD. In-situ monitoring of woven glass fibre reinforced composites under flexural loading through embedded aligned carbon nanotube sheets. J. Compos. Mater. Vol. 52, 2018, p. 2777-2788.

[24]Wang Y. et.al. Influence of temperature on the impact behaviour of woven-ply carbon fibre reinforced thermoplastic composites. Compos. Struct. Vol. 185, 2018, pg. 435-445.

[25]Yang B., Wang Z., Zhou L., Zhang J., Liang W. Experimental and numerical investigation of interplay hybrid composites based on woven fabrics and PCBT resin subjected to low-velocity impact. Comps. Struct. Vol. 132, 2015, p. 464-476.

[26]Hung P., Lau K., Cheng L., Leng J., Hui D. Impact response of hybrid carbon/glass fibre reinforced polymer composites designed for engineering applications. Compos. Part B. Vol 133, 2018, p. 86-90.

[27]Swolfs Y., Geboes Y., Gorbatikh L., Pinho ST. The importance of translaminar fracture toughness for the penetration impact behaviour of woven carbon/glass hybrid composites. Compos. Part A. Vol. 103, 2017, p. 1-8.

[28]Rijsijk Van K., Bersee HEN. Reactive processing of textile fibre-reinforced thermoplastic composites-an overview. Compos Part A, Vol.38, 2007, p.666-681.

[29]The composite institute facilities thermoplastic composite development for wind turbine blades through innovative project. IACMI, 2017, http://iacmi.org/2017/01/17/iacmi-composites-insitutefacilties-thermoplastic-composite-I-wind-turbine-blades-innovative-project/.

[30]Rijsijk Van K., et.al. Sustainable vacuum-infused thermoplastic composites for MW-size wind turbine blades-preliminary design and manufacturing issues. J. of Solar Ener. Eng. Vol. 127, 2005, p.570-580.

[31]Abrate S. Impact Engineering of Composite Structures. Springer, ISBN 978-3-7091-0522-1.

[32]Sun F., Yu T., Hu C., Li Y. Influence of functionalised graphene by grafted phosphorus containing flame retardant on the flammability of carbon fibre/epoxy resin (CF/ER) composite. Compos. Sci. Techno. Vol. 136, 2016, p. 76-84.

[33]Subadra SP., Yousef S., Griskevicius P., Makarevicius. High-performance fibreglass/epoxy reinforced by functionalised CNTs for vehicle applications with less fuel consumption and greenhouse gas emissions. Polymer Testing. Vol. 86, 2020, 106480.

[34]Yousef S., Subadra SP., Griskevicius P., Varnagiris S., Milcius D., Makarevicius V. Superhydrophilic functionalized graphene/fibreglass/epoxy laminates with high mechanical, impact and thermal performance and treated by plasme. Polymer Testing, Vol 90, 2020, 106701.

[35]Subadra SP., Griskevicius P., Yousef S. Low velocity impact and pseudo-ductile behaviour of carbon/glass/epoxy and carbon/glass/PMMA hybrid composites laminated for aircraft application at service temperature. Polymer Testing. Vol. 89, 2020, 106711.

[36]Subadra SP., Griskevicius P. Sustainability of polymer composites and its critical role in revolutionising wind power for green future. Sustain. Technol. Green Econ. Vol. 1, 2021, pg. 1-7.

[37]Subadra SP., Griskevicius P. Effect of hybridisation and ply waviness on the flexural strength of polymer composites: An experimental and numerical study. Polymer. Vol. 14, 2022, 1360.

[38]Ranjbar M., Feli S. Mechanical and low-velocity impact properties of epoxy-composite beams reinforced by MWCNTs. J. Compos. Mater. Vol. 53, 2018, p. 693-705.

[39]Adeniyi AG., Onifade DV., Ighalo JO., Adeoye AS. A review of coir fibre reinforced polymer composites. Comos. B Eng. Vol. 176, 2019. 107305

[40]Korkiakoski S., Brondsted P., Sarlin E., Saarela O. Influence of specimen type and reinforcement in measured tension-tension fatigue life of unidirectional GFRP laminates. Int. J. Fatig. Vol. 85, 2016, pg: 114-129.

[41]Antoniou A., Mikkelsen LP., Goutianos S., Bagemiel O., Gebauer I., Flindt R., Sayer F. Influence of the glass non-crimp fabric intrinsic undulation on the stiffness of the composite ply: A micromechanical approach. IOP Conf. Ser.: Mater. Sci. Eng. 942, 2020. 012017.

[42]Liu H., Zhang Z., Jia H., Liu Y., Leng J. A modified composite fatigue damage model considering stiffness evolution for wind turbine blades. Compos. Struct. Vol. 233, 2020, 111736.

[43]Moriniere FD. Low-velocity impact on fibre-metal laminates. PhD Thesis, TU Delft. Link: https://doi.org/10.4233/uuid:022e1a88-f48e-493e-805e-014f396a05dc

[44]Dubary N., Taconet G., Bovet C., Vieille B. Influence of temperature on the impact behaviour and damage tolerance of hybrid woven-ply thermoplastic laminates for aeronautical applications. Compos. Struct. Vol. 168, 2017, pg. 663-674.

[45]Vieille B., Casado VM., Bouvet C. Influence of matrix toughness and ductility on the compression-after-impact behaviour of woven-ply thermoplastic- and thermosetting- composites: A comparative study. Compos. Struct. Vol. 110, 2014, pg. 207-218.

[46]Boumbimba RM. et.al. Glass fibres reinforced acrylic thermoplastic resin-based tri-block copolymers composites: Low velocity impact response at various temperatures. Compos. Struct. Vol. 160, 2017, pg. 939-951.

[47]Rojstaczer S., Cohen D., Marom G. Thermal expansion of Kevlar fibres and composites. J Mater Lett. Vol. 4, 1985, 1233.

[48]Yousef S., Tatariants M., Tichonovas M., Kliucininkas L., Lukosiute SI., Yan L. Sustainable green technology for recovery of cotton fibres and polyster from textile waster. J. Clean. Prod. Vol. 254. 2020, 120078.

[49]Hayashi T., Koyama K., Yamazaki A., Kihira M. Development of new material properties by hybrid composition. 2nd report. Fukugo Zairyo (Composite Materials) Vol. 1, 1972, pg.21-25.

[50]Raouf RA. Effects of layer waviness on interlaminar stresses in thick composite plates. J of Thermoplastic Compos Materials. Vol. 7, 1994. pg. 261-269.

[51]Christian WJR., DiazDelao FA., Atherton K., Patterson EA. An experimental study on the manufacture and characterisation of in-plane fibre-waviness defects in composites. R. Soc. Open sci. Vol. 5. 2018, 180082

[52]Murray RE., Roadman J., Beach R. Fusion joining of thermoplastic composite wind turbine blades: lap-shear bond characterisation. Renewable Energy, Vol. 140, 2019, p. 501-512.

[53]Hsiao HM., Isaac MD. Effect of fibre waviness on stiffness and strength reduction of unidirectional composites under compressive loading. Compos. Mater. Vol. 5, 1993, p. 344-369.

[54]Jones RM. Mechanics of Composite Materials, Second Edition. Taylor & Francis, Inc.; Philadelphia, PA, USA, 1999.

[55]Reddy JN. Mechanics of Laminated Composite Plates and Shells Theory and Analysis, Second Edition. CRC Press LLC. ISBN: 0-8493-1592-1.

[56]Hallquist JO. LS-Dyna Theoretical Manuel. Livermore Software Technology Corporation; 2005.

[57]Jackson K., Littell JD., Horta LG., Annett MS., Fasanella EL., Seal MD. Impact testing and simulation of composite airframe structures. Technical Memorandum (TM), NASA (https://ntrs.nasa.gov/citations/20140011934).

[58]Xiao X. Modelling energy absorption with a degree mechanics based composite material model. J Compos Mater. Vol. 43, 2009, pg. 427-44.

[59] Feraboli P., Wade B., Deleo F., Rossaian M., Higgins M., Byar A. LS-Dyna MAT54 modeling of the axial crushing of a composite tape sinusoidal specimen. Composites Part A. Vol. 42, 2011, pg. 1809-1825.

[60]Chang FK, Chang KY. A progressive damage model for laminated composites containing stress concentration. J Compos Mater. Vol. 21, 1987, pg-834-55.

[61]Liu D. Impact-induced delamination-A view of bending stiffness mismatching. J. of Compos. Mat. Vol 22, 1988, 674.

[62]Zeng XL., Tang BL., Shen XJ., Dan CY., Shi YC., Feng MJ., Fu SY. Effect of graphene oxide size on interlaminar shear strength of glass fabric/epoxy composites. Mat. Res. Express. Vol 6. 2019, 105306.

[63]Yousef S., Eimontas J., Striugas N., Tatariants M., Abdelnaby MA., Tuckute S., Kliucininkas L. A sustainable bioenergy conversion strategy for textile waster with self-catalysts using mini-pyrolysis plant. Energy Conv. Manag. Vol. 196. 2019, p. 688-704.

[64]LS-DYNA Keyword User´s Manual, version 971; Livermore Software Technology Corporation, CA, USA, 2006.

[65]Han S., Meng S., Araby T., Liu T., Demiral M. Mechanical and electrical properties of graphene and carbon nanotube reinforced epoxy adhesives: Experimental and numerical analysis. Compos. Appl. Sci. Manuf. Vol. 120, 2019, p. 116-126.

[66]Godara A. et al. Influence of carbon nanotube reinforcement on the processing and the mechanical behaviour of carbon fibre/epoxy composites. Carbon. Vol. 47, 2009, p. 2914-2923.

[67]Ferreira JAM. et al. Impact response of nano reinforced mat glass/epoxy laminated. Fibres Polym. Vol 16, 2015, p. 173-180.

[68]Ahmadi-Moghadam B., Sharafimasooleh M., Shadlou S., Taheri F. Effect of functionalisation of graphene nanoplatelets on the mechanical response of graphene/epoxy composites. Mater. Des. Vol. 66, 2015, p. 142-149.

[69]Ashori A., Fallah M., Ghiyasi M., Rabiee M. Reinforcing effects of functionalised graphene oxide on glass fibre/epoxy composites. Polym. Compos. Vol. 39, 2017, p. 2324-2333.

[70]Beauson J., Lilholt H., Brondsted P. Recycling solid residues recovered from glass fibre-reonforced composites-a review applied to wind turbine blade materials. J. of Reinforced Plastics. Vol. 33, 2014, p. 1542-1556.

[71]Pimenta S., Pinho ST. Recycling carbon fibre reinforced polymers for structural application: technology Review and market outlook. Waster Manage, Vol.31, 2011, p. 378-392.

[72]Chen J., Wang J., Ni A. Recycling and reuse of composites materials for wind turbine blades: An overview. Journal of Reinforced Plastics and Composites, Vol. 38, 2019, p. 567-577.

[73]Giorgini L., Leonardi C., Mazzocchettu L. Pyrolysis of fibreglass/polyester composites: recovery and characterisation of obtained products. FME Transactions, Vol. 44, 2016, p. 404-414.

[74]Pickering SJ., Kelly RM., Kennerley JR. Fluidised-bed process for recovery of glass fibres from scrap thermoset composites. Composites Science Technology, Vol. 60, 2000, p. 509-523.

[75]Mcconnell VP. Launching the carbon fibre recycling industry. Reinforced Plastic, Vol. 54, 2010, p. 33-37.

[76]Dogan A., Arikan V. Low-velocity impact response of E-glass reinforced thermoset and thermoplastic based sandwich composites. Compos. B Eng. Vol. 127, 2017, p. 63-69.

[77]Xu., J Li., Ding J. Chemical recycling of carbon fibre/epoxy composites in a mixed solution of peroxide hydrogen and N,N-dimethylformamide. Composite Science and Technology, Vol. 82, 2013, p. 54-59.

[78] Li X., Bai R., Mckechnie J. Environmental and financial performance of mechanical recycling of carbon fibre reinforced polymer and comparison with conventional disposal routes. Journal of Clean Productions, Vol. 127, 2016, p. 451-460.

[79] Murray RE., et.al. Techni-economic analysis of a megawatt-scale thermos-plastic resin wind turbine blade. Renewable Energy, Vol. 131, 2019, p. 111-119.

[80] The composites institute facilities thermoplastic composite development for wind turbine blades through innovative project. IACML, 2017, http://iacmi.org/2017/01/17/iacmi-composites-insitutefacilties-thermoplastic-composite-developement-wind-turbine-blades-innovative-project/.

[81] Cousins DS., et.al. Recycling glass fibre thermoplastic composites from wind turbine blades. Journal of Clean Production, Vol. 209, 2019, p. 1252-1263.

[82]Naaman AE., Jeong SM. Structural ductility of concrete beams prestressed with FRP tendons, in: Proceeding of the second international RILEM symposium (FRPRCS-2), 1995, p. 379-401.

[83]Grace NF., Soliman AK., Abdel-Sayed G., Saleh KR. Behavior and ductility of simple and continuous FRP reinforced beams. J. Compos. Construct. Vol. 2, 1998, p. 186-194.

[84]Ghallab A. Ductility of externally prestressed continuous concrete beams, KSCE Journal of Civil Engineering. Vol. 18, 2014, p. 595-606.

[85]Foo CC., Seah LK., Chai GB. A modified energy-balance model to predict low-velocity impact response for sandwich composites. Compos. Struct. Vol. 93, 2011, p. 1385-1393.

[86]Andreas A., Phillip G., Klaus D. Strength prediction of ply waviness in composite materials considering matrix dominated effects. Compos. Struct. Vol. 127. 2015, p. 51-59.

[87]Zein S., Neaz Sheik M., Alex MR., Abheek B. Numerical investigation on the flexural behaviour of GFRP-RC beams under monotonic loads. Structures, Vol. 20, 2019, p. 255-267.

[88]Jun Z., Jihui W., Aiqing N., Wantao G., Xiang L., Yibo W. A multi-parameter model for stiffness prediction of composite laminates with out-of-plane waviness. Compos. Struct. Vol. 185, 2018, p. 327-337.

[89]3B-fibreglass SPRL, Technical Data Sheet for SE 2020 Direct Roving. Available online: https://www.3b-fibreglass.com/sites/ default/files/products-data-sheets/TDS-SE-2020-DR-for-Epoxy-Resins-2015-sans-trame-LR.pdf (accessed on 19 June 2020

CURRICULUM VITAE

Personal data:

Name surname: Sharath Peethambaran Subadra
Date and place of birth: November 21, 1989, India
E-mail: sharadhsub@outlook.com

Education:

09/18–present	PhD Candidate in Mechanical Engineering, Kaunas University of Technology (KTU), Lithuania. Research: Impact mechanics of polymer composites. Supervisor: Prof. Dr. Paulius Griškevičius.
09/14–06/16	Master of Science in Mechanical Engineering, Kaunas University of Technology, Lithuania. Thesis: Acoustic study of damage propagation in polymer composites.
2009–2012	Bachelor of Engineering, Mechanical Engineering, Visvesvaraya Technological University, India.
2004–2009	High school and Higher secondary school, Kendriya Vidyalaya and St. Claret's PU College, Bangalore, India.

Work experience:

11/22–present	Research Assistant Hochschule für Angewandte Wissenschaften, Hamburg, Germany. Research: Calibration of UTMs through acoustics.
12/21–10/22	R&D Mechanical Engineer VIEZO, Vilnius, Lithuania. Work: Improving performance of energy harvesting device for IoT sensors in railways.

Internships in science and institutions abroad:

08/20–10/20	Erasmus Exchange-Researcher
09/21–11/21	Fraunhofer Institute for Wind Energy Systems (IWES), Bremerhaven, Germany. Research: Failure modelling in lap shear joints in polymer composites.

Scientific activity (scientific publications):

Subadra, S.P., Griškevičius, P. (2022). Effect of Hybridization and Ply Waviness on the Flexural Strength of Polymer Composites: An Experimental and Numerical Study. *Polymers*, *14*(7), 1360.

Subadra, S.P., Griškevičius, P. (2021). Sustainability of polymer composites and its critical role in revolutionising wind power for green future. *Sustainable Technologies for Green Economy*, *1*(1), 1–7.

Yousef, S., Subadra, S.P., Griškevičius, P., Varnagiris, S., Milcius, D., Makarevicius, V. (2020). Superhydrophilic functionalized graphene/fiberglass/epoxy laminates with high mechanical, impact and thermal performance and treated by plasma. *Polymer Testing*, *90*, 1–11.

Subadra, S.P., Griskevicius, P., Yousef, S. (2020). Low velocity impact and pseudo-ductile behaviour of carbon/glass/epoxy and carbon/glass/PMMA hybrid composite laminates for aircraft application at service temperature. *Polymer Testing*, *89*, 1–10.

Subadra, S.P., Yousef, S., Griskevicius, P., Makarevicius, V. (2020). High-performance fibreglass/epoxy reinforced by functionalized CNTs for vehicle applications with less fuel consumption and greenhouse gas emissions. *Polymer Testing*, *86*, 1–10.

LIST OF PUBLICATIONS

Articles published in peer-reviewed scientific publications

Indexed in the Web of Science with Impact Factor

1. [S1;GB] Subadra, Sharath P.; Griskevicius, Paulius; Yousef, Samy. Low velocity impact and pseudo-ductile behaviour of carbon/glass/epoxy and carbon/glass/PMMA hybrid composite laminates for aircraft application at service temperature // Polymer Testing. Oxford : Elsevier. ISSN 0142-9418. eISSN 1873-2348. 2020, Vol. 89, art. no. 106711, p. 1-10. DOI: 10.1016/j.polymertesting.2020.106711. [Science Citation Index Expanded (Web of Science); Scopus] [IF: 4,282; AIF: 3,771; IF/AIF: 1,135; Q1 (2020, InCites JCR SCIE)] [M.kr.: T 009] [Indelis: 0,334]
2. [S1;GB] Yousef, Samy; Subadra, Sharath P.; Griškevičius, Paulius; Varnagiris, Sarunas; Milcius, Darius; Makarevicius, Vidas. Superhydrophilic functionalized graphene/fiberglass/epoxy laminates with high mechanical, impact and thermal performance and treated by plasma // Polymer Testing. Oxford : Elsevier. ISSN 0142-9418. eISSN 1873-2348. 2020, Vol. 90, art. no. 106701, p. 1-11. DOI: 10.1016/j.polymertesting.2020.106701. [Science Citation Index Expanded (Web of Science); Scopus] [IF: 4,282; AIF: 3,771; IF/AIF: 1,135; Q1 (2020, InCites JCR SCIE)] [M.kr.: T 006, T 008] [Indelis: 0,166]
3. [S1;GB] Subadra, Sharath P.; Yousef, Samy; Griškevicius, Paulius; Makarevicius, Vidas. High-performance fiberglass/epoxy reinforced by functionalized CNTs for vehicle applications with less fuel consumption and greenhouse gas emissions // Polymer Testing. Oxford : Elsevier. ISSN 0142-9418. eISSN 1873-2348. 2020, vol. 86, art. no. 106480, p. 1-10. DOI: 10.1016/j.polymertesting.2020.106480. [Science Citation Index Expanded (Web of Science); Scopus] [IF: 4,282; AIF: 3,771; IF/AIF: 1,135; Q1 (2020, InCites JCR SCIE)] [M.kr.: T 009 T 008] [Indelis: 0,250]
4. [S1;CH;OA] Subadra, Sharath P.; Griskevicius, Paulius. Effect of hybridization and ply waviness on the flexural strength of polymer composites: an experimental and numerical study // Polymers. Basel : MDPI. ISSN 2073-4360. 2022, vol. 14, iss. 7, art. no. 1360, p. 1-19. DOI: 10.3390/polym14071360. [Science Citation Index Expanded (Web of Science); Scopus; DOAJ] [IF: 4,967; AIF: 5,162; IF/AIF: 0,962; Q1 (2021, InCites JCR SCIE)] [M.kr.: T 009] [Indelis: 0,500]

Indexed in the Web of Science without Impact Factor

1. [S3; LT; OA] Subadra, Sharath P.; Griskevicius, Paulius. Sustainability of polymer composites and its critical role in revolutionising wind power for green future // Sustainable technologies for green economy. Kaunas : JVE Journals. ISSN 2669-2457. 2021, vol. 1, iss. 1, p. 1-7. DOI: 10.21595/stge.2021.21974. [M.kr.: T 009] [Indelis: 0,500]

Articles published in conference proceedings

1. [Pld; LT] Subadra, Sharath P.; Griškevičius, Paulius; Jurėnas, Vytautas. Analysis of damage in fibre reinforced polymer composites using acoustic-laser vibrometer // Mechanika 2019: proceedings of the 24th international scientific conference, 17 May 2019, Kaunas University of Technology, Lithuania / Kaunas University of Technology, Lithuanian Academy of Science, IFTOMM National Committee of Lithuania, Baltic Association of Mechanical Engineering. Kaunas : Kaunas University of Technology. ISSN 1822-2951. 2019, p. 141-144. [M.kr.: T 009] [Indelis: 0,334]

Other conference abstracts and articles in conference proceedings

1. [T2; PT; OA] Peethambaran Subadra, Sharath; Balčiūnas, Justas; Griskevicius, Paulius. Influence of temperature on the impact-static and dynamic-performance of fibre reinforced polymer composites // MECHCOMP 2019: 5th international conference on mechanics of composites, Instituto Superior Técnico, Lisbon, Portugal, 1-4 July 2019: book of abstracts. [S.l.] : [s.n.]. 2019, p. 120-121. [M.kr.: T 008]

2. [T2; LV; OA] Subadra, Sharath P.; Griskevicius, Paulius. Impact induced damage in fibre reinforced composites and the effect of matrix dominant properties on the effect of damage propagation // Advanced composites and applications: 80th international scientific conference of the University of Latvia, February 15, 2022: book of abstracts. Riga : University of Latvia. 2022, p. 11. [M.kr.: T 009]

High-performance fiberglass/epoxy reinforced by functionalized CNTs for vehicle applications with less fuel consumption and greenhouse gas emissions

Sharath P. Subadra [a], Samy Yousef [a,c,*], Paulius Griskevicius [a], Vidas Makarevicius [b]

[a] Department of Mechanical Engineering, Kaunas University of Technology, LT-51424, Kaunas, Lithuania
[b] Lithuanian Energy Institute, Breslaujos 3, LT-44403, Kaunas, Lithuania
[c] Department of Materials Science, South Ural State University, Lenin Prospect 76, 454080, Chelyabinsk, Russia

ABSTRACT

Carbon Nanotubes (CNTs) is among the most promising nanofiller materials that could be used for enhancing the properties of fiberglass/epoxy laminates for vehicle industries with less CO_2 emission (the key player in the climate change). However, usually the commercialized CNTs are supplied in the shape of heavily entangled tubes what leads to random dispersion of CNTs in the polymer matrix and decrease in their performance, especially at industrial scale. Within this frame, the chemical functionalization process was used in the present research to avoid this problem and to modify the surface properties of CNTs at the same time, thus improving compatibility and solubility of CNTs in epoxy solutions. Afterwards, probe sonicator (pre-dispersion), ultrasonic path (main dispersion), mechanical mixer (mixed CNTs/Epoxy solutions with hardener), and vacuum infiltration (to remove air bubbles) were used to disperse functionalized CNTs with different concentrations (in the range 0.05–0.4 wt%) in the epoxy-hardener solutions. Then, vacuum-assisted resin transfer technique followed by curing process were used to prepare 4 layers-fiberglass/CNTs/epoxy panels. The mechanical and impact properties of the prepared panels were tested according to ASTM D7025 and ISO 6603-2 standards, respectively. Also, thermal behavior of the panels was investigated using thermogravimetric (TG-DTG). Finally, the environmental performance in terms of greenhouse gas emission (GHGE) was evaluated according to ISO-14040 standard, taking the resulting strength and changes in density into account. The results showed that 0.35 wt% of FCNTs were enough to improve the strength of panels by ~60%, compared to pure sample. Which means that weight structure of vehicles can decrease by 23%. Also, fuel consumption and GHGE can decrease significantly by 16% and ~26%, respectively. In addition, thermal stability and energy impact absorption at the same concentration of CNTs were improved by 5% and 31%, respectively.

1. Introduction

Recently, various governments and decision makers have taken several serious actions in order to face challenges of climate change. One of the made decisions is pushing designers and manufacturers to decrease amount of fuel consumption in transport vehicles, where more than 15% of CO_2 emission are generated from different fuels used in transportation sector [1–3]. Lightweight materials, including fiber reinforced composites (FRC) are among the most promising materials that can be employed to achieve this strategy, where vehicle mass reduced by 100 kg saves about 0.7 l fuel for each 100 km (directly and indirectly). This can contribute greatly to ecologically friendly issues and help to adopt the suggested strategy [4,5]. FRC is a thermoset plastic reinforced with fibers and currently used widely in many distinct engineering fields (from household to aerospace industries) alternatively to high-performance metal and metal-based alloys, including aerospace, construction, transportation, automotive, sports utilities, etc. [6,7]. Fiberglass/epoxy laminates are mainly composed of fiber layers (made from glass, carbon, etc.) assembled together using epoxy resin to provide the obtained panels better design flexibility, mechanical properties, good chemical performance and electrical resistance. Among FRC materials, glass fiber reinforced composite materials (GFRP) of different

* Corresponding author. Department of Production Engineering, Faculty of Mechanical Engineering and Design, Kaunas University of Technology, LT-51424, Kaunas, Lithuania.
E-mail address: ahmed.saed@ktu.lt (S. Yousef).

types (plain, twill, satin) are used frequently because of their good stiffness to density ratio, mechanical, thermal, acoustic properties, fatigue, impact, endurance limit, corrosive resistance, easy manufacturing, etc., when compared to traditional engineering materials [8,9]. Therefore, the researchers hastened to study their properties, including mechanical, thermal, acoustic, fatigue, impact, etc. [10–16]. In addition, many models were developed to simulate their failure and fracture modes using different types of nonlinearity and incorporating smart materials (PZT piezo elements) [10–18]. Despite of all the above advantages, their poor recyclability was a great challenge, especially as these types of waste contain a lot of Bromine, what can cause several problems related to health and environment. Within this frame, Yousef et al. (2017, 2018) developed a new approach to recover all fiberglass layers from the end-life-panels using dissolution treatments with organic solvents [19–21]. Also, mechanical and thermal characterizations of the recovered fiberglass layers were investigated and the results showed that due to polymer degradation, strength of the recovered fiberglass was smaller by −40% [22,23]. Based on these advantages and recently developed recycling technologies, demand for fiberglass/epoxy laminates has been increasing rapidly.

In order to meet this huge demand, laminated hybrid composites have been introduced. They are composed of a multi-phase material comprised of polymer matrix and reinforcing filler, thus producing composite materials with synergistic mechanical properties [24–26]. In the literature, there are some examples when several nanoparticles have been used for this purpose (like Carbon nanotubes (CNTs), Boron nitride, alumina, TiO$_2$, Al$_2$O$_3$, Graphene, etc.) [27–32]. Among these nanofillers, CNTs with high aspect ratio provide high mechanical strength up to 42%, especially at lower concentrations in the range 0.05–0.4 wt% of fibre composite matrix, whereas at high concentrations, CNTs started to agglomerate in the prepared matrix system causing a slight decrement of mechanical properties [33–38]. Also, CNTs are more cost-effective, compared to graphene [39]. However, the commercialized CNTs are usually supplied as a mixture of various diameters and chiralities of nanotubes that are normally contaminated with metallic and amorphous impurities in the form of heavily entangled tubes, what impedes CNTs to disperse uniformly in the prepared matrix, especially at industrial scale [40]. Therefore, different surface functionalization process (using different chemicals like aromatic, aliphatic, aliphatic ether, etc.) was developed for this purpose and the results revealed greater adhesion of the epoxy composite to the functionalized CNTs because of covalent bonding [41–44]. Based on these results, CNTs were used as nanofiller in the present study after having been modified using the functionalization process.

With regard to preparation of laminated hybrid composite panels, this process usually starts with dispersion of CNTs in epoxy using Probe sonicator or ultrasonic path or magnate string or combination of some of them in probable presence of some solvent (e.g. Ethonal, Dimethylformamide, etc.) to decrease viscosity of epoxy, thus improving dispersion, followed by mixing of prepared solution with hardener mechanically. Although the results in presence of solvent were promising, but another step is needed to remove solvent less costly. Finally, hand lay-up technique or vacuum assisted resin technique can be used for preparing fiberglass/CNTs/epoxy panels, followed by curing process [29,45,46]. In the present research, vacuum assisted resin technique was used to produce fiberglass/functionalized CNTs/epoxy panels with high mechanical, thermal, and impact properties. Also, a new model was developed to evaluate fuel reduction and greenhouse gas emission (GHGE) based on the obtained strength and panel density in order to use the developed panels in vehicle industries.

2. Experimental

2.1. Materials and chemicals

CNTs with an average diameter of 30 nm and a few micrometers in length were synthesized using CVD multi-quartz (Fig. (1A)) [47]. Fig. (1B) shows the high resolution transmission electron microscopy (TEM) photo of the synthesized CNTs at 650 °C contaminated with amorphous impurities at the ends (indicated by orange circles). In order to remove these components, the synthesized CNTs were oxidized by refluxing at 130 °C in an acid mixture (Sulfuric acid: Nitric acid = 3:1) for 30 min and then diluted with water and filtered. The filtered samples were washed by distilled water and dried in an oven at 50 °C for overnight, thus obtaining the functionalized CNTs (FCNTs) as shown in Fig. (1C) [48]. Epoxy resin and its hardener (EPIKOTE Resin MGS® RIMR 135 and EPIKURE Curing Agent MGS® RIMH 1366) were purchased from Momentive. Glass fabric Panda™ (Weave: Twill 2/2 type and weight: 163 g/m^2) were supplied by R&G Faserverbundwerkstoffe GmbH, Waldenbuch, Germany. All other chemicals used in this work were purchased from Sigma-Aldrich.

2.2. Design of the experiments

The experiments were started by preparing fiberglass/epoxy laminate nanocomposite panels with different concentrations of FCNTs in the scope 0.05 to 0.4 wt% and each sample had a code (based on the concentrations of FCNTs), as illustrated in Table 1. Then mechanical, impact, and thermal behaviors of the fabricated nanocomposite panels were analyzed, as shown in Fig. (2). Finally, a model was developed to simulate and evaluate the GHG emission from the obtained panels so that they could be used in the future designing plans of the vehicles, structure. All these steps, including optimum conditions of each process, are explained in detail in the following sections.

2.2.1. Preparation of FCNTs/epoxy/hardener solutions

In order to disperse specified amount of FCNTs with uniform distribution in epoxy resin, initially, the required quantity of FCNTs was predispersed in 48 g of epoxy resin solution (70 wt% of the total matrix weight) using a Probe sonicator at 50 Hz for 30 min to overcome high viscosity of epoxy resin, folowed by preparation of the pre-dispersed FCNTs/Epoxy solutions (without any additional chemicals or solvents). It is worth mentioning that the pre-dispersion process was performed at 30 °C and the temperature was controlled using thermocouple sensor. After that, the pre-dispersed FCNTs/Epoxy solutions were treated again by ultrasonicaon at 50 °C for 2 h to prepare FCNTs/epoxy solutions [49]. Finally, the prepared FCNTs/Epoxy solutions were mixed with −16 g of hardener solution (30 wt% of the total matrix weight) using a mechanical mixer for 30 mints., then maintaining them in vacuum infiltration at −100 bar for 15 mints. to remove any cavities and entrapped air bubbles from the mixture, and then preparing final FCNTs/Epoxy/Hardener (FCEH) solutions [37–39].

2.2.2. Preparation of fiberglass/FCNTs/epoxy panels

Four Glass fabric Panda™ sheets with average weight of 94 g and nominal size of 270 mm × 320 mm were cut from the supplied fabric roller for each batch. Vacuum assisted resin transfer method was employed to prepare fiberglass/FCNTs/epoxy laminate nanocomposite panels with four layers of fabric with thickness of 1 ± 0.05 mm (depending on the concentration of FCNTs in the prepared FCEH solutions). Also, one neat fiberglass/epoxy laminate panel was prepared for comparison. Finally, the panels were post-cured using infra-red lamp at 80 °C for 8 h, then exposed to the main curing process in the oven at 80–100 °C for 6hr. for toughening or hardening of the prepared panels by cross-linking of polymer chains and for achieving of homogeneity in the structure of panels. In order to get the aforementioned optimum conditions, three panels with different concentrations of FCNTs (FGCE0 "Neat", FGCE1 "low concentration", and FGCE0 "low concentration") were prepared as initial experiments at different conditions, in particular a) without vacuum infiltration of FCEH solutions, b) without vacuuming of the prepared panels, c) without post-curing, and d) with post-curing at 50 °C for 6 h. After that, Metallographic microscope was used

111
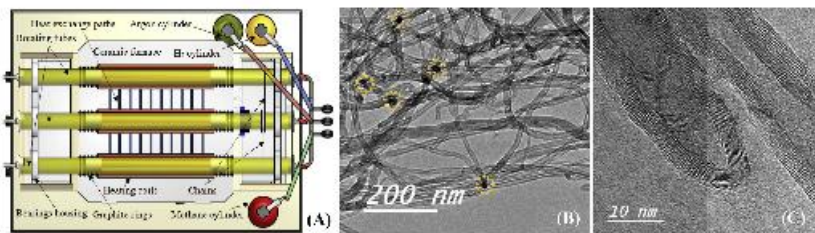
Fig. 1. A) Schematic drawing of CVD multi-quartz, B) TEM photo of the synthesized CNTs, and C) TEM photo of FCNTs.

Table 1
Fiberglass/epoxy laminate nanocomposite panel codes.

Sample codes	FGCE0	FGCE1	FGCE2	FGCE3	FGCE4	FGCE5	FGCE6	FGCE7	FGCE8
CNTs (wt.%)	0	00.5	0.15	0.20	0.25	0.30	0.35	0.40	0.45

Fig. 2. Fiberglass/FCNTs/epoxy laminate nanocomposite panels – preparation and characterization flowchart.

to examine the panel surface after each preparation and treatment process to study the effect of preparation parameters on morphology and features of the obtained panels and to select the optimal conditions.

Fig. (3A–D) shows microscope images of the obtained neat panel. It is clear that the panel without vacuum infiltration of FCEH solution contains a lot of exploded cavities (pockets), where big-size fiber became bare (Fig. (3A)). By vacuuming the FCEH solution, the size of these pockets decreased gradually (Fig. (3B)), then started to disappear after UV post-curing (Fig. 3C)) and main curing process at 50 °C for 6hr. (Fig. (3C)). However, it was noted that after the main curing process, the panel still contained a very small amount of exploded air bubbles (white circles), what can cause stress concentration in these regions and affect negatively final properties of the obtained panels. Therefore, based on the results of the initial experiments, the panels were cured again at 80

°C for 6 h and then dried for 24 h to obtain the final treated panels.

With regard to FGCE1 panel (Fig. (3E,F)) and FGCE8 (Fig. (3G,H)) panel, it was noted that the samples had almost the same features as the neat panel (pockets and bare fiber) after post-curing and main curing process. In addition, some epoxy infusion particles remained on the surface because of chemical modification of epoxy, what leads to increase in its viscosity. These particles can be eliminated by increasing the curing temperature up 100 °C to obtain a smooth surface containing some FCNTs agglomerations (orange circles). Based on these initial results, the main curing process was performed at 80 °C for FGCE0 and 100 °C for nanocomposite panels and Fig. (4A) shows the panels at the optimum conditions. Finally, automatic cutter was used to trim the panel edges and to cut the mechanical (25 mm × 270 mm) and impact (80 mm × 80 mm) samples according to ASTM D7025 and ISO 6603-2

3
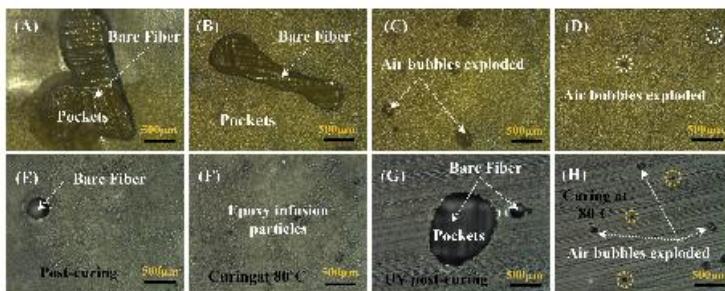
Fig. 3. Microscope photos of the obtained panels at different preparation and treatment conditions.

standards, as shown in Fig. (4B).

2.2.3. Greenhouse gas emissions modeling

The environmental performance in terms of Greenhouse Gas emission (GHGE) factor of the fabricated fiberglass/FCNTs/epoxy laminated nanocomposites was evaluated in order to study their potential applications in the vehicle industries. GHGE factor was calculated based on the developed approach by Turner et al. (2015) and according to ISO-14040 standard [50]. This approach suggested that each material has equivalent CO_2 values (reported in the literature) that can be decreased significantly by reducing their size or mass or density [51,52]. In the present research and as mentioned before, reduction of a vehicle mass by 100 kg saves about 0.7 l fuel for each 100 km (directly and indirectly), leading to decreased CO_2 emissions by 1800 kgCO2-eq/ton [53]. In order to simulate that and to calculate this reduction in mass after adding FCNTs, a new model was developed. The GHGE model was started by establishing a relationship between the resultant strength and the final mass or density of the obtained panels. The relationship was formulated based on theories of failures, particularly the maximum principal stress theory (safe design against the brittle failure mode "Fiberglass/Epoxy") with applied load uniaxial-normal load as illustrated in Eqs. (1)-(3) [54], while the optimum cross-section area of panels was calculated based on mass and length of panels, and the measured density using Eqn. (4).

$$\sigma_{max.} \leq \sigma_{all} \tag{1}$$

$$\sigma_{all} = \frac{\sigma_{ult.}}{2 \times SF} \tag{2}$$

$$\sigma_{max.} = \frac{F_{max.}}{A} \tag{3}$$

$$A = \frac{m}{\rho \times L} \tag{4}$$

where $\sigma_{max.}$, σ_{all}, $\sigma_{ult.}$, SF, $F_{max.}$, A, m, ρ, and L are the maximum applied stress (MPa), allowable strength (MPa), ultimate strength (MPa), Factor of safety, maximum applied axial load, cross-section area of Fiberglass/Epoxy and its nanocomposite panels, mass of panels (g), the measured density (g/mm³), length of the panels (mm), respectively. It is worth mentioning that density of the panels was measured using Archimedes' principle in ethanol media.

The maximum applied stress can be calculated based on mass and density by combining Eq. (3) and Eq. (4) as written in Eqn (5). Based on that, the mass can be expressed as shown in Eq. (6) and (7).

$$\sigma_{max.} = \frac{F_{max.} \times \rho \times L}{m} \tag{5}$$

$$\frac{F_{max.} \times \rho \times L}{m} = \left(\frac{\sigma_{ult.} \ (FG)}{2 \times SF}\right)FG = \left(\frac{\sigma_{ult.} \ (CNTs/FG \ )}{2 \times SF}\right) \tag{6}$$

$$m = \frac{2 \times SF \times F_{max.} \times \rho \times L}{\sigma_{ult.}} \tag{7}$$

Since the obtained panels are supposed to work at the same conditions, in particularly, $F_{max.}$, SF, and length, it was assumed that all these parameters can be merged in Eqn (8). as a constant (C), and in this case, mass can be formulated as shown in Eqn (9).
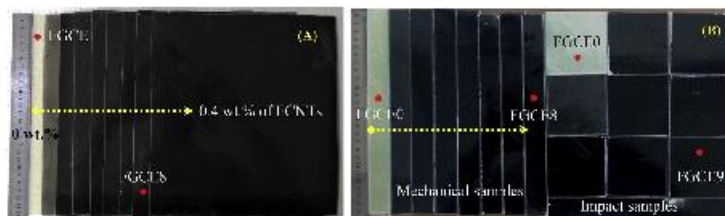
Fig. 4. A) Fiberglass/epoxy laminate nanocomposite panels and B) Mechanical and impact standard samples.

4

113

$$C = 2 \times SF \times L \times F_{max}. \tag{8}$$

$$m = \frac{Cp(\text{neat panel or nanocomposite panel})}{\sigma ult.(\text{neat panel or nanocomposite panel})} \tag{9}$$

Finally, mass reduction (m_R), fuel reduction (F_R), and GHG emission factor was calculated based on the obtained mass using Eqs. (10)-(12), respectively [5,53].

$$m_R = \frac{m(\text{nanocomposite panel}) - m(\text{neat panel})}{m(\text{neat panel})} \tag{10}$$

$$F_R = \frac{mR}{100} \frac{\times 0.7}{\times 100} \tag{11}$$

$$CO_{2\ \text{emission reduction}} = \frac{FR\ (\%) \times 1800\ (\text{kgCO2} - \text{eq/ton})}{100\ \times\ 1149\ (1\ \text{ton oil to liter})} \tag{12}$$

3. Characterizations

Scanning Electron Microscope (SEM) was used to check dispersion and morphology of the obtained fiberglass/FCNTs/epoxy laminate panels. Mechanical tensile properties of the panels (five specimens from each batch) were measured by a Lloyd Universal Testing Machine (model LR10K) connected to high-resolution camera. The tests were performed on five specimens from each batch, then taking the average of these measurements. Thermal stability of the panels was determined by Thermogravimetric/Derivative Thermogravimetric analysis (TGA-DTG), TA instruments TGA Q500 being in the following conditions, N_2 flow rate 10 °C/min. The impact test was performed using Coesfeld Magnus 1000 High-speed drop tower with cylindrical steel impactor with 20 mm in diameter and hemispherical end with a mass of 5.129 kg. The low-velocity impact response of the obtained fiberglass was received in accordance to ISO 6603-2 and the impact experiment was investigated at constant impact energy (50J) and room temperature.
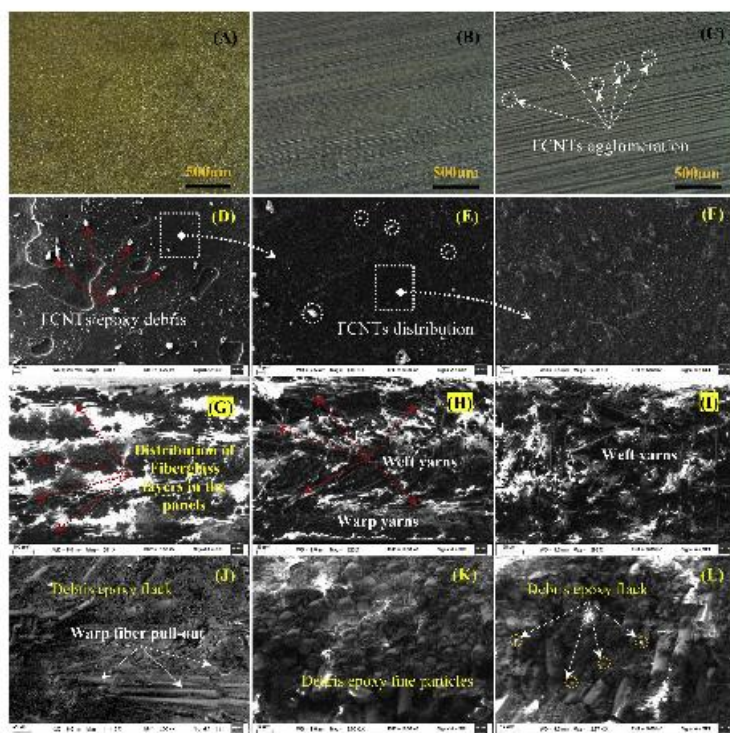
Fig. 5. A-D) Optical Microscope images and M – P) SEM micrograph of the fracture surfaces of fibreglass.

114

4. Results and discussions

This section is focused on the investigation of morphology, mechanical, impact and thermal properties of the obtained and treated panels at the optimum preparation conditions, particularly, vacuumed FCEH solutions at − 100 bar for 15 mints., Infra-red post-curing at 80 °C for 8 h, and main curing at 80 °C for 6 h (for FGCE0 sample) and 100 °C for FGCE1 to FGCE8 samples.

4.1. Dispersion and morphology of the obtained panels

In order to check the surface morphology of the obtained panels at the optimum preparation conditions, three samples were selected for observation: FGCE0 (pristine panel), FGCE7 (optimum concentration of FCNTs-based on the obtained results in the next sections), and FGCE8 (higher concentration of FCNTs). Afterwards, the selected samples were cleaned in ethanol emulsion using ultrasound to remove any contaminated elements on the surfaces, and then the examination process was started using the color optical microscope. Fig. (5A–C) shows the surface morphology of FGCE0, FGCE7, and FGCE8 panels at 500 μm. As shown in optical images, the surface of FGCE0 sample is very clean, without any cavents or bubbles. The same features were noted during observation of FGCE7 and FGCE8 samples and the surface became smoother due to surface modification by mixing with modified CNTs [55], which means that the selected preparation and cooling conditions were suitable to achieve the goal. However, at the highest concentration of FGCE8 sample, little black particles (indicated in white circles) appeared due to FCNTs agglomeration. SEM examination was used to check morphology and dispersion of FCNTs in the surface of FGCE7 (optimum concentration of FCNTs) sample at 30 μm, 10 μm, 3 μm. As shown in SEM photos, the surface contaminated by several FCNTs/epoxy debris (of different shapes and sizes) was formed during solidification and cutting processes in SEM sample (Fig. (5D)). At the lower scale, the amount and size of FCNTs/epoxy debris decreased significantly and the features of FCNTs started to appear in the form of very fine particles distributed uniformly inside the panel with strong crosslinking. The surfaces became a little bit rough (Fig. (5E,F)). Also, SEM was used to examine morphology of cross-section after coating by the gold layer. As shown in Fig. (5G), the matrix composed of four layers of fibreglass distributed uniformly in the vertical direction and glued by epoxy resin was obtained. Also, the fabric composed of two types of yarns (weft and warp) interlaced at a certain angle was receictved, as shown in (Fig. (5H,I)).

With regard to fracture type, in general epoxy is classified as a brittle material after having been mixedwith hardener and having dried. This characteristic becomes even more evident after mixing epoxy with FCNTs because of chemical modification of their molecules [56]. Under the applied load, the fracture occurred in the epoxy by breaking their van der waals bonds in the form of cracks, then it started to spread inside the matrix (that propagated further along epoxy) followed by separating epoxy in form of debris (flack or large particles) in case of pure epoxy, as shown in Fig. (5J). By adding FCNTs and reaching the optimum amount (FGCE7), the fracture surface became more brittle with debris in the form of fine particles, which means that the prepared panels became harder Fig. (5K). At high concentration of FCNTs (FGCE7), the panels became more brittle with numerous FCNTs agglomerations (orange circles) (Fig. (5L)). With regard to fiberglass bundle breakage, it is known that epoxy is bonding with bundles through two types of bonds; chemical and mechanical bonds and these bonds increases by adding FCNTs due to their higher ratio of surface area to volume that leads to rapid and strong interaction between CNTs and epoxy molecular, thus improving their chemical and physical behaviors [57,58]. Under the applied load in neat sample, bundles were pulled out because of weaker bonding between fiber and epoxy Fig. (5J), while after having mixed them with FCNTs, the bonding became stronger, what led to fracture in fibers and epoxy at the same time and the same plan as shown in Fig. (5K,L).

4.2. Mechanical properties of the obtained panels

The stress-strain curves, mechanical and density data of the produced panels are presented in Fig. (6) and Table 2. The stress-strain curves manifest that strain doesn't affect significantly mixture with FCNTs, because glass fiber composites are classified as a brittle material, whereas tensile strength and elasticity modulus of the panel were increased by −7% and 6% (compared with neat sample), respectively, after adding 0.05 wt% of FCNTs to epoxy matrix. By increasing the concentration of FCNTs up to 0.35 wt%, the strength increased gradually until reaching to 250 Mpa (with improved 30% compared with neat sample). Similar elasticity modulus was increased by 31% and the panels became more rigid with hard structure; then it decreased again due to FCNTs agglomeration. This happened because mixing of FCNTs with epoxy restricted the molecular rearrangement of epoxy chains during the mixing, preparation and solidification processes. Also, it can be explained by good miscibility and higher interaction between FCNTs nanofiller and panel composite [59]. These features can be improved after the functionalization process which leads to better cross-linked epoxy-CNTs nanocomposites [42].

This means that preparation processes succeeded to disperse FCNTs uniformly in the obtained panels, especially in FGCE7 sample [60]. Above this concentration (0.35 wt%), the strength and elastic modulus decreased drastically due to FCNTs agglomeration. Finally, density doesn't change significantly by adding FCNTs due to adding a very small amount compared to the total weight of the prepared matrix up to 0.4 wt %. Also, this indicated that all panels were prepared under the same conditions without any voids or internal defects between laminates, which can affect the composite performance. In addition, these results are promising compared to the results available in the literature: it was reported that 0.75–1.2 wt% of CNTs show higher tensile strength with improved 20–28% [38,39,61]. Therefore, the amount of used raw materials in the preparation of panels and the production costs may be reduced.

4.3. Impact properties of the obtained panels

Fig. (7A, B) shows the damages that occurred in the panels by the end of the impact tests on the front and back sides of the tested samples, respectively. Also, the images show the overall damage areas including glassfiber bundles breakages, matrix cracks and delaminations for all the panels. As shown in the images and due to high applied energy (50J), the steel impactor penetrates completely in all the specimens with the approximately similar damage shapes. The resulting damages are characterized by three main features: Rhombus shape, two diamonds, and damage tip point. These features and geometry represent the projection of semi-spherical impactor on the tested samples after failure, where rhombus shape represents the damage limitations (damage zones) and the failure point resulted from the intersection of two diamonds and represent the end of failure. Presence of these features confirms that the preparation, testing, and failure were happening based on the standard conditions [62]. Although the front and back sides had the same features, but usually the front view of the matrix is exposed to high compression load creating conditions for failure, while the opposite side is exposed to high tensile stress what causes a tension failure on the other side at the same time [63]. Also, it was noted that the projected failure areas seem to be close to each other (especially delamination areas occurring at interfaces of the edges). In addition, the size of these areas decreases slowly by increasing the amount of FCNTs as a result of improving the elasticity modulus of the panels.

Fig. (8) shows the impact response in terms of impact load and impact energy versus displacement in the projection of damage areas. As seen in the load-displacement curves (Fig. (8A)), all samples have similar features with two sharp peaks at 3.75 mm and 3.94 mm. The first peak corresponds to maximum impact load and this location refers to maximum impact energy too, while the second peak is referred to
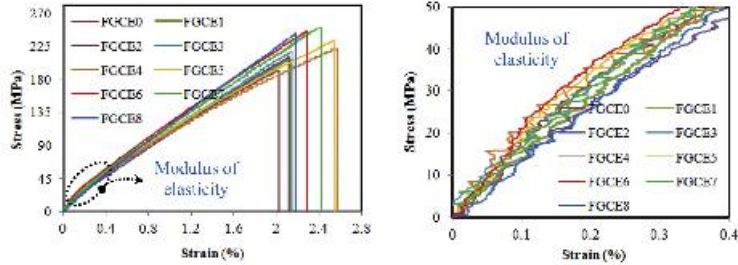
Fig. 6. Stress-Strain curves of the prepared panels.

Table 2
Density and mechanical data of fiberglass/epoxy and its nanocomposites.

Sample Code	Density (kg/ m³)	Tensile modulus (MPa)	Stress at break (MPa)	Strain at break (%)
FGCE0	1620.37 ± 0.004	6712 ± 56	191.48 ± 3.6	2.02 ± 0.06
FGCE1	1620.77 ± 0.007	7143 ± 78	205.93 ± 4.8	2.13 ± 0.07
FGCE2	1621.18 ± 0.006	7335 ± 62	207.41 ± 4.4	2.09 ± 0.05
FGCE3	1621.45 ± 0.005	7584 ± 54	216.3 ± 3.8	2.13 ± 0.05
FGCE4	1623.61 ± 0.004	7762 ± 42	220.74 ± 3.4	2.56 ± 0.04
FGCE5	1623.05 ± 0.004	7905 ± 38	231.88 ± 3.1	2.54 ± 0.04
FGCE6	1624.38 ± 0.002	8431 ± 32	244.81 ± 2.3	2.28 ± 0.03
FGCE7	1625.21 ± 0.001	8746 ± 28	249.62 ± 2.1	2.42 ± 0.03
FGCE8	1625.21 ± 0.003	8294 ± 37	240.37 ± 2.4	2.17 ± 0.03

fracture impact load and fracture impact energy. Since designers are usually looking for maximum load before failure point (just to be in the safe zone), therefore, the impact analysis was focused on these parameters (maximum impact load and energy), as shown in Fig. (8A,B). It is clear from these curves that the maximum impact load and energy were increased by adding FCNTs up to 0.35% by −31% (from 2.13 KN to 2.80 KN) and −20 (from 9.68 J to 11.79J). Then FCNTs started to agglomerate what led to decrease in values of these parameters again. This means that by enhancing FCNTs to Fiberglass/epoxy panels, elimination of damage initiation energy was started, while improving bonds between epoxy molecular and bundles of fiber, leading to delay in crack propagation and absorbtion of more energy until breakage point. Compared to the results available in literature, the functionalization of CNTs can be regarded as an approach to improve the impact response of Fiberglass/epoxy composites with a significant improving result, compared to the results available in literature [64-68].

4.4. Greenhouse gas analysis

Fig. (9) shows the effect of FCNTs on the mass, fuel consumption, and carbon emission reduction of the obtained panels based on the improved resultant strength and density. It seems that the specified parameters
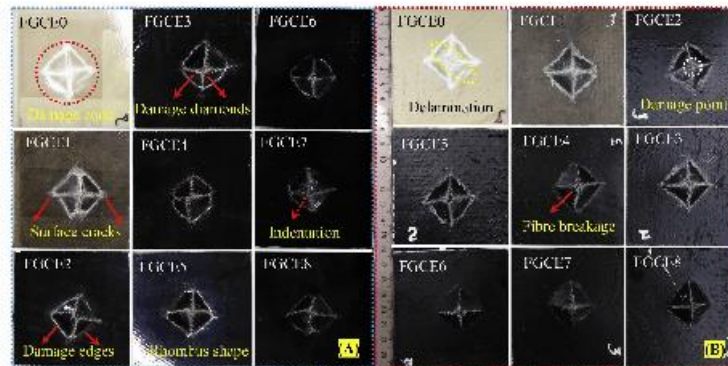
Fig. 7. Photographs of impacted panels on front and back views.

116
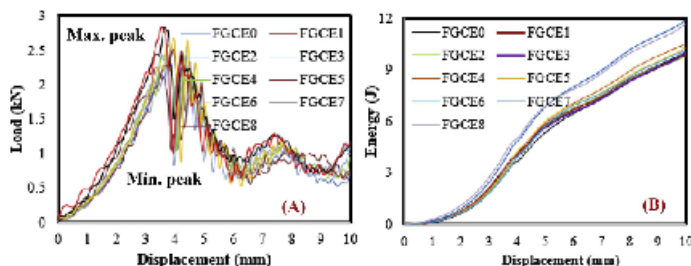
Fig. 8. A) Impact load versus displacement, and B) Impact energy versus displacement of the obtained panels.

were affected gradually by CNTs addition, where the mass decreased by −7% (compared with virgin panel) by adding CNTs at lower concentration (0.05 wt%), leading to decrease in fuel consumption and CO_2 emission by 4.9% and 7.7%, respectively. These improvements in the specified terms were increased gradually by increasing the amount of CNTs in the obtained matrix until 0.35 wt% of CNTs. At this concentration of CNTs, the mass decreased by −23% (compared with virgin panel), which caused significant fuel consumption and CO2 emission by 16.1% and 25.3%, respectively. When CNTs loading was increased up to 0.4 wt%, the analyzed terms decreased by −3%, 2%, and 3.2%, respectively. This was due to agglomeration of CNTs, which led to decrease in panel strength. This required to increase the cross-section of the panel during the design process to be able to withstand the applied load, thus increasing the mass, fuel consumption, and carbon reduction of the obtained panels. Based on these values and environmental performance of the obtained panels, application of present technology on an industrial scale in structure of cars gives a possibility to

decrease CO_2 emission by − 9581 kg CO2-eq/t and to decrease energy consumption by 16.1%, as shown in Fig. (9B).

4.5. Thermal properties of recovered epoxy resin

Fig. (10) shows the results of TGA-DTG analysis for the obtained panels. As illustrated in the TGA analysis curves (Fig.(10A)), all panels exhibit similar thermal degradation features distributed in successive three regions. The first degradation zone is located in the range of 50 °C-316 °C with a very small weight fraction loss −2.4% due to evaporation of water and some organic components in the decomposed epoxy and hardener. After that, a significant weight loss (−40%) is manifested in the temperature range of 317 °C-467 °C and maximum decomposition temperature at 430 °C due to the complete composition of epoxy and their compound, especially Bromine [69]. Also, it was noted that the nanocomposite panels had a higher thermal stability in terms of less weight loss (64% for neat and 60% for with reduction −4%), while the last decomposition zone showed significant decomposition (42–46%) and this fraction represented the fiberglass that needs a very high temperature for decomposition [70]. Also, it was not possible to determine the amount of PCNTs because of smaller mixing amount (0.35 wt%). Based on these results, only −62 wt% of the total weight of the obtained matrix were decomposed and these results agree with the percentages used before to prepare the panels.

5. Conclusion

In the present research, the functionalized carbon nanotubes (FCNTs) were used to improve the mechanical, thermal, and impact properties of fiberglass/epoxy laminates by 60, 5, and 31%, respectively. FCNTs were dispersed uniformly in epoxy and hardener solutions using probe sonicator, ultrasonic path, mechanical mixer, and vacuum infiltration. Then, they were assembled with fiberglass layers using vacuum-assisted resin transfer followed by preparation of final panels after exposure to curing process. Also, an environmental model was developed to evaluate greenhouse gas emission (GHGE) in order to study their potential applications in vehicle industries. According to the model developed using the panel fiberglass/0.35 wt% of FCNTs/epoxy laminated panels in vehicle applications, fuel consumption and GHGE can decrease significantly by 16% and −26%, respectively as a result of a significant reduction of the obtained panels by 23%. Based on these results, fiberglass/epoxy nanocomposites could be classified as an eco-friendly material with high potential for application in vehicle industries with less fuel consumption and GHGE.
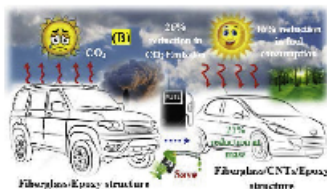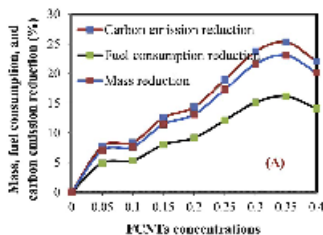
Fig. 9. A) Effect of FCNTs on the mass, fuel, and CO_2 reduction of the obtained panels, and B) CO_2 emission from neat fiberglass and nanocomposite panels.

117
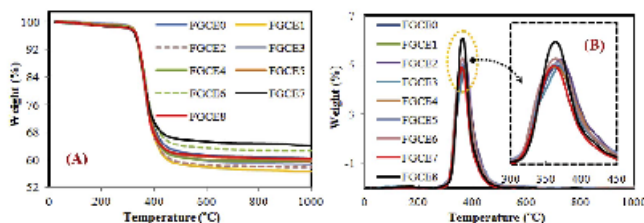
Fig. 10. TGA-DTG analysis of the prepared panels.

Declaration of competing interest

The authors declare that they have no known competing financial interests or personal relationships that could have appeared to influence the work reported in this paper.

CRediT authorship contribution statement

Sharath P. Subadra: Data curation, Software. **Samy Yousef:** Conceptualization, Formal analysis, Writing - original draft. **Paulius Griskevicius:** Writing - review & editing. **Vidas Makarevicius:** Visualization.

References

[1] E. Baltar do Souza Leão, L. F. M. do Nascimento, J.C.S. de Andrade, J.A. Puppim de Oliveira, Carbon accounting approaches and reporting gaps in urban emissions: an analysis of the Greenhouse Gas inventories and climate action plans in Brazilian cities, J. Clean. Prod. (2019), https://doi.org/10.1016/j.jclepro.2019.118930.

[2] A.K.M. Tarigan, Expectations, attitudes, and preferences regarding support and purchase of eco-friendly fuel vehicles, J. Clean. Prod. (2019), https://doi.org/10.1016/j.jclepro.2019.04.190.

[3] https://www.carbonbrief.org/analysis-fossil-fuel-emissions-in-2018-increasing-at-fastest-rate-for-seven-years.

[4] F. Del Pero, M. Delogu, M. Pierini, The effect of lightweighting in automotive LCA perspective: Estimation of mass-induced fuel consumption reduction for gasoline turbocharged vehicles, J. Clean. Prod. (2017), https://doi.org/10.1016/j.jclepro.2017.04.013.

[5] J. Fan, J. Njuguna, An introduction to lightweight composite materials and their use in transport structures, in: Lightweight Composite Structures in Transport: Design, Manufacturing, Analysis and Performance, 2016, https://doi.org/10.1016/B978-1-78242-325-6.00001-3.

[6] Q. Dasgupta, G. Madras, K. Chatterjee, Gradient platform for combinatorial screening of thermoset polymers for biomedical applications, Mater. Sci. Eng. C (2019), https://doi.org/10.1016/j.msec.2018.10.023.

[7] A.B.M. Supian, S.M. Sapuan, M.Y.M. Zuhri, E.S. Zainudin, H.H. Ya, Hybrid Reinforced Thermoset Polymer Composite in Energy Absorption Tube Application: A Review, Defence Technology, 2018, https://doi.org/10.1016/j.dt.2018.04.004.

[8] V.R. Raman Bharath, R. Vijaya Ramnath, N. Manoharan, Kenaf fibre reinforced composite: a review, ARPN Journal of Engineering and Applied Sciences (2015), https://doi.org/10.1016/j.matdes.2011.04.008.

[9] M.F.M. Alkbir, S.M. Sapuan, A.A. Nuraini, M.R. Ishak, Fibre properties and crashworthiness parameters of natural fibre-reinforced composite structure: a literature review, Compos. Struct. (2016), https://doi.org/10.1016/j.compstruct.2016.01.098.

[10] R. Polanský, P. Prosr, M. Čermák, Determination of the thermal endurance of PCB FR4 epoxy laminates via thermal analyses, Polym. Degrad. Stabil. (2014), https://doi.org/10.1016/j.polymdegradstab.2014.03.043.

[11] D.S. Lobanov, O.A. Staroverov, The fatigue durability GFRP under increased temperatures, Procedia Structural Integrity (2019), https://doi.org/10.1016/j.prostr.2019.08.087.

[12] A. Jafari, M. Bazli, H. Ashrafi, A. Vatani Oskouei, S. Azhari, X.L. Zhao, H. Gholipour, Effect of fibers configuration and thickness on tensile behavior of GFRP laminates subjected to elevated temperatures, Construct. Build. Mater. (2019), https://doi.org/10.1016/j.conbuildmat.2019.01.003.

[13] A. Gliniczynski, T. Kubiak, P. Rozylo, P. Jakubczak, J. Bieniaś, The response of laminated composite plates and profiles under low-velocity impact load, Compos. Struct. (2019), https://doi.org/10.1016/j.compstruct.2018.09.005.

[14] L. Li, S.V. Lomov, X. Yan, Correlation of acoustic emission with optically observed damage in a glass/epoxy woven laminate under tensile loading, Compos. Struct. (2015), https://doi.org/10.1016/j.compstruct.2014.12.029.

[15] W. Chen, Q. Meng, H. Hao, J. Cui, Y. Shi, Quasi-static and dynamic tensile properties of fiberglass/epoxy laminate sheet, Construct. Build. Mater. (2017), https://doi.org/10.1016/j.conbuildmat.2017.03.074.

[16] B. Shivamurthy, K. Udaya Bhat, S. Anandhan, Mechanical and sliding wear properties of multi-layered laminates from glass fabric/graphite/epoxy composites, Mater. Des. (2013), https://doi.org/10.1016/j.matdes.2012.07.059.

[17] L. Lampani, F. Sarasini, J. Tirillò, P. Gaudenzi, Analysis of damage in composite laminates with embedded piezoelectric patches subjected to bending action, Compos. Struct. (2018), https://doi.org/10.1016/j.compstruct.2018.04.073.

[18] E. Lomakin, B. Fedulov, Nonlinear deformation and failure analysis of laminated composites, in: Procedia Structural Integrity, 2018, https://doi.org/10.1016/j.prostr.2018.12.110.

[19] M. Tatariants, S. Yousef, G. Denafas, M. Tichonovas, R. Bendikiene, Recovery of gold, other metallic and non-metallic components of full-size waste random access memory, J. Clean. Prod. (2018), https://doi.org/10.1016/j.jclepro.2017.11.132.

[20] S. Yousef, M. Tatariants, M. Tichonovas, R. Bendikiene, G. Denafas, Recycling of bare waste printed circuit boards as received using an organic solvent technique at a low temperature, J. Clean. Prod. (2018), https://doi.org/10.1016/j.jclepro.2018.03.227.

[21] M. Tatariants, S. Yousef, G. Denafas, R. Bendikiene, Separation and purification of metal and fiberglass extracted from waste printed circuit boards using milling and dissolution techniques, in: Environmental Progress and Sustainable Energy, 2018, https://doi.org/10.1002/ep.12899.

[22] S. Yousef, M. Tatariants, R. Bendikiene, G. Denafas, Mechanical and thermal characterizations of non-metallic components recycled from waste printed circuit boards, J. Clean. Prod. (2018), https://doi.org/10.1016/j.jclepro.2017.08.195.

[23] M. Tatariants, S. Yousef, R. Sidaraviciute, G. Denafas, R. Bendikiene, Characterization of waste printed circuit boards recycled using a dissolution approach and ultrasonic treatment at low temperatures, RSC Adv. (2017), https://doi.org/10.1039/c7ra07034a.

[24] G.L. Devnani, S. Sinha, Effect of nanofillers on the properties of natural fiber reinforced polymer composites, Mater. Today: Mater. Today. Proc. (2019), https://doi.org/10.1016/j.matpr.2019.06.460.

[25] M.D. Kiran, H.K. Govindaraju, T. Jayaraju, Evaluation of mechanical properties of glass fiber reinforced epoxy polymer composites with alumina, titanium dioxide and silicon carbide, in: Materials Today: Proceedings, 2018, https://doi.org/10.1016/j.matpr.2018.06.602.

[26] M.D. Kiran, H.K. Govindaraju, T. Jayaraju, N. Kumar, Review-effect of fillers on mechanical properties of polymer matrix composites, in: Materials Today: Proceedings, 2018, https://doi.org/10.1016/j.matpr.2018.06.611.

[27] S. Sharma, B.P. Singh, S.S. Chauhan, J. Jyoti, A.K. Arya, S.R. Dhakate, T. Yokozeki, Enhanced thermomechanical and electrical properties of multiwalled carbon nanotube paper reinforced epoxy laminar composites, Compos. Appl. Sci. Manuf. (2018), https://doi.org/10.1016/j.compositesa.2017.10.023.

[28] A.D. Kelkar, Q. Tian, D. Yu, L. Zhang, Boron nitride nanoparticle enhanced prepregs: a novel route for manufacturing aerospace structural composite laminate, Mater. Chem. Phys. (2016), https://doi.org/10.1016/j.matchemphys.2016.03.044.

[29] G.V. Seretis, G. Kouzilos, D.E. Manolakos, C.G. Provatidis, On the graphene nanoplatelets reinforcement of hand lay-up glass fabric/epoxy laminated composites, Compos. B Eng. (2017), https://doi.org/10.1016/j.compositesb.2017.03.015.

[30] Longitudinal and Transverse Compressive Properties of Alumina Nanoparticles Filled Epoxy/unidirectional Glass Fiber Composite Laminate under In-Plane Loading.

[31] R.K. Nayak, Influence of seawater aging on mechanical properties of nano-Al2O3 embedded glass fiber reinforced polymer nanocomposites, Construct. Build. Mater. (2019), https://doi.org/10.1016/j.conbuildmat.2019.06.043.

[32] R.K. Nayak, R.C. Ray, Influence of seawater absorption on retention of mechanical properties of nano-TiO2 embedded glass fiber reinforced epoxy polymer matrix composites, Archives of Civil and Mechanical Engineering (2018), https://doi.org/10.1016/j.acme.2018.07.002.

[33] A. Deep, K.K. Singh, P. Rawat, C. Kumar, R.P. Behera, Effect of nano and macro carbon fillers on flexural properties of glass fiber/epoxy composite laminates, IOP

Conf. Ser. Mater. Sci. Eng. (2018), https://doi.org/10.1088/1757-899X/455/1/012007.

[34] W.A.D.W. Dalina, S.H. Tan, M. Mariatti, Properties of fiberglass/MWCNT buckypaper/epoxy laminated composites, Procedia Chemistry (2016), https://doi.org/10.1016/j.proche.2016.03.138.

[35] K. Aly, A. Li, P.D. Bradford, In-situ monitoring of woven glass fiber reinforced composites under flexural loading through embedded aligned carbon nanotube sheets, J. Compos. Mater. (2018), https://doi.org/10.1177/0021998317754120.

[36] Md Musthak, M. Madhavi, P.M. Ahamullah, Study on effects of E-glass fiber hybrid composites enhanced with multi-walled carbon nanotubes under tensile load using full factorial design of experiments, Appl. Nanosci. (2017), https://doi.org/10.1007/s13204-017-0569-8.

[37] S. Sharma, B.P. Singh, S.S. Chauhan, J. Jyoti, A.K. Arya, S.R. Dhakate, T. Yokozeki, Enhanced thermomechanical and electrical properties of multiwalled carbon nanotube paper reinforced epoxy laminar composites, Compos. Appl. Sci. Manuf. (2018), https://doi.org/10.1016/j.compositesa.2017.10.023.

[38] M. Ranjbar, S. Feli, Mechanical and low-velocity impact properties of epoxy-composite beams reinforced by MWCNTs, J. Compos. Mater. (2019), https://doi.org/10.1177/0021998318790049.

[39] S. Han, Q. Meng, S. Araby, T. Liu, M. Demiral, Mechanical and electrical properties of graphene and carbon nanotube reinforced epoxy adhesives: Experimental and numerical analysis, Compos. Appl. Sci. Manuf. (2019), https://doi.org/10.1016/j.compositesa.2019.02.027.

[40] S. Yousef, A. Khattab, T.A. Osman, M. Zaki, Effects of increasing electrodes on CNTs yield synthesized by using arc-discharge technique, J. Nanomater. (2013), https://doi.org/10.1155/2013/392126.

[41] M. Yoonessi, M. Lebrón-Colón, D. Scheiman, M.A. Meador, Carbon nanotube epoxy nanocomposites: the effects of interfacial modifications on the dynamic mechanical properties of the nanocomposites, ACS Appl. Mater. Interfaces (2014), https://doi.org/10.1021/am5056849.

[42] K.S. Khare, F. Khabaz, R. Khare, Effect of carbon nanotube functionalization on mechanical and thermal properties of cross-linked epoxy-carbon nanotube nanocomposite: Role of strengthening the interfacial interactions, ACS Appl. Mater. Interfaces (2014), https://doi.org/10.1021/am405317x.

[43] M.R.A. Salam, M.V. Hosur, S. Zainuddin, S. Jeelani, Improvement in mechanical and thermo-mechanical properties of epoxy composite using two different functionalized multi-walled carbon nanotubes, Open J. Compos. Mater. (2013), https://doi.org/10.4236/ojcm.2013.32a001.

[44] X. Chen, J. Wang, M. Lin, W. Zhong, T. Feng, X. Chen, F. Xue, Mechanical and thermal properties of epoxy nanocomposites reinforced with amino-functionalized multi-walled carbon nanotubes, Mater. Sci. Eng. (2008), https://doi.org/10.1016/j.msea.2008.04.044.

[45] R. Meier, I. Kahraman, A.T. Seyhan, S. Zaremba, K. Drechsler, Evaluating vibration assisted vacuum infusion processing of hexagonal boron nitride sheet modified carbon fabric/epoxy composites in terms of interlaminar shear strength and void content, Compos. Sci. Technol. (2016), https://doi.org/10.1016/j.compscitech.2016.03.022.

[46] K.K. Panchagnula, P. Kuppan, Improvement in the mechanical properties of neat GFRPs with multi-walled CNTs, Journal of Materials Research and Technology (2019), https://doi.org/10.1016/j.jmrt.2018.02.009.

[47] S. Yousef, A. Mohamed, Mass production of CNTs using CVD multi-quartz tubes, J. Mech. Sci. Technol. (2016), https://doi.org/10.1007/s12206-016-1031-7.

[48] A. Mohamed, S. Yousef, M. Ali Abdelnaby, T.A. Osman, B. Hamawandi, M. S. Toprak, A. Uheida, Photocatalytic degradation of organic dyes and enhanced mechanical properties of PAN/CNTs composite nanofibers, Separ. Purif. Technol. (2017), https://doi.org/10.1016/j.seppur.2017.03.051.

[49] G.V. Seretis, et al., Effect of sonication on the mechanical response of graphene nanoplatelets/glass fabric/epoxy laminated nanocomposites, Compos. B Eng. (2018), https://doi.org/10.1016/j.compositesb.2018.04.034.

[50] D.A. Turner, I.D. Williams, S. Kemp, Greenhouse gas emission factors for recycling of source-segregated waste materials, Resour. Conserv. Recycl. (2015), https://doi.org/10.1016/j.resconrec.2015.10.026.

[51] S. Yousef, M. Tatariants, M. Tichonovas, L. Kliucininkas, S.I. Lukošiūtė, L. Yan, Sustainable green technology for recovery of cotton fibers and polyester from textile waste, J. Clean. Prod. (2020), https://doi.org/10.1016/j.jclepro.2020.120078.

[52] S. Yousef, M. Tatariants, M. Tichonovas, V. Makarevicius, Sustainable technology for mass production of Ag nanoparticles and Al microparticles from damaged solar cell wafers, Waste Manag. (2019), https://doi.org/10.1016/j.wasman.2019.08.019.

[53] S. Yousef, J. Eimontas, N. Striūgas, M. Tatariants, M.A. Abdelnaby, S. Tuckute, L. Kliucininkas, A sustainable bioenergy cceversion strategy for textile waste with self-catalysts using mini-pyrolysis plant, Energy Convers. Manag. (2019), https://doi.org/10.1016/j.enconman.2019.06.050.

[54] S. Yousef, Polymer nanocomposite components: a case study on gears, in: Lightweight Composite Structures in Transport: Design, Manufacturing, Analysis and Performance, 2016, https://doi.org/10.1016/B978-1-78242-325-6.00016-5.

[55] N. Wang, et al., Efficient surface modification of carbon nanotubes for fabricating high performance CNT based hybrid nanostructures, Carbon (2017), https://doi.org/10.1016/j.carbon.2016.10.027.

[56] S. Roy, R.S. Petrova, S. Mitra, Effect of carbon nanotube (CNT) functionalization in epoxy-CNT composites, Nanotechnol. Rev. (2018), https://doi.org/10.1515/ntrev-2018-0068.

[57] S. Yousef, et al., Wear characterization of carbon nanotubes reinforced acetal spur, helical, bevel and worm gears using a TS universal test rig, JOM (2015), https://doi.org/10.1007/s11837-014-1268-5.

[58] S. Yousef, A. Visco, G. Galtieri, J. Njuguna, Flexural, impact, rheological and physical characterizations of POM reinforced by carbon nanotubes and paraffin oil, Polym. Adv. Technol. (2016), https://doi.org/10.1002/pat.3801.

[59] X. Liu, et al., Characterization of enhanced interfacial bonding between epoxy and plasma functionalized carbon nanotube films, Compos. Sci. Technol. (2017), https://doi.org/10.1016/j.compscitech.2017.04.004.

[60] H. Tanabi, M. Erdal, Effect of CNTs dispersion on electrical, mechanical and strain sensing properties of CNT/epoxy nanocomposites, Results in Physics (2019), https://doi.org/10.1016/j.rinp.2018.11.081.

[61] A. Godara, et al., Influence of carbon nanotube reinforcement on the processing and the mechanical behaviour of carbon fiber/epoxy composites, Carbon (2009), https://doi.org/10.1016/j.carbon.2009.06.039.

[62] A. Gliszczynski, et al., The response of laminated composite plates and profiles under low-velocity impact load, Compos. Struct. (2019), https://doi.org/10.1016/j.compstruct.2018.09.005.

[63] A. Mishra, N.K. Naik, Failure initiation in composite structures under low-velocity impact: Analytical studies, Compos. Struct. (2010), https://doi.org/10.1016/j.compstruct.2009.08.024.

[64] J.A.M. Ferreira, et al., Impact response of nano reinforced mat glass/epoxy laminates, Fibers Polym. (2015), https://doi.org/10.1007/s12221-015-0173-z.

[65] D. Sadykov, I. Nouicer, C. Lekakou, Hybrid woven glass fibre fabric-multi-walled carbon nanotube-epoxy composites under low rate impact, Journal of Composites Science (2017), https://doi.org/10.3390/jcs1010010.

[66] V.A. Kolnev, et al., Structural and functional properties of composites with carbon nanotubes for space applications, in: Materials Today: Proceedings, 2018, https://doi.org/10.1016/j.matpr.2018.08.036.

[67] N. Li, et al., Interlaminar properties of GFRP laminates toughened by CNTs buckypaper interlayer, Compos. Struct. (2019), https://doi.org/10.1016/j.compstruct.2018.10.002.

[68] M. Ranjbar, S. Feli, Mechanical and low-velocity impact properties of epoxy-composite beams reinforced by MWCNTs, J. Compos. Mater. (2019), https://doi.org/10.1177/0021998318790049.

[69] M. Tatariants, S. Yousef, R. Sidaravicius, G. Denafas, R. Bendikiene, Characterization of waste printed circuit boards recycled using a dissolution approach and ultrasonic treatment at low temperatures, RSC Adv. (2017), https://doi.org/10.1039/c7ra07034a.

[70] G. Fredi, et al., Multifunctional epoxy/carbon fiber laminates for thermal energy storage and release, Compos. Sci. Technol. (2018), https://doi.org/10.1016/j.compscitech.2018.02.005.

119

Superhydrophilic functionalized graphene/fiberglass/epoxy laminates with high mechanical, impact and thermal performance and treated by plasma

Samy Yousef [a, d, *], Sharath P. Subadra [a], Paulius Griškevičius [a], Sarunas Varnagiris [b], Darius Milcius [b], Vidas Makarevicius [c]

[a] Department of Mechanical Engineering, Kaunas University of Technology, LT-51424, Kaunas, Lithuania
[b] Center for Hydrogen Energy Technologies, Lithuanian Energy Institute, Breslaujos 3, 44403, Kaunas, Lithuania
[c] Lithuanian Energy Institute, Breslaujos 3, LT-44403, Kaunas, Lithuania
[d] Department of Materials Science, South Ural State University, Lenin prospect 76, 454080, Chelyabinsk, Russia

ABSTRACT

This research aims to develop superhydrophilic fiberglass/epoxy nanocomposite (FGEC) laminates with high mechanical, thermal, and impact properties. In order to achieve this goal, functionalized graphene (FGA) was used as a nanofiller material to improve the mechanical, impact, and thermal behaviors of FGEC, while the plasma treatment helped to form the oxidized polar functional groups (C9O groups and C–O groups) on the fabricated FGEC laminates, thus modifying their hydrophilic behavior. The experiments were started with production of FGEC laminates by mixing FGA (0.05-0.4 wt%) with epoxy resin in presence of Acetone (to obtain better dispersion), followed by preparation of FGEC laminates using vacuum-assisted resin transfer and curing processes. Afterwards, the surfaces of the fabricated FGEC laminates were treated by air plasma at 13Pa and 30W for different treatment times in the range 5–30 min. Mechanical and impact properties of the untreated and treated laminates were investigated according to ASTM-D7025 and ISO 6603-2 standards, respectively. Also, thermal behavior of the laminates was investigated using a thermogravimetric analysis, while a high resolution camera was used to record and calculate a contact angle of the untreated and treated laminates. SEM and Optical Microscope was used to observe dispersion of FGA, microstructure, impact mechanism, and surface morphology of the fabricated FGEC matrix. Meanwhile, XPS was used to evaluate changes in the surface structures of the untreated and treated samples. The results showed that 0.35 wt% of FGA and 15-min exposure to plasma treatment were enough to improve tensile strength and impact energy of the laminates by 18% and 70%, respectively, and to decrease the water contact angle from 67° to 14°.

1. Introduction

Currently, fiberglass/epoxy resin laminates have been used increasingly in manufacture of structures of the components applied for work in critical environments, including marine, aerospace, etc. This means that majority of these components, including laminates, are subject to harsh and versatile loading conditions in the course of their use in the specified environments, which requires adjustment of special properties (e.g., mechanical, impact, hydrophobic) to such applications. Also, these behaviors should be manifested individually or as a combination of two or more components (depending on operating conditions) [1–3]. In order to meet these requirements of high performance, fiberglass/epoxy resin nanocomposite (FGEC) laminates were introduced. Generally, FGERC laminates are composed of fiberglass layers and epoxy resin modified by different types of nanofiller materials (e.g. Carbon nanotubes, Si, Graphene, etc.) to enhance the bonding and adhesive behavior [4–8]. The recent studies have proved that FGERC laminates have many promising advantages that make them suitable for such environments, including low costs and density, high strength and stiffness, good fatigue, and corrosion resistance [9,10]. Also, these studies showed that Graphene (GA) has better performance compared to other nanofillers due to high surface-area-to-volume ratio of GA [11,12]. In the literature, the studies which were focused on incorporating of GA with fiberglass/epoxy resin (GFGR) laminates have branched into several paths within the following frames: mechanical performance, impact, friction and wear behavior, thermal properties, fracture and failure modes, electromagnetic
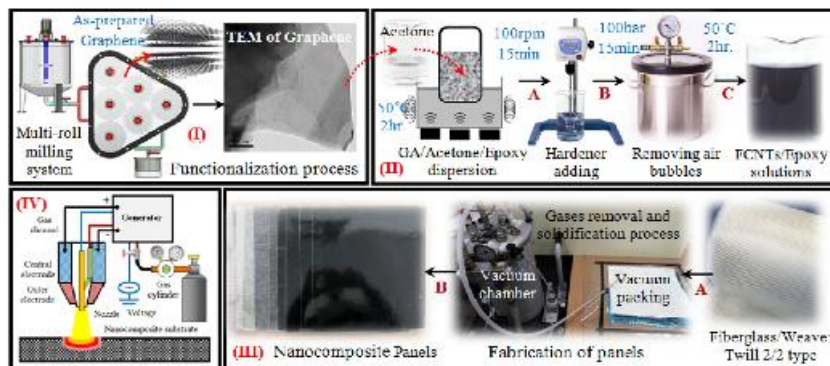
Fig. 1. FGEC laminates – preparation and plasma treatment flowchart.

properties, and advanced applications [13–19].

With regard to the mechanical performance of FGERC, they cover a wide scope, including many different topics such as tensile performance, shear strength, buckling behavior, impact energies, flexural strength, and toughness. All these behaviors were studied at different concentrations of GA in the range 0.05–30 wt% (relative to epoxy and full matrix) and different testing conditions [20–24]. The results showed that GA with lower concentrations (< 0.5 wt%) has a significant effect on mechanical performance in general by improving its strength, flexural strength, shear strength, absorbed energy by 10%, 29%, 36%, 24%, respectively. On the second path, the researchers were focused on the study of fracture and failure modes for most of the previous listed topics. The majority of failure modes occurred as a result of brittle fracture increased by 70% and 206% in mode I and mode II of interlaminar fracture energies, respectively [14,25–27]. Meanwhile, the third path was focused on investigation of thermal properties of the FGEC laminates and the results showed that FGERC is more stable than virgin panels [20,28]. The other path was focused on electromagnetic properties and growing electrical conductivity and studied their potential application in the advanced technologies, including Energy, sensors, vibration, etc. [19,29–31].

As it is evident from the previous section, adding of GA to FGERC laminates resulted in the improvement of many behaviors and these results were a strong motivation for researchers to try to improve these behaviors more by controlling properties of GA itself. With this regard, the effect of GA particle size on mechanical, interlaminar shear property of FGERC laminates was studied and the results showed that small-sized GA particles have better performance compared to the particles of bigger size [32,33]. Also, the effect of surface morphology of GA on performance of FGERC laminates was investigated. The results revealed that the functionalization process has a significant impact on GA surface modification and removal of amorphous impurities of the GA particles, which leads to reduced agglomeration of GA and greater adhesion with epoxy composite when covalent bonding is used [34–36].

Also, preparation of GA/epoxy solutions and FGERC laminates is considered to be one more challenge. It is known that high viscosity of epoxy resin impedes dispersion of GA in epoxy uniformly; therefore, Marra et al. (2018) used acetone as a green solvent to decrease viscosity of epoxy, thus obtaining better dispersion [37]. However, it was noted that the addition of GA increases roughness of FGERC laminates significantly [38–40], which affects negatively their hydrophobic

properties and increases the water contact angle from 70° to 108° [41, 42]. In order to improve the surface morphology of the fiber/epoxy laminates, Li et al. (2018) used a plasma process as a surface treatment to repair damaged composites successfully and to reduce the water contact angle of carbon fiber/epoxy laminates from 78° to 35° [43]. Based on the optimum conditions reported in the literature, in the present work the functionalized GA (FGA) was used as a nanofiller material for enhancing mechanical, thermal, and impact properties of FGEC laminates in the presence of acetone as a mixing assistant. Afterwards, hydrophobic properties of the fabricated panels were improved using plasma treatment without a significant effect on the aforementioned properties, thus developing superhydrophilic FGEC laminates with high mechanical, thermal, and impact properties that could be used for self-cleaning, treatment of ground water, anti-corrosion, and for other water applications.

2. Experimental

2.1. Materials and chemicals

Epoxy resin and its hardener (EPIKOTE Resin MGS® RIMR 135 and EPIKURE Curing Agent MGS® RIMH 1366) were purchased from Momentive. Glass fabric Panda™ (Weave: Twill 2/2 type and weight: 163 g/m²) was supplied by R&G Faserverbundwerkstoffe GmbH, Waldenbuch, Germany. All other chemicals used in this work were purchased from Sigma-Aldrich.

2.2. Design of the research experiments

The layout of the present research was designed according to the main concept of fiberglass/epoxy laminate panel production technologies combined with other advanced processing technologies used to improve the dispersion process and surface treatment. Fig. 1 shows the designed layout that is composed of four phases: I) Production and functionalization process of GA, II) dispersion of FGA in epoxy/hardener solutions, III) preparation of fiberglass/epoxy laminate nanocomposite panels, and IV) plasma treatment of the obtained panels. Finally, morphology, hydrophobic, mechanical, impact, and thermal properties of the treated panels were observed and tested based on the standard methods. All these phases are explained in detail in the following sections.
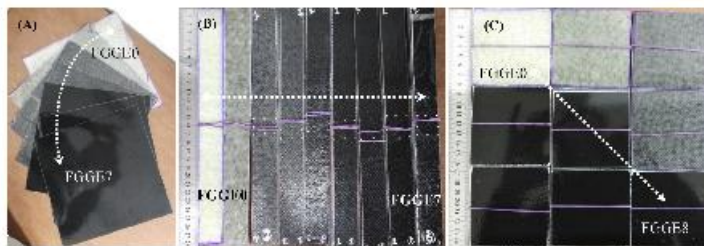
2

Fig. 2. A) Images of the fabricated FGEC laminates, and B,C) Photos of the mechanical and impact standard specimens, respectively.

2.2.1. Production and functionalisation of graphene

Graphene used in the present study was synthesized using multi-roll milling device and low-temperature expandable graphite as a raw material (Fig. 1I) [11]. The synthesized process was conducted at 500 rpm for 45 min to produce as-prepared GA with an average thickness of 15 nm and 15 μm in length. Afterwards, the prepared GA was exposed to chemical functionalization process at 120 °C in an acid mixture (H2SO4: HNO3 = 3:1) for 30 min to remove the exfoliated particles and impurities from the as-prepared GA and to reduce the agglomeration between their layers [34–36], thus obtaining the functionalized GA (FGA) as shown in high-resolution transmission electron microscopy (TEM) image (Fig. 1I).

2.2.2. Dispersion of graphene in epoxy solutions

In order to prepare uniformly distributed FGA/epoxy solutions and to avoid any probability of FGA agglomeration during the dispersion process, at first FGA with concentrations 0.05, 0.1, 0.15, 0.2, 0.25, 0.3, 0.35, 0.4 wt% (relative to epoxy) was dispersed in acetone (FGA: Acetone 100mg/20 ml) under the effect of sound wave for 1 h at 50 kHz [37]. Then liquid epoxy resin (70 wt% of the total matrix weight) was added to the prepared suspension (FGA/Acetone), and everything was mixed together using ultrasonication bath for 4 h at room temperature and at 50 kHz. Evaporation of acetone from the prepared solutions followed, when a magnetic stirrer was engaged at a speed of 300 rpm for 2 h at a temperature of 70 °C (to avoid segmentation and agglomeration of FGA again). Later, a hardener solution (30 wt% of the total matrix weight) was added to FGA/Epoxy solutions and everything was mixed together using a mechanical mixer for 20 min. Finally, the cavities and entrapped air bubbles were removed from the FGA/Epoxy/Hardener solutions by keeping the solutions in vacuum infiltration at −100 bar for 10 min, thus preparing the final solutions as shown in Fig. 1II.

2.2.3. Fabrication of FGEC laminate panels

According to ASTM standards, it is necessary to maintain the laminate thickness of at least 1 mm (after shrinkage) for mechanical and impact property measurements. To achieve and maintain that, 4 layers of Glass fabric Panda™ (Weave: Twill 2/2 type) with 92 g and nominal size of 260 mm × 310 mm were cut from the supplied roller for each FGA batch. FGA/Epoxy/Hardener solutions with different concentrations of FGA (0.05–0.4 wt%) were used as an adhesive material for fabricating a 1-mm-thickness FGEC laminates composed of four layers of fiberglass. Vacuum assisted resin transfer method was used to fabricate FGEC

laminates. Then the laminates were post-cured using infra-red lamp at 80 °C for 8 h followed by a main curing process in the industrial oven at 90 °C for 6 h, where the curing process had a significant effect on the cross-linking of FGA/Epoxy chains and achieving of the homogeneity in the structure of the obtained laminates (Fig. 1III) [39], thus obtaining the final FGEC laminates as shown in Fig. 2A. Finally, automatic cutter was used to cut the mechanical specimens (25 mm × 270 mm; according to ASTM D7025) and impact specimens (80 mm × 80 mm; according to ISO 6603-2 standard) from the obtained FGEC laminates as shown in Fig. 2B,C, respectively. For simplicity, each sample was given a code based on the concentrations of FGA, as shown in Table 1.

2.2.4. Plasma treatment

The low-temperature air plasma treatment was performed in a vacuum chamber at constant pressure (13Pa) and applied power 30W (700V) produced by a DC generator as shown in Fig. 3. In order to select the optimum plasma treatment conditions (particularly plasma treatment time) constrained by achieving minimum contact angle, the initial plasma experiments were performed only with two samples from the prepared FGEC laminates; FGCE0 (neat sample) and FGCE7 (higher concentration of FGA). The initial plasma experiments were started by cutting small pieces (50 mm × 30 mm) from the selected samples, then exposing them to plasma treatment under the conditions specified above for different treatment times: 5, 10, 15, 20, 25, 30 min, followed by measurement of the contact angle of each sample as a function of treatment time, and then selecting the optimum plasma treatment time.

3. Characterizations

Scanning Electron Microscope (SEM) was employed to observe dispersion of GA in the fabricated FGEC laminates, microstructure, and surface morphology of the untreated and treated laminates, while Optical Microscopy (Hirox digital microscope KH 8700) was used to analyze the impact mechanism. The effect of plasma treatment on the surface elemental compositions and functional group of the fabricated FGEC laminates was assessed by X-ray photoelectron spectroscopy (XPS). The contact angles (θ°) of the fabricated FGEC laminates were calculated using sessile drops method (using Eq. (1)), where h and d represent the height (mm) and diameter (mm) of the droplet itself. Finally, the changes in surface energy (in terms of contact angle of a distilled water droplet) of the untreated and treated FGEC laminates were measured with Laboratory-made apparatus connected to a digital

Table 1
Sample codes of the fabricated FGEC laminates.

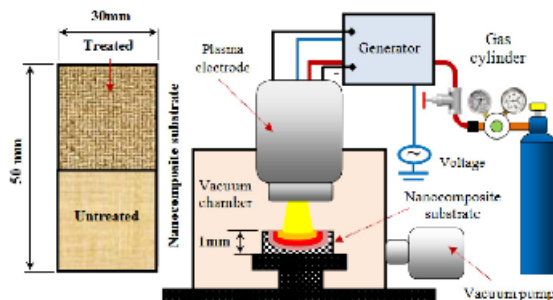| Sample codes	FGGE0	FGGE1	FGGE2	FGGE3	FGGE4	FGGE5	FGGE6	FGGE7
PGA (wt.%)	0	00.5	0.15	0.20	0.25	0.30	0.35	0.40

122

Fig. 3. Diagrammatic sketch of the main components of plasma treatment.

camera to record the formulated water droplet on the tested surfaces within 5 s. Then the open source software ImageJ (image processing and analysis) was employed to measure the contact angles of the formulated water droplets. It is worth mentioning that the contact angles of the treated samples were measured within 5 min after extracting the treated samples from the vacuum chamber into an ambient atmosphere. Also, the measured contact angles were the average of 10 measurements.

$$\theta = 2 arctg(\frac{2A}{d}) \qquad (1)$$

The mechanical tensile behaviors of the fabricated FGEC laminates were determined by a Lloyd Universal Testing Machine (model LR10K) connected to a high-resolution camera to indicate the actual deformation. Meanwhile, the impact energies of the FGEC laminates were measured at room temperature and constant impact energy (50J) using Coesfeld Magnus 1000 High-speed drop tower with cylindrical steel impactor with 20 mm in diameter and hemispherical end with a mass of 5.129 kg. The mechanical and impact tests were performed on five specimens from each FGA batch. Finally, the thermal stability of the fabricated FGEC laminates in terms of weight loss was measured by Thermogravimetric analysis (TA instruments TGA Q500) at N_2 flow rate 15 °C/min.

4. Results and discussions

4.1. Dispersion and microstructure of the fabricated FGEC laminates

In order to check dispersion of FGA in the obtained FGEC laminates and its effect on the microstructure of the panels, four samples were selected for examination process using SEM: FGGE0 (neat panel for comparison), FGGE1 (lowest concentration of FGA), FGGE6 (optimum concentration of FGA based on the illustrated results in the next sections), and FGGE7 (highest concentration of FGA). The selected samples for SEM observation were cut from the obtained panels (had size within 5 mm × 10 mm), then cleaned in ethanol under the effect of sound waves for 1 h to remove any contaminated elements, followed by coating with a very thin layer of gold to avoid blurring of contours of epoxy during the high voltage-observation process. Afterwards, the coated samples were fixed on a carbon grid holder in a vertical direction and the examination process was started. Fig. 4 shows the microstructure cross-section of FGGE0, FGGE1, FGGE6, and FGCE7 panels within the scale range 3–30 μm. As shown in SEM images, the fabricated FGEC panels are composed of several laminates containing destroyed yarns (weft and warp interlaced at a certain angle) as a result of the shear stress generated during the cutting process. Also, it is clear that the yarns

are distributed in the horizontal direction (parallel to cutting edge "Weft") and in the vertical direction in the form of round shapes representing the cross section of the warp yarns. All of these laminates stick together using epoxy resin. It was noted that weft and wrap yarns had almost the same shape and size in all the examined samples, but the morphology of FGA/Epoxy matrix changed depending on the case (depending on FGA concentration). Therefore, the examination process using SEM was focused on features of FGA/Epoxy in each sample. Generally, failure was occurring in neat epoxy due to ductile fracture in the form of debris (flakes and bulk particles) as shown in Fig. 4A-C [17].

With regard to FGGE1 sample, it seems that the interfacial microstructure did not change significantly when compared with that of FGGE0 sample, where the amount of FGA was not enough to distribute well and to bond with molecules of epoxy, thus obtaining poor dispersion of GA with epoxy Fig. 4D-F. Also, it is evident that fibres in FGGE0 and FGGE1 samples are very smooth with very little traces of adhering matrix, which manifests relatively weak interface. For FGGE6 sample, it was noted that the epoxy debris changed from flakes and bulk particles into small particles, which means that fracture became brittle as a result of increasing viscosity of epoxy and high cross-linking of FGA/Epoxy chains (Fig. 4G-I) [39]. In addition, the destroyed fibers of FGGE6 sample were very rough (compared with neat sample) and had some traces of adhering matrix (indicated by white circles) with less fiber debonding and pullout in the fabricated matrix, which means that such loading of FGA (0.35 wt%) was enough to improve the adherence and satisfactory interfacial adhesion of FGA sheets and fiberglass/epoxy laminates [26,44]. Distribution of undulation in SEM photos also shows a reasonably uniform dispersion of FGA throughout the fabricated matrix. Presence of these features indicates that the tested sample became more rigid with higher resistance to fracture and these results agree with mechanical and impact tests in the following sections. At the highest concentration of FGA (FGGE7) (Fig. 4J-L), the fracture surface with neat epoxy is seen to be smooth, without any surface undulation and the fracture became more brittle with very fine particles due to agglomerates of FGA (indicated in white ellipse).

4.2. Analysis of the contact angles

The wettability experiments were performed in two stages; the first stage (initial experiments) was focused on obtaining the optimum plasma time by exposing the neat sample and FGGE7 (high GA concentration) to plasma treatment for 5, 10, 15, 20, 25, 30 min, followed by measuring of a contact angle of each sample as a function of time, then selecting the optimum plasma treatment time. Fig. 5A shows the effect of plasma treatment time on a contact angle. As shown in the
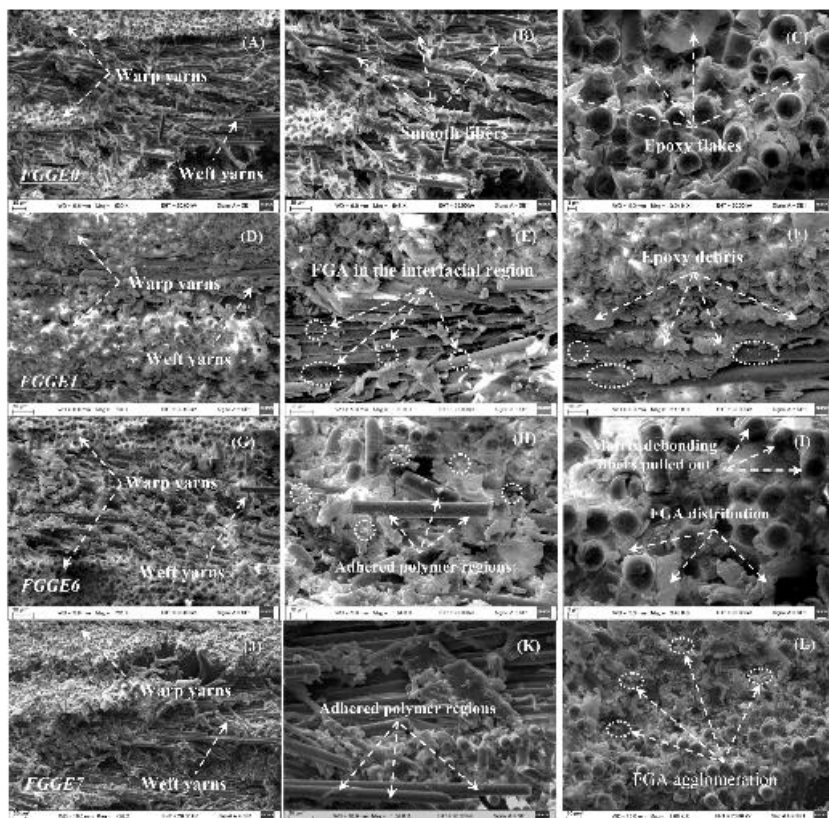
Fig. 4. SEM micrograph of the fracture cross-section of the fabricated FGEC laminates.

figure, the neat sample without treatment has a better contact angle when compared with GA sample, due to the higher roughness of GA, which led to decrease in the angle [41].

After having exposed both samples to plasma treatment, the angle was reduced significantly due to surface modifications as explained in the next sections, then it became stabler after 15 min, keeping the same value. Based on the initial results, 15 min were selected as an optimum plasma time. In the second stage of the experiments, all samples were treated by plasma for 15 min followed by measuring of contact angles as shown in Fig. 5B. It seems that the contact angle of the untreated samples increased significantly after GA had been added as a result of its increased roughness. Once these samples were exposed to plasma process, the contact angles of all the samples were reduced by up to 14° for all the batches as a result of surface modifications.

4.3. Surface analysis of the fabricated FGEC laminates

4.3.1. Surface morphology

Fig. 6 shows surface morphologies of the untreated and treated FGEC laminates observed by SEM. The observation process was focused on FGGE0, FGGE1, FGGE6, and FGGE7 samples. As shown in the SEM image of the untreated FGCE0 sample (Fig. 6A), the untreated surface seems to be very smooth with little debris generated during the cutting process. At the lowest concentration of FGA (FGCE1), it seems that the surface morphology, amount and shape of debris do not change (Fig. 6B). At the optimum loading of FGA (FGCE6), a little debris in the form of fine particles was formulated during the curing process (Fig. 6C). When the amount of FGA was increased up to 0.4 wt% (FGCE7), these fine particles joined together and formed very hard and bulk particles as

5
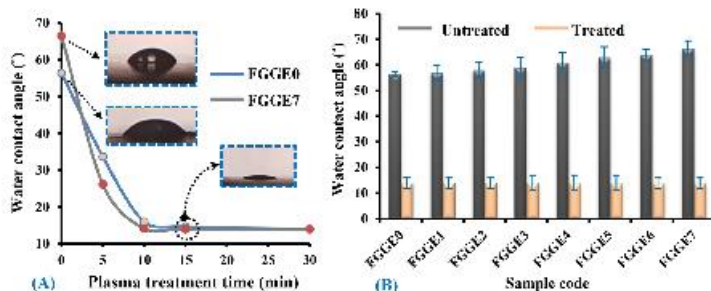
Fig. 5. Effect of plasma treatment time on contact angle measurements of FGGE0 and FGGE7 samples and B) contact angle measurements of all samples at optimum plasma time.
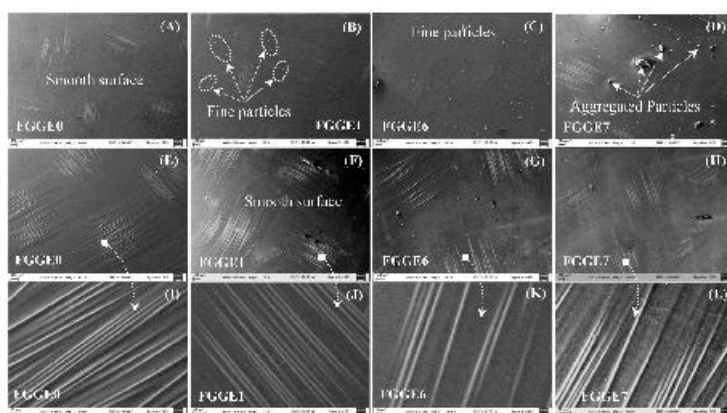
Fig. 6. SEM images of (A–D) the untreated samples and (E–L) the treated FGEC laminates.

a result of FGA agglomeration (Fig. 6D), which led to increased viscosity of the resin and their surface tension during the solidification process [45].

After having exposed the fabricated FGEC laminates to plasma treatment (at the optimum conditions), it was noted that the surface features of the treated samples had not changed a lot and the resin surface layers remained smooth, while most of FGA/epoxy debris was removed or destroyed into fine particles under the effect of plasma treatment. These fine particles can be rearranged again by increasing the treatment time and they can be distributed uniformly with high cross-linking on the treated panel surfaces (Fig. 6E-H). Also, it was observed that glass fibers were emerging gradually without causing any damage to the bare glass fibers resulting from etching of epoxy debris and removal of organic contamination as shown in Fig. 6I-L. These contaminated elements were removed through physical ablation of hydrocarbons on the treated panel surfaces and the selective action of plasma on the composite constituents. Also, addition of FGA to epoxy

matrix manifested high heat conductivity which allowed plasma jet to penetrate inside of the epoxy layer and cause the etching process for epoxy debris, stopping with collision with the layer of fiberglass that had smaller conductivity [43,46]. On the other side, it was noted that the surface of FGGE7 sample became a little rough and hard due to FGA agglomeration (Fig. 6L). Based on these results, low-temperature plasma treatment (30W) can be used as a promising technology for surface epoxy modification without causing any damage to fiberglass.

4.3.2. XPS analysis of the fabricated FGEC laminates

The surface elements and valence structures of neat and nano-composite laminates were analyzed by XPS. Fig. 7A-C shows the survey scan spectra of some batches of the untreated and treated fiberglass laminates, in particular neat sample (FGGE0), low concentration of FGA (FGGE1), and optimum condition of FGA (FGGE6) based on the dispersion results in the above section. As shown in the survey scan spectra results (Fig. 7A-C), all the untreated samples (FGGE0, FGGE1,
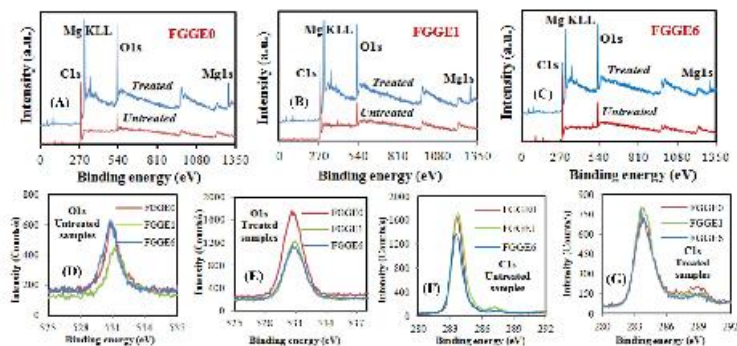
Fig. 7. A-C) Survey scan spectra of the untreated and treated samples, D,E) O1s spectra of the untreated and treated samples, respectively, and F,G) C1s spectra of the untreated and treated samples, respectively.
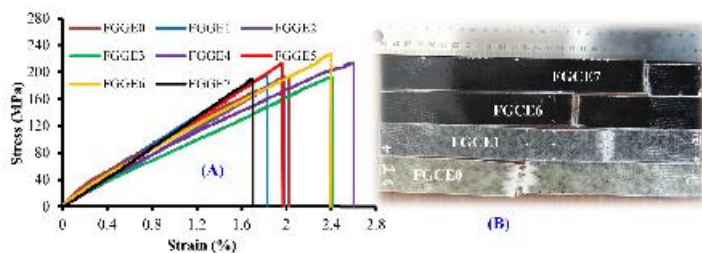
Fig. 8. Stress-Strain curves of the fabricated FGEC laminates and B) Image of the fracture mechanical samples.

and FGGE6) contain the same profiles with two main element orbitals: C1s at 282 eV and O1s at 531 eV.

It was noted that the intensity of these elements decreased significantly at the lowest concentration of FGA, then increased again at higher loading of FGA (Fig. 7D,F). In addition to appearance of new elemental orbital (Mg1s at 1304 eV), the same main element orbitals (C1s at 282 eV and O1s at 531 eV) were observed in all the treated samples (Fig. 7A-C). The presence of new peak at 1304 (Mg1s) means that the surface modification has caused successfully the change of the valence structure of the element [43]. Also, it was noted that the intensity of O1s peak increased significantly after plasma treatment (Fig. 7E), while the intensity of C1s peak decreased (Fig. 7G) due to formed oxidized polar functional groups (C9O groups and C–O groups) and increased number of O-containing functional groups on the surface of the treated samples, which led to improved activity of the treated surface by inducing oxygenation and thus enhancing the molecular bonding of epoxy and GA [46,47], thus decreasing water contact angle and increasing surface energy. These results agree with the contact angle measurement results obtained in section 4.2.

4.4. Mechanical properties of the fabricated FGEC laminates

Fig. 8A and Table 2 show the stress-strain curves and mechanical

Table 2
Mechanical data of untreated and treated fiberglass/FGA/epoxy nanocomposites.

Untreated samples			
Sample Code	Tensile modulus (MPa)	Stress at break (MPa)	Strain at break (%)
FGCE0	6693	191.7	2.02
FGCE1	7262	189.6	1.96
FGGE2	7436	192.1	1.98
FGCE3	7686	194.8	2.41
FGCE4	7837	207.3	1.9
FGCE5	8330	213.8	2.62
FGCE6	8596	226.3	2.41
FGCE7	8604	190	1.69
Treated samples			
FGCE0	6642	193.8	2.09
FGCE6	8536	231.4	2.54

measurements of the untreated panels. As shown in the curves, the deformation of the obtained panels in terms of strain was decreasing gradually with the addition of FGA because the matrix became brittle, especially at the highest loading of FGA. With regard to tensile strength, it is clear that the strength of the panels decreased by adding several FGA

7

126
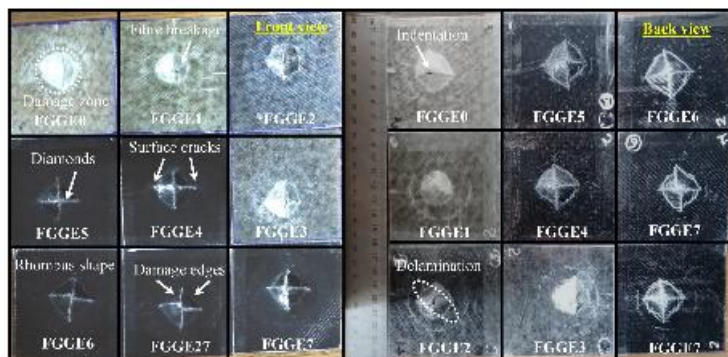
Fig. 9. Photographs of impacted FGEC laminate panels from front and back.

because of poor distribution of FGA in the fabricated matrix followed by gradual improvment in the strength by increasing amounts of FGA upto 0.35 wt% (FGGE6). It improved by 18% when compared with the neat sample and by 8%, when compared with the results obtained by Kiran et al. (2019) due to the effect of surface modification of GA and their uniform dispersion in the fabricated matrixs [25]. At the highest loading of FGA, the strength decreased again due GA agglomeration. Modulus of elasticity (E) also had the same trend, where E increased by 28% at 0.35 wt% loading of FGA and the panels became more rigid, where the addition of FGA to epoxy restricted the molecular rearrangement of epoxy chains and modified their structure during the mixing and solidification processes [28]. Also, use of solvent during the mixing process led to decrease in viscosity of epoxy and allowed GA to penetrate inside of epoxy and incorporate with epoxy molecules, thus improving the elasticity of the panels [37].

Moreover, functionalization contributes strongly to good miscibility and higher interaction between GA through increase of the surface to volume ratio and cross-linked epoxy-GA, thus increasing adhesive properties and energy for fracture, thus increasing amount of pulled-out fibers [35]. Based on the mechanical results confirmed by SEM observations, 0.35 wt% of FGA (FGGE6) were enough to achieve good miscibility and higher interaction between panels and FGA. Therefore,

FGGE6 sample was selected as an optimal nanocomposite panel; then it was exposed to plasma treatment (at 30 W for 15 min) to study the effects of surface treatment on its mechanical behaviors. Also, the neat panel (FGGE0) was treated by plasma for comparison and the resulting data are presented in Table 2. It is clear that the strength and strains of the treated samples were not affected significantly by plasma treatment, because the effects of plasma process only extend on some hundreds of nanometres in depth in the fabricated FGEC laminates without causing any changes in laminate properties [43].

4.5. Impact properties of the fabricated FGEC laminates

4.5.1. Characteristics of the damage areas

The impact test usually accompanies many of the characteristics in the damage areas as a result of collision of the impactor (steel impactor in the present research) with the tested panels under the applied energy (50J). These characteristics in the damage areas can be specified in the following terms: broken fibers, cracks, and delaminations [48]. All these features were observed in all the tested impact samples with some variation as shown in Fig. 9. As shown in the photographs of impacted untreated panels (from front and back views), the impactor penetrates completely in the neat panel (FGCE0) and FGA panels of low
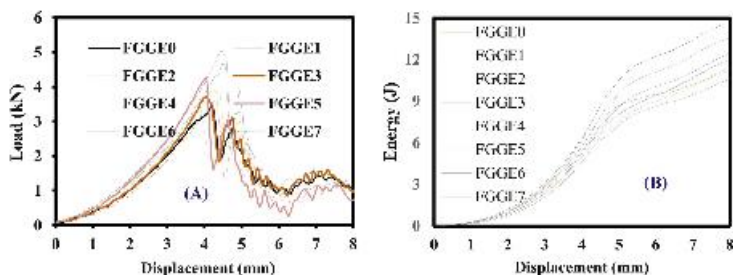
Fig. 10. A) Impact load versus displacement, and B) Impact energy versus displacement of the untreated panels.

8

127
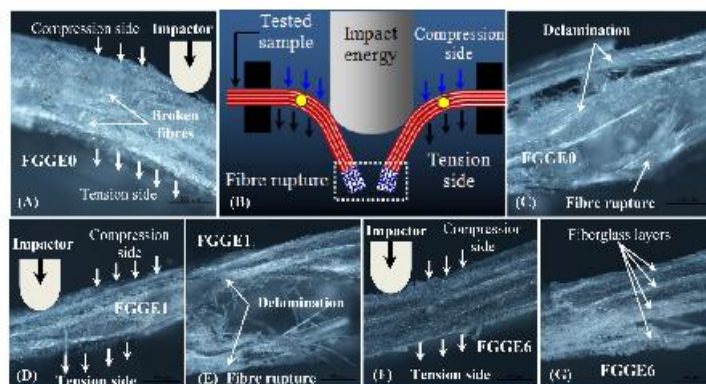
Fig. 11. A,C-G) Microscopic images of the damage impacted samples and B) Diagrammatic sketch of the impact fracture features.

concentration (FGCE1-FGCE3). By increasing the concentration of GA (FGCE4-FGCE7), the panels became more rigid and hard what led to interruption of the impactor's penetration. Also, it was noted that each batch had approximately similar damage features and geometry, including Rhombus profile (damage limitations), diagonals of Rhombus, and damage corners. As shown in the photographs (Fig. 9), all these characteristics and geometries exist in all the batches and some of them have sharp edges, especially at high loading of FGA. Also, the size of the projected failure areas decreases gradually by increasing the amount of FGA. In addition, it seems that the damage edges in the front view is much clearer and sharper than on the back, because during the impact test the front side of the panel was subjected to high compression causing a deformation mode, while backside was exposed to tension stress causing a full fracture with sharp edges (as shown in 4.5.3). This confirms that the fabrication, impact, impact testing, and damage occurred under ideal conditions [49].

4.5.2. Impact load and energy curves of the fabricated FGEC laminates

Fig. 10A, B shows impact load-displacement curves and impact energy-displacement curves of the projection of damage areas, respectively. As shown in the load-displacement curves (Fig. 10A), all sample curves have similar profiles with two sharp peaks corresponding to maximum impact load (at 3.87 mm) and fracture impact load (at and 4.12 mm), respectively. Since all the design theories have been built on the maximum load before failure zone (to increase the safety of the products), therefore, the analysis process of the impact results was focused on maximum impact load and energy of each panel. According to Fig. 10A, B, it seems that by increasing the loading of FGA up to 0.35% (FGCE6), the maximum impact load and impact energy increased by −70% (from 2.81 KN to 4.78 KN) and −48% (from 9.68 J to 14.27 J) due to improved chemical and friction bonds between epoxy molecules and bundles of fiber, resulting in increased rigidity of panels, thus delaying the crack propagation under the applied load and absorbtion of more energy until full failure occurs. At the highest concentration of FGA, the maximum impact load and energy deceased again as a result of agglomeration. These results have a great potential to improve more than 40% of the impact energy, when compared with the results obtained by Kamar et al. (2015) [27].

Finally, the impact test was performed again on FGCE0 sample (neat sample) and FGCE6 sample (as an optimum sample) after the plasma treatment. It was noted that plasma treatment did not have a significant effect on the impact properties (by improving impact load and impact energy by 3–5%) due to the same reasons that were listed in section 4.4 above. Based on these results, the functionalization of FGA and its mixing with epoxy in presence of solvent can be considered as an appropriate approach to improve the impact response of fiberglass/epoxy composites.

4.5.3. Observation of the impact fracture

In order to observe the fracture cross section surface of the impacted untreated-samples, the damaged samples (FGGE0, FGGE1, and FGGE6) were cut in the middle, then cleaned using ethanol and examined using Optical Microscopy within scale 800 μm. As shown in the diagrammatic sketch (Fig. 11B), the impact on the tested sample is similar to a simple supported beam. During the impact test, the upper surface of this beam was subject to compression stress, while the bottom side was subjected to tensile stress leading to failure. Based on the schematic sketch, the damage area in the horizontal direction is limited by two corners (indicated by yellow circles), while the vertical damage is limited by fibre rupture. The observation process using Optical Microscopy was focused on two zones: damage limitations (yellow circles) and the end of damage (fibre rupture). Fig. 11A, C-G shows microscopic photos of the impact fracture surfaces of FGGE0, FGGE6, and FGGE7 samples. The examination of FGGE0 in the horizontal direction shows a high deformation at this point with few broken fibers attached to the surface (Fig. 11A), while the end of fracture presents fibre rupture combined with delamination features (Fig. 11C). FGGE1 sample introduced the same features like in case of FGGE0 sample with relatively strong interface (Fig. 11D,E). At 0.35 wt% concentration of FGA (FGGE6), the impact fracture surface is seen to be smooth without any surface undulation compared with a neat sample. Also, the damage became brittle with little black particles and low deformation and relatively smaller matrix deformation and few microcracks. These results demonstrate that addition of FGA to fiberglass/epoxy matrix using the developed technique leads to increase in rigidity of the panels and these results agree with the results obtained from the impact load and energy curves in the previous section.
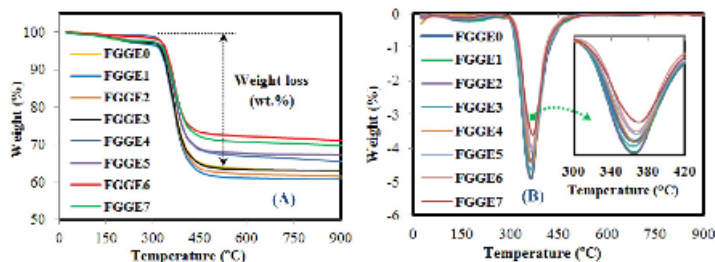
128

Fig. 12. TGA-DTG analysis of the fabricated panels, respectively.

4.6. Thermal properties of the fabricated FGEC laminates

Fig. 12 shows TGA-DTG profiles of the fabricated panels in the range from room temperature to 900 °C. As shown in TGA results (Fig. 12A), all panels were decomposed in three consecutive stages in the ranges of 50–310 °C, 311–410 °C, and 411–900 °C with total estimated weight loss in the range 29.2–38.6 wt% (depending on the loading of FGA in the prepared matrix). The decomposition of the first stage (2.6 wt%) occurred due to evaporation of moisture and degradation of few organic components in the fabricated panels, while the second decomposition (in the range 311–410 °C) corresponds to the complete degradation of epoxy and hardener. It seems that this stage represents the major degradation stage with weight loss estimated by 22.3–34.1 wt%. Also, it is clear that the nanocomposite panels showed better thermal stability (in terms of weight loss) with 16% improvement, when compared with neat panels due to two reasons: a) the pyrolysis of oxygen containing functional groups of CO, CO_2, and steam during the thermal reaction and b) the structural modification of the epoxy system and improvement in their crystallinity [16,50]. For the last degradation stage, it seems that a very small decomposition was occurring during this phase (~3%) as a result of decomposed remaining epoxy components and organic components in the fiberglass fraction (converted into a char energy product), while the inorganic components in the fiberglass need high temperature for decomposition [51,52]. Based on TGA results, addition of FGA to epoxy in presence of solvent influences the thermal degradation profile of the fabricated panels with total decomposition of 29 wt% for FGGE6 and 37 wt% for FGGE0, what means that the thermal stability of nanocomposite panels is stabler (with 22% improvement), when compared with a neat epoxy without a significant effect on the maximum degradation temperatures as shown in DTG results (Fig. 12B).

5. Conclusion

In the present research, the authors succeeded to make superhydrophobic fiberglass nanocomposites with high mechanical and impact performance and thermal stability, as well. The functionalized graphene (FGA) was used in the presence of green solvent to modify the epoxy molecular matrix, thus improving the strength, impact energy, and thermal behavior of the made fiberglass/epoxy laminates. The low temperature plasma treatment was used to etch the resin debris from the manufactured surfaces and it increased the oxygen functional groups on the panel surfaces leading to decrease in their contact angle by ~80%, thus improving their hydrophobic property and converting it into superhydrophobic material that can be used for many applications, including water-resistant, construction, anti-icing surfaces, lightweight, marine, anticorrosion surfaces etc. Also, the treated nanocomposite panels showed a high thermal stability with 22% improvement, when

compared with a neat panel. According to these results, the developed approach can serve as a promising technology for mass production of high strength, impact, and superhydrophobic fiberglass nanocomposite panels for multi-functional applications.

Authorship statement

All experiments and results analysis were performed equally between all authors.

Declaration of competing interest

The authors declare that they have no known competing financial interests or personal relationships that could have appeared to influence the work reported in this paper.

CRediT authorship contribution statement

Samy Yousef: Formal analysis, Funding acquisition, Investigation, Methodology, Writing - original draft, Writing - review & editing. Sharath P. Subadra: Formal analysis, Investigation, Methodology, Writing - original draft. Paulius Griškevičius: Writing - review & editing. Sarunas Varnagiris: Investigation, Methodology, Writing - original draft, Formal analysis. Darius Milcius: Writing - original draft, Formal analysis. Vidas Makarevicius: Methodology, Visualization.

References

[1] A.P. Mouritz, Advances in understanding the response of fibre-based polymer composites to shock waves and explosive blasts, Compos. Appl. Sci. Manuf. (2019), https://doi.org/10.1016/j.compositesa.2019.105502.

[2] A. Jafari, M. Bazli, H. Ashrafi, A. Vatani Oskouei, S. Azhari, X.L. Zhao, H. Gholipour, Effect of fibers configuration and thickness on tensile behavior of GFRP laminates subjected to elevated temperatures, Construct. Build. Mater. (2019), https://doi.org/10.1016/j.conbuildmat.2019.01.003.

[3] C.M. Vu, T.V. Nguyen, L.T. Nguyen, H.J. Choi, Fabrication of adduct filled glass fiber/epoxy resin laminate composites and their physical characteristics, Polym. Bull. (2016), https://doi.org/10.1007/s00289-015-1553-7.

[4] A.D. Kelkar, Q. Tian, D. Yu, L. Zhang, Boron nitride nanoparticle enhanced prepregs: a novel route for manufacturing aerospace structural composite laminate, Mater. Chem. Phys. (2016), https://doi.org/10.1016/j.matchemphys.2016.03.044.

[5] S. Yousef, A. Mohamed, Mass production of CNTs using CVD multi-quartz tubes, J. Mech. Sci. Technol. (2016), https://doi.org/10.1007/s12206-016-1031-7.

[6] G.V. Seretis, G. Kouzilos, D.E. Manolakos, C.G. Provatidis, On the graphene nanoplatelets reinforcement of hand lay-up glass fabric/epoxy laminated

10

129

composites, Compos. B Eng. (2017), https://doi.org/10.1016/j.compositesb.2017.03.015.

[7] Longitudinal and transverse compressive properties of alumina nanoparticles filled epoxy/unidirectional glass fiber composite laminate under in-plane loading.

[8] R.K. Nayak, B.C. Ray, Influence of seawater absorption on retention of mechanical properties of nano-TiO2 embedded glass fiber reinforced epoxy polymer matrix composites, Arch. Civ. Mech. Eng. (2018), https://doi.org/10.1016/j.acme.2018.07.002.

[9] B. Rairan, M. Dimilović, A. Veg, A. Grbović, A. Bengin, Harmonization of new wind turbine rotor blades development process: a review, Renew. Sustain. Energy Rev. (2014), https://doi.org/10.1016/j.rser.2014.07.137.

[10] M.P.M. Alikhir, S.M. Sapuan, A.A. Nuraini, M.R. Ishak, Fibre properties and crashworthiness parameters of natural fibre-reinforced composite structure: a literature review, Compos. Struct. (2016), https://doi.org/10.1016/j.compstruct.2016.01.098.

[11] S. Yousef, A. Mohamed, M. Tatariants, Mass production of graphene nanosheets by multi-roll milling technique, Tribol. Int. (2018), https://doi.org/10.1016/j.triboint.2018.01.040.

[12] J. Keyte, K. Pancholi, J. Njuguna, Recent developments in graphene oxide/epoxy carbon fiber-reinforced composites, Front. Mater. (2019), https://doi.org/10.3389/fmats.2019.00224.

[13] G.V. Seretis, A.K. Polyzos, D.E. Manolakos, C.G. Provatidis, Tensile performance of graphene nanoplatelets/glass fabric/epoxy nanocomposite laminae, Procedia Struct. Integr. (2018), https://doi.org/10.1016/j.prostr.2018.09.035.

[14] N.T. Kamar, M.M. Hossain, A. Khomenko, M. Haq, L.T. Drzal, A. Loos, Interlaminar reinforcement of glass fiber/epoxy composites with graphene nanoplatelets, Compos. Appl. Sci. Manuf. (2015), https://doi.org/10.1016/j.compositesa.2014.12.010.

[15] S.P. Subadra, S. Yousef, P. Griskevicius, V. Makarevicius, High-performance fiberglass/epoxy reinforced by functionalized CNTs for vehicle applications with less fuel consumption and greenhouse gas emissions, Polym. Test. (2020), https://doi.org/10.1016/j.polymertesting.2020.106480.

[16] Y. He, Q. Chen, H. Liu, L. Zhang, D. Wu, C. Lu, Z. Guo, Friction and wear of MoO3/graphene oxide modified glass fiber reinforced epoxy nanocomposites, Macromol. Mater. Eng. (2019), https://doi.org/10.1002/mame.201900166.

[17] M. Rafiee, P. Nitzsche, J. Laliberte, S. Hind, F. Robitaille, M.R. Labrosse, Thermal properties of doubly reinforced fiberglass/epoxy composites with graphene nanoplatelets, graphene oxide and reduced-graphene oxide, Compos. B Eng. (2019), https://doi.org/10.1016/j.compositesb.2018.11.051.

[18] D.A. Hawkins, A. Haque, Fracture toughness of carbon-graphene/epoxy hybrid Nanocomposites, Procedia Eng. (2014), https://doi.org/10.1016/j.proeng.2014.11.833.

[19] F. Marra, J. Lecini, A. Tamburrano, L. Pisu, M.S. Sarto, Electromagnetic wave absorption and structural properties of wide-band absorber made of graphene-printed glass-fibre composite, Sci. Rep. (2018), https://doi.org/10.1038/s41598-018-30498-3.

[20] D.A. Hawkins, A. Haque, Strain energy release rate and mode-I delamination growth in carbon-graphene/epoxy hybrid nanocomposites, Procedia Eng. (2015), https://doi.org/10.1016/j.proeng.2015.05.080.

[21] S. Zerg, M. Shen, S. Chen, L. Yang, F. Lu, Y. Xue, Mechanical and thermal properties of carbon nanotube- and graphene-glass fiber fabric-reinforced epoxy composite: a comparative study, Textil. Res. J. (2019), https://doi.org/10.1177/0040517518792750.

[22] Z. Asaee, M. Mohamed, S. Soumik, F. Taheri, Experimental and numerical characterization of delamination buckling behavior of a new class of GNP-reinforced 3D fiber-metal laminates, Thin-Walled Struct. (2017), https://doi.org/10.1016/j.tws.2016.12.015.

[23] G.V. Seretis, G. Kouzilos, D.E. Manolakos, C.G. Provatidis, On the graphene nanoplatelets reinforcement of hand lay-up glass fabric/epoxy laminated composites, Compos. B Eng. (2017), https://doi.org/10.1016/j.compositesb.2017.03.015.

[24] J. Jia, X. Du, C. Chen, X. Sun, Y.W. Mai, J.K. Kim, 3D network graphene interlayer for excellent interlaminar toughness and strength in fiber reinforced composites, Carbon (2015), https://doi.org/10.1016/j.carbon.2015.09.001.

[25] J. Wang, X. Jin, C. Li, W. Wang, H. Wu, S. Guo, Graphene and graphene derivatives toughening polymers: toward high toughness and strength, Chem. Eng. J. (2019), https://doi.org/10.1016/j.cej.2019.03.229.

[26] B.V. Kiran, K.M. Rao, D.L. Raju, An investigation on mechanical properties of e-glass fiber reinforced polymer nanocomposites, Mater. Today: Proceedings (2019), https://doi.org/10.1016/j.matpr.2019.07.575.

[27] M. Sánchez, R. Moriche, S.G. Prolongo, A.R. Marrón, A. Jiménez-Suárez, A. Ureña, Evaluation of sensitivity for detecting different failure modes of epoxy matrix composites doped with graphene nanoparticles, Compos. Struct. (2019), https://doi.org/10.1016/j.compstruct.2019.111167.

[28] J. Jia, X. Du, C. Chen, X. Sun, Y.W. Mai, J.K. Kim, 3D network graphene interlayer for excellent interlaminar toughness and strength in fiber reinforced composites, Carbon (2015), https://doi.org/10.1016/j.carbon.2015.09.001.

[29] M. Rafiee, P. Nitzsche, J. Laliberte, S. Hind, F. Robitaille, M.R. Labrosse, Thermal properties of doubly reinforced fiberglass/epoxy composites with graphene

nanoplatelets, graphene oxide and reduced-graphene oxide, Compos. B Eng. (2019), https://doi.org/10.1016/j.compositesb.2018.11.051.

[30] X. Wan, H. Lu, J. Kang, S. Li, Y. Yue, Preparation of graphene-glass fiber-resin composites and its electromagnetic shielding performance, Compos. Interfac. (2018), https://doi.org/10.1080/09276440.2018.1439641.

[31] J. Chu, A.J. Marsden, R.J. Young, M.A. Bissett, Graphene-based materials as strain sensors in glass fiber/epoxy model composites, ACS Appl. Mater. Interfaces (2019), https://doi.org/10.1021/acsami.9b09862.

[32] M. Rafiee, F. Nitzsche, M.R. Labrosse, Fabrication and experimental evaluation of vibration and damping in multiscale graphene/fiberglass/epoxy composites, J. Compos. Mater. (2019), https://doi.org/10.1177/0021998318822706.

[33] F. Wang, L.T. Drzal, Y. Qin, Z. Huang, Size effect of graphene nanoplatelets on the morphology and mechanical behavior of glass fiber/epoxy composites, J. Mater. Sci. (2016), https://doi.org/10.1007/s10853-015-9649-x.

[34] X.L. Zeng, B.L. Tang, X.J. Shen, C.Y. Dang, Y.C. Shi, M.J. Feng, S.Y. Fu, Effect of graphene oxide size on interlaminar shear strength of glass fabric/epoxy composites, Mater. Res. Express (2019), https://doi.org/10.1088/2053-1591/ab34b9.

[35] B. Ahmadi-Moghadam, M. Sharafimasooleh, S. Shadlou, F. Taheri, Effect of functionalization of graphene nanoplatelets on the mechanical response of graphene/epoxy composites, Mater. Des. (2015), https://doi.org/10.1016/j.matdes.2014.10.047.

[36] A. Ashori, A. Fallah, M. Ghiyasi, Y. Yue, Reinforcing effects of functionalized graphene oxide on glass fiber/epoxy composites, Polym. Compos. (2018), https://doi.org/10.1002/pc.24646.

[37] F. Sun, T. Yu, G. Hu, Y. Li, Influence of functionalized graphene by grafted phosphorus containing flame retardant on the flammability of carbon fiber/epoxy resin (CF/EP) composite, Compos. Sci. Technol. (2016), https://doi.org/10.1016/j.compscitech.2016.10.002.

[38] F. Marra, J. Lecini, A. Tamburrano, L. Pisu, M.S. Sarto, Electromagnetic wave absorption and structural properties of wide-band absorber made of graphene-printed glass-fibre composite, Sci. Rep. (2018), https://doi.org/10.1038/s41598-018-30498-3.

[39] R. Umer, Y. Li, Y. Dong, H.J. Haroosh, K. Liao, The effect of graphene oxide (GO) nanoparticles on the processing of epoxy/glass fiber composites using resin infusion, Int. J. Adv. Manuf. Technol. (2015), https://doi.org/10.1007/s00170-015-7427-1.

[40] G.V. Seretis, S.F. Nitodas, P.D. Mimigianni, G.N. Kouzilos, D.E. Manolakos, C.G. Provatidis, On the post-curing of graphene nanoplatelets reinforced hand lay-up glass fabric/epoxy nanocomposites, Compos. B Eng. (2018), https://doi.org/10.1016/j.compositesb.2017.12.041.

[41] N. Jamali, H. Khosravi, A. Rezvani, E. Tohidlou, J.A. Poulis, Viscoelastic and dry-sliding wear properties of basalt fiber-reinforced composites based on a surface-modified graphene oxide/epoxy matrix, J. Ind. Textil. (2019), https://doi.org/10.1177/1528083719850839.

[42] S.G. Prolongo, R. Moriche, A. Jiménez-Suárez, M. Sánchez, A. Ureña, Advantages and disadvantages of the addition of graphene nanoplatelets to epoxy resins, Eur. Polym. J. (2014), https://doi.org/10.1016/j.eurpolymj.2014.09.022.

[43] Z. Xiong, S. Ma, L. Fan, Z. Tang, R. Zhang, H. Na, J. Zhu, Surface hydrophobic modification of starch with bio-based epoxy resins to fabricate high-performance polylactide composite materials, Compos. Sci. Technol. (2014), https://doi.org/10.1016/j.compscitech.2014.01.007.

[44] C. Qing Li, H. Bin Dong, W. Wei Zhang, Low-temperature plasma treatment of carbon fibre/epoxy resin composite, Surf. Eng. (2018), https://doi.org/10.1080/02670844.2017.1420417.

[45] R. Brighenti, A. Carpinteri, D. Scorza, Mechanics of interface debonding in fibre-reinforced materials, J. Compos. Mater. (2016), https://doi.org/10.1177/0021998315612537.

[46] Y. Cheng, et al., Preparation, structure, and properties of surface modified graphene/epoxy resin composites for potential application in conductive ink, Coatings (2018), https://doi.org/10.3390/COATINGS8110387.

[47] G. Zhang, X. Dai, Y. Wang, G. Sun, P. Li, L. Qu, Y. Dou, Preparation and corrosion resistance of ETEO modified graphene oxide/epoxy resin coating, Coatings (2019), https://doi.org/10.3390/coatings9010046.

[48] P.H. Chen, T.C. Chang, K.C. Chang, et al., Effects of plasma treatment time on surface characteristics of indium-tin-oxide film for resistive switching storage applications, Appl. Surf. Sci. 414 (2017) 224-229.

[49] A. Glianczymki, et al., The response of laminated composite plates and profiles under low-velocity impact load, Compos. Struct. (2019), https://doi.org/10.1016/j.compstruct.2018.09.005.

[50] D. Sadykov, L. Nouicer, C. Lekakou, Hybrid woven glass fibre fabric-multi-walled carbon nanotube-epoxy composites under low rate impact, J. Compos. Sci. (2017), https://doi.org/10.3390/jcs1010010.

[51] A. Ashori, M. Ghiyasi, A. Fallah, Glass fiber-reinforced epoxy composite with surface-modified graphene oxide: enhancement of interlaminar fracture toughness and thermo-mechanical performance, Polym. Bull. (2019), https://doi.org/10.1007/s00289-018-2387-z.

[52] S. Hredi, et al., Multifunctional epoxy/carbon fiber laminates for thermal energy storage and release, Compos. Sci. Technol. (2018), https://doi.org/10.1016/j.compscitech.2018.02.005.

130

Sustainability of polymer composites and its critical role in revolutionising wind power for green future

Sharath P. Subadra[1], Paulius Griskevicius[2]
Department of Mechanical Engineering, Kaunas University of Technology, Kaunas, Lithuania
[1]Corresponding author
E-mail: [1]*sharath.peethambaran@ktu.edu*, [2]*paulius.griskevicius@ktu.lt*

Check for updates

Abstract. Fibre reinforced polymer composites are gaining wide acceptability in different sectors due their high specific mechanical properties. They have effectively replaced conventional material like metals in many applications thus imparting lighter weight with higher efficiency. Wind energy sector has grown tremendously over the last decade and as per "The Global Wind Turbine Market-Forecasts from 2020 to 2025", global wind turbine market was valued at US$ 90.144 billion in 2019 and is expected to grow at a CAGR of 5.34 % to reach an estimated market size of US$123.154 billion by 2025. Wind turbine blades are fabricated using fibre reinforced composites with ideally a balsa or foam core. The composites used in this case are essentially glass reinforced in epoxy resins, and these highly engineered materials are difficult to recycle as epoxy is a thermoset resin and are not re-mouldable. This poses an environmental problem and a loss in terms of recoverable capital. Thermoplastics as against thermosets could be an alternative resin material for the blades but this has been less explored by the wind sector. The use of thermoplastic could impart cost reductions due to shorter manufacturing cycle times, recovery of raw materials and reduced tooling adjustments in terms of heating. Recovery of composite constituent parts can provide economic benefits because those constituent parts have high embedded energy. In the context of this dilemma of recyclability of wind turbine blades, this review paper intent to explore the current research and future prospect of recycling wind turbine blade materials.

Keywords: polymer composites, thermosets, thermoplastics, wind turbines, recycling, green economy.

1. Introduction

Fibre reinforced polymer composites are characterised by their higher strength and lower weight which has made them an ideal replacement where metals were used historically especially in the transport sector to significantly reduce the energy consumption and hence reduce the environmental fallout. Three types of composites found in general application are polymer-matrix composites (PMC), metal-matrix composites (MMC) and ceramic-matrix composites (CMC). Based on the reinforcements composites are classified into particulate composites, fibre-reinforced composites and structural composites. Polymer based composites dominates the market and thermosets are the most widely used [1].

Based on a recent market survey by Grand View Research (India & U.S. based market research and consulting company), the composites market size which stood at UD$ 89.04 billion in 2019 is expected to grow at a compounded annual growth rate (CAGR) of 7.6 % from 2020 until 2027. Automotive sector is poised to drive this growth fuelled by a demand for lightweight fuel-efficient vehicles. Aerospace sector is another sector that will lead the growth in composites, especially to be used in aircraft, rockets, satellites, and missiles. Constituent wise, glass fibres where the most widely used fabric in 2019 which accounted for 61.8 % of the revenues. While the same report suggested a robust growth in the carbon fabric segment with a CAGR of 7.6 % from 2020 to 2027. Resins form an important constituent, and thermosetting resins dominate the market contributing

131

72 % of the revenues in 2019 the demand driven by transportation and defence sectors.

As mentioned earlier, thermosetting resins dominate the market and this is true of the wind turbine industry, used in the vacuum infusion of blades. The industry has been hesitant using thermoplastic resins though other sectors are gradually using them, but there is a growing interest on these resins within the wind sector [2]. Typically wind turbine blades are made of reinforcements of fibres (glass or carbon) in plastic polymer such as epoxy, with balsa wood or polyvinyl chloride (PVC) as sandwich core materials and bonded joints, coatings and lightning conductors (fig 1). Wind turbines are estimated to have life cycle of about 25 years and there exist a concern as to what to do with them post expiry [3].
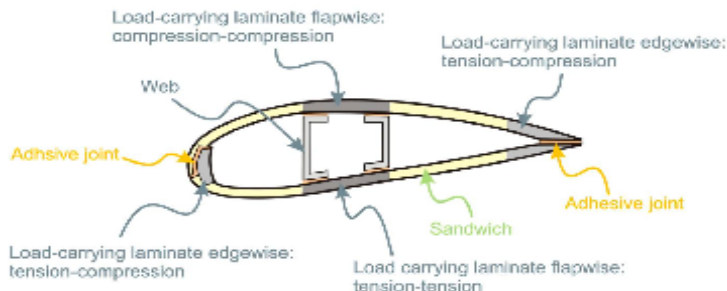
Fig. 1. Wind turbine profile showing its parts and load carrying parts [4]

Professor Henning Albers from the Institute für Umwelt und Biotechnik (Hochschule Bremen, Germany) estimated that for each 1 kW installed an equivalent of 10 kg of rotor blade material would be required. This means a 7.5 MW turbine would require 75 tonnes of material! The associated problems concerns with recycling of the wind turbine blade constituent materials, and as per experts since the sector is quite young, there exists only limited amount of practical knowledge and experience on recycling of the turbines and it takes considerable amount of time to gain experience in dismantling, separation, recycling, and disposal of the system constituent parts [3]. In the context of retiring wind turbines, it was estimated that between 3.9 and 4.8 GW will be decommissioned and most of these are expected to be in Denmark, Germany, the Netherlands, Spain, and Italy (Wind Europe 2019). Around the year 2022, an expected amount of 50,000 tonnes of end-of-life blades is to be handled [5]. In the same parlance a global cumulative waste from retiring wind turbine blades is estimated to be at 43,400,000 tonnes by 2050 considering 20 years lifetime without considering the offshore wind turbines [5]. Therefore, this paper intents to review existing literature on current techniques on recycling wind turbine blades and looking into alternative materials that could make the recycling more sustainable.

2. Current techniques available to recycle wind turbine blades

There are a few technologies available to recycle thermoset composites that go into the manufacture of wind turbine blades and they could be put under the broad category of mechanical, thermal and chemical recycling [6-8]. Each of these methods are further elaborated in the following sub-sections.

2.1. Mechanical recycling

This method involves the use of crushed waste composites as raw material for secondary raw

2

132

materials. Thus, in the context of wind turbine blade this involves pre-cutting and crushing. This recycling method is classified into two basic methods/process, the first method involves breaking up the waste into particles of fine powder while the second method is to shred/crush the waste and the recycled material obtained by the two methods are used as fillers/reinforcements or as raw materials that go into cements/concrete. Few researchers used these techniques for instance, Palmer et al. [9] tried a closed-loop recycling on thermoset composites where in, the material was grinded and later used the recycled GFRP as an ideal replacement for pristine composites. Rotor blades with glass fibre reinforced thermosetting resin was recycled through the mechanical method and used in cement production [10]. On a whole mechanical recycling method is economical and simple and is widely used in recycling of fibre reinforced polymer composites. But on the downside the final product obtained through this method is of low value due to the material especially the fibre being damaged during the recovery process and the process's inability to deliver longer fibres [2].

2.2. Thermal recycling

This method is further classified into three types namely, pyrolysis, fluidized bed recycling process and microwave pyrolysis. The first type essentially involves recovering fibres by decomposing the resin into organic small molecules using inert gas heat. Thus, clean fibres can be obtained by pyrolysis and oxidation and could be subsequently used as reinforcements and can compete with pristine new fibres [11]. Carbon fibres were found to be suitable for this process vis-à-vis the pristine quality of the fibres obtained after pyrolysis but Thomason et al. (2014) found that the strength of the glass fibre after pyrolysis was reduced significantly and there was limited strength re-generation from acid and silane post-treatments of the fibres. Fluidised bed method involves using air as fluidising gas in a fluidised bed reactor to decompose the matrix material through high temperature air heat flow and the heat thus generated recycles the fibre material. This method too has been found to degrade the glass fibre strength by about 50 % [12]. The last documented method under this category is the microwave pyrolysis which decomposes the resin in the composite material by microwave radiation in the microwave cavity. The resin could also be internally heated by absorbing microwave energy from the fibre which then decompose the resin faster. This method was found to be suitable for carbon fabric composites [13, 14].

2.3. Chemical recycling

This method involves the use of chemicals to chemically modify or decompose to make waste into materials that can be recycled. This method when used to recycle thermoset matrix composites is found to be harder and more expensive but the recycling per se is better vis-à-vis the mechanical method. Supercritical fluid method and solvolysis method are the two important methods under this recycling method. The first method refers to a special state in which the temperature and pressure of the fluid exceeds that of its critical temperature and pressure. At this stage, the fluid could decompose/degrade polymer waste, and water or alcohol is used as the decomposition medium [15]. In the context of this method Oliveux et al. recycled GFRP using subcritical water and it was seen that washing of the recycled GF contaminated by residual organic substance was necessary [16]. This method is advantageous on the virtue of it being a clean and less polluting method, in addition to its ability to reproduce clean and good performance fibres. But this method requires high temperature and high pressure and thus adding to the cost of equipments that can withstand such conditions. The solvolysis method involves de-polymerisation of the polymer using the chemical properties of the solvent under heating conditions. This method is good at obtaining carbon fibres from composites [17-19], the strength of the fibre was found to be good. This method has its drawback in the form of using toxic solvents and is expensive.

133

3. Alternatives for wind turbine blades and the sustainability of recycling methods

Thermoplastic resins are gaining acceptability as a replacement to thermoset resins in the fabrication of composite panels for various applications. As explained in the previous sections recycling thermosets are limited by its commercial exploitability on a large scale, this also reveals the small margins on which they operate. In this context thermoplastics can limit the extent of downcycling that thermosets require [20-21]. With the development of infusible thermoplastic resins for the blades, there exists a potential for recycling being more sustainable [22]. 40 % of the costs of a wind turbine blade come from the labour cost and this cost is linked to the cycle time, thus by replacing thermoset with thermoplastic in the manufacturing process, there exists a possibility to reduce the cycle time [23]. This could be attributed to the polymerisation process associated with thermoplastic resins, which is its ability to polymerise at room temperature and thus eliminating heated tooling and ovens for post cure [24, 25]. Thermoplastics can lend itself to be reformed by the application of heat thus enabling maintenance by not degrading the material properties [26]. This particular property of mouldability enables blades components to be thermally bonded without the need for separate adhesives [27]. Subadra et al. (2020) studied the impact performance of Poly methyl methacrylate (PMMA) and it was seen that they had similar impact resistance vis-à-vis epoxy resins [28]. In the context of these natural advantages, recently there is a growing interest in acrylic thermoplastic resin commercially known as Elium by Arkema which lends itself to large scale re-cycling of wind turbine blade components. Following two sections deals with Elium's capability to lends itself to be more sustainable vis-à-vis recycling and being as structurally sturdy as thermoset resin-based blade structure.

3.1. Thermoplastic as a suitable re-placement for thermoset resin

A wind turbine blade was manufactured using Elium as the resin by National Wind Technology Centre (NWTC) at National Renewable Energy Laboratory (NREL) in Denver, USA by R. E. Murray et al (2021). This blade was compared structurally (both static and fatigue) with an epoxy blade manufactured by TPI Composites. The thermoplastic blade was able to polymerise at room temperature and there was no requirement for a pre-heated or post-cure equipment thus reducing the manufacturing complexity and hence the costs. It was observed that the thermoplastic blade had a 3-11 % more displacement under the same static-load and this was attributed to differences in the fibreglass weight between the two blades and the adhesive used, though the thermoplastic blade was more flexible than its epoxy counterpart.

Fatigue test on both blades revealed less than 0.5 % variation in stiffness over a million cycles of loading, with no large scale observable degradation in structural or material properties degradation. Both the blade types had natural frequencies within 2.5 % in both the flatwise and edgewise directions while the thermoplastic blade had 5 to 7 times more structural damping. With these structural performances, which is on par with epoxy blades, Elium could serve as an ideal replacement for epoxy thus making recyclability of blade material a real possibility and hence making wind energy more sustainable part of the energy basket [29].

3.2. Recycling thermoplastic

The investigation carried out by D. S. Cousins et al. (2019). highlights the feasibility of using Elium since it can facilitate the recycling of wind turbine parts on a larger scale. In his study four recycling techniques were implemented namely, thermal decomposition of the polymer matrix, mechanical grinding, thermoforming, and dissolution. While thermal decomposition forms a process classified under the thermal recycling method, mechanical grinding and dissolution are classified under the broad category of mechanical and chemical recycling methods, respectively. Thermoforming involves heating thermoplastic composite sheets above the glass transition temperature of the polymer so that the shape can be altered in mould. Based on these four methods

the research team weighed in the pro and cons of these methods vis-à-vis the recycled material.

Thermal decomposition (pyrolysis) required less energy to decompose the polymer matrix from the composites when compared to other recovery techniques. But the loss of the high-embedded-energy polymer could be counted as a disadvantage when this method is considered. Thermoplastic resin has an edge over its thermoset counterparts because the resin can be recovered by dissolution. In addition to this the glass fibre rovings recovered from the composite by this method retained its tensile strength with a reduction of only 12 %, while the mechanical property reduction was significant when pyrolysis (thermal decomposition) was employed to recover the fabric. Thermoforming enabled the straightening of a spar cap thus demonstrating the ability of thermoplastic composites ability to be downcycled into other products. An economic analysis on the feasibility of recycling thermoplastic composites and the recovery of the constituent materials revealed that they can replace the virgin materials within the supply chain. And a meaningful reduction in labour costs, obtaining a minimal knockdown on the polymer, and maximising the glass fibre for resale can be realised [22].

Thus, the possibility of up-scaling established recycling methods is a real time possibility. Adopting these methods, gradual replacement of thermosets and further validating its feasibility could pave the way for a fully integrated industrial cycle beginning with blade structure fabrication, installing them, recycling them and further reusing them in the same blade structure. Finally, an attempt towards green economy and an industry that is sustainable could be realised in the context of wind turbine sector.

4. Conclusions

The review paper explored the various recycling methods/processes developed and adopted for the recycling of thermoset matrix composites and its sustainability in the context of wind turbine blades. The three main methods namely mechanical, thermal and chemical methods were elaborated with an emphasis on its feasibility. Thermoplastic composites were discussed and its ability to lend itself to recycling was stressed and the ability of the novel resin by Arkema, Elium was discussed. Elium's ability to replace thermoset matrix in wind turbine blades and its ability to sustains loads both static and dynamic was studied and later the ability of this thermoplastic to be recycled was also seen. Thermoplastics can replace the conventional thermosets albeit in a gradual manner as some thermoplastics can bear similar loads as the one bore by the thermosets and this has been proven through two case studies in this paper. Similarly, more studies should be carried out studying the ability and feasibility of these thermoplastics especially Elium which has PMMA as its constituent polymer. The ability of this resin to lend itself to conventional recycling methods can be a better option vis-à-vis epoxy-based composites. Thus, the wind turbine sector could gradually mature into a sector on par with conventional material sector and thus making composites more environmentally sustainable.

References

[1] Yang Y., Boom R., Irion B., Heerden Kuiper Wit D. J. P. H. Recycling of composites materials. Chemical Engineering and Processing: Process Intensification, Vol. 51, 2012, p. 53-68.
[2] Chen J., Wang J., Ni A. Recycling and reuse of composite materials for wind turbine blades: An overview. Journal of Reinforced Plastics and Composites, Vol. 38, 2019, p. 567-577.
[3] Larsen K. Recycling wind turbine blades. Renewable Energy Focus, Vol. 9, 2009, p. 70-73.
[4] Mishnaevsky Jr L., Branner K., Petersen H. N., Beauson J., Mcgugan M., Sørensen F. Materials for wind turbine blades: An overview. Materials, Vol. 10, 2017, p. 1285.
[5] Liu P., Barlow C. Y. Wind turbine blade waster in 2050. Waste Management, Vol. 62, 2017, p. 229-240.
[6] Beauson J., Lilholt H., Brøndsted P. Recycling solid residues recovered from glass fibre-reinforced composites-a review applied to wind turbine blade materials. Journal of Reinforced Plastic Composites, Vol. 33, 2014, p. 1542-1556.

[7]   Pickering S. J. Recycling technologies for thermoset composite materials-current status. Composite A, Vol. 37, 2006, p. 1206-1215.

[8]   Pimenta S., Pinho S. T. Recycling carbon fibre reinforced polymers for structural application: technology review and market outlook. Waste Manage, Vol. 31, 2011, p. 378-392.

[9]   Palmer J., Ghita O. R., Savage L. Successful closed loop recycling of thermoset composites. Composite A, Vol. 40, 2009, p. 490-498.

[10] Schmidl E., Hinrichs S. Geocycle provides sustainable recycling of rotor blades in cement plant. Dewi Magazine, Vol. 36, 2010, p. 6-14.

[11] Giorgini L., Leonardi C., Mazzocchetti L. Pyrolysis of fibreglass/polyester composites: recovery and characterisation of obtained products. FME Transactions, Vol. 44, 2016, p. 405-414.

[12] Pickering S. J., Kelly R. M., Kennerley J. R. A fluidised-bed process for the recovery of glass fibres from scrap thermoset composites. Composites Science and Technology, Vol. 60, 2000, p. 509-523.

[13] Mcconnell V. P. Launching the carbon fibre recycling industry. Reinforced Plastic, Vol. 54, 2010, p. 33-37.

[14] Lester E., Kingman S., Wong K. H. Microwave heating as a means for carbon fibre recovery from polymer composites: a technical feasibility study. Materials Research Bulletin, Vol. 39, 2004, p. 1549-1556.

[15] Okajima I., Sako T. Recycling of carbon fibre reinforced plastic using supercritical and subcritical fluids. Journal of Mater Cycles Waste Management, Vol. 19, 2015, p. 15-20.

[16] Oliveux G., Bailleul J. L., Salle E. L. G. L. Chemical recycling of glass fibre reinforced composites using subcritical water. Composites A, Vol. 43, 2012, p. 1809-1818.

[17] Xu P., Li J., Ding J. Chemical recycling of carbon fibre/epoxy composites in a mixed solution of peroxide hydrogen and N,N-dimethylformamide. Composite Science and Technology, Vol. 82, 2013, p. 54-59.

[18] Jiang Y., Deng G., Chen X. On the successful chemical recycling of carbon fibre/epoxy resin composites under the mild condition. Composite Science and Technology, Vol. 151, 2017, p. 243-251.

[19] Wang Y., Cui X., Ge H. Chemical recycling of carbon fibre reinforced epoxy resin composites via selective cleavage of the carbon-nitrogen bond. ACS Sustainable Chemistry and Engineering, Vol. 3, 2015, p. 3332-3337.

[20] Li X., Bai R., Mckechnie J. Environmental and financial performance of mechanical recycling of carbon fibre reinforced polymers and comparison with conventional disposal routes. Journal of Clean Production, Vol. 127, 2016, p. 451-460.

[21] Witik R. A., Teuscher R., Michaud V., Ludwig C., Månson J. Carbon fibre reinforced composite waste: an environmental assessment of recycling, energy recovery and landfilling. Composites Part A: Applied Science and Manufacturing, Vol. 49, 2013, p. 89-99.

[22] Cousins D. S., et al. Recycling glass fibre thermoplastic composites from wind turbine blades. Journal of Clean Production, Vol. 209, 2019, p. 1252-1263.

[23] Murray R. E., et al. Techno-economic analysis of a megawatt-scale thermo-plastic resin wind turbine blade. Renewable Energy, Vol. 131, 2019, p. 111-119.

[24] Rijswijk Van K., Bersee H. E. N. Reactive processing of textile fibre-reinforced thermoplastic composites-an overview. Composites Part A: Applied Science and Manufacturing, Vol. 38, 2007, p. 666-681.

[25] The composites Institute facilities thermoplastic composite development for wind turbine blades through innovative project. IACMI, 2017, http://iacmi.org/2017/01/17/iacmi-composites-insitute-facilties-thermoplastic-composite-developement-wind-turbine-blades-innovative-project/.

[26] Rijswijk van K., et al. Sustainable vacuum-infused thermoplastic composites for MW-size wind turbine blades-preliminary design and manufacturing issues. Journal of Solar Energy Engineering, Vol. 127, Issue 4, 2005, p. 570-580.

[27] Murray R. E., Roadman J., Beach R. Fusion joining of thermoplastic composite wind turbine blades: lap-shear bond characterization. Renewable Energy, Vol. 140, 2019, p. 501-512.

[28] Subadra S. P., Griskevicius P., Yousef S. Low velocity impact and pseudo-ductility behaviour of carbon/glass/PMMA hybrid composite laminates for aircraft application at service temperature. Polymer Testing, Vol. 89, 2020, p. 106711.

[29] Murray E. R., et al. Structural validation of a thermoplastic composite wind turbine blade with comparison to a thermoset composite blade. Renewable Energy, Vol. 164, 2021, p. 1100-1107.

136

Sharath P. Subadra current Ph.D. student at Kaunas University of Technology, Department of Mechanical Engineering. His current research interests Polymer composites damage modelling.

Paulius Griskevicius hold a Ph.D. degree from Kaunas University of Technology. Now he works KTU as an Associate Professor. His current research includes polymer composite with non-destructive test methods to detect damage in polymer composites.

137

Low velocity impact and pseudo-ductile behaviour of carbon/glass/epoxy and carbon/glass/PMMA hybrid composite laminates for aircraft application at service temperature

Sharath P. Subadra [a], Paulius Griskevicius [a], Samy Yousef [a,b,*]

[a] *Department of Mechanical Engineering, Kaunas University of Technology, LT-51424, Kaunas, Lithuania*
[b] *Department of Materials Science, South Ural State University, Lenin Prospect 76, 454080, Chelyabinsk, Russia*

ARTICLE INFO

ABSTRACT

Carbon/glass hybrid composite (CGHC) laminates are some of the most promising composites for lightweight applications. Sometimes these laminates are used in warm environment, such as aircraft frame structures, and this may affect their performance. In order to investigate this issue, the present research aims to study the effect of temperatures on the impact behavior and pseudo-ductile behaviour of CGHC in presence of different types of thermosets "epoxy" and thermoplastic "acrylic poly-methyl methacrylate-PMMA". The experiments were started with making of CGHC laminates from different stacking sequences of unidirectional carbon and woven glass fibre layers, using a vacuum-assisted resin transfer method followed by curing treatment. In addition to CGHC laminates, four other neat batches (Carbon/epoxy, Carbon/PMMA, Glass/epoxy, Glass/PMMA) were prepared for comparison. The low velocity impact behaviour of the fabricated panels was evaluated at high temperatures (60 °C and 80 °C) according to ISO 6603-2 standard, using drop tower, while pseudo-ductile behaviour and ductility index (DI) of the specimens were estimated based on the measured total energy and elastic energy. Also, the low-velocity impact response was modeled mathematically based on a modified energy-balance model to predict the absorbed energies. Finally, the failure mechanisms were examined using optical microscope to determine the influence of these damage growth on DI of the composites under different temperatures. The results showed that the impact energy response of both hybrid composites i.e. epoxy and PMMA was stable even as the temperature rose, however, carbon/glass/PMMA exhibited better performance compared with carbon/glass/epoxy with an increase in impact energy response estimated at 50% (25 °C) and 53% (80 °C). Also, the pseudo-ductile phenomenon was strongly evident, which facilitates the predictability of failure.

1. Introduction

Currently, demand for Glass Fiber Reinforced Polymer (GFRP) laminates in aircrafts and vehicle structures is on the upswing due to their light weight, damage tolerance, high specific strength, durability, maturity in processing, smaller gas emission, smaller fuel consumption, etc. compared with metals. Also, recently, they have been generalized as an alternative energy absorbing material for producing light armour and impact related applications instead of metals and alloys [1–3]. While used for the structure of the specified applications, GFRP is subjected occasionally to low velocity impact resulting from bird strikes while the aircraft is parked and taxiing, from dropped tools in the course of assembly and maintenance works, or from runway debris encountered during take-off, which can cause damage even at very low impact energies [4]. Therefore, several types of nano fillers, including graphene and carbon nanotubes, nanoceramic particles, etc. have been used to improve the impact properties [5–7]. Although the energy impact absorption was improved by the added filler up to 31%, the resultant failure was described as a brittle fracture which means that the failure is sudden and catastrophic with no significant visible damage or warning [8]. This type of failure makes designers hesitant in exploiting the performance advantages of polymer composites and render them unsuitable for applications where load conditions are not fully predictable and catastrophic failure cannot be tolerated. To ensure safe operation in this case, much greater safety factor is applied to ductile material, which affects negatively economic performance of the final product.

To overcome this problem, a Pseudo or semi ductility concept was introduced [9]. This phenomenon can be achieved in the material by incorporating both glass and carbon fibres in one composite panel "Hybrid-composites", which leads to enhanced strains to failure of carbon fibres measured in glass/carbon hybrid composites [10,11]. As carbon fabrics can bear higher loads, it has been accepted that they can take in less strain energy when compared to glass fabrics [12]. Also, the hybridisation allows for a compromise of mechanical properties while alleviating the individual fibre drawbacks [13]. The hybrid effect can be defined as the apparent increase in the initial failure strain of low elongation fibre composite in the hybrid composite relative to the composite with only low elongation fibres. The studies concluded that hybridisation can induce pseudo-ductility [14]. The low-velocity impact behavior of Carbon fiber reinforced polymer (CFRP), GFRP, and their hybrids was studied extensively and the studies concluded that damage is caused in this case is in the form of indentation, matrix cracking, fibre/matrix de-bonding, de-lamination and fibre-breakage [15,16]. These damages are quite dangerous as they can reduce significantly the residual mechanical properties of the material and leave very limited visible marks on the impacted surface leading to failure on the long run [17,18]. The features of these damages are dependent on the fibre architecture, resin type, stacking sequence (in case of hybrid), thickness, and environmental conditions [19–22].

With regard to the fibre architecture, it was reported that defects of carbon fabrics appear in their unidirectional glass/carbon hybrids in the form of gradual failure and multiple cracking of the carbon plies without unstable delamination in their hybrid composites [22–24]. Meanwhile, resin can be divided into thermoplastic and thermosets. Recent studies have showed that thermoplastic composites have higher productivity and better recyclability compared with thermosets resin. These characteristics make thermoplastic resins a viable alternative when compared to its thermoset counterparts in the automotive sector [25, 26]. Acrylic resins are lightweight thermosetting plastics with excellent wetting properties and high strength, making them useful for ultralight orthopaedic appliances, too. Due to its non-toxicity, poly(methyl methacrylate)-PMMA is widely used in medicine to make prostheses [27,28]. However, the impact behavior of PMMA is still missing, especially when it is reinforced by such fibres as glass or carbon.

A big scope of environmental conditions has been reviewed, including many conditions related to ambient gases, chemicals, heating, etc. Among these conditions, the focus was on warm surrounding conditions since the current research was developed to cover this area. As mentioned before, these composites have gained wide acceptance in different sectors, such as aircraft structures. They are subjected to thermal loading resulting from heat generation from aircraft's engines during service that may affect their performance [29–31]. Within this context, many studies have been developed to investigate the effect of temperature on damages and the morphology of the failure within, taking into account thicknesses and matrix type factors. The results revealed that the fracture mechanism of laminates is quite complicated at higher temperature and that the impact-induced delamination area decreases as the temperature increases, while the lowering of

temperature resulted in a decrease in the damage area. Also, it was observed that high temperatures had little influence on the penetration impact and that the laminate thickness had the biggest influence [32–34]. For better understanding of the fracture mechanism and to study the pseudo ductile behavior of CFRP and GFRP, several numerical models were developed based on pseudo-plastic law [18,35]. The results revealed that the panels exhibited semi-ductility with less brittleness and allowed it to undergo inelastic deformation prior to complete failure [36]. As illustrated in the literature, the impact and pseudo-ductile behaviour of carbon/glass/epoxy and carbon/glass/PMMA hybrid composite laminates at low and high temperatures are missing and hence should be understood and quantified with appropriate mathematical equations. Since hybrid composites are gaining wider traction within the aerospace sector [15], so it is necessary to understand if these materials are able to exhibit a hybrid effect on elevated operating temperatures. Within this frame, this research was developed to cover this area and to assess the performance of thermoplastic and thermosets at high temperatures. Also, the pseudo ductile performance of carbon/glass/epoxy and carbon/glass/PMMA hybrid composite laminates at low and high temperatures was studied.

2. Experimental

2.1. Materials and design of the research experiments

Unidirectional Carbon fabrics (areal density-120 g/m^2) and Glass fabric Panda™ (Weave: Twill 2/2 type and weight: 163 g/m^2) were supplied by R&G Faserverbundwerkstoffe GmbH and Otto Bock Healtcare GmbH, Waldenbuch, Germany. Epoxy based on Bisphenol A and its hardener (modified cycloaliphatic polyamine free of alkyl phenol and benzyl alcohol) and Methyl methacrylate (MMA: 617H119-Orthocryl Resin) resin and its polymerizer (Benzoyl peroxide-BPO: Orthocryl resin 617P37, Otto Bock) were purchased from Otto Bock. The experiments in the present work were designed in three stages: a) making of fiber/resin laminate composites, b) investigation of impact properties of the prepared panels and their microstructure, and c) estimation of ductility of the obtained panels using an energy concept (based on the impact data results). Also, the experiments were carried out on six sets of composite panels having different types of resin, fabric (Carbon "c" and Glass "g"), and architecture, as shown in Table 1. All these stages and their conditions are explained in detail in the following sections.

2.2. Making of fiber/resin laminate composites

In order to prepare the listed sets of panels, 8 layers of unidirectional carbon fabric and another 8 layers of Glass fabric with nominal size of 350 mm × 350 mm were cut from each supplied roller to prepare T-1, T-2, T-4, and T-5 samples. 2 other layers of unidirectional carbon fabrics and 8 layers of Glass fabric with same nominal size were used to make T-3 and T-6 samples. In parallel, epoxy resin and its hardener solution with ratio 70:30 wt% of the total panel weight were mixed together using a mechanical mixer for 15 min, followed by keeping the solutions in a vacuum chamber at −100 bar for 10 min to eliminate the cavities and entrapped air bubbles created during the mixing process. PMMA resin solution was prepared by mixing MMA monomer with BPO as an initiation system in the free-radical polymerization with a weight ratio of 100:2 (MMA:BPO) using a mechanical mixer for 15 min, then removing entrapped air bubbles as before [37]. After that, vacuum assisted resin transfer method was employed to prepare composite panels followed by infra-red lamp post-cured process (at 70 °C for 6 h) and the main curing process (at 90 °C for 5 h). Lastly, an automatic cutter was used to cut impact specimens (80 mm × 80 mm; according to ISO 6603-2 standard) from the obtained composite panels.

Table 1
Panel codes, architecture, and composition.

Panel Code	Architecture	Fabric	Fibre oreintation	Resin
T - 1	[0$_c$/90$_c$/90$_c$/0$_c$]	Carbon	Uni-directional	Epoxy
T - 2	[0$_g$/0$_g$/0$_g$/0$_g$]	Glass	2/2 Twill	Epoxy
T - 3	[0$_g$/0$_g$/0$_c$/0$_g$/0$_g$]	Glass & Carbon	Glass-2/2 twill Carbon-Uni	Epoxy
T - 4	[0$_c$/90$_c$/90$_c$/0$_c$]	Carbon	Uni-directional	PMMA
T - 5	[0$_g$/0$_g$/0$_g$/0$_g$]	Glass	2/2 Twill	PMMA
T - 6	[0$_g$/0$_g$/0$_c$/0$_g$/0$_g$]	Glass & Carbon	Glass-2/2 twill Carbon-Uni	PMMA

2.3. Low velocity impact test

The impact tests were conducted using Coesfeld Magnus 1000 High Speed Drop Tower (built according to ISO 6603-2) with a maximum impactor speed of 42 m/s. The measurements were performed at constant impact energy (50 J, as it was enough to penetrate completely) using a cylindrical steel impactor with 20 mm in diameter and hemispherical end with a mass of 5.129 kg. The specimens were placed over a circular support with an outer diameter of 80 mm and inner diameter of 40 mm. The pneumatically activated clamps from above restrained the specimens during impact (built according to ISO 6603-2). The equipment provided the impact velocity just before impact, along with the force, energy (absorbed by the material), displacement and time histories. Later, the cross-section of all the specimens was examined to study the growth of crack at room temperature (25 °C) and at 80 °C respectively. Finally, the calculations of velocity, displacement and force histories by the drop weight impacter can be found in the supplementary material.

2.4. Estimation of ductility of the obtained panels

Usually, ductility of beams structure is expressed in terms of a dimensionless ductility factor or DI based on the generated curvatures, rotations, or reflections. However, this criteria was based on yield and the ultimate strains, which are not suitable in case of brittle materials like in the present research. Therefore, energy criterion was introduced to estimate DI of the brittle materials based on consumed energy until the failure [38,39]. Within this framework, Naaman and Jeong (1995) and Grace et al. (1998) developed two different models to compute DI based on the total energy (E_{total}), elastic energy ($E_{elastic}$), failure energy ($E_{in-elastic}$), as described in Eqs [1,2,40,41]. E_{total} represents the area under load impact – a deflection curve up to the failure (elastic and failure energies), and $E_{elastic}$ is defined as the area of the triangle formed at the failure load by the line having the weighted average slope of two initial straight lines of the load-deflection curve, as shown in Fig. (1). Both methods gave accurate results that served as a strong motivation for their use in calculation of ductility of several brittle materials, such as concrete, etc. [42]. Therefore, both energy methods were used in the present research to estimate DI of the prepared panels.

$$DI \text{ (Naaman)} = \frac{1}{2}\left(\frac{E_{total}}{E_{elastic}} + 1\right) \tag{1}$$

$$DI \text{ (Grace's)} = \frac{E_{in-elastic}}{E_{total}} \tag{2}$$

3. Results and discussion

3.1. Load impact characteristics of hybrid carbon/glass fiber composites

Figure (2A, B) shows impact load-time curves of carbon/glass fiber-epoxy specimens (T-1, T-2, T-3) and carbon/glass fiber-PMMA specimens (T-4, T-5, T-6) at room temperature. It seems that the curves of T-1, T-2, T-4, and T-5 samples have similar profiles, in particular two sharp peaks corresponding to maximum impact load (at 0.87, 1.12 ms for epoxy batches and 0.47, 1.14 ms for PMMA batches) and another peak due to fracture impact load (at 0.92, 1.20 ms for epoxy batches and 0.57, 1.59 ms for PMMA batches). Meanwhile, another additional peak was generated in both T-3 and T-6 (at 0.91 and 0.86 ms) due to the hybrid effect [43].

Since the designers are interested in the elastic zone (maximum impact load before failure), the analysis was focused on maximum load before failure zone for all the panels. It is clear that PMMA is characterized by higher performance compared with epoxy in terms of maximum impact load and fracture load. As shown in the figure, the fiberglass/epoxy and fiberglass/PMMA have the highest impact performance load estimated at 2.72 kN and 4.66 kN, respectively, which means that fiberglass/PMMA has better performance estimated by 42%. The same trend was noticed in carbon fiber/epoxy (1.16 KN) and carbon fiber/epoxy (1.29 KN), but with a small increase estimated at 13%. It was caused by higher molecular weight of thermoplastic resin leading to strong joining with fibers through two types of bonding: mechanical and chemical [44]. In case of hybrid carbon/glass fiber composites, the phenomenon of pseudo ductility was evident (explained in subsequent sections) in both samples (yellow marker) with impact load estimated at 2.32 KN (T-3) and 3.1 KN (T-6) respectively. Also, the impact load in presence of epoxy did not change much compared to the pure glass (reduction 10% only compared), while in case of PMMA, the impact load decreased significantly from 4.66 KN to 3.76 KN (with reduction 19%). However, carbon-fiberglass/PMMA panels still had better impact performance compared with carbon-fiberglass/epoxy with increase by 28%.

3.2. Characteristics of the damage areas

A closer look into the damages suffered by individual specimens revealed an interesting scenario with respect to the shape of the damage. The damage observed in all the specimens resembled the shape of a rhombus or a diamond irrespective of the temperature. Figure (3) illustrates these scenarios and the influence of fabric architecture, resin type, and temperature on the damages at the end of the impact tests on the front and back sides. It was noted that the damage in all samples can be characterized by many features that can be classified as external features (damage limitations and geometry) and internal features. As shown in the images, the external features are confined to two forms; rhombus and round shape (based on fabric architecture). These geometries appeared due to the applied energy (50 J), which led to a print of the projection of semi-spherical impactor on the upper surface of the impacted samples followed by creation of an intersection of two diagonals (usually along the warp and weft directions). After complete penetration of the steel impactor into the tested specimens, internal
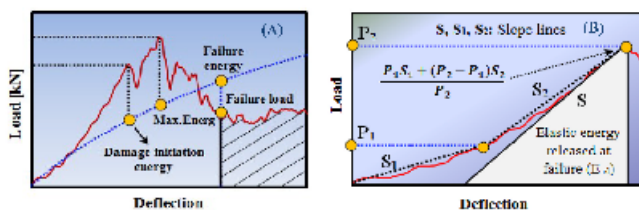
Fig. 1. (A) Impact characteristics and (B) evaluation of elasticity energy.
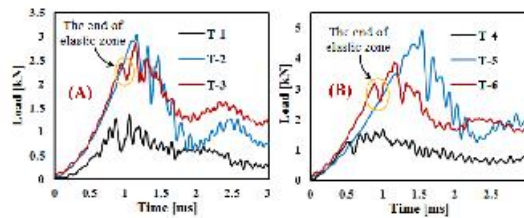
Fig. 2. Load-time characteristics of (A) Carbon/glass-epoxy specimens and (B) Carbon/glass-PMMA specimens at room temperature.
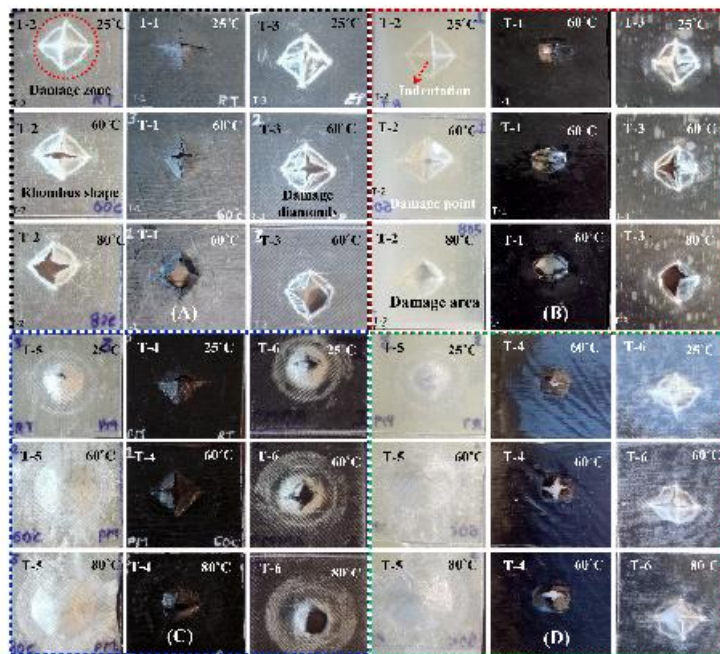
Fig. 3. A)-Obverse and B)-Impact side of impact of T-2, T-1 and T-3 respectively. Rhombus-shaped damage is seen in all the types and depth of indentation rose with increasing temperature. C)-Obverse and D)-Impact side of the impact of T-5, T-4 and T-6 respectively. Rhombus-shaped fracture is seen at room temperature in T-5, while permanent indentation is seen as the temperature rises. T-4 and T-6 exhibited rhombus-shaped fracture and underwent complete penetration as the temperature rose.

features appeared in the damage zones. They can be summarized as glassfiber bundles breakages, cracks, delaminations, etc. in all the panels. Although these features were manifested in all the specimens with approximate temperatures and architecture, this means that making, testing, and failure of the panels took place under the standard conditions [2,31].

T-3 and T-6 behaved differently when compared to their pure counterparts. The load of T-3 and T-6 was increasing gradually at room temperature until the initial drop started (yellow marker in Fig. 2). This initial drop in load was conspicuously absent in T-2 and T-5. Following

4

141

this drop, the load rose to a maximum before dropping down to fail completely. The damage suffered by the specimens was quite different from their pure counterparts. The shape of damage (rhombus shaped) was quite the same as seen in the case of pure specimens, but there seems to be considerable delamination along the splits in case of T-3 and T-6, while no delamination was observed in case of T-2. The delamination contributes considerably to development of ductility in composites. The depth of penetration was increasing as the temperature was rising and the ductility seen in lower temperature was not observed here. Plasticisation arrested greatly the growth of the crack and the penetration was preceded by elastic deformation as temperature was rising.

A close look into the load-time characteristics reveals the same in case of T-3 and T-6. It is seen that at room temperature there is an initial drop in load attributed to the transfer of load by carbon fibres to the glass fibres after the former had failed by rupture. The final rupture corresponding to that of glass coincides with the maximum load taken by the entire specimen. Considerable adhesion problem was observed in T-6 as temperature rose. As the temperature rose, the acrylic resin became more plastic and lost adhesion with the fibres [45]. Delamination was seen along the splits at room temperature, but at higher temperatures, in addition to the elastic deformation, the fibres lost the adhesion (can be termed as de-bonding) with the fibres and ultimately suffered penetration. Also, as the temperature rose, unlike in T-3 where the delamination and split coincided with the maximum load, in T-6 a shearing tear (not necessarily along the diagonal direction) was observed in glass fibres after the carbon fibre had failed by rupture. This failure resulted in penetration of rather round shape in some specimens than a rhombus-shaped (with splits along the diagonal direction) fracture seen in other specimens. The main factor contributing to this is the plasticisation of the resin along with the inherent high strain characteristic of glass fibres [46]. Where the plasticisation process results in modification of the polymer molecules in the form of copolymerization, which leads to the plasticizer molecules neutralize van der Waal's bonds between the polymer molecules and increases the mobility of the polymer chains, thus reducing the crystallinity degree of the resin, especially with increases the service temperature, where plasticizer can be lossed through volatilization or extraction during use of a plasticized polymer causing thermal agent [47].

3.3. Effect of temperature on load and energy impact

Figure (4A,B) illustrates the influence of temperatures (60 °C and 80 °C) on the load borne and impact energy by specimens. As shown in Fig. (4A), the respective load bearing capacity of T-1 and T-2 samples did not change much as the temperature was rising. This could be attributed to the fact that epoxy tends to retain its ambient temperature properties up to 160 °C (melting temperature) with less degradation [48]. Also, it was noted that GFRP still retained better impact performance against CFRP at higher temperature, whereas T-2 and T-5

behaved differently as the temperature was rising. T-5 undertook significantly more load estimated at 46%, when compared with T-2, which was taking smaller load as the temperature was rising. This significant increase in impact load of PMMA hassled to higher mechanical and thermal stability, compared with epoxy resin, which needs more energy to break the moloular bonds of PMMA [29].

With regard to energy absorption, generally, the amount of energy applied to the specimens is absorbed and utilized in many ways, including elastic and in-elastic deformation, the latter through damages like crack propagation, delamination, perforation etc. Figure (4b) shows the maximum energy absorbed by the specimens at different temperatures (60 °C and 80 °C). At room temperature, the energy was expended in the form of either crack growth, delamination and/or fibre rupture [32,33]. As the temperature rose, more energy was spent in the form of elastic deformation and finally fibre rupture, though the maximum energy absorbed remained constant in individual cases, which means constant energy absorption with the rise of temperature. This can be seen in case of all the samples except for T-5; for example, T-2 showed constant absorption throughout the temperature increase, while T-5 took in more energy in the form of elastic deformation, which could be attributed to the high-strain glass fibres and the pliability of acrylic resins [49]. In case of hybrid samples (T-3 and T-6), T-3 displayed similar energy characteristic as T-2, whereas T-6 was seen as a compromise between T-5 and T-2/T-3.

3.3.1. Evaluation of elastic and in-elastic energies

The elastic and in-elastic energy plays an important role in quantifying ductility in polymer composites. The in-elastic energy is defined as the energy spent in damage initiation and propagation [42]. Figure (5A, B) shows the in-elastic and elastic energy absorbed by the tested specimens, respectively. As can be seen in Fig. (5A), as the temperature was rising the material was taking less energy to propagate damage in the form of delamination, de-bonding, and crack growth, as shown in failure mechanisms section while the absorbed energy was taken in the form of elastic deformation (Fig. (5B)). Also, it was observed that the in-elastic energy either was decreasing gradually with increasing temperature or remained constant. This implies that as temperature increases, the plasticisation of matrix leads to an arrest in the development of conventional forms of composite damage experienced at room temperature [30].

The decrease was more obvious in case of T-4 and T-6 as they had the acrylic PMMA containing resin. As the temperature rose, these specimens became more pliable and took in more energy to undergo elastic deformation seen in Fig. (5B) [29]. T-1, T-2 and T-3 having epoxy as resin exhibited a near constant behaviour in the case of in-elastic energy. No significant drops in energy were seen, but they too took in more elastic energy as the temperature rose. The elastic energy component of the total energy increased as the temperature rose and there was a pronounced increase in case of T-5. T-5 suffered more indentation rather
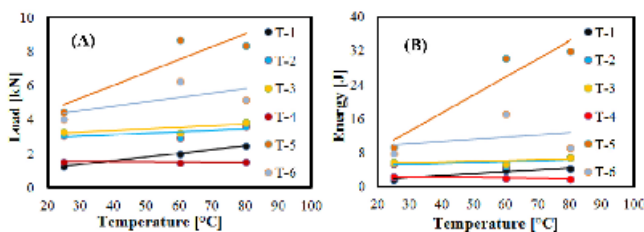

Fig. 4. Effect of temperatures on (A) load characteristics and (B) Energy characteristics.
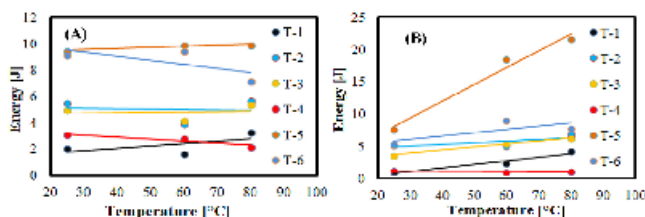
142

Fig. 5. (A) In-elastic energy-temperature and (B) elastic energy-temperature.

than splitting along the warp and weft direction (Fig. (3C)) and this prompted an elastic response and hence the elastic component saw an abrupt rise. But, in case of all other specimens, the rise in elastic component was modest as they suffered penetration and prior to this, they took elastic energy in the form of elastic deformation with either a constant or decreasing in-elastic component throughout three studied temperatures.

3.3.2. Evaluation of ductility index

Ductility index was estimated using Eq. (2) and based on the in-elastic and elastic energies obtained from the above section at different temperatures. Based on the value of the obtained DI, the behavior of the material can be defined, in particular brittle <69%, ductile failure >75%, semi-ductile between 70 and 74% [42]. Figure (6A, B) shows DI estimated by Naaman et al. (DI- Naaman) and Grace et al. (DI- Grace) methods. According to the indexes, it seems that DI decreased with increasing temperature due to the reduction in in-elastic energy component taken by the material as the temperature rose. Also, it was noted that DI is directly proportional to in-elastic energy and in-directly proportional to the elastic energy. These figures help to ascertain that ductility fell and thus the material became more brittle in nature or the material was just taking more elastic energy before failure in the form of fibre splitting along the warp and weft and then rupture [50].

A low DI does not necessarily mean a very brittle material; it could also mean a rebound of the impactor. In this scenario, a large part of the elastic energy taken by the material is returned back to the impactor, in such a case the index value would approach 0. In such a scenario, a close look into the load-deflection curve would help to understand better nature of the failure. All the specimens manifested a considerable decrease in DI, which could be attributed to the in-ability of the material to undergo classical composite failure modes, such as crack propagation, delamination and de-bonding. In such a scenario, the material is taking in more elastic energy in the form of elastic deformation (as its getting pliable), and as this energy reaches a critical level (which is above the elastic limit) the specimens are simply punctured without undergoing any of the above mentioned failure mechanisms [51,52].

Also, it is clear that T-4 performed better on the ductility scale even though they took a smaller load when compared to all others. The hybrids T-3 and T-6 exhibited a compromise between all the types studied. They had an average ductility of 0.65/1.94 (Grace and Naaman respectively) at room temperature, which fell down to an average of 0.45/1.45. This range of ductility is good, as the material is losing its tendency to fail abruptly and fails in a controlled manner, as in case of pure glass (T-2 and T-5), where average ductility of average 0.5/1.6 at room temperature fell to 0.35/1.3 at higher temperatures. Structural applications exposed to impact might not bode well in this case. The total amount of energy absorbed by the material during impact is expended in the form of elastic deformation and damage propagation (in-elastic deformations). Thus, according to the DI analysis, both hybrid samples (T3 and T6) exhibited better DI at room temperature, but as temperature rose DI dropped, which means the materials was loosing its hybrid characteristic i.e. its ability to fail in a controlled manner was lost. Also, it seems that pure form of carbon with PMMA smanifested better DI even as temperature dropped. Thus, the incorporation of carbon in a pure glass composite reduces its unpredictability while failing under impact at room temperature.

3.3.3. Energy based model to predict the absorbed energy during impact

In order to predict the absorbed energies during the low-velocity impact empirically, Foo et al. (2011) developed a new approach but for carbon-sandwich composites only [53]. The same approach was adopted in the present research to predict the absorbed energy at room temperature through plotting a normalized absorbed energy (E_{total}/E_{el}) against the inverse of the normalized impact energy ratio (E_{el}/E_{imp}) for all samples, as shown in Fig. (7), where E_{imp} is the incident impact energy of the impactor; here it was 50 J. The power regression curve was found to be the best fit and based on that, Eq. (3) links the absorbed energy to the elastic energy and the incipient impact energy, giving an approximate estimate of the total absorbed energy in the form of elastic
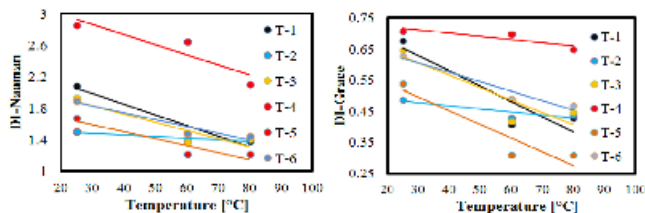

Fig. 6. Ductility Index (DI) with respect to temperature. (A) DI-Naaman and (B) DI-Grace.
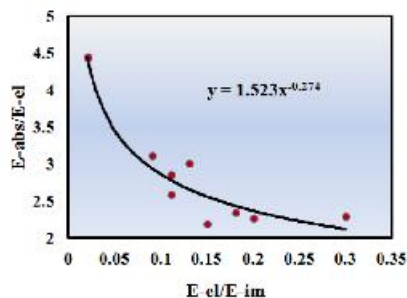
143

Fig. 7. A normalized energy plot for nine specimens at room temperature.

deformation and in-elastic deformation. This expression is almost similar to the formula obtained by Wisnom et al. (2017) [54]. Also, it was noted that the values of (E_{el}/E_{imp}) obtained from Fig (7) are located in the range 0.02 and 0.4, but if similar test data were used, the range could be further extended. Thus, in conclusion, the absorbed energy could be estimated approximately by just knowing the elastic energy [56], which, as mentioned in the previous sections, can be obtained from experiments until an accurate method is found. This means the power regression curve was found to be the best fit and the equation of the curve predicted the absorbed energy of the specimen quite accurately.

$$\frac{E_{total}}{E_{el}} = 1.52 * \left(\frac{E_{el}}{E_{imp}}\right)^{-0.27} \tag{3}$$

3.4. Analysis of damage and failure mechanisms

It was quite hard to arrive to a conclusion as to what the energy has been expended for in the course of impact through visual inspections only or by studying the maximum energy absorbed by the specimens.

Therefore, optical microscope was used to infer the micro mechanism involved during the damage of composites under impact, and to determine the possible influence of the damage growth on ductility of the composites, as explained in the previous sections.

3.4.1. Epoxy resin

The observation process using the optical microscope was performed on the cross section of the impact region after having it cut by an automatic cutter. Figure (8) shows the micrographic images of the damages of carbon/glass-epoxy resin samples at 25 °C (the lowest temperature) and 80 °C (the highest temperature). The examination process revealed the failure mechanism of T-1 sample (Fig. (8A)) at 25 °C resulting from crack growth, which tends to branch out from the edge towards the impact centre. Also, a fibre rupture was noted extensively on the impact side due to the compressive stress involved, along with crushing and the resultant debris formation, which can be seen as reflections close to the fibre rupture. These failure mechanisms contributed to a substantially high DI at room temperature in T-1 samples. At 80 °C (Fig. (8B)), the resin became more pliable with deformed edges with less fibre rupture. Also, the significant cracks could be seen on the obverse side of impact, while crack growth is seen in the middle of the specimen away from the impact side towards the centre of impact. These cracks maintained effectively DI at higher temperatures albeit lower than room temperature. Thus, it could be concluded that carbon with epoxy tend to maintain considerable DI even at higher temperatures, making it more compatible under impact loading at higher temperatures. Figure (8C,D) shows the damaged edges of T-2 at 25 °C and 80 °C, respectively. At 25 °C, the sample suffered significant delamination along the edges as can be seen in the first figure along with significant fibre-pull outs. The de-lamination was limited within the perimeter of the rhombus of the entire impact damage, especially along the edges and the splits. The damage features at 80 °C do not change significantly due to the fact that fiberglass has high strain fibres and when coupled with plasticity of the resin, the material took in more elastic energy in the form of elastic deformation than in the form of damage. These results explain why DI at low and high temperature and at 80 °C was rather constant as insignificant.

Figure (8E,F) shows the examination of T-3 at 25 °C and 80 °C, respectively. As shown in Fig. (8E), the damaged edges make it quite
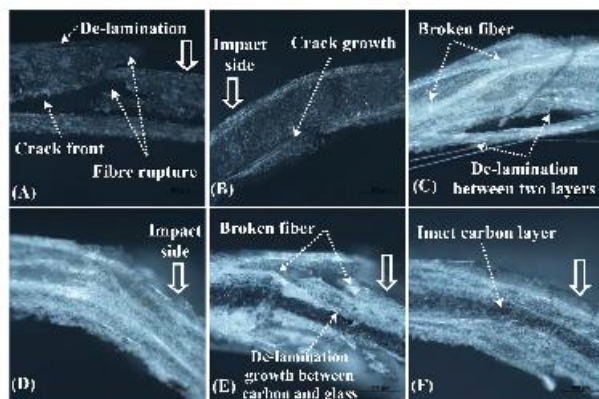
Fig. 8. A) and B) are T-1 at 25 °C and 80 °C respectively. At 25 °C unstable propagation of crack is seen especially at the interface between alternatively oriented plies and at 80 °C resin is more plastic and hence become pliable. C) and D) are T-2 at 25 °C and 80 °C respecitvley. At 25 °C crack growth is seen at alternating plies in combination with fibre pull out and at 80 °C resin is more plastic. E) and D) are T-3 at 25 °C and 80 °C respecitvley. At 25 °C the carbon layer at the centre arrests the unstable crack growth, while more damage is seen in pure glass layer and at 80 °C, more plasticity is seen as temperature rises, thus arresting damage to an extent.

144

evident that the inclusion of carbon layer in the middle has increased the complexity of the damage having a direct bearing on the DI. On the impact side fibre rupture was seen along the edges with the carbon fibre being intact while delaminations were seen along the interface between glass layers. Moving towards the impact centre, the carbon fibre ruptured, following which the load was borne by the neighbouring glass fibres, which too had ruptured after reaching its critical load bearing capacity. Delamination was seen along the split (forming the diagonal of the rhombus-shaped damage) and along the edges of the impact (perimeter of the rhombus). Based on the results, the damage mechanism became more complex and affected DI, which at 25 °C was quite high when compared to its pure glass counterpart. However, this complexity of damage is quite necessary, as this chain of damage events would delay the abrupt failure of the material in the event of an impact, as seen in pure glass composites.

3.4.2. PMMA resin

Figure (9) shows the micrographic images of the damages of carbon/glass-PMMA resin samples (T-4, T-5, T-6) at 25 °C and 80 °C. As shown in Fig. (9A), the damage area of T-4 at 25 °C contains a mix of damage modes dominated by inter-ply delamination and intra-ply crack growth. These modes contributed effectively to the in-elastic energy (damage propagation energy) absorption, thus exhibiting higher DI when compared to T-1 at 25 °C. By increasing the temperature, it gave way to more elastic deformation rather than damage propagation in the form of in-elastic energy absorption, that led to a drop in DI. Also, it is clear that the edges were conspicuous in absence of any delaminations or cracks both in the inter and intra-ply region, as shown in Fig. (9B). Figure (9C, D) shows the fracture of T-5 sample at 25 °C and 80 °C, respectively. At 25 °C, the damage had a lot of reflections along the warp directions as most fibres were de-bonded, while fibres along the weft directions is clearly visible (Fig. (9C)). Comparing T-5 at 25 °C vis-à-vis T-2, T-5 suffered considerable damage within the impact region, including delamination and de-bonding. Also, it was observed that there existed a general adhesion problem between glass and the acrylic resin and this was evident in the large number of fibre pull outs seen in the front of impact. At 80 °C, thermoplastic resin became more mouldable and

underwent deformation taking in more elastic energy, as can be seen in Fig. (9D). The specimen suffered permanent indentation, with cavities being developed along the layers (not necessarily cracks). This could be accounted to the plasticity of the thermoplastic resin, as at higher temperatures there were not enough resins to mould into the shape and hence they were behind the cavities.

Fig. (9E, F) shows T-6 (hybrids with acrylic PMMA as resin) at 25 °C and 80 °C, respectively. At room temperature, delaminations were seen along the edges and along the splits of the impact region, the same as in T-3, on the obverse side of impact (Fig. (9E)). Fibre rupture was seen along the edges of impact on the impact side, with resin debris collecting in the gaps seen as reflections in the first picture. These micro-mechanisms contributed naturally to higher DI at room temperature comparable to that of T-3. However, as the temperature rose like in case of all the other types studied, they underwent elastic deformation with a drop in DI evident from Fig. (9F). The effect of temperature had a profound impact on PMMA, as can be seen from the above discussions. It was generally observed that at lower temperature, PMMA along with the fibres exhibited a generally brittle damage mode, but as temperature rose the PMMA became more rubbery and this had a profound impact on the damage propagation. Especially at higher temperatures, if the impactor perforated the specimens (true in case of T-4 and T-6), the perforation would induce a hole enlargement without any cracks and there is a possibility of later hole re-closing termed as spring-back mechanism. This could be attributed to the elastic recovery arising from the rubbery state of the amorphous chains within the PMMA [56].

Finally, based on the results of current study, it is evident that the hybrid effect is more pronounced when the amount of glass and carbon fibres is controlled. Also, the most important factor governing the failure behaviour of ply-by-ply hybrid laminates is mode II energy release rate, which controls delamination after the failure of the lower strain plies [53,54]. For a given material combination, the energy release rate depends on the thickness of the low strain layer. Delamination was restricted to the edges of the obverse side of the impact and along the diagonal split of the rhombus-shaped fracture. Fibre rupture was not seen on the edges except across the split. An increase in plasticity reduced delamination and made the material pliable along the edges.
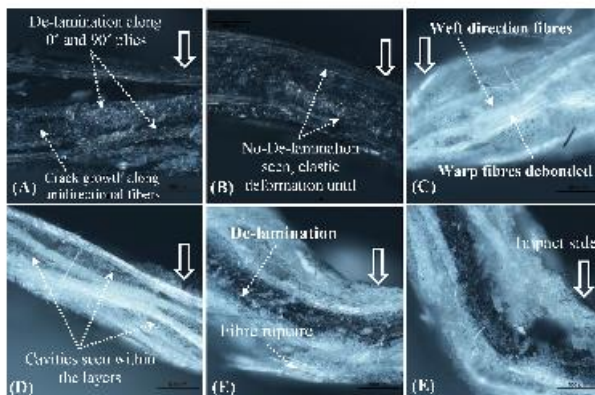
Fig. 9. A) and B) T-4 at 25 °C and 80 °C respectively. At 25 °C cracks and delamination were seen while at 80 °C the resin became more pliable. C) and D) T-5 at 25 °C and 80 °C respectively. At 25 °C fibre pull out was seen in more reflections. At 80 °C the specimen became more pliable and permanent indentation appeared. E) and F) are T-6 at 25 °C and 80 °C respectively. At 25 °C the carbon layer at the centre arrests the unstable crack growth and at 80 °C the specimens were more plastic.

8

Lesser DI implies an increase in elastic deformation of the material with smaller in-elastic component. The microanalysis made this quite evident. Smaller in-elastic energy component implies lesser fracture mechanisms like crack growth, delamination etc. As temperature rose, the normal failure mechanisms, such as delamination, de-bonding etc. were contained and instead the material took in more energy in the form of elastic deformation and finally a diagonal split along the warp and weft direction of the fibre appeared.

If these observations were made within the context of aircrafts, few observations could be provided. Firstly, within the service temperature mentioned in this study, T-3 and T-6 loose their hybrid characteristic when the temperature approaches 80 °C. The failure was generally catastrophic in nature without any prior warning which is characteristic to hybrids at lower temperatures. However, as it has been mentioned above, as the hybrid effect is more pronounced when the amount of carbon is smaller vis-à-vis glass, an optimum amount of carbon and glass along with thickness could be achieved through experimental and numerical analysis. These could then be subjected to tests within the service temperatures and hence there is a possibility of retaining the hybrid characteristic within the service temperatures. Secondly, both epoxy and PMMA behaved similarly at lower temperatures, especially in case of hybrids thus, PMMA is biocompatible and could replace easily some epoxy-based parts of aircrafts, especially in the airframe. Thirdly, glass-based composites were found to fail catastrophically even at lower temperatures and hence is not an advisable material, but their combination with carbon makes them a viable and cheap alternative to pure carbon-based composites.

4. Conclusions

In the present research, the low velocity impact behaviour of carbon and glass fibre and its hybrids was investigated at 25, 60, and 80 °C respectively. The experiments were carried out on two resin sets, namely thermpset-epoxy and thermoplastic-PMMA, and later their failure mechanism and Ductility Index (DI) were studied at the specified temperatures. Also, a normalized energies curve was plotted to deduce the empirical relation and to predict the absorbed energies based on the incident impact energy of the impactor, total energy, and elastic energy. The results revealed that the hybrid effect is more obvious when the weight percentage of carbon fabrics are smaller vis-à-vis glass fabrics, which could be estimated through experimental and theoretical analysis. Also, thermosets and thermoplastic behaved similarly at lower temperatures, while at higher temperature thermoplastic was more stable, especially in the case of hybrids. In addition, the hybrid of thermoplastic can be retaining their characteristics within the high service temperatures, what make it has a big potential application in airframe and could replace easily some thermosets-based components of aircrafts.

Authorship statement

All experiments and results analysis were performed equally between all authors.

Declaration of competing interest

The authors declare that they have no known competing financial interests or personal relationships that could have appeared to influence the work reported in this paper.

Acknowledgements

Appendix A. Supplementary data

References

[1] A.G. Adeniyi, D.V. Onifade, J.O. Ighalo, A.S. Adeoye, A review of coir fiber reinforced polymer composites, Compos. B Eng. (2019), https://doi.org/10.1016/j.compositesb.2019.107305.

[2] S.P. Subadra, S. Yousef, P. Griskevicius, V. Makarevicius, High-performance fiberglass/epoxy reinforced by functionalized CNTs for vehicle applications with less fuel consumption and greenhouse gas emissions, Polym. Test. (2020), https://doi.org/10.1016/j.polymertesting.2020.106480.

[3] S. Korkiakoski, P. Brøndsted, E. Sarlin, O. Saarela, Influence of specimen type and reinforcement on measured tension-tension fatigue life of unidirectional GFRP laminates, Int. J. Fatig. (2016), https://doi.org/10.1016/j.ijfatigue.2015.12.008.

[4] N.R. Mathivanan, J. Jerald, Experimental investigation of woven E-glass epoxy composite laminate subjected to low-velocity impact at different energy levels, J. Miner. Mater. Char. Eng. (2010), https://doi.org/10.4236/jmmce.2010.97046.

[5] M. Ranjbar, S. Feli, Mechanical and low-velocity impact properties of epoxy-composite beams reinforced by MWCNTs, J. Compos. Mater. (2019), https://doi.org/10.1177/0021998318790049.

[6] A.Y. Al-Maharma, P. Sendur, The effect of interlaminar graphene nano-sheets reinforced e-glass fiber/epoxy on low velocity impact response of a composite plate, Mater. Res. Express (2018), https://doi.org/10.1088/2053-1591/aac1cf.

[7] H. Kallagunta, J.S. Tate, Low-velocity impact behavior of glass fiber epoxy composites modified with nanoceramic particles, J. Compos. Mater. (2019), https://doi.org/10.1177/0021998319893435.

[8] R.M. Marat-Mendes, M.M. Freitas, Failure criteria for mixed mode delamination in glass fibre epoxy composites, Compos. Struct. (2010), https://doi.org/10.1016/j.compstruct.2009.07.017.

[9] Y. Swolfs, Y. Meerten, P. Hine, I. Ward, I. Verpoest, L. Gorbatikh, Introducing ductility in hybrid carbon fibre/self-reinforced composites through control of the damage mechanisms, Compos. Struct. (2015), https://doi.org/10.1016/j.compstruct.2015.04.069.

[10] G. Czel, M.R. Wisnom, Demonstration of pseudo-ductility in high performance glass/epoxy composites by hybridisation with thin-ply carbon prepeg, Composites Part A 52 (2013) 23–30.

[11] G. Czél, M. Jalalvand, M.R. Wisnom, T. Czigány, Design and characterisation of high performance, pseudo-ductile all-carbon/epoxy unidirectional hybrid composites, Compos. B Eng. (2017), https://doi.org/10.1016/j.compositesb.2016.11.049.

[12] H. Yu, M.L. Longana, M. Jalalvand, M.R. Wisnom, K.D. Potter, Pseudo-ductility in intermingled carbon/glass hybrid composites with highly aligned discontinuous fibres, Compos. Appl. Sci. Manuf. (2015), https://doi.org/10.1016/j.compositesa.2015.02.014.

[13] D.K. Jesthi, R.K. Nayak, Improvement of mechanical properties of hybrid composites through interply rearrangement of glass and carbon woven fabrics for marine application, Compos. B Eng. (2019), https://doi.org/10.1016/j.compositesb.2019.03.042.

[14] S. Kar, S. Pattnaik, M.K. Sutar, Development of pseudo ductile behavior of carbon fiber reinforced composites-An overview, in: Materials Today: Proceedings, 2019, https://doi.org/10.1016/j.matpr.2019.07.390.

[15] M. Damghani, N. Ersoy, M. Piorkowski, A. Murphy, Experimental evaluation of residual tensile strength of hybrid composite aerospace materials after low velocity impact, Compos. B Eng. (2019), https://doi.org/10.1016/j.compositesb.2019.107537.

[16] J.J. Andrew, S.M. Srinivasan, A. Arockiarajan, H.N. Dhakal, Parameters influencing the impact response of fiber-reinforced polymer matrix composite materials: a critical review, Compos. Struct. (2019), https://doi.org/10.1016/j.compstruct.2019.111007.

[17] P. yan Hung, K. tak Lau, L. kwan Cheng, J. Leng, D. Hui, Impact response of hybrid carbon/glass fibre reinforced polymer composites designed for engineering applications, Compos. B Eng. (2018), https://doi.org/10.1016/j.compositesb.2017.09.026.

[18] M. Fotouhi, M. Jalalvand, M. Saeedifar, B. Xiao, M.R. Wisnom, High performance quasi-isotropic thin-ply carbon/glass hybrid composites with pseudo-ductile behaviour loaded off-axis, Compos. Struct. (2020), https://doi.org/10.1016/j.compstruct.2020.112444.

[19] A. Pandian, M.T.H. Sultan, U. Marimuthu, A.U.M. Shah, Low velocity impact studies on fibre-reinforced polymer composites and their hybrids – review, Encyclopedia of Renewable and Sustainable Materials (2020), https://doi.org/10.1016/b978-0-12-803581-8.11289-5.

[20] X.C. Sun, S.R. Hallett, Failure mechanisms and damage evolution of laminated composites under compression after impact (CAI): experimental and numerical study, Compos. Appl. Sci. Manuf. (2018), https://doi.org/10.1016/j.compositesa.2017.10.026.

[21] M. Dahale, G. Neale, R. Lupicini, L. Cascone, C. McGarrigle, J. Kelly, A. McIlhagger, Effect of weave parameters on the mechanical properties of 3D woven glass composites, Compos. Struct. (2019), https://doi.org/10.1016/j.compstruct.2019.110947.

[22] A. Rogani, P. Navarro, S. Marguet, J.F. Ferrero, C. Lanouette, Tensile post-impact behaviour of thin carbon/epoxy and glass/epoxy hybrid woven laminates – Part I:

146

experimental study, Compos. Struct. (2019), https://doi.org/10.1016/j.compstruct.2019.111508.

[23] A. Rogani, P. Navarro, S. Marguet, J.F. Ferrero, C. Lanouette, Tensile post-impact behaviour of thin carbon/epoxy and glass/epoxy hybrid woven laminates – Part II: numerical study, Compos. Struct. (2019), https://doi.org/10.1016/j.compstruct.2019.111455.

[24] S. Fotouhi, J. Clamp, A. Bolouri, T.R. Pozegic, M. Fotouhi, Investigating polyethersulfone interleaved Glass/Carbon hybrid composite under impact and its comparison with GLARE, Compos. Struct. (2019), https://doi.org/10.1016/j.compstruct.2019.111268.

[25] N.H. Nash, A. Portela, C.I. Bachour-Sirerol, I. Manolakis, A.J. Comer, Effect of environmental conditioning on the properties of thermosetting- and thermoplastic-matrix composite materials by resin infusion for marine applications, Compos. B Eng. (2019), https://doi.org/10.1016/j.compositesb.2019.107271.

[26] Q. Charlier, F. Lortie, J.F. Gérard, Interfacial adhesion in glass-fiber thermoplastic composites processed from acrylic reactive systems, a multi-scale experimental analysis, in: International Journal of Adhesion and Adhesives, 2020, https://doi.org/10.1016/j.ijadhadh.2019.102536.

[27] W. Jiang, X. Jin, H. Li, S. Zhang, T. Zhou, H. Xie, Modification of nano-hybrid silicon acrylic resin with anticorrosion and hydrophobic properties, Polym. Test. (2020), https://doi.org/10.1016/j.polymertesting.2019.106287.

[28] M. Pourhajibagher, R. Ghorbanzadeh, A. Bahador, Antimicrobial properties of acrylic resins doped with Undaria pinnatifida exposed to light-emitting diode: in silico and in vitro assessments on multispecies biofilm-producing microbiota, Photodiagnosis Photodyn. Ther. (2019), https://doi.org/10.1016/j.pdpdt.2019.05.039.

[29] A. Dogan, V. Arikan, Low-velocity impact response of E-glass reinforced thermoset and thermoplastic based sandwich composites, Compos. B Eng. (2017), https://doi.org/10.1016/j.compositesb.2017.06.027.

[30] Y.O. Shen, B. Jiang, Y. Li, X. Jiang, Low velocity impact response and energy absorption behavior on glass fibre reinforced epoxy composites, Sci. China Technol. Sci. (2017), https://doi.org/10.1007/s11431-016-9061-3.

[31] C. Zhang, Y. Rao, W. Li, Low-velocity impact behavior of intralayer hybrid composites based on carbon and glass non-crimp fabric, Compos. Struct. (2020), https://doi.org/10.1016/j.compstruct.2019.111713.

[32] A.A.M. Badawy, Impact behavior of glass fibers reinforced composite laminates at different temperatures, Ain Shams Engineering Journal (2012), https://doi.org/10.1016/j.asej.2012.01.001.

[33] T. Sreekantha Reddy, P. Rama Subba Reddy, V. Madhu, Low velocity impact studies of E-glass/epoxy composite laminates at different thicknesses and temperatures, Defence Technology (2019), https://doi.org/10.1016/j.dt.2019.02.003.

[34] I. Papa, A. Langella, V. Lopresto, CFRP laminates impacted at low velocity: influence of the matrix and temperature, in: AIP Conference Proceedings, 2018, https://doi.org/10.1063/1.5045889.

[35] A. Varadevan, S. Senthil Kumaran, K. Naresh, R. Velmurugan, Layer-wise damage prediction in carbon/Kevlar/S-glass/E-glass fibre reinforced epoxy hybrid composites under low-velocity impact loading using advanced 3D computed tomography, Int. J. Crashworthiness (2020), https://doi.org/10.1080/13588265.2018.1511234.

[36] M. Fotouhi, M. Jalalvand, M.R. Wisnom, Demonstration of pseudo-ductility in all fibre directions of high performance quasi-isotropic thin ply carbon/glass hybrid composites, in: ICCM International Conferences on Composite Materials, 2017.

[37] H.A. Samad, M. Jaafar, Effect of polymethyl methacrylate (PMMA) powder to liquid monomer (P/L) ratio and powder molecular weight on the properties of PMMA cement, Polym. Plast. Technol. Eng. (2009), https://doi.org/10.1080/03602550902824374.

[38] B.W. Jo, G.H. Tae, B.Y. Kwon, Ductility evaluation of prestressed concrete beams with CFRP tendons, J. Reinforc. Plast. Compos. (2004), https://doi.org/10.1177/0731684404035492.

[39] F. Oudah, R. El-Hacha, A new ductility model of reinforced concrete beams strengthened using Fiber Reinforced Polymer reinforcement, Compos. B Eng. (2012), https://doi.org/10.1016/j.compositesb.2012.01.071.

[40] A.E. Naaman, S.M. Jeong, Structural ductility of concrete beams prestressed with FRP tendons, in: Proceeding of the Second International RILEM Symposium (FRPRCS-2), 1995, pp. 379–401. London.

[41] N.F. Grace, A.K. Soliman, G. Abdel-Sayed, K.R. Saleh, Behavior and ductility of simple and continuous FRP reinforced beams, J. Compos. Construct. 2 (4) (1998) 186–194. November.

[42] A. Ghallab, Ductility of externally prestressed continuous concrete beams, KSCE Journal of Civil Engineering (2014), https://doi.org/10.1007/s12205-014-0443-0.

[43] A. Rajpurohit, S. Joannès, V. Singery, P. Sanial, L. Laiarinandrasana, Hybrid effect in in-plane loading of carbon/glass fibre based inter- and intraply hybrid composites, Journal of Composites Science (2020), https://doi.org/10.3390/jcs4010006.

[44] S.S. Yao, F.L. Jin, K.Y. Rhee, D. Hui, S.J. Park, Recent advances in carbon-fiber-reinforced thermoplastic composites: a review, Compos. B Eng. (2018), https://doi.org/10.1016/j.compositesb.2017.12.007.

[45] Y. Wang, J. Zhang, G. Fang, J. Zhang, Z. Zhou, S. Wang, Influence of temperature on the impact behavior of woven-ply carbon fiber reinforced thermoplastic composites, Compos. Struct. (2018), https://doi.org/10.1016/j.compstruct.2017.11.056.

[46] A. Gliszczynski, et al., The response of laminated composite plates and profiles under low-velocity impact load, Compos. Struct. (2019), https://doi.org/10.1016/j.compstruct.2018.09.005.

[47] M.K. Moghaddam, J. Hellmann, W. Lang, Plasticisation of epoxy resin transfer molding substrate for fabrication of interdigital capacitive sensors, Procedia Engineering (2016), https://doi.org/10.1016/j.proeng.2016.11.358.

[48] S. Yousef, M. Tatariants, R. Bendikiene, G. Denafas, Mechanical and thermal characterizations of non-metallic components recycled from waste printed circuit boards, J. Clean. Prod. (2017), https://doi.org/10.1016/j.jclepro.2017.08.195.

[49] W. Jiang, X. Jin, H. Li, S. Zhang, T. Zhou, H. Xie, Modification of nano-hybrid silicon acrylic resin with anticorrosion and hydrophobic properties, Polym. Test. (2020), https://doi.org/10.1016/j.polymertesting.2019.106287.

[50] C. Zhang, Y. Rao, W. Li, Low-velocity impact behavior of intralayer hybrid composites based on carbon and glass non-crimp fabric, Compos. Struct. (2020), https://doi.org/10.1016/j.compstruct.2019.111713.

[51] V. Carvelli, H. Nishida, T. Fujii, K. Okubo, Low velocity impact and CAI of woven carbon fibre reinforced highly polymerized thermoplastic epoxy modified with submicron diameter glass fibres, Composite Structures, 2020, https://doi.org/10.1016/j.compstruct.2019.111835.

[52] C. Zhang, Y. Rao, Z. Li, W. Li, Low-velocity impact behavior of interlayer/intralayer hybrid composites based on carbon and glass non-crimp fabric, Materials (2018), https://doi.org/10.3390/ma11122472.

[53] C.C. Foo, L.K. Seah, G.B. Chai, A modified energy-balance model to predict low-velocity impact response for sandwich composites, Compos. Struct. (2011), https://doi.org/10.1016/j.compstruct.2010.11.008.

[54] M.R. Wisnom, G. Czél, Y. Swolfs, M. Jalalvand, L. Gorbatikh, L. Verpoest, Hybrid effects in thin ply carbon/glass unidirectional laminates: accurate experimental determination and prediction, Compos. Appl. Sci. Manuf. (2016), https://doi.org/10.1016/j.compositesa.2016.04.014.

[55] I.E. Tabrizi, A. Kefal, J.S.M. Zanjani, C. Akalin, M. Yildiz, Experimental and numerical investigation on fracture behavior of glass/carbon fiber hybrid composites using acoustic emission method and refined zigzag theory, Compos. Struct. (2019), https://doi.org/10.1016/j.compstruct.2019.110971.

[56] D. Garcia-Gonzalez, A. Rusinek, A. Bendarma, R. Bernier, M. Klosak, S. Bahi, Material and structural behavior of PMMA from low temperatures to over the glass transition: quasi-static and dynamic loading, Polym. Test. (2020), https://doi.org/10.1016/j.polymertesting.2019.106263.

10

147

Article

Effect of Hybridization and Ply Waviness on the Flexural Strength of Polymer Composites: An Experimental and Numerical Study

Sharath P. Subadra [1,2,*] and Paulius Griskevicius [1]

[1] Department of Mechanical Engineering, Faculty of Mechanical Engineering and Design, Kaunas University of Technology, LT-51424 Kaunas, Lithuania; paulius.griskevicius@ktu.lt

[2] Vezo, Kirtimu Str. 61b, LT-02244 Vilnius, Lithuania

[*] Correspondence: sharath.peethambaran@ktu.edu

Abstract: The study aims to ascertain the influence of hybridisation and ply waviness on the flexural behaviour of polymer composites. Two different resin systems, namely epoxy and Poly(methyl methacrylate)-PMMA, were chosen for the study, wherein two batches of carbon/glass hybrid composites (CGHC) were fabricated with the two resin systems. In addition to CGHC samples, four other neat batches with waviness (glass/epoxy and glass/PMMA) were prepared to study the effect of out-of-plane ply waviness. Two sets were additionally made with in-plane waviness (angles ranging from 15–35°) with epoxy to further understand the effect of waviness on flexural behaviour. Thereafter, two more batches of samples with neither waviness nor hybrid architectures were tested to achieve a better understanding of hybridization and the presence of waviness. It was seen that the hybridization of polymer composites introduces a pseudo-ductile behaviour in brittle composites, which makes the failure more predictable. An energy-based model was implemented to quantify the ductility introduced by hybridization. The presence of in-plane waviness increased the flexural load but reduced the modulus considerably. The presence of out-of-plane waviness decreased the flexural properties of composites drastically, though the displacement rate was seen to increase considerably. From the comparison between epoxy and PMMA, it was seen that PMMA exhibited similar flexural properties vis-à-vis epoxy. PMMA is easy to re-cycle and thus could serve as an ideal replacement for epoxy resin. Finally, a numerical model was built based on an LS-DYNA commercial solver; the model predicted the flexural behaviour close to what was seen in the experiments. The model could be calibrated correctly by ascertaining the influence of failure strain in the longitudinal direction, which is fibre dependent, and the failure strain in the transverse direction, which is matrix dependent.

Keywords: fibre-reinforced polymer composites; wind energy; composite stiffnesses degradation; numerical modelling

1. Introduction

The demand for polymer composites has been on the upswing due to their light weight, damage tolerance, high specific strength, durability, maturity in processing, lower gas emissions, lower fuel consumption, etc., compared to metals [1–3]. The failure of polymer composites is sudden and catastrophic, owing to their brittle nature; thus, to ensure safe operations, higher safety factors are applied for components made from polymer composites. This could lead to over-designed components of composites, hence affecting their potential weight-saving benefits. Introducing ductility into a brittle material, i.e., achieving gradual failure [4], in composite structures could enhance their functionality, widening their application scope.

The hybridisation of composite architecture has been accepted as an approach to introduce gradual failure in polymer composites [4–12]. This essentially includes combining

148

low-strain materials (LSM) and high-strain materials (HSM) in an appropriate configuration. Though different possibilities of hybridising exists, the one most exploited is the inter-layer hybrid configuration, where mixing of different materials occurs on the ply level [8,9]. Extensive studies have been conducted on the hybrid effect exhibited by specimens under tension [13–17]. It has been found that thin carbon/epoxy pre-impregnated plies produced using tow spreading technology have suppressed damage mechanisms by obtaining lower energy release rates, delaying the propagation of intralaminar and interlaminar cracks [18–22]. This has introduced fragmentation of carbon plies as a new damage mechanism in composites, thus lending to gradual failure instead of catastrophic failure [4]. As the need arises to make polymer composites environmentally sustainable, alternative resin systems that are more recyclable need to be explored [23]. The hybrid effect in such resins needs to be confirmed and quantified.

Fibre waviness is a common manufacturing-induced defect associated with thick composite structures. Two primary causes of waviness are the residual stress originating during curing and local buckling of fibres during filament winding [24–29]. Ideal properties associated with straight fibre materials are assumed when conducting structural analysis; this is a flawed practice, because these properties are either over-estimated or under-estimated in terms of the true experimental values (these take into account the presence of waviness) [30–36]. Loading of composite structures with ply waviness causes a three-dimensional stress state that can reduce their stiffness and strength, which is of particular concern in real-time applications such as wind turbines. Load-bearing parts with ply waviness in wind turbines, such as spar caps, lead to early global failure and kinking of the entire blade structure; thus ply waviness can cause structural problems, which must be considered in the analysis and design process of wind turbine blades [36]. An important parameter controlling the waviness-dependent properties is the wave amplitude and wavelength ratio (a/λ) [31,37–39]. Rai et al. [39] proved this theoretically, and the latter has been experimentally proven [24–39].

Making composite architectures to achieve gradual failure with flexural loading has not been an objective in many studies; maximising the flexural strength and modulus has been the concern [40–43]. Most flexural studies on hybrid composites [4] have identified the ideal combinations of different fabrics to achieve the hybrid effect, while quite few have quantified the hybrid effect achieved. Ductility Index is a mathematical term that can be employed to determine the energy expended during failure and hence better understand the damage propagation. While studying waviness in polymer composites, the current research has sought to understand the mechanical performance in tension, compression, and fatigue [44]. Several studies [24–39] have aimed to predict the strength and stiffness reduction in the presence of waviness. The effect of waviness on flexural strength has been less explored experimentally, Allison and Evans [45] studied the effect of waviness on flexural performance. The same study derived a failure criterion that could predict the load and location where failure will begin. Taking the lead from this research, the current study explores the effect of waviness on composites with two different resin systems. Matrix-dominated properties play an important role [46] in the presence of waviness; hence, this becomes the rationale to understand the role of different matrices while studying waviness. The study further explores a numerical model that predicts the flexural behaviour of hybrid composites and laminates with waviness. The numerical model is an attempt to explore the effect of carbon fabric on the hybrid effect and the matrix dominant properties in the presence of waviness.

2. Experimental Methodology

2.1. Materials and Design of Experiments

Uni-directional glass (areal density 220 g/m^2) and carbon fabrics (areal density 120 g/m^2) were supplied by R&G Faserverbundwerskstoffe GmbH (Waldenbuch, Germany). Epoxy resin based on Bisphenol A and its hardener (modified cycloaliphatic polyamine free of alkyl phenol and benzyl alcohol) was also sourced from the same firm.

149

The methyl methacrylate (MMA: 617H119-Orthocryl Resin) resin and its polymeriser (Benzoyl Peroxide-BPO: Orthocryl resin 617P37, Otto Bock) were sourced from Otto Bock HealthCare Deutschland GmbH (Duderstadt, Germany). The composite architecture and the resin viscosity and density are elaborated in Tables 1 and 2 respectively as per the data sheets from the manufacturer. The experimental work here was designed in four stages: (a) making of fibre/resin laminate composites, (b) investigation of flexural properties of the prepared panels and subsequent micro-structure, (c) estimation of the ductility of hybrid composites, and (d) validation of the numerical model. The experiments were carried out for 10 batches of specimens with different fibre architectures, resin, etc., as elaborated in Table 1, where T-3, T-4, T-7, T-8 were specimens with out-of-plane waviness, and T-9 and T-10 with in-plane waviness. T-3 and T-7 had waviness defined as concave up and T-4 and T-8 as concave down.

Table 1. Composite architecture.

Specimen Code	Symbol	Architecture	Fabric	Fibre Orientation	Resin
T-1		●●●●●●●●	Glass	Uni-directional	Epoxy
T-2		●●●●●●●●	Glass and Carbon	Uni-directional	Epoxy
T-3/T-9		●●●●●●●●	Glass	Uni-directional	Epoxy
T-4/T-10	Glass ◆	●●●●●●●●	Glass	Uni-directional	Epoxy
T-5	Carbon ◆	●●●●●●●●	Glass	Uni-directional	PMMA
T-6		●●●●●●●●	Glass and Carbon	Uni-directional	PMMA
T-7		●●●●●●●●	Glass	Uni-directional	PMMA
T-8		●●●●●●●●	Glass	Uni-directional	PMMA

Table 2. Resin viscosity and density.

Resin Material	Property	Value	Units
Epoxy (Bisphenol A)	Viscosity at 25 °C	710	mPas
	Density at 25 °C	1.15	g/cm^3
Epoxy (Bisphenol A)	Viscosity at 25 °C	14	mPas
	Density at 25 °C	0.94	g/cm^3
PMMA	Viscosity at 20 °C	500	mPas
	Density at 20 °C	1	g/cm^3

2.2. Fabrication of Fibre/Resin Laminate Composites and the Flexural Test

The preparation of the panels was preceded by cutting the fabrics in accordance with the size of the panels; EN ISO 14125:1998/AC was followed for the preparation of specimens. Epoxy resin and its hardener solution with a ratio of 70:30 wt% of the total panel weight were mixed together using a mechanical mixer for 15 min, followed by keeping the solutions in a vacuum chamber at −100 bar for 10 min to eliminate air bubbles introduced during mixing. PMMA resin mix was prepared by mixing MMA monomer with BPO as an initiation system in the free-radical polymerization, with a weight ratio of 100:2 (MMA:BPO), using a mechanical mixer for 15 min; subsequently, the air bubbles were removed as before. The hand lay-up method was adopted to fabricate the panels, and in the case of introducing out-of-plane waviness into the laminates, a semi-circular die made

of plastic was used. The plastic die had a length of 110 mm and diameter of 10 mm; the waviness angle obtained by the placement of this die was approximately 14 degrees. The fabric was placed over the die (wax was used a releasing agent on the die) one after the other, and the resin was spread over it by a roller; subsequently, the panels were vacuum bagged. This method gives repeatability in the results of post-flexural tests, as the method ensures a constant thickness of 1.9 ± 0.1 mm through the fabricating process. This can be achieved by thoroughly sealing the vacuum bag and maintaining the vacuum pressure constant by ensuring that there are no leakages. In-plane waviness was introduced by pushing the fabric upwards while immersed in resin. Thus, by doing so, T-9 was introduced with an in-plane wave angle of $-15°$, and T-10 with an in-plane angle of $-35°$. An infra-red lamp post-cure process was adopted (at 70 °C for 6 h), and the main curing process was carried out on an electronically controlled oven (temperature range 30–350 °C) (at 90 °C for 5 h). An automatic cutter was used to cut the specimens, and the cutting parameters were set as per the ISO standard adopted for this study. Five samples were assigned to each code mentioned in Table 1, and the accuracy of the cut specimens in terms of dimensions was satisfactory to obtain consistency in the experimental results. Later, 3-point bending tests were performed on a Tinius Olsen universal testing machine (UTM) having a maximum load capacity of 10 kN, within a span length of 60 mm and at a loading rate of 3 mm/min.

2.3. Determination of Ductility of Specimens Subjected to Flexural Loading

Ductility of beams can be expressed in terms of a dimensionless ductility factor or DI based on the general curvatures, rotations, or reflections. However, this criteria is based on a yield and an ultimate strain found in ductile metals as opposed to brittle materials. Thus, an energy criterion was introduced to estimate the DI of brittle materials based on the consumed energy until failure [47–50]. Based on this framework, Naaman and Jeong (1995) [49] and Grace et al. (1998) [50] developed two different models to compute the DI, which is based on the total energy (E_{total}), elastic energy ($E_{elastic}$), and the failure energy ($E_{in-elastic}$), as seen in Equations (1) and (2). E_{total} represents the area under the load-displacement curve up until the final failure, whereas $E_{elastic}$ is defined as the area of the triangle formed at the failure load by the line having the weighted average slope of two initial straight lines of the load-displacement curve (Figure 1). Both methods gave accurate results, which served as a motivation for its use in calculation of ductility of brittle materials, such as concrete, [49,50]. Thus, both these methods were employed in this paper.

$$DI\ (Naaman) = \frac{1}{2}\left(\frac{E_{total}}{E_{elastic}} + 1\right) \tag{1}$$

$$DI\ (Grace's) = \frac{E_{in-elastic}}{E_{total}} \tag{2}$$
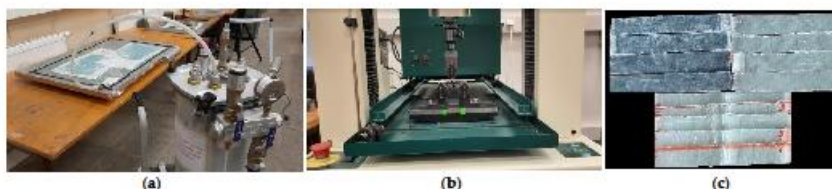

Figure 1. (a) Composite panel preparation using the vacuum bagging method. (b) Flexural test on a specimen with waviness. (c) Specimens for flexural test.

2.4. Numerical Analysis of the Flexural Behaviour of All the Architectures Currently Studied

The finite element method (FEM) was adopted in the current work to understand the effect of hybridization of composite architecture and to ascertain the effect of waviness on composite flexural properties. The analysis was carried out using LS-DYNA software, which is classified as the most-used program for solving nonlinear problems using explicit time integration with precise results [51]. The use of LS-DYNA as a software was validated by its original developers (Livermore Software Technology Corporation, acquired by Ansys in 2019) for its generic applications. Thus, common applications of LS-DYNA include automotive, aerospace, metal forming and multi-physics problems [52]. Thus, in the context of the current research, a finite element model was to predict the flexural performance of composites with hybrid architecture and degradation of flexural properties in the presence of waviness. The modelling techniques require several parameters to be defined, and these include material properties, meshing size, loading conditions, and constraints. These parameters were defined and used as input for LS-DYNA modelling for each of the samples studied in this paper (Figure 2).

In the material section, two composite material properties were defined for carbon and glass. The material properties were determined from static tests on the specimens and from the mathematical model developed based on the rule of mixtures, as elaborated in [53]. Thus, based on these methods, Table 3 gives an overview of the material properties used in this paper. The table has information on both glass and carbon composites with both resin types used.

A.　The composite plies were modelled using 4 Node Shell formulation, available in the LS DYNA Shape Mesher library. The mesh size (mesh type: square) was kept constant at 1 mm throughout the modelling. The size of the specimens was as per the ISO standard mentioned in Section 3.2. The number of layers in the model is as per Table 1. Regarding the boundary conditions, the specimens were constrained as a pin and roller [54] support. This implies a completely constrained motion in the z-direction and free in the y-direction (along the width), while in the x-direction (along the length), the specimens were fixed at one end and were allowed a translation motion at the other end.

B.　On defining the loading conditions, initially, a set of nodes on which the load would be applied were defined using the Boundary_SPC_SET option. Later, the loading curve was defined based on the actual experimental loading conditions, and the curve was assigned to the nodes through the option Boundary_Prescribed_Motion_Set.

C.　The composite failure was modelled using the material model MAT 54, which is a progressive-failure model that uses the Chang–Chang failure criterion [55]. The model takes in 21 parameters that should be defined, 15 of which are physically based and 6 of which are numerical parameters. Among the 15 physical parameters, 10 are material constants; these are elaborated in Table 2. The remaining 5 parameters are tensile and compressive failure strain in fibre directions, the matrix and shear failure strains, and the effective failure strain. The 6 numerical parameters were set at their default values. By conducting a parametric, study it was inferred that only DFAILT and DFAILM (DFAILT-Max strain for fibre tension, DFAILM-Max strain for matrix straining in tension and compression) needed to be adjusted. These terms and their explanations can be found in [51]. Adjusting the above two parameters helps simulate the tension/compression within the matrix between layers and the tension of fibres along the bottom of the specimen [51].
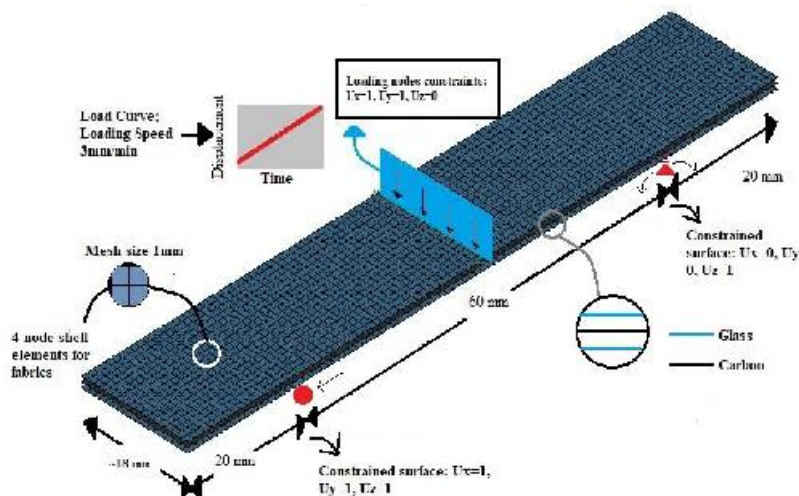
152

Figure 2. FEM schematic of the specimens, including modelling, materials, meshing, constraints, contact definition, and loading conditions.

Table 3. Composite specimen properties for numerical modelling. X_T: strength in tension (longitudinal); X_C: strength in compression (longitudinal); Y_T: strength in tension (transverse); Y_C: strength in compression (transverse); S_L: shear strength.

Resin Type	E_1 (GPa)	E_2 (GPa)	G_{12}/G_{13} (GPa)	ν_{12}	X_T (MPa)	X_C (MPa)	Y_T (MPa)	S_L (MPa)	Y_C (MPa)
Epoxy/Glass	32.4	8.1	2.6	0.22	680	600	35	37	35
Epoxy/Carbon	63	40	9	0.16	709	473	501	146	199
PMMA/Glass	23.16	2.1	2.62	0.38	325	246	16	42	128
PMMA/Carbon	47	3	1.8	0.13	1300	882	15	40	120

3. Results and Discussion

3.1. Flexural Characteristics of Composite Specimens: Pure, Hybrid, and with Waviness

Figure 3a,b shows the load displacement plots for the tested samples from both epoxy and PMMA. Since consistent plots were obtained among the samples studied, the presented plots are just for one sample set. It can be inferred that the PMMA and epoxy samples exhibited similar flexure response; though a significant increase in load was seen, it was generally comparable to epoxy specimens. A direct consequence of this outcome is the eventual replacement of epoxy with more recyclable PMMA. A closer observation shows the specimens with waviness tend to lose their flexural strength in comparison to those with no waviness in them. Though the specimens without any waviness/hybridisation tend to carry the highest flexural load, the failure post-maximum was abrupt. Hybrid specimens with both glass and carbon within the architecture failed gradually, with intermittent load drops, characterised as the hybrid effect. Though the maximum load is lesser when compared to pure glass specimens, the increasing complexity of composite

153

damage mechanisms increased its ductility and hence reduced the abruptness of the damage, which is less desirable in real-time applications of these materials. The presence of waviness within the architecture is less desirable from a strength perspective; the reduction in flexural modulus was approximately 30% when compared to pure specimens in the case of epoxy and 36% in the case of PMMA. The presence of waviness hinders the normal damage mechanisms associated with composites when subjected to flexural loading. Most specimens with waviness failed abruptly, not because of any noticeable fibre failure, but due to delaminations in the waviness region. A noticeable increase in displacement was observed in specimens with waviness; this was noticed in the case of T-3 (epoxy) and T-8 (PMMA), which could be attributed to the geometry of the specimens. A microscopic inspection and observations are made in a later section in this research.

In addition to out-of-plane waviness, the effect of in-plane waviness in the case of epoxy specimens was studied; PMMA was not considered in this case. As mentioned in the previous section, five sets of samples were subjected to flexure in each code, and Figure 3d is the mean of the results obtained. This was to avoid too much data and to keep the research more concise as to study the effect of waviness on the flexural behaviour rather than ascertaining material properties with different resin systems. As can be seen in the figure (Figure 3c-e), the introduction of in-plane waviness (angle ranging from 15° to 35°) had a profound influence on the flexural behaviour of composites. Even though a reduction in flexural modulus was observed as is the case with the introduction of waviness, an increase of 22% in load was observed between T1 and T9/T10. This increase was expected because, mathematically, when using classical laminate theory to ascertain the influence of in-plane and out-of-plane waviness on the various material properties (E_x, E_y, E_z, G_{xy}, G_{xz}, G_{yz}), an increase in G_{xy} is observed in the case of in-plane waviness; in the case of out-of-plane waviness, an increase in G_{xz} is observed [56]. In practice, the increase in the case of G_{xz} cannot be realised because of early interlaminar failure [56], as can be seen earlier in the case of the out-of-plane waviness specimens studied in this paper. As can be seen in Figure 3e, the ultimate failure in the case of T-1 and T-9 was due to fibre rupture, as is the case with most flexural tests. However, in the case of T-10, no fibre failure was seen, but the specimen lost its load-bearing capacity due to shear failure, which is the major reason behind de-lamination failure. This is in stark contrast to the failure seen in T-1 and T-9, where no shear failure was seen. A direct implication of the introduction of in-plane waviness is an increase in in-plane shear modulus. This could translate to a higher load-bearing capacity, where the load is equitably shared by both the reinforcing fibres and the resin used. To prove this hypothesis, further studies should be conducted in this regard.

The results are indications that hybrid composites can be beneficial by altering damage mechanisms, though compromises on strength and stiffnesses are to be expected. Figure 4a,b below illustrates the maximum strength and flexural stiffness (EN ISO 14125:1998/AC), which can be obtained by the following equations:

$$\sigma_F = \frac{3PL}{2bd^2} \tag{3}$$

$$E_F = \frac{L^3 m}{4bd^3} \tag{4}$$

where P, L, b, d, and m are the maximum load, span, width, height, and initial slope from the load-displacement curve, respectively. The figure below is the average plot of the five samples studied in each code set, as there was consistency in the results obtained. As can be inferred from the figure below, a considerable drop in flexural strength was witnessed with the presence of waviness in the architecture. Though the drop in the case of the hybrid specimen (T-2) is negligible, waviness in T-3 and T-4 saw a considerable reduction in strength. Similar results are seen in PMMA samples, thus favouring them to replace epoxy for better recyclability.
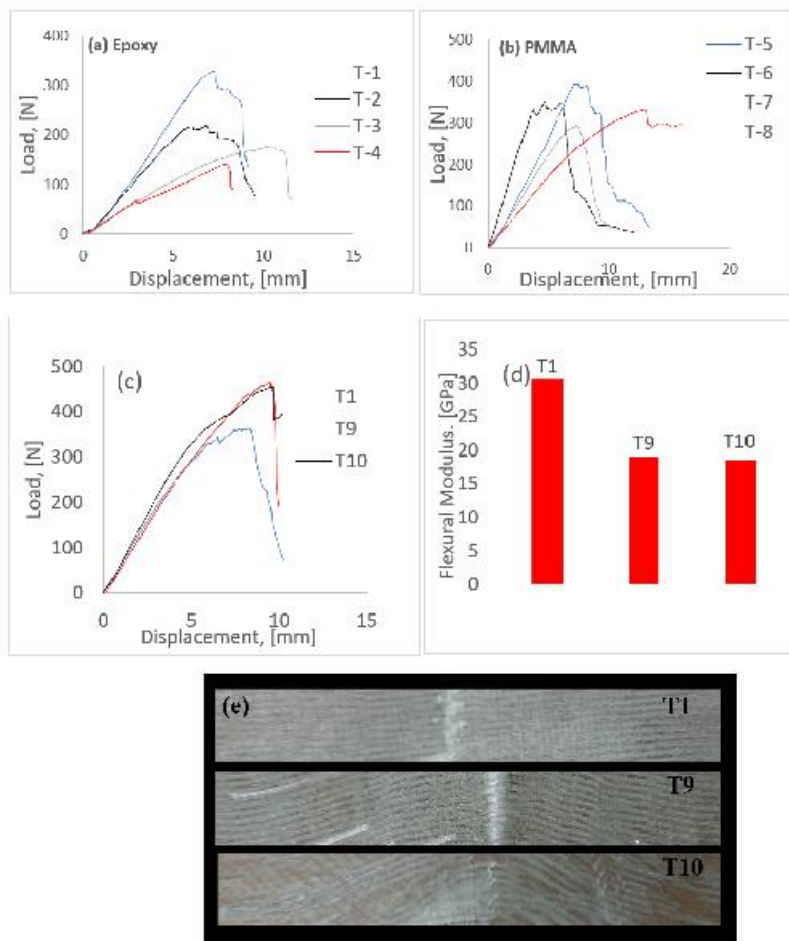
154

Figure 3. Load displacement curve from the flexural test. (**a**) Specimens with epoxy resin, (**b**) specimens with PMMA as resin, (**c**) specimens with in-plane waviness, (**d**) flexural modulus of specimens with in-plane waviness, and (**e**) specimens post-failure (in-plane waviness).
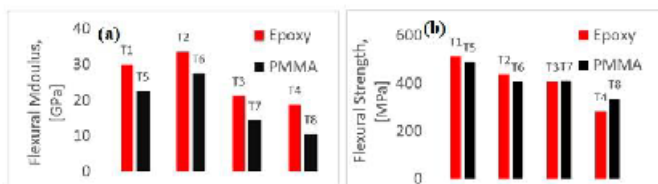
155

Figure 4. Flexural modulus and strength of pure glass, hybrids, and samples with waviness. (a) Flexural modulus comparisons from T-1 to T-8 and (b) Flexural strength comparison from T-1 to T-8.

While an alternative resin that is more environmentally friendly than epoxy is a better choice, the alternative should be as good as epoxy. Though PMMA was less stiff when compared to its epoxy counterparts, the strengths were comparable to epoxy in all cases studied. In addition to this, it was seen that the presence of waviness did reduce the strength of the specimens, but the percentage difference between the sample without waviness (T-5) and the one with waviness (T-7 and T-8) was approximately 20%. A considerable amount of reduction was seen in flexural properties while studying PMMA samples. Though T5 had lower modulus than T-1, the introduction of hybrid architecture increased the modulus significantly. Hybridising samples with PMMA considerably increased the ductility index (DI), which is indicative of an increment in the inelastic energy absorption capabilities of these samples; this will be detailed in the next section. When introducing PMMA as an alternative to epoxy, there is the drawback of making the structure more elastic in nature (more pliable). Thus, there exists a rationale to hybridise, resulting in a slight increase in stiffness, but an insignificant reduction in strength. Thus, to conclude, it can be ascertained that with some trade-offs, based on the requirements, an appropriate hybrid structure with correct distribution of carbon fabrics can be engineered with PMMA, as an alternative. The presence of manufacturing-induced damage like waviness and undulations seems to have lesser impact on strength loaded under flexure.

3.2. Energy Absorption and Estimation of Ductility Index of Samples under Flexure

The energy absorbed by specimens can be divided into two major components, the elastic and inelastic components, and these components quantify the ductility of composites. The inelastic energy is defined as the energy spent in damage initiation and propagation [49]. As mentioned in Section 2.3, the ductility index (DI) can be estimated from Equations (1) and (2) based on the calculated elastic and inelastic components. Figure 5A,B compares the ductility index estimated from both the equations for pure T1 and T5 samples against the hybrid T-2 and T-6. As ductility of any structure quantifies the ability to absorb inelastic energy without losing the loading capacity, a higher ductility would naturally signify a higher ability to absorb inelastic energy [47–50]. This is true mathematically, as ductility is directly proportional to the inelastic component [50]. Though the energy model proposed in [50] considers the total energy component, the inelastic part of this total energy cannot be discounted. Thus, based on these arguments, the T-2 and T-6, due to their hybrid architecture, fail in a controlled manner when loaded under flexure. The introduction of a single layer of carbon within multiple layers of glass introduced the hybrid effect considerably, as is evident from the figure below. The increase in ductility can be attributed to an increase in the inelastic component of the total energy, which was calculated to be 520 J in the case of T-2 and 861 J in the case of T-6. The hybrid effect can be attributed to the effect of interplay of low-strain carbon and high-strain glass fibres; the inter-laminar stresses also have an effect and cannot be neglected, as is evident from this study. Another important observation from the current study is that of the elastic component from the total energy. In the case of the non-hybrid specimens, the elastic component was the

dominant energy absorption segment. This component does make the material brittle and less predictable, while the introduction of a hybrid architecture increased the inelastic component, reducing the elastic component to 40% of the total energy. Thus, in conclusion, hybridising of composites can reduce the unpredictability of composites considerably and make them an ideal choice for structural applications.
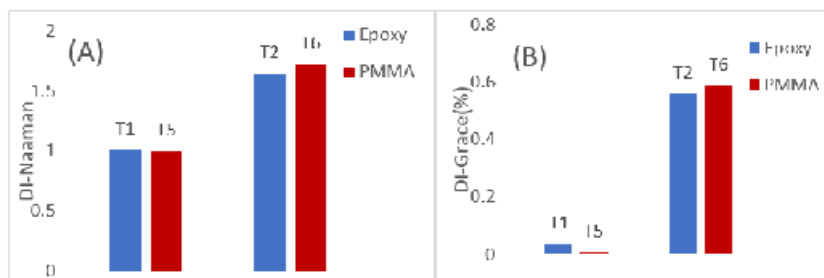

Figure 5. Ductility index (DI) based on the energy model developed by Naaman et al. [50] and Grace et al. [51]. (**A**) DI as per Naaman, (**B**) DI as per Grace.

3.3. Analysis of Damage in the Composite Architecture Subjected to External Loading

As seen in the previous sections, T-2 and T-6 had comparable load-bearing capacity and higher ductility effect as opposed to T-1 and T-5; thus, it becomes imperative to check the damage at the microscale. An optical microscope was used to check the damage and infer the mechanisms leading to a higher ductility effect in T-2 and T-6. Therefore, T-1, T-5, T-2, and T-6 were examined to check the progression of damage.

3.3.1. Epoxy Resin

The cross section of the specimens were analysed (in the case of epoxies: T-1 and T-2) using an optical microscope with 4 lens head with $4\times$, $10\times$, $40\times$, and $100\times$ lenses, in addition to a 5MPx camera for image transfer to a PC. It must be noted that the waved architecture was omitted in the case of epoxy and PMMA from this study. This was because no noticeable ductility was observed in the case of specimens with waved architecture, apart from an increase in displacement to final load drop. This was true in the case of T-3 and T-8, where it can be seen (Figure 3) that the maximum displacement to final load was approximately 10 mm. It was observed that in the case of T-1 (Figure 6), when the load drops, the fabrics ruptured and there was considerable delamination on the other side of the loading. After this event, the specimens lost their load-bearing capacity and ultimately failed completely. However, in the case of hybrids (T-2 in Figure 6), the carbon fabric was still intact. Therefore, a combination of rupture of high-strain fabric such as glass, and no rupture in a high-strength fabric such as carbon, contributes to the hybrid effect, which introduces ductility into composites and makes their failure more predictable.
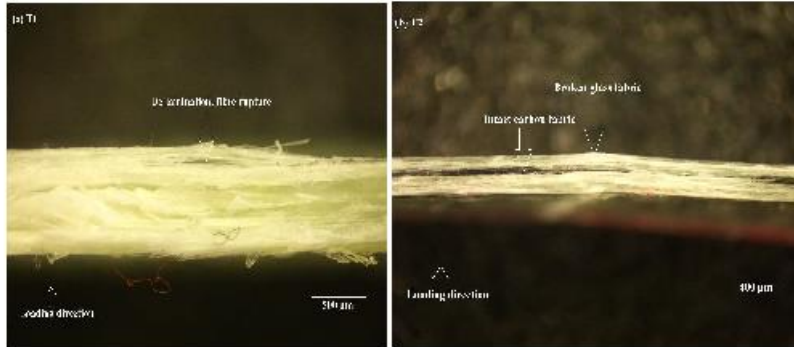
157

Figure 6. Magnified image of damaged cross-section of T1 (a) and T2 (b).

3.3.2. PMMA Resin

The damage observed in the case of T-5 and T6 (Figure 7) was clearer, as there was less reflection, as was the case in T-1 and T-2. Nevertheless, the damage observed here is similar to that seen in the previous case. T-5 failed by complete rupture of the glass fabric on the opposite side of the loading, though no de-lamination was observed. T6 exhibited the hybrid effect due to the reasons mentioned in the previous paragraph, but no delamination was observed among the fabrics in this case. The carbon fabric remained intact, which could have contributed to a higher ductility index as compared to T-2; in addition, the effect of matrix cannot be neglected. It is in this context that the effect of "bending–stiffness mismatch" [57] plays an important role in contributing to the ductility effect.
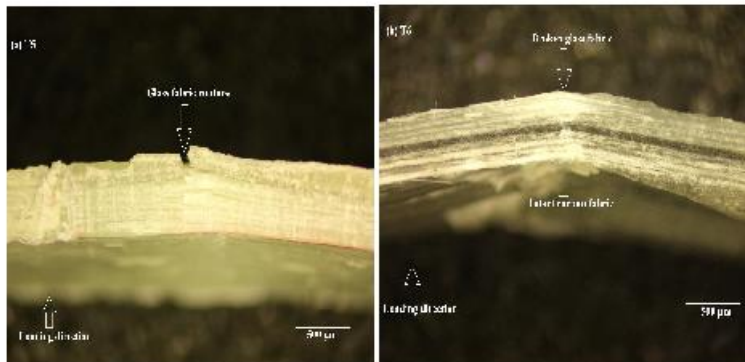

Figure 7. Magnified image of damaged cross-section of T5 (a) and T6 (b).

Bending–stiffness mismatch could be attributed to several reasons, including differing material properties, stacking sequence, and ply thickness. It was observed in [58] that delamination along the thickness direction was caused by differing stiffness among the

plies, rather than viewing them in the context of stress distribution. It has to be noted that while considering this hypothesis in the context of the hybrids studied here, no observable delamination was observed; it was the systematic rupture of low-strength glass fabric with an intact carbon in the middle that contributed to a differing bending–stiffness mismatch in the architecture. This mismatch in properties among the plies could be one of the major factors contributing to the ductility effect, though this has to be verified analytically using the classical laminate theory and additional experiments with differing thickness of glass and carbon fabrics.

3.4. Numerical Results

The numerical modelling approach elaborated in Section 2.4 was able to generate results that could capture the experimental behaviour with good compatibility. This compatibility is illustrated below in Figure 8 and Table 4, where the first three rows bearing columns marked *a, b, c,* and *d* and the last three rows bearing columns marked *e, f, g,* and *h* are dedicated for the epoxy (T-1, T-2, T-3, and T-4) and PMMA (T-5, T-6, T-7, and T-8), respectively. It can be noticed that the modelling approach was able to capture the load displacement in the elastic region with good precision. In the first row below, the stress field along the x-direction (along the length) is elucidated, and the second row elucidates the stress field in the xy-direction; similarly, the stress fields are elucidated for PMMA in fourth and fifth rows, respectively. All the figures below were captured at the same moment (steps) to adhere to a uniformity in results.

Table 4. Comparison between experimental and numerical loads obtained in flexure.

Specimen Code	T-1	T-2	T-3	T-4	T-5	T-6	T-7	T-8
Experimental Load (N)	329.60	226.25	172.40	139.95	428.21	440.50	230.00	295.20
Numerical Load (N)	341.34	229.78	165.92	138.38	439.94	492.21	205.47	296.44

From the stress fields, it was observed that T-4 and T-8 did not have a stress concentration along the mid-span (where the load is applied), while the same could be seen for all other types. It was also seen that T-4 and T-8 had the maximum displacement before failure. An inference on these two observations could be that the actual span length of these specimens is large if the waviness region is imagined to be a straight line. That would make the specimens naturally more elastic in nature than those without any waviness. In addition to this, the same advantage can be realised in PMMA, while in the case of epoxy, a reduction in strength was observed with the introduction of waviness. In the case of PMMA, there was an observable reduction in strength when compared to straight counterparts, but this was not drastic. These could be simulated on LD DYNA using the MAT 54 model, as this keyword uses strain-based criteria to arrive at failure; especially in the case of flexure, DFAILT and DFAILM plays an important role.

Failure strains DFAILT and DFAILM are calculated by dividing the material modulus by their strengths, i.e., $DFAILT = \frac{XT}{E_1}$ and $DFAILM = \frac{YT}{E_2}$. In this study, a parametric study was carried out to determine the correct value, and a range between 0.01 to 0.05 was found to give good compatibility with experiments; higher values were found to over-estimate the failure load to a large extent. It was also found that DFAILC, which is the failure strain in the compressive direction, had some influence on the results, and its value was taken in the range of -0.01 to -0.03 ($DFAILC = \frac{XC}{E_1}$). Other parameters in MAT 54, such as FBRT, TFAIL, DFAILS, SOFT, and YCFAC, were given default values. With these parameters, MAT 54 could be an ideal material model to study the flexural behaviour of composites within any kind of architecture. The next section checks the sensitivity of the model to DFAILT and DFAILM, in the range as shown in Table 3. T1 was chosen for the study, as the parameters for glass composite needed to be adjusted; this avoided the complication involved when hybrids are considered, as the parameters for carbon must be changed as well.
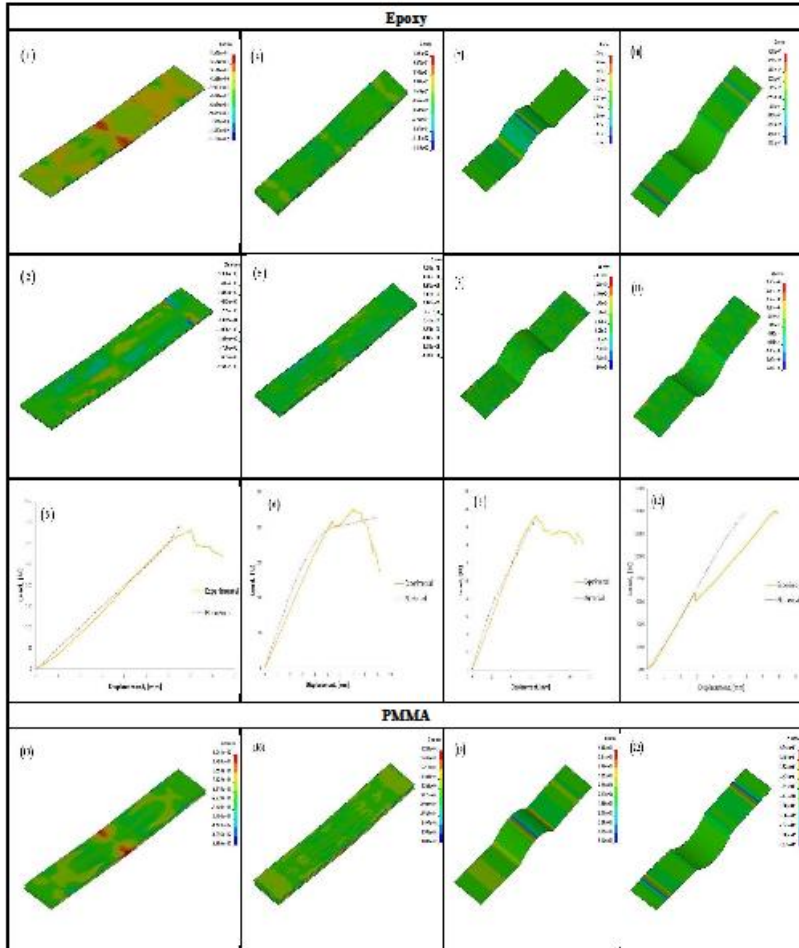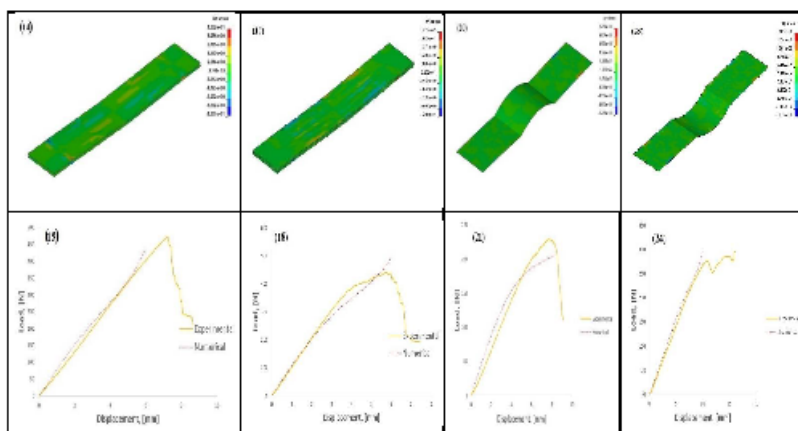
Figure 8. Cont.

160

Figure 8. Numerical results (stress fields along the -x and -xydirections, load displacement plots) captured on LS DYNA for all the specimen types studied. **(1)** Stress in x-direction for T-1, **(2)** Stress in xy-direction for T-1, **(3)** Load curve for T-1. **(4–6)** Stresses and load curve for T-2. **(7–9)** Stresses and load curve for T-3. **(10–12)** Stresses and load curve for T-4. **(13–15)** Stresses and load curve for T-5. **(16–18)** Stresses and load curve for T-6. **(19–21)** Stresses and load curve for T-7. **(22–24)** Stresses and load curve for T-8.

Sensitivity of the Model to Different Modelling Parameters

Figure 9 elucidates the theoretical and numerical strain values that were subsequently used for the parametric study in this section. The numerical values were obtained using the rule of mixture model available in the literature [58]. The theoretical strains seen in Figure 8 can be determined by knowing the material properties of the fabric and the resin used. Thus, the glass fabric stiffness was taken from literature [59] and is listed in Table 5 along with that of the resin (epoxy) used for the current study. The resin properties were ascertained through quasi-static tests, as per ISO 527(2). The aim here was to arrive at the correct calibration and hence to ascertain the influence of the respective parameters on the flexural response, which is otherwise difficult to obtain experimentally. With the theoretical values available, it gives an idea of how much the numerical model can be calibrated and its accuracy. From the figure below (Figure 9), a DFAILT of 0.048 and DFAILM of 0.1 was used in the parametric study (PS-2 and PS-6, respectively).

Table 5. Fibre and matrix mechanical properties.

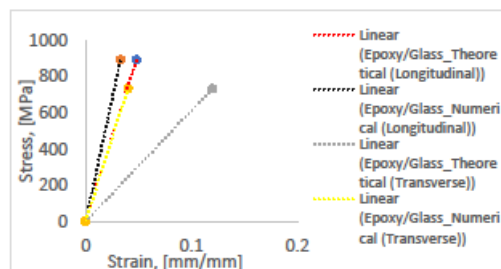| Material	Young's Modulus (GPa)	Tensile Strength (MPa)
Epoxy	3.2	70
Glass Fabric	81.0	2200

161

Figure 9. Theoretical and numerical strains for the parametric study.

Figure 10 elucidates the influence of MAT 54 parameters DFAILT and DFAILM on the behaviour of T1 under flexure. Shear stress distribution was chosen in this study because it was found that DFAILM had an influence on the failure. A parametric study in this case is necessary to benchmark a numerical model to further validate its future use in similar applications. Thus, in this study, it was found that DFAILT and DFAILM influence the model outcome to a greater extent. The range of different parameters adopted in this study is shown in the Table 6. Six parametric studies (PS) were conducted on T1, since the rest should show similar results with the same set of parameters and to avoid the accumulation of extensive results, which would be harder to analyse. From this study, it can be inferred that material properties in the longitudinal and transverse directions to a greater extent influenced the flexural response of the composite beam. From the six parametric studies, PS-1 and PS-6 gave responses that closely resembled that of the experimental ones. PS-2 and PS-4 slightly overestimated the response, and as can be seen in Table 3, DFAILM was constant at 0.04 and DFAILT was in the range of 0.048–0.1. It should be noted that DFAILM at 0.1, obtained theoretically, calibrated the model similarly to that of the experimental response. PS-3 and PS-5 underestimated the response to a greater extent, wherein lower strain values were adopted (0.009). As was explained in the previous section, DFAILT and DFAILM are max strain for fibre tension and max strain for matrix straining in tension and compression, respectively; parameters related to fibre and matrix play an important role in the flexural response. In Section 3.1, the effect of in-plane waviness was found to increase the flexural strength and modulus. As seen in this section, an increase in the matrix strain had a profound influence in the flexural response. Relating this study to in-plane waviness could highlight the importance of flexural modulus and strength, as seen in Section 3.1.

Table 6. Parameters adopted for the parametric study.

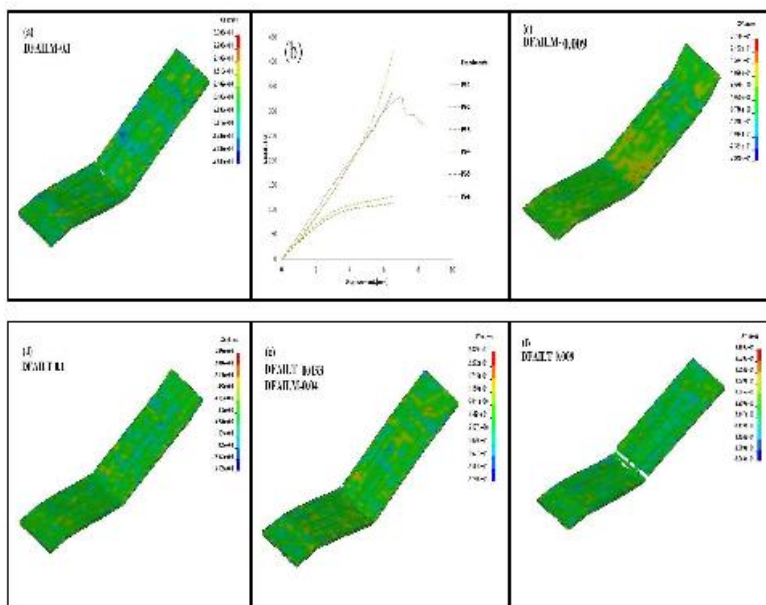| Parametric Study (PS)	DFAILT	DFAILM
1	0.033	0.04
2	0.048	0.04
3	0.009	0.04
4	0.1	0.04
5	0.033	0.009
6	0.033	0.1

Figure 10. Parametric study on influence of DFAILT and DFAILM on flexural behaviour of T1. (a) XY-stress when DFAILM = 0.1. (b) Load-displacement plot for the six parametric studies listed in Table 4. (c) XY-stress when DFAILM = 0.009. (d) XY-stress when DFAILT = 0.1. (e) XY-stress when DFAILT = 0.033 and DFAILM = 0.04. (f) XY-stress when DFAILT = 0.009.

Figure 10b shows the effect of an over-estimated DFAILT and DFAILM at 0.1. At 0.1, the failure strain is very high, and this makes the composites very stiff in the elastic region; as seen from Figure 10a,d, shear stress distribution, the element deletion that signifies failure, was not observed. It was observed that a lower strain than 0.015 in this regard was detrimental to the result, and hence it was not considered. Strains lower than 0.01 showed instabilities in the model, with non-uniform element failure. DFAILT at 0.009 saw the specimen fail (Figure 10f) pre-maturely (evident from the element deletion) and be less stiff than the experimental plots. The ideal strains that reflected the experimental results were 0.033 and 0.04 (Figure 10e), and hence these should be considered. These strains are the baseline values at which the model predicts the failure of the specimens correctly for the given material properties. It was noted that these strains are dependent on a variety of factors having direct co-relation to the material properties, such as specimen thickness, fibre volume fraction, etc.

4. Conclusions

In the current study, an attempt to ascertain the influence of hybridisation and ply waviness on the flexural behaviour of polymer composites was carried out. Epoxy and PMMA was chosen for the study, and hence 10 batches of specimens where cut and tested

163

(each batch was named, from T1–T10, with specimens each). Based on the study, the following conclusions were drawn:

- PMMA was found to have similar flexural strength to that of epoxy, though the flexural modulus was found to be lower. Hybridising the architecture did not alter the modulus, but a drop in strength was observed in the case of epoxy specimens. In the case of PMMA, hybridisation increased the modulus, but the increase was not significant, and the strength did not change significantly. Thus, from a strength perspective, PMMA could be a good alternative for epoxy, thus making composites more recyclable.
- The presence of waviness was found to be detrimental in both epoxy and PMMA specimens; in the case of the former, there was severe reduction in strength and modulus. However, the presence of in-plane waviness was found to increase the load significantly; thus, waviness could have some positive effects on composites.
- Hybridisation introduces ductility into composites, and this can be quantified using an energy-based model. Thus, it was observed that hybridised specimens (T2 and T6) exhibited higher ductility when compared to their purer counterparts. A level of 60% ductility was seen in T2 and T6, while in T1 and T5, it was abysmally low.
- The hybrid effect was further studied using an optical microscope, and it was observed that the carbon fabric was still intact, without failure. The hybrid effect was introduced by a controlled failure of first the glass fabrics and subsequently the carbon. Bending–stiffness mismatch was another reason for this observation, though this must be studied further using the classical laminate theory.
- Numerical models were built on LS DYNA using the material model MAT 54, available in the LS DYNA MAT library. The modelling approach selected was found to predict the flexural behaviour similar to experiments. Tensile strain-to-failure (DFAILT) and matrix strain-to-failure (DFAILM) was seen to influence the modelling outcome proportionately, and hence a parametric study was conducted to establish the correct values of DFAILT and DFAILM.

Author Contributions: Conceptualization, S.P.S. and P.G.; methodology, S.P.S.; software, S.P.S.; validation, S.P.S. and P.G.; formal analysis, S.P.S.; investigation, S.P.S.; resources, S.P.S.; data curation, S.P.S.; writing—original draft preparation, S.P.S.; writing—review and editing, P.G.; visualization, S.P.S.; supervision, P.G.; project administration, P.G.; funding acquisition, P.G. All authors have read and agreed to the published version of the manuscript.

Institutional Review Board Statement: Not applicable.

Informed Consent Statement: Not applicable.

Data Availability Statement: Not applicable.

Conflicts of Interest: The authors declare no conflict of interest.

References

1. Adewale, G.A.; Damilola, V.O.; Joshua, O.I.; Akorede, S.A. A review of coir fibre reinforced polymer composites. *Compos. B Eng.* **2019,** *176,* 107305. [CrossRef]
2. Sharath, P.S.; Samy, Y.; Paulius, G.; Vidas, M. High-performance fibreglass/epoxy reinforced by functionalised CNTs for vehicles applications with less fuel consumption and greenhouse gas emissions. *Polym. Test.* **2020,** *86,* 106480. [CrossRef]
3. Samuli, K.; Povl, B.; Essi, S.; Olli, S. Influence of specimen type and reinforcement on measured tension-tension fatigue life of unidirectional GFRP laminates. *Int. J. Fatig.* **2016,** *85,* 114–129. [CrossRef]
4. Guillermo, I.; Meisam, J.; Mohamad, F.; Juan, M.; Michael, R.W. Gradual failure in high-performance uni-directional thin-ply carbon/glass hybrid composites under bending. *Compos. Struct.* **2021,** *271,* 114128. [CrossRef]
5. Hayashi, T. Development of new material properties by hybrid composition. 1st Report. *Fukugo Zair. Compos. Mater.* **1972,** *1,* 18–20.
6. Summerscales, J.; Short, D. Carbon fibre and glass fibre hybrid reinforced plastics. *Composites* **1978,** *9,* 157–166. [CrossRef]

7. Manders, P.W.; Bader, M.G. The strength of hybrid glass/carbon fibre composites-Part 1 Failure strain enhancement and failure mode. *J. Mater. Sci.* **1981**, *16*, 2233–2245. [CrossRef]
8. Gergely, C.; Michael, R.W. Demonstration of pseudo-ductility in high performance glass-epoxy composites by hybridisation with thin-ply carbon prepeg. *Compos. Part A Appl. Sci. Manuf.* **2013**, *52*, 23–30.
9. Yentl, S.; Larissa, G.; Ignaas, V. Fibre hybridisation in polymer composites: A review. *Compos. A* **2014**, *67*, 181–200.
10. Gergely, C.; Meisam, J.; Michael, R.W.; Tibor, C. Design and characterisation of high performance, pseudo-ductile all-carbon/epoxy unidirectional hybrid composites. *Compos. Part B Eng.* **2017**, *111*, 348–356.
11. Yentl, S.; Ignaas, V.; Larissa, G. Recent Advances in fibre-hybrid composites: Material selection, opportunities and applications. *Int. Mater. Rev.* **2019**, *64*, 181–215.
12. Putu, S.; Mohamad, F.; Gergely.; Marco, L.; Michael, R.W. Fatigue behaviour of pseudo-ductile unidirectional thin-ply carbon/epoxyglass/epoxy hybrid composites. *Compos. Struct.* **2019**, *224*, 110996.
13. Meisam, J.; Gergely, C.; Michael, R.W. Numerical modelling of the damage modes in UD thin carbon/glass hybrid laminates. *Compos. Sci. Technol.* **2014**, *94*, 39–47.
14. Yentl, S.; Ignaas, V.; Larissa, G. A review of input data and modelling assumptions in longitudinal strength models for unidirectional fibre-reinforced composites. *Compos. Struct.* **2016**, *150*, 153–172.
15. Gergely, C.; Meisam, J.; Michael, R.W. Design and characterisation of advanced pseudo-ductile unidirectional thin-ply carbon/epoxy-glass/epoxy hybrid composites. *Compos. Struct.* **2016**, *143*, 362–370.
16. Michael, R.W.; Gergely, C.; Yentl, S.; Meisam, J.; Larissa, G.; Ignaas, V. Hybrid effects in thin ply carbon/glass unidirectional laminates: Accurate experimental determination and prediction. *Compos. A* **2016**, *88*, 131–139.
17. Guerrero, J.M.; Mayugo, J.A.; Costa, J.; Turon, A. A 3D Progressive failure model for predicting pseudo-ductility in hybrid unidirectional composites materials under fibre tensile loading. *Compos. Part A Appl. Sci. Manuf.* **2018**, *107*, 579–591. [CrossRef]
18. Sangwook, S.; Ran, Y.K.; Kazumasa, K.; Stephen, W.T. Experimental studies of thin-ply laminated composites. *Compos. Sci. Technol.* **2007**, *67*, 996–1008.
19. Tomohiro, Y.; Akiko, K.; Akinori, Y.; Toshi, O.; Takahira, A. Damage characterisation in thin-ply composite laminates under out-of-plane transverse loadings. *Compos. Struct.* **2010**, *93*, 49–57.
20. Hiroshi, S.; Mitsuhiro, M.; Kazumasa, K.; Manato, K.; Hiroki, T.; Mototsugo, T.; Isao, K. Effect of ply-thickness on impact damage morphology in CFRP laminates. *J. Reinf. Plast. Compos.* **2011**, *30*, 1097–1106.
21. Amacher, R.; Cugnoni, J.; Botsis, J.; Sorensen, L.; Smith, W.; Dransfeld, C. Thin ply composites: Experimental characterisation and modelling of size-effects. *Compos. Sci. Technol.* **2014**, *101*, 121–132.
22. Joel, G. Thin-ply composite laminates: A review. *Compos. Struct.* **2020**, *236*, 111920.
23. Subadra, S.P.; Griskevicius, P. Sustainability of polymer composites and its critical role in revolutionising wind power for green future. *Sustain. Technol. Green Econ.* **2021**, *1*, 1–7. [CrossRef]
24. Heoung-Jae, C.; Jai-Yoon, S.; Isaac, M.D. Effects of material and geometric nonlinearities on the tensile and compressive behaviour of composite materials with fibre waviness. *Compos. Sci. Technol.* **2001**, *61*, 125–134.
25. Hsiao, H.M.; Isaac, M.D. Elastic properties of composites with fibre waviness. *Compos. Part A Appl. Sci. Manuf.* **1996**, *27*, 931–941. [CrossRef]
26. Shi-Chang, W.; Isaac, M.D. Wave propagation in composite material with fibre waviness. *Ultrasonics* **1995**, *33*, 3–10.
27. Travis, A.B.; John, W.G., Jr.; Mark, A.L. Influence of ply waviness on the stiffness and strength reduction on composite laminates. *J. Thermoplast. Compos. Mater.* **1992**, *5*, 344–369.
28. Hsiao, H.M.; Isaac, M.D. Effect of fibre waviness on stiffness and strength reduction of unidirectional composites under compressive loading. *Compos. Sci. Technol.* **1996**, *56*, 581–593. [CrossRef]
29. Chan, W.S.; Wang, J.S. Influence of fibre waviness on the structural response of composite laminates. *J. Thermoplast. Compos. Mater.* **1994**, *7*, 243–260. [CrossRef]
30. Mark, R.G.; Ghodrat, K. Localised fibre waviness and implications for failure in unidirectional composites. *J. Compos. Mater.* **2005**, *36*, 1225–1244.
31. Karami, G.; Garnich, M. Micromechanical study of thermoplastic behaviour of composites with periodic fibre waviness. *Compos. Part B Eng.* **2005**, *36*, 241–248. [CrossRef]
32. Jumahat, A.; Soutis, C.; Jones, F.R.; Hodzic, A. Fracture mechanism and failure analysis of carbon fibre/toughened epoxy composites subjected to compressive loading. *Compos. Struct.* **2010**, *92*, 295–305. [CrossRef]
33. Karami, G.; Garnich, M. Effective moduli and failure considerations for composites with periodic fibre waviness. *Compos. Struct.* **2005**, *67*, 461–475. [CrossRef]
34. Potter, K.; Khan, B.; Wisnom, M.; Bell, T.; Stevens, J. Variability, fibre waviness and misalignment in the determination of the properties of composite materials and structures. *Compos. Part A Appl. Sci. Manuf.* **2008**, *39*, 1343–1354. [CrossRef]
35. Travis, A.B.; John, W.G., Jr.; Mark, A.L. Influence of ply waviness with nonlinear shear on the stiffness and strength reduction of composite. *J. Thermoplast. Compos. Mater.* **1994**, *7*, 76–90.
36. Alves, M.P.; Cimini, C.A., Jr.; Ha, S.K. Fibre waviness and its effect on the mechanical performance of fibre reinforced polymer composites: An enhanced review. *Compos. Part A* **2021**, *149*, 106526. [CrossRef]
37. Heoung-Jae, C.; Jai-Yoon, S. Non-linear behaviours of thick composites with fibre waviness under pure bending. *Mater. Sci. Res. Int.* **1999**, *48*, 243–260.

165

38. Michael, R.W. Effect of fibre waviness on the relationship between compressive and flexural strengths of unidirectional composites. *J. Compos. Mater.* **1994**, *28*, 66–76.
39. Rai, H.G.; Rogers, C.W.; Crane, D.A. Mechanics of curved fibre composites. *J. Reinf. Plast. Compos.* **1992**, *11*, 552–566. [CrossRef]
40. James, W.G.; Christis, G.P.; Balaguru, P.N. Flexural response of inorganic hybrid composites with E-Glass and carbon fibres. *J. Eng. Mater. Technol.* **2010**, *132*, 021005.
41. Ary Subagia, I.D.G.; Yonjig, K.; Leonard, D.T.; Cheol, S.K.; Ho, K.S. Effect of stacking sequence in the flexural properties of hybrid composites reinforced with carbon and basalt fibres. *Compos. B Eng.* **2014**, *58*, 251–258. [CrossRef]
42. Mehdi, K.; Chensong, D.; Ian, J.D. Multi-objective analysis for optimal and robust design of unidirectional glass/carbon fibre reinforced hybrid epoxy composites under flexural loading. *Compos. Part B Eng.* **2016**, *84*, 130–139.
43. Mehdi, K.; Chensong, D.; Ian, J.D. Effect of matrix voids, fibre misalignment and thickness variation on multi-objective robust optimization of carbon/glass fibre-reinforced hybrid composites under flexural loading. *Compos. B* **2017**, *123*, 136–147.
44. Maragoni, L.; Modenato, G.; De Rossi, N.; Vescovi, L.; Quaresimin, M. Effect of fibre waviness on the comprsisive fatigue behaviour of woven carbon/epoxy laminates. *Compos. Part B* **2002**, *199*, 108282. [CrossRef]
45. Allison, B.D.; Evans, J.L. Effect of fibre waviness on the bending behaviour of S-glass/epoxy composites. *Mater. Des.* **2012**, *36*, 316–322. [CrossRef]
46. Andreas, A.; Philipp, G.; Klaus, D. Strength prediction of ply waviness in composite materials considering matrix dominated effect. *Compos. Struct.* **2015**, *127*, 51–59.
47. Sharath, P.S.; Paulius, G.; Samy, Y. Low velocity impact and pseudo-ductile behaviour of carbon/glass/epoxy and carbon/glass/PMMA hybrid composite laminates for aircraft application at service temperature. *Polym. Test.* **2020**, *89*, 106711.
48. Ahmed, G. Ductility of externally prestressed continuous concrete beams. *KSCE J. Civ. Eng.* **2014**, *18*, 595–606.
49. Naaman, A.E.; Jeong, S.M. Structural ductility of concrete beams prestressed with FRP tendons. In Proceedings of the Second International RILEM Symposium (FRPRCS-2), Ghent, Belgium, 23–25 August 1995; pp. 379–401.
50. Grace, N.F.; Soliman, A.K.; Abdel-Sayed, G.; Saleh, K.R. Behaviour and ductility of simple and continuous FRP reinforced beams. *J. Compos. Constr.* **1998**, *2*, 186–194. [CrossRef]
51. Paolo, F.; Bonnie, W.; Francesco, D.; Mostafa, R.; Mark, H.; Alan, B. LS-DYNA MAT54 modelling of the axial crushing of a composite tape sinusoidal specimen. *Compos. Part A* **2011**, *42*, 1809–1825.
52. Egle, R.; Panagiotis, K.; Guillermo, R. Model parameter sensitivity and benchmarking of the explicit dynamic solver of LS-DYNA for structural analysis in case of fire. *Fire Saf. J.* **2017**, *90*, 123–138.
53. Antoniou, A.; Mikkelsen, L.P.; Goutianos, S.; Bagemiel, O.; Gebauer, I.; Flindt, R.; Sayer, F. Influence of the glass non-crimp fabric intrinsic undulation on the stiffness of the composite ply: A micromechanical approach. *IOP Conf. Ser. Mater. Sci. Eng.* **2020**, *942*, 012017. [CrossRef]
54. Zein, S.; Neaz Sheikh, M.; Alex, M.R.; Abheek, B. Numerical investigation on the flexural behaviour of GFRP-RC beams under monotonic loads. *Structures* **2019**, *20*, 255–267.
55. *LS-DYNA Keyword User'S Manual*, version 971; Livermore Software Technology Corporation: Livermore, CA, USA, 2006.
56. Jun, Z.; Jihui, W.; Aiqing, N.; Wantao, G.; Xiang, L.; Yibo, W. A multi-parameter model for stiffness prediction of composite laminates with out-of-plane waviness. *Compos. Struct.* **2018**, *185*, 327–337.
57. Dahsin, L. Impact-induced delamination-A view of bending stiffness mismatching. *J. Compos. Mater.* **1988**, *22*, 674.
58. Robert, M.J. *Mechanics of Composite Materials*, 2nd ed.; Taylor & Francis Inc.: Philadelphia, PA, USA, 1999; pp. 121–184.
59. 3B-Fibreglass SPRL, Technical Data Sheet for SE 2020 Direct Roving. Available online: https://www.3b-fibreglass.com/sites/default/files/products-data-sheets/TDS-SE-2020-DR-for-Epoxy-Resins-2015-sans-trame-LR.pdf (accessed on 19 June 2020).

166